

**University of Alberta**

**Insights into Selenium-77 NMR Interaction Tensors:  
Multinuclear Magnetic Resonance Investigations of  
Iminobis(dialkylphosphine chalcogenide) Systems in the Solid State**

by

**Bryan Adam Demko**



A thesis submitted to the Faculty of Graduate Studies and Research  
in partial fulfillment of the requirements for the degree of

**Doctor of Philosophy**

**Department of Chemistry**

**Edmonton, Alberta**

**Fall 2008**



Library and  
Archives Canada

Published Heritage  
Branch

395 Wellington Street  
Ottawa ON K1A 0N4  
Canada

Bibliothèque et  
Archives Canada

Direction du  
Patrimoine de l'édition

395, rue Wellington  
Ottawa ON K1A 0N4  
Canada

*Your file* *Votre référence*  
*ISBN: 978-0-494-46303-1*  
*Our file* *Notre référence*  
*ISBN: 978-0-494-46303-1*

**NOTICE:**

The author has granted a non-exclusive license allowing Library and Archives Canada to reproduce, publish, archive, preserve, conserve, communicate to the public by telecommunication or on the Internet, loan, distribute and sell theses worldwide, for commercial or non-commercial purposes, in microform, paper, electronic and/or any other formats.

The author retains copyright ownership and moral rights in this thesis. Neither the thesis nor substantial extracts from it may be printed or otherwise reproduced without the author's permission.

**AVIS:**

L'auteur a accordé une licence non exclusive permettant à la Bibliothèque et Archives Canada de reproduire, publier, archiver, sauvegarder, conserver, transmettre au public par télécommunication ou par l'Internet, prêter, distribuer et vendre des thèses partout dans le monde, à des fins commerciales ou autres, sur support microforme, papier, électronique et/ou autres formats.

L'auteur conserve la propriété du droit d'auteur et des droits moraux qui protègent cette thèse. Ni la thèse ni des extraits substantiels de celle-ci ne doivent être imprimés ou autrement reproduits sans son autorisation.

---

In compliance with the Canadian Privacy Act some supporting forms may have been removed from this thesis.

Conformément à la loi canadienne sur la protection de la vie privée, quelques formulaires secondaires ont été enlevés de cette thèse.

While these forms may be included in the document page count, their removal does not represent any loss of content from the thesis.

Bien que ces formulaires aient inclus dans la pagination, il n'y aura aucun contenu manquant.

  
**Canada**

*To my family and friends*

## Abstract

Solid-state nuclear magnetic resonance permits access to the orientation-dependent NMR interaction tensors. A review of the solid-state  $^{77}\text{Se}$  NMR literature introduces areas of active research and places the presented experimental work into context. A comprehensive investigation of selenium chemical shift tensors provides a theoretical foundation using density functional theory for the level of relativistic theory, via the zeroth order regular approximation, required to reproduce experimentally determined values and trends. The selenium chemical shift tensors for a number of organoselenium, organophosphine selenide, and inorganic selenium systems are reported for the first time. Multinuclear magnetic resonance investigations of iminobis(dialkylphosphine chalcogenide) systems,  $\text{HN}(\text{R}_2\text{PE})_2$  ( $\text{E} = \text{O}, \text{S}, \text{Se}$ ;  $\text{R} = \text{Ph}, {}^i\text{Pr}$ ), together with their respective calculated values demonstrate the sensitivity of the selenium chemical shift tensor to hydrogen bonding and disorder within their solid-state structures. Indirect one-bond selenium-phosphorus coupling constants,  ${}^1J(^{77}\text{Se}, {}^{31}\text{P})_{\text{iso}}$ , are diagnostic with respect to the presence of an acidic N-H proton. The magnitudes of  ${}^1J(^{77}\text{Se}, {}^{31}\text{P})_{\text{iso}}$  for the  $\text{HN}(\text{R}_2\text{PSe})_2$  ( $\text{R} = \text{Ph}, {}^i\text{Pr}$ ) species,  $> 700$  Hz, are on the order of 200 Hz larger than those found for  $[\text{N}({}^i\text{Pr}_2\text{PSe})_2]^-$  systems. The study of metal(II) tetraisopropyldiselenoimido-diphosphinato complexes,  $\text{M}[\text{N}({}^i\text{Pr}_2\text{PSe})_2]_2$ , by solid-state NMR presents a novel non-symmetric inorganic X-Se-Y moiety for solid-state  $^{77}\text{Se}$  NMR investigation. The characterized M-Se-P linkages are members of six-membered,  $\text{MSe}_2\text{P}_2\text{N}$ , rings. The pseudo-boat or distorted chair conformations of the heterocyclic rings, commonly encountered in  $\text{M}^{n+}[\text{N}(\text{R}_2\text{PSe})_2]_n$  systems, have been differentiated by solid-state  $^{77}\text{Se}$

NMR. The selenium chemical shift tensors for the pseudo-boat  $MSe_2P_2N$  rings possess spans,  $\Omega = \delta_{11} - \delta_{33}$ , that are on the order of 100-200 ppm larger than those from rings with a distorted chair conformation. Calculated orientations for the selenium chemical shift tensors are also found to differ depending on the conformation of the heterocyclic ring. The selenium chemical shift tensor for the central selenium in the square-planar complex  $Se[N(^iPr_2PSe)_2]_2$  was described by qualitative molecular orbital theory, and its computation was found to require spin-orbit relativistic corrections in order to accurately reproduce the principal components,  $\delta_{ij}$ . The largest magnitudes reported for  $^1J(^{77}Se, ^{77}Se)_{iso}$  and  $^1J(^{125}Te, ^{77}Se)_{iso}$  were found for the  $Se[N(^iPr_2PSe)_2]_2$  and  $Te[N(^iPr_2PSe)_2]_2$  complexes, respectively.

## Acknowledgments

I would like to begin by thanking my supervisor, Roderick Wasylshen, for accepting me into his research group in the Fall of 2002. From synthetic chemistry, to experimental spectroscopy, to theoretical computational chemistry, the array of research pursuits available as a member of Rod's group is exceptional in scope and quality.

The research presented in this thesis could not have been accomplished without the valued contributions of some of my coworkers. Mathew Willans and Kris Harris also joined Rod's group in the Fall of 2002 and quickly became the fundamental support system for many of my research struggles. Devin Sears joined the group as a post-doctoral fellow in the Summer of 2004 and subsequently taught me much of research preparation, planning and execution. The knowledge shared to me by these three chance colleagues, and their willingness to serve as soundboards for my thoughts and concerns, has been invaluable to me both personally and professionally. Today, the bonds that I have formed with Mat, Kris and Devin transcend the working environment and I am glad to count them among my closest of friends.

Some more specific acknowledgements in regards to the research conducted for the preparation of this thesis are also required. The work presented in Chapter 4 was accomplished in no small part due to the efforts of Klaus Eichele. I thank Klaus for performing the majority of the experimental work, some simulations and a number of helpful discussions. Additionally, the contributions of Prof. Glenn H. Penner for preparing the trimethylphosphine selenide and tris-(*tert*-butyl)phosphine selenide samples, Prof. Gang Wu for some preliminary experiments on ammonium

selenotungstate, and Prof. P.-N. Roy for generous use of some computing resources, are humbly acknowledged. As for the research presented in Chapters 5 through 7, I would like to thank Prof. Martin Cowie and his research group for access to their solvent stills, and Dr. Devin Sears for use of his computational resources.

Before acknowledging the non-research related support that I have received, I would like to thank several funding agencies that have financially supported me through the pursuit of this degree. These include the Natural Sciences and Engineering Research Council of Canada, the Alberta Ingenuity Fund, and the University of Alberta for various research grants and scholarships.

The existence of things in my life that are outside the laboratory, outside chemistry, and outside science are what allows me to keep returning to the laboratory. The day-in day-out love and support of my wife, Sarah, has been the hearthstone of my faith in my self and my work. With Sarah, there is no accomplishment that is achieved alone which makes every future success all the more worth pursuing.

The support system upon which Sarah and I rely most heavily, I feel fortunate to say, is our immediate families. My parents, Victor and Marlene, are what every child could desire in their parents; an endless fount of love and support. The desire in me to emulate them is only matched by my efforts to make them proud. My brother and sister, Nick and Kate, are more than just my siblings; they are my oldest, dearest, and most personal of friends. Douglas and Flora Ord have welcomed me into their equally wonderful family with open arms and open hearts. Their care and concern is always appreciated. From my sister-in-law, Megan, Sarah and I receive nothing but optimism and best wishes. I am truly blessed with a family unlike any other.

While I have already listed a number of those that I count among my close friends, those that have yet to be mentioned are equally valued for their friendship and support. Mike Ius has brought more fun times to my life than can be listed; however, his visit in the Spring of 2003 will forever be remembered as a response to a friend in need. Chris Kanakos knows me like few people do and our nearly daily conversations almost always leave me smiling. Mike Kanakos has served admirably throughout our friendship as my substitute big brother. Tina Grant is a constant inspiration at her command of positive energy. Andrew Grosvenor has been a welcome friendly face during the past couple years, especially during our often biweekly conversations over beer. And the treasured support of Dr. Anna Jordan has often gone above and beyond for me.

The social activities that I have participated in during my graduate degree have served me well and deserve their own credit. From my first month at the University of Alberta I have belonged to the softball team of many names and count our victories and losses among some of my fondest memories of my time here. With the arrival of Devin Sears in 2004, I found someone to share my enjoyment of football with, and nearly every Monday night in the Fall found us at Scholars/The Library/Hudsons. The Monday Night Football gang slowly grew to include Andrew Grosvenor and Glen Elliot, and served as an often much needed weekly escape. The various ski trips that I have been able to join in on were valued weekend vacations to the mountains.

Finally, I would like to recognize the tutelage of my former supervisors; Professors Yining Huang, David Shoesmith and Derek Leaist. Their instruction during my early experiences with scientific research laid a strong foundation for my current and future research endeavors.



## Table of Contents

<b>Chapter 1 – Introduction and Overview.....</b>	<b>1</b>
<b>1.1 Introduction.....</b>	<b>1</b>
1.1.1 Selenium .....	1
1.1.2 Nuclear Magnetic Resonance .....	3
1.1.3 Focus System .....	5
<b>1.2 Overview .....</b>	<b>7</b>
<b>1.3 References.....</b>	<b>10</b>
<b>Chapter 2 – Solid-State Selenium-77 NMR.....</b>	<b>14</b>
<b>2.1 Introduction.....</b>	<b>14</b>
2.1.1 Selenium-77 NMR.....	14
2.1.2 Solid-State <sup>77</sup> Se NMR.....	15
2.1.3 Structure.....	16
<b>2.2 Solid-State <sup>77</sup>Se NMR.....</b>	<b>19</b>
2.2.1 Selenium .....	19
2.2.2 Selones.....	21
2.2.2.1 <i>Seleno-Carbonyls</i> .....	21
2.2.2.2 <i>Phosphine Selones</i> .....	22
2.2.3 Bridging Selenium Systems.....	26
2.2.3.1 <i>Bridging Organic Centers</i> .....	27
2.2.3.1.1 Selenoethers .....	27
2.2.3.1.2 Organic Conductors .....	29
2.2.3.2 <i>Bridging Organic and Inorganic Centers</i> .....	40
2.2.3.3 <i>Bridging Inorganic Centers</i> .....	44
2.2.3.3.1 Symmetric X-Se-X Linkages.....	44
2.2.3.3.2 Non-symmetric X-Se-Y Linkages .....	47
2.2.4 Inorganic Systems.....	49
2.2.4.1 <i>Selenium Oxides</i> .....	49
2.2.4.2 <i>Inorganic Mono-, Di-, and Poly-selenides</i> .....	54
2.2.4.2.1 Inorganic Monoselenides .....	54
2.2.4.2.2 Inorganic Diselenides.....	57
2.2.4.2.3 Inorganic Polyselenides .....	61
2.2.4.3 <i>Vitreous Systems</i> .....	63
2.2.5 Miscellaneous Selenium Systems .....	65
2.2.5.1 <i>Miscellaneous Organoselenium Systems</i> .....	65
2.2.5.2 <i>Miscellaneous Inorganic Systems</i> .....	69
<b>2.3 Summary.....</b>	<b>70</b>
<b>2.4 References.....</b>	<b>72</b>

**Chapter 3 – Theory and Methods..... 89**

<b>3.1 NMR Interactions</b> .....	89
3.1.1 The Zeeman Interaction .....	90
3.1.2 The Nuclear Magnetic Shielding Interaction .....	91
3.1.3 The Direct Dipolar Interaction.....	94
3.1.4 The Indirect Nuclear Spin-Spin Interaction.....	95
3.1.5 The Quadrupolar Interaction.....	97
<b>3.2 Experimental Techniques in Solid-State NMR</b> .....	98
3.2.1 Magic Angle Spinning .....	99
3.2.2 High-Power Heteronuclear Decoupling.....	101
3.2.3 Cross Polarization .....	102
<b>3.3 Quantum Chemical Calculation of NMR Parameters</b> .....	104
3.3.1 Density Functional Theory .....	105
3.3.2 The Zeroth Order Regular Approximation .....	108
<b>3.4 References</b> .....	111

**Chapter 4 – A Combined Experimental and Quantum Chemistry Study of Selenium Chemical Shift Tensors ..... 114**

<b>4.1 Introduction</b> .....	114
<b>4.2 Background Theory</b> .....	116
<b>4.3 Experimental</b> .....	118
<b>4.4 Results and Discussion</b> .....	122
4.4.1 Comparison of Observed and Calculated Selenium Chemical Shift Tensors	122
4.4.2 Organoselenium Compounds.....	127
4.4.3 Organophosphine Selenides.....	138
4.4.4 Inorganic Selenium Compounds.....	150
<b>4.5 Summary</b> .....	156
<b>4.6 References</b> .....	158

**Chapter 5 – Probing Solid Iminobis(dialkylphosphine chalcogenide) Systems with Multinuclear Magnetic Resonance ..... 167**

<b>5.1 Introduction</b> .....	167
<b>5.2 Experimental</b> .....	169
5.2.1 Sample Preparation .....	169
5.2.2 NMR Experiments .....	171
5.2.3 DFT Computations.....	172
<b>5.3 Results &amp; Discussion</b> .....	173
5.3.1 Solid-State <sup>31</sup> P NMR.....	174
5.3.1.1 <i>HN(R<sub>2</sub>PO)<sub>2</sub> (R = Ph, <sup>i</sup>Pr)</i> .....	174

5.3.1.2 $HN(R_2PS)_2$ ( $R = Ph, ^iPr$ )	178
5.3.1.3 $HN(R_2PSe)_2$ ( $R = Ph, ^iPr$ )	181
5.3.2 Solid-State $^{77}Se$ NMR	184
5.3.3 The Effect of the E-P··P-E ‘Torsion’ Angle	188
<b>5.4 Summary</b>	190
<b>5.5 References</b>	192

**Chapter 6 – A Solid-State NMR Investigation of Single-Source Precursors for Group 12 Metal Selenides;  $M[N(^iPr_2PSe)_2]_2$  ( $M = Zn, Cd, Hg$ ) ..... 200**

<b>6.1 Introduction</b>	200
<b>6.2 Experimental</b>	202
6.2.1 Sample Preparation	202
6.2.2 NMR Experiments	203
6.2.3 DFT Computations	205
<b>6.3 Results &amp; Discussion</b>	206
6.3.1 Solid-State $^{31}P$ NMR	207
6.3.2 Solid-State $^{77}Se$ NMR	214
6.3.3 Solid-State $^{113}Cd$ NMR	219
6.3.4 Solid-State $^{199}Hg$ NMR	221
<b>6.4 Summary</b>	223
<b>6.5 References</b>	225

**Chapter 7 – Comparing Main Group and Transition Metal Square-Planar Complexes of the Diselenoimidodiphosphate Anion: A Solid-State NMR Investigation of  $M[N(^iPr_2PSe)_2]_2$  ( $M = Se, Te; Pd, Pt$ ) ..... 235**

<b>7.1 Introduction</b>	235
<b>7.2 Experimental</b>	236
7.2.1 Sample Preparation	236
7.2.2 NMR Experiments	238
7.2.3 DFT Computations	240
<b>7.3 Results &amp; Discussion</b>	242
7.3.1 Solid-State $^{31}P$ NMR	243
7.3.2 Solid-State $^{77}Se$ NMR Results of the Diselenoimidodiphosphinato Selenium Environments	251
7.3.3 Solid-State NMR of the Central Atom of $M[N(^iPr_2PSe)_2]_2$ ( $M = ^{195}Pt, ^{77}Se, ^{125}Te$ )	259
<b>7.4 Summary</b>	268
<b>7.5 References</b>	270

<b>Chapter 8 – Conclusions and Outlook .....</b>	<b>278</b>
<b>8.1 Conclusions.....</b>	<b>278</b>
8.1.1 Experimental Solid-State <sup>77</sup> Se NMR Parameters.....	279
8.1.2 Theoretical Insight into <sup>77</sup> Se Nuclear Magnetic Shielding .....	282
8.1.3 Specific Chemical Information .....	285
<b>8.2 Outlook.....</b>	<b>286</b>
8.2.1 Lone Electron Pair Stereochemical Activity.....	287
8.2.2 Paramagnetic Systems .....	287
8.2.3 Tellurium Analogues .....	288
<b>8.3 References .....</b>	<b>290</b>
<b>Appendix A .....</b>	<b>292</b>
<b>Appendix B .....</b>	<b>293</b>
<b>Appendix C .....</b>	<b>295</b>
<b>Appendix D .....</b>	<b>301</b>
<b>Appendix E .....</b>	<b>304</b>

## List of Tables

### Chapter 2

Table 2.1 Isotropic selenium chemical shifts of various $^{77}\text{Se}$ NMR reference compounds. ....	18
Table 2.2 Solid-state $^{77}\text{Se}$ NMR chemical shifts and chemical shift tensors for elemental selenium. ....	20
Table 2.3 Solid-state $^{77}\text{Se}$ chemical shifts and chemical shift tensors for seleno-carbonyl systems. ....	22
Table 2.4 Solid-state $^{77}\text{Se}$ chemical shifts and chemical shift tensors for phosphine seleno systems. ....	23
Table 2.5 Indirect spin-spin coupling constants, $^nJ(^{77}\text{Se}, ^m\text{X})_{\text{iso}}$ ( $m < 77$ ). ....	25
Table 2.6 Solid-state $^{77}\text{Se}$ chemical shifts and chemical shift tensors for selenium bridging organic centers. ....	28
Table 2.7 Solid-state $^{77}\text{Se}$ NMR monitored phase transitions in the organic conductors, $\text{A}_2\text{X}$ . ....	34
Table 2.8 Solid-state $^{77}\text{Se}$ chemical shifts and chemical shift tensors for selenium bridging organic and inorganic centers. ....	42
Table 2.9 Indirect spin-spin coupling constants, $^nJ(^{77}\text{Se}, ^m\text{X})_{\text{iso}}$ ( $m > 77$ ). ....	44
Table 2.10 Solid-state $^{77}\text{Se}$ chemical shifts and chemical shift tensors for inorganic X-Se-X bridging moieties. ....	46
Table 2.11 Solid-state $^{77}\text{Se}$ chemical shifts and chemical shift tensors for inorganic X-Se-Y bridging moieties. ....	48
Table 2.12 Solid-state $^{77}\text{Se}$ chemical shifts and chemical shift tensors for selenium oxides. ....	50
Table 2.13 Solid-state $^{77}\text{Se}$ chemical shifts and chemical shift tensors for inorganic selenium systems. ....	55
Table 2.14 Solid-state $^{77}\text{Se}$ chemical shifts found in vitreous selenium systems. ....	64
Table 2.15 Solid-state $^{77}\text{Se}$ chemical shifts and chemical shift tensors for miscellaneous organoselenium systems. ....	66

### Chapter 4

Table 4.1 Experimental and Theoretical Chemical Shift Tensors for Organoselenium Compounds. ....	129
Table 4.2 Experimental and Theoretical Chemical Shift Tensors for Tris-Organophosphine Selenides. ....	139
Table 4.3 Experimental and Theoretical Chemical Shift Tensors for Inorganic Selenium Compounds. ....	151

## Chapter 5

Table 5.1 Solid-state  $^{31}\text{P}$  NMR parameters for  $\text{HN}(\text{R}_2\text{PE})_2$  ( $\text{E} = \text{O}, \text{S}, \text{Se}$ ;  $\text{R} = \text{Ph}, {}^i\text{Pr}$ ). 175

Table 5.2 Solid-state  $^{77}\text{Se}$  NMR parameters for  $\text{HN}(\text{R}_2\text{PSe})_2$  ( $\text{R} = \text{Ph}, {}^i\text{Pr}$ ). ..... 186

## Chapter 6

Table 6.1 Solid-state  $^{31}\text{P}$  NMR parameters for  $\text{M}[\text{N}({}^i\text{Pr}_2\text{PSe})_2]_2$  ( $\text{M} = \text{Zn}, \text{Cd}, \text{Hg}$ ). ..... 209

Table 6.2 Solid-state  $^{77}\text{Se}$  NMR parameters for  $\text{M}[\text{N}({}^i\text{Pr}_2\text{PSe})_2]_2$  ( $\text{M} = \text{Zn}, \text{Cd}, \text{Hg}$ )..... 216

Table 6.3 Solid-state  $^{113}\text{Cd}$  and  $^{199}\text{Hg}$  NMR parameters for  $\text{M}[\text{N}({}^i\text{Pr}_2\text{PSe})_2]_2$  ( $\text{M} = \text{Cd}, \text{Hg}$ ). ..... 221

## Chapter 7

Table 7.1 Experimental and theoretical solid-state  $^{31}\text{P}$  NMR parameters for  $\text{M}[\text{N}({}^i\text{Pr}_2\text{PSe})_2]_2$  ( $\text{M} = \text{Pd}, \text{Pt}; \text{Se}, \text{Te}$ ). ..... 245

Table 7.2 Experimental and theoretical solid-state  $^{77}\text{Se}$  NMR parameters for the anion of  $\text{M}[\text{N}({}^i\text{Pr}_2\text{PSe})_2]_2$  ( $\text{M} = \text{Pd}, \text{Pt}; \text{Se}, \text{Te}$ ). ..... 253

Table 7.3 Experimental and theoretical solid-state NMR parameters for  $\text{M}[\text{N}({}^i\text{Pr}_2\text{PSe})_2]_2$  ( $\text{M} = {}^{105}\text{Pd}, {}^{195}\text{Pt}; {}^{77}\text{Se}, {}^{125}\text{Te}$ )..... 260

## Appendix A

Table A1 Linear Fit Parameters for Experimental vs. Calculated Selenium Chemical Shift Tensors. .... 292

## Appendix B

Table B1 Theoretical phosphorus chemical shift tensors for  $\text{HN}(\text{R}_2\text{PE})_2$  ( $\text{E} = \text{O}, \text{S}, \text{Se}$ ;  $\text{R} = \text{Ph}, {}^i\text{Pr}$ )..... 293

Table B2 Theoretical selenium chemical shift tensors for  $\text{HN}(\text{R}_2\text{PSe})_2$  ( $\text{R} = \text{Ph}, {}^i\text{Pr}$ ). .. 294

## Appendix C

Table C1 Theoretical phosphorus chemical shift tensors for  $\text{M}[\text{N}({}^i\text{Pr}_2\text{PSe})_2]_2$  ( $\text{M} = \text{Zn}, \text{Cd}, \text{Hg}$ )..... 295

Table C2 Theoretical selenium chemical shift tensors for  $\text{M}[\text{N}({}^i\text{Pr}_2\text{PSe})_2]_2$  ( $\text{M} = \text{Zn}, \text{Cd}, \text{Hg}$ ). ..... 296

Table C3 Theoretical cadmium and mercury magnetic shielding tensors for  $\text{M}[\text{N}({}^i\text{Pr}_2\text{PSe})_2]_2$  ( $\text{M} = \text{Cd}, \text{Hg}$ ). ..... 297

Table C4 Traceless phosphorus chemical shift tensors for  $\text{M}[\text{N}({}^i\text{Pr}_2\text{PSe})_2]_2$  ( $\text{M} = \text{Zn}, \text{Cd}, \text{Hg}$ ). ..... 298

Table C5 Table C5 Traceless selenium chemical shift tensors for  $\text{M}[\text{N}({}^i\text{Pr}_2\text{PSe})_2]_2$  ( $\text{M} = \text{Zn}, \text{Cd}, \text{Hg}$ ). ..... 299

Table C6 Traceless cadmium and mercury chemical shift tensors for  $\text{M}[\text{N}({}^i\text{Pr}_2\text{PSe})_2]_2$  ( $\text{M} = \text{Cd}, \text{Hg}$ )..... 300

## Appendix D

Table D1 Theoretical phosphorus shielding tensors for $M[N(^iPr_2PSe)_2]_2$ ( $M = Pd, Pt; Se, Te$ ). .....	301
Table D2 Theoretical selenium shielding tensors for the anion of $M[N(^iPr_2PSe)_2]_2$ ( $M = Pd, Pt; Se, Te$ ). .....	302
Table D3 Theoretical shielding tensors for nucleus $M$ of $M[N(^iPr_2PSe)_2]_2$ ( $M = {}^{105}Pd, {}^{195}Pt; {}^{77}Se, {}^{125}Te$ ). .....	303

## List of Figures

### Chapter 2

- Figure 2.1 Representative examples of the seleno-carbonyls (a-c) and phosphine selones (d-g) that have been studied by solid-state  $^{77}\text{Se}$  NMR. .... 24
- Figure 2.2 Selenium coronands that have been studied by solid-state  $^{77}\text{Se}$  NMR. .... 30
- Figure 2.3 Structurally rigid selenoethers that have been studied by solid-state  $^{77}\text{Se}$  NMR. .... 31
- Figure 2.4 Examples of the bridging selenium environments that have been studied by solid-state  $^{77}\text{Se}$  NMR. .... 41
- Figure 2.5 Miscellaneous structures that have been studied by solid-state  $^{77}\text{Se}$  NMR. .... 68

### Chapter 3

- Figure 3.1 Diagram illustrating the orientation of the external applied magnetic field, as defined by the polar angles  $\theta$  and  $\phi$ , with respect to the nuclear magnetic shielding tensor. .... 93
- Figure 3.2 Relative angles describing the orientation of the external applied magnetic field,  $B_0$ , internuclear vector,  $r_{\text{IS}}$ , and the sample rotation, rotor, axes. .... 100
- Figure 3.3 The effect of MAS on the  $^{77}\text{Se}$  NMR spectrum of  $(\text{NH}_4)_2\text{SeO}_4$ . .... 101
- Figure 3.4 Typical cross polarization pulse sequence. .... 103

### Chapter 4

- Figure 4.1 Compounds investigated. .... 119
- Figure 4.2 Experimental vs. calculated isotropic chemical shifts,  $\delta_{\text{iso}}$ , for the selenium-containing compounds investigated. .... 123
- Figure 4.3 Experimental vs. calculated values for (a)  $\delta_{11}$ , (b)  $\delta_{22}$ , and (c)  $\delta_{33}$  for the selenium-containing compounds investigated. .... 125
- Figure 4.4 Experimental vs. calculated spans,  $\Omega = \delta_{11} - \delta_{33}$ , for the selenium-containing compounds investigated. .... 127
- Figure 4.5 CP MAS  $^{77}\text{Se}$  NMR spectrum of *N,N*-dimethylselenourea. .... 128
- Figure 4.6 RACP MAS  $^{77}\text{Se}$  NMR spectrum of *N*-methylbenzothiazole-2-selone. .... 132
- Figure 4.7 Selenium-77 RACP MAS NMR center band spectrum of  $\text{Ph}_2\text{SeCl}_2$ . .... 135
- Figure 4.8 (a) CP MAS  $^{77}\text{Se}$  NMR spectrum of  ${}^t\text{Bu}_3\text{PSe}$ . (b) CP  $^{77}\text{Se}$  NMR spectrum of stationary  ${}^t\text{Bu}_3\text{PSe}$ . .... 141
- Figure 4.9 Selenium-77 RACP MAS NMR spectrum for  $\text{Cyc}_3\text{PSe}$ . .... 143
- Figure 4.10 5-phenyldibenzophosphine 5-selenide RACP MAS  $^{77}\text{Se}$  spectrum. .... 146
- Figure 4.11 CP MAS  $^{77}\text{Se}$  NMR spectrum for *p*- $\text{Tol}_3\text{PSe}$ . .... 148
- Figure 4.12  $^{77}\text{Se}$  CP MAS NMR spectrum for  $\text{TTMPSe}$ . .... 149



Figure 4.13 CP static $^{77}\text{Se}$ NMR spectrum for $(\text{NH}_4)_2\text{SeO}_4$ .	152
Figure 4.14 $^{77}\text{Se}$ CP MAS spectrum for $(\text{NH}_4)_2\text{WSe}_4$ .	154

## Chapter 5

Figure 5.1 Common conformations encountered in iminobis(dialkylphosphine chalcogenide), $\text{HN}(\text{R}_2\text{PE})_2$ (E = O, S, Se), systems.	170
Figure 5.2 RACP MAS $^{31}\text{P}$ NMR spectra for (a) $\text{Ph}_2\text{P}(\text{OH})\text{NP}(\text{O})\text{Ph}_2$ and (b) $\text{HN}(\text{}^i\text{Pr}_2\text{PO})_2$ .	176
Figure 5.3 RACP MAS $^{31}\text{P}$ NMR spectra for (a) $\text{HN}(\text{Ph}_2\text{PS})_2$ and (b) $\text{HN}(\text{}^i\text{Pr}_2\text{PS})_2$ .	179
Figure 5.4 RACP MAS $^{31}\text{P}$ NMR spectra for (a) $\text{HN}(\text{Ph}_2\text{PSe})_2$ and (b) $\text{HN}(\text{}^i\text{Pr}_2\text{PSe})_2$ .	182
Figure 5.5 RACP MAS $^{77}\text{Se}$ NMR spectra for (a) $\text{HN}(\text{Ph}_2\text{PSe})_2$ and (b) $\text{HN}(\text{}^i\text{Pr}_2\text{PSe})_2$ .	185
Figure 5.6 Isotropic region of the $^{77}\text{Se}$ NMR spectra for (a) $\text{HN}(\text{Ph}_2\text{PSe})_2$ and (b) $\text{HN}(\text{}^i\text{Pr}_2\text{PSe})_2$ .	187
Figure 5.7 Effect of rotation about the E-P•••P-E ‘torsion’ angle for $\text{HN}(\text{Me}_2\text{PSe})_2$ on (a) $\delta_{\text{iso}}(^{31}\text{P})$ and (b) $\delta_{\text{iso}}(^{77}\text{Se})$ .	189

## Chapter 6

Figure 6.1 Representation of the solid-state structure of $\text{M}[\text{N}(\text{}^i\text{Pr}_2\text{PSe})_2]_2$ (M = Zn, Cd, Hg).	207
Figure 6.2 VACP MAS $^{31}\text{P}$ NMR spectrum of $\text{Hg}[\text{N}(\text{}^i\text{Pr}_2\text{PSe})_2]_2$ .	208
Figure 6.3 Isotropic $^{31}\text{P}$ NMR regions for $\text{M}[\text{N}(\text{}^i\text{Pr}_2\text{PSe})_2]_2$ (M = Zn, Cd, Hg) at 4.7 T, 7.0 T, and 11.7 T.	211
Figure 6.4 (a) VACP MAS $^{77}\text{Se}$ NMR spectra for $\text{M}[\text{N}(\text{}^i\text{Pr}_2\text{PSe})_2]_2$ (M = Zn, Cd, Hg). (b) Expansion of the isotropic region of the $^{77}\text{Se}$ NMR spectra.	215
Figure 6.5 VACP $^{113}\text{Cd}$ NMR spectrum of stationary $\text{Cd}[\text{N}(\text{}^i\text{Pr}_2\text{PSe})_2]_2$ .	220
Figure 6.6 (a) VACP MAS $^{199}\text{Hg}$ NMR spectrum of $\text{Hg}[\text{N}(\text{}^i\text{Pr}_2\text{PSe})_2]_2$ . (b) Expansion of the isotropic region of the $^{199}\text{Hg}$ NMR spectrum.	222

## Chapter 7

Figure 7.1 Representation of the solid-state structures of $\text{M}[\text{N}(\text{R}_2\text{PSe})_2]_2$ (R = $^i\text{Pr}$ , Ph) (a) M = Se, Te; (b) M = Pd, Pt.	237
Figure 7.2 VACP MAS $^{31}\text{P}$ NMR spectra for (a) $\text{Pd}[\text{N}(\text{}^i\text{Pr}_2\text{PSe})_2]_2$ and (b) $\text{Pt}[\text{N}(\text{}^i\text{Pr}_2\text{PSe})_2]_2$ .	244
Figure 7.3 VACP MAS $^{31}\text{P}$ NMR spectra for (a) $\text{Se}[\text{N}(\text{}^i\text{Pr}_2\text{PSe})_2]_2$ and (b) $\text{Te}[\text{N}(\text{}^i\text{Pr}_2\text{PSe})_2]_2$ .	247
Figure 7.4 Isotropic $^{31}\text{P}$ NMR regions for $\text{M}[\text{N}(\text{}^i\text{Pr}_2\text{PSe})_2]_2$ (M = Pd, Pt; Se, Te) at 4.7 T, 7.0 T, and 11.7 T.	248

Figure 7.5 VACP MAS $^{77}\text{Se}$ NMR spectra for (a) $\text{Pd}[\text{N}(\text{}^i\text{Pr}_2\text{PSe})_2]_2$ and (b) $\text{Pt}[\text{N}(\text{}^i\text{Pr}_2\text{PSe})_2]_2$ .....	252
Figure 7.6 (a) Experimental VACP MAS $^{77}\text{Se}$ NMR spectrum for $\text{Se}[\text{N}(\text{}^i\text{Pr}_2\text{PSe})_2]_2$ . (b-d) Simulations of the selenium environments for $\text{Se}[\text{N}(\text{}^i\text{Pr}_2\text{PSe})_2]_2$ . (e) VACP MAS $^{77}\text{Se}$ NMR spectrum for $\text{Te}[\text{N}(\text{}^i\text{Pr}_2\text{PSe})_2]_2$ , and (f) its simulation.....	255
Figure 7.7 Isotropic regions of the $^{77}\text{Se}$ NMR spectra at 7.0 T for the diselenoimidodiphosphinate anion of the square-planar complexes $\text{M}[\text{N}(\text{}^i\text{Pr}_2\text{PSe})_2]_2$ , M = (a) Pd, (b) Pt, (c) Se, (d) Te.....	258
Figure 7.8 VACP MAS $^{195}\text{Pt}$ NMR spectrum of $\text{Pt}[\text{N}(\text{}^i\text{Pr}_2\text{PSe})_2]_2$ . .....	261
Figure 7.9 Molecular orbital diagram for an idealized $\text{Pt}^{\text{II}}\text{L}_4$ anion. ....	263
Figure 7.10 Molecular orbital diagram for an idealized $\text{M}^{\text{II}}\text{L}_4$ (M = Se, Te) anion.....	265
Figure 7.11 VACP MAS $^{125}\text{Te}$ NMR spectrum of $\text{Te}[\text{N}(\text{}^i\text{Pr}_2\text{PSe})_2]_2$ . .....	267

## List of Symbols

$A$	hyperfine coupling constant
$\alpha, \beta, \gamma$	Euler angles
$\mathbf{B}_0$	external applied magnetic field
$B_0$	external magnetic field strength
$B_1$	radiofrequency field strength
$B_{0,c}$	superconducting magnetic field strength
$B_{0,MI}$	metal-insulator magnetic field strength
$C_Q$	nuclear quadrupolar coupling constant
$C_3$	three-fold rotation axis
$c$	speed of light
$\mathbf{D}$	direct dipolar coupling tensor
$\delta_{ii}$	principal component of the chemical shift tensor
$\delta_{iso}$	isotropic chemical shift
$\Delta\sigma$	anisotropy of the chemical shift tensor
$\Delta J$	anisotropy of the indirect spin-spin coupling tensor
$e$	elementary charge
$\theta, \phi$	polar angles
$\gamma_I$	magnetogyric ratio for spin $I$
$\hat{\mathcal{H}}$	Hamiltonian operator
$h$	Planck's constant
$\hbar$	reduced Planck's constant
$\eta_\sigma$	asymmetry of the chemical shift tensor

$\eta_I$	asymmetry of the indirect spin-spin coupling tensor
$\eta_Q$	asymmetry of the electric field gradient tensor
$\mathbf{I}$	nuclear spin angular momentum operator
$I$	nuclear spin quantum number
$\mathbf{J}$	indirect spin-spin coupling tensor
$J_{\text{iso}}$	indirect spin-spin coupling constant
$J_{\text{ii}}$	principal component of the indirect spin-spin coupling tensor
$\mathbf{K}$	reduced indirect spin-spin coupling tensor
$K$	reduced indirect spin-spin coupling constant
$\kappa$	skew of the nuclear magnetic shielding or chemical shift tensor
$m_e$	electron mass
$m_I$	magnetic quantum number for spin $I$
$\mu_I$	nuclear magnetic moment for spin $I$
$\mu_0$	vacuum permeability
$\mu_B$	Bohr magneton
$\nu_L$	Larmor frequency
$\nu_{\text{rot}}$	rotor spinning frequency
$Q$	nuclear quadrupole moment
$\Omega$	span of the nuclear magnetic shielding or chemical shift tensor
$P_{\text{MI}}$	metal-insulator transition pressure
$P_c$	superconducting transition pressure
$R_{\text{DD}}$	direct dipolar coupling constant

$R_{eff}$	effective direct dipolar coupling constant
$\rho(\mathbf{r})$	electron density
$S_4$	four-fold improper rotation axis
$\sigma$	nuclear magnetic shielding tensor
$\sigma_{ii}$	principal component of the nuclear magnetic shielding tensor
$\sigma_{iso}$	isotropic nuclear magnetic shielding constant
$T$	temperature
$T_{AO}$	anion ordering temperature
$T_{MI}$	metal-insulator transition temperature
$T_c$	superconducting transition temperature
$T_g$	glass transition temperature
$T_1$	nuclear spin-lattice relaxation time
$T_1^{-1}$	nuclear spin-lattice relaxation rate
$T_2$	nuclear spin-spin relaxation time
$T_2^{-1}$	nuclear spin-spin relaxation rate
$\mathbf{V}$	electric field gradient tensor
$V_{ii}$	principal component of the electric field gradient tensor
$\Xi$	frequency ratio

## List of Abbreviations

ADF	Amsterdam Density Functional
<i>acac</i>	acetylacetonate
<i>aq</i>	aqueous
BETD-TSF	bis(ethylenedithio)tetraselenafulvalene
BETD-TTF	bis(ethylenedithio)tetrathiafulvalene
bpy	2,2'-bipyridine
Bu	butyl
CDW	charge density wave
CP	cross polarization
CW	continuous wave (decoupling)
Cyc	Cyclohexyl
DFT	density functional theory
DFPT	density functional perturbation theory
DZ	double- $\zeta$
EFG	electric field gradient
Et	ethyl
FID	free induction decay
FISC	field induced superconducting
FISDW	field induced spin density wave
GIAO	gauge including atomic orbital
HF	Hartree-Fock

HETCOR	heteronuclear correlation
HOMO	highest occupied molecular orbital
IGLO	individualized gauge for localized orbitals
<sup>i</sup> Bu	isobutyl
<sup>i</sup> Pr	isopropyl
LUMO	lowest unoccupied molecular orbital
<i>l</i>	liquid
MAS	magic angle spinning
MAE	magic angle effect
Me	methyl
N.A.	natural abundance
NMR	nuclear magnetic resonance
NQR	nuclear quadrupole resonance
NR	non-relativistic
o.d.	outside diameter
PAS	principal axis system
Ph	phenyl
ppm	parts per million
<i>p</i> -Tol	<i>para</i> -tolyl
RACP	ramped-amplitude cross polarization
RH	relative humidity
rf	radiofrequency

SC	superconducting
SDW	spin density wave
SEDOR	spin echo double resonance
SO	scalar with spin-orbit relativistic
SOS	sum over states
SR	scalar relativistic
TMDTDSF	tetramethyldithiadiselenafulvalene
TMTSF	tetramethyltetraselenafulvalene
TMTTF	tetramethyltetrathiafulvalene
TPPM	two-pulse phase-modulated (decoupling)
TTMPSe	tris-2,4,6-trimethoxyphenylphosphine selenide
TZ2P	triple- $\zeta$ doubly polarized
<sup>t</sup> Bu	<i>tert</i> -butyl
VACP	variable amplitude cross polarization
XRD	X-ray diffraction
X <sub>2</sub> TCNQ	2,5-dihalo-tetracyanoquinodimethane
ZORA	zeroth order regular approximation



# Chapter 1

## Introduction and Overview

### 1.1 Introduction

#### 1.1.1 Selenium

Since its initial discovery by Berzelius in 1818, selenium has steadily been incorporated in nearly all areas of chemistry. While the early chemistry involving selenium was predominately inorganic in nature,<sup>1</sup> the development of organoselenium chemistry in the 1970s<sup>2-4</sup> paved the way for many of the studies probing the suspected importance of selenium in biological systems over the next thirty years.<sup>5</sup> With the function of selenium as an essential nutrient in mammalian systems firmly solidified,<sup>6-8</sup> attention has returned to selenium within inorganic systems particularly with regard to materials chemistry.

The protective function of selenium in biology has been associated with numerous diseases including thyroid and reproductive function,<sup>7</sup> heart and cardiovascular diseases,<sup>5,7</sup> as well as cancer.<sup>9,10</sup> Although selenium compounds generally show structural properties similar to those of their sulfur analogues,<sup>11</sup> organoselenium compounds frequently possess unique chemical reactivities and biological activities.<sup>12</sup> Glutathione peroxidase, the first selenoprotein identified in mammals, blocks the formation of peroxides and free radicals both of which are believed to trigger various forms of cancer.<sup>5,8</sup> The discovery that the TGA codon directs the incorporation of selenium has ultimately led to the acceptance of selenocysteine as the 21<sup>st</sup> amino acid.<sup>13,14</sup> Selenocysteine is generally located at the active site of selenoproteins,<sup>7</sup> and a recently

identified selenoprotein family exhibiting a diselenide bond between selenocysteine residues<sup>15</sup> has been highlighted as a potential source of cellular redox regulation.<sup>16</sup>

Selenium is also found in a wide range of materials that have found applications in many industrial fields such as photoelements, in solar technology, in metal coatings, as well as lubricants, and pharmaceuticals.<sup>17</sup> The discovery of electrical conduction within organic quasi one- or two-dimensional charge transfer complexes containing tetraselenafulvalene species led to the first organic superconducting material tetramethyltetraselenafulvalene hexafluorophosphate, (TMTSF)<sub>2</sub>PF<sub>6</sub>.<sup>18,19</sup> Subsequent studies of these materials have ventured to investigate the nature of the conducting phases as well as any transitions into the various ground states expected for these materials including charge and spin density wave, as well as singlet and triplet superconductivity states.<sup>20</sup>

Recently, selenium has witnessed an increasingly important role within nano-scale systems. Selenium has been utilized in the structure of various nanoparticles, nanowires, and nanotubules.<sup>21-29</sup> Applications of selenium in nano systems are known in the preparation of indium and gallium selenide materials,<sup>30-32</sup> selenium incorporation within nanochannels of porous materials,<sup>33,34</sup> in thermoelectric materials,<sup>35,36</sup> as memory devices,<sup>37</sup> and for selenium nanowires themselves,<sup>38,39</sup> as well as their use as templating agents for the formation of nanotubes of other materials.<sup>40,41</sup>

Vitreous systems containing selenium are classified as a member of the chalcogenide glasses and comprise one of two families of non-oxide glasses.<sup>42</sup> These glasses are typically formed with neighboring elements of the periodic table, i.e., phosphorus, germanium, arsenic, tellurium, etc. Modern developments and applications

of chalcogenide glasses have recently been reviewed.<sup>43</sup> These materials are sought after primarily as a result of their unique optical applications in the mid-infrared.<sup>42</sup> For example, P-Se-Al glasses are optical and electronic materials with prospective applications as infrared optical fibers, reversible conductivity switching devices, semiconductors, photoconductors, photo-resists, and solid electrolytes.<sup>44</sup>

### 1.1.2 Nuclear Magnetic Resonance

For physicists, chemists, material scientists, biochemists, and medical researchers, nuclear magnetic resonance, NMR, is one of the most important characterization techniques at their disposal.<sup>45,46</sup> The discovery that the chemical shift and indirect spin-spin coupling interactions were resultant from the local environment of the nucleus being investigated demonstrated the potential of NMR in characterizing a variety of chemical species. As virtually every element in the periodic table possesses an NMR-active isotope, NMR is accessible to essentially any chemical system of interest.

Nuclear magnetic resonance of neat liquids or dilute solutions may be considered the conventional application of NMR due to its widespread use. Rapid molecular tumbling of the chemical species in the liquid phase typically results in averaging of the NMR parameters of interest to their isotropic values. The resulting NMR spectra of liquids are generally composed of narrow and well-defined peaks, which can be readily described by the isotropic chemical shift,  $\delta_{\text{iso}}$ , of each non-equivalent nucleus present in the sample and where applicable the isotropic indirect spin-spin coupling constant,  $J_{\text{iso}}$ , between NMR-active nuclei. In addition, nuclear magnetic relaxation data can yield information on the overall motion of the molecule in solution, as well as modes of motion

within the molecule itself. For all of this available information, NMR of liquids has been utilized in the routine characterization of synthetic products, in the structure determination of complex biomolecules, and in the pursuit of reaction mechanisms and other dynamics in solution. However, nuclear magnetic resonance studies in solution provide only a portion of the information available from NMR in general. The anisotropic NMR interactions hold valuable orientation-dependent information. In addition to the anisotropies of those already mentioned, the chemical shift and indirect spin-spin coupling interactions that are averaged to their scalar isotropic values, the dipolar and quadrupolar interactions are averaged to zero in solution.

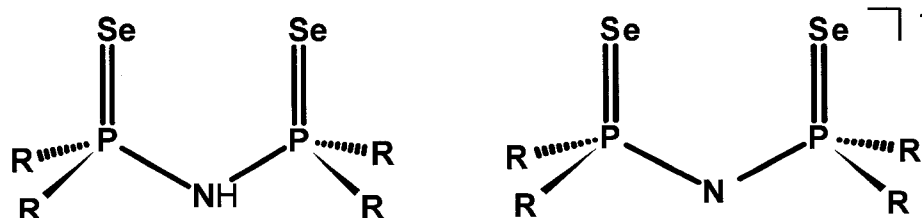
As a result of these additional interactions as well as their anisotropic contributions, solid-state NMR is more complicated than that of solution phases and potentially more informative. The strong anisotropic chemical shift, dipolar, and possibly quadrupolar interactions typically found in NMR of polycrystalline solids generally result in broad, featureless lineshapes. Additionally, nuclear magnetic relaxation times are known to be significantly longer in the solid state, typically an order of magnitude larger or more. The lack of definition in these obtained spectra is of little use for characterization purposes; however, recent developments in methodology provide the experimentalist with the power of discretion over many NMR interactions including their anisotropies. One such approach in modern solid-state NMR that provides high-resolution ‘solution-like’ spectra involves the combination of magic angle spinning, high-power decoupling, and cross polarization, which will be discussed in more detail in Chapter 3.

With the continual improvement of computational power and the development of scientific computing software, the theoretical calculation of NMR parameters has developed into an entirely complementary approach to modern solid-state NMR spectroscopy.<sup>47</sup> The accurate reproduction of experimental NMR values is a good test of the level of theory employed in calculating such second-order properties as the nuclear magnetic shielding and indirect spin-spin coupling interactions. As calculations are performed on predefined structures, either from computational geometry optimizations or via crystal structure determinations, calculated parameters correspond to explicit structural sites and can often be assigned to specific resonances in the experimental spectrum. Additionally, the orientation-dependent interactions are calculated within the frame of reference of the predefined structure, and the relative orientation of the principal axis system of the calculated interaction tensor within the molecular frame is an important piece of information that is not readily extracted from solid-state NMR spectra of polycrystalline solids. These calculated orientations, in the case of nuclear magnetic shielding tensors, have been found to be in good agreement with the corresponding experimentally determined orientations of chemical shift tensors from single-crystal NMR studies.<sup>48</sup>

### 1.1.3 Focus System

In the process of pursuing an increase to the literature available on <sup>77</sup>Se NMR, the majority of the experimental chapters of this thesis are each focused on the solid-state NMR results of a specific compound; iminobis(dialkylphosphine selenide), HN(R<sub>2</sub>PSe)<sub>2</sub>, and the complexes of its mono-anionic bidentate ligand form; tetraalkyldiselenoimido-

diphosphinate,  $[N(R_2PSe)_2]^-$ , Scheme 1.1. In addition to characterizing the NMR parameters from these complexes, by studying this class of compounds, system specific questions, information, and answers are sought.



**Scheme 1.1** Iminobis(dialkylphosphine chalcogenide) and tetraalkyl-diselenoimidodiphosphinato systems.

Tetraalkyldichalcogenoimidodiphosphinato complexes,  $M^{n+}[N(R_2PE)_2]_n$  ( $E = O, S, Se, Te$ ), display variable binding geometries about the metal center that have been shown to depend on the choice of  $E$ ,  $R$ , and  $M$ .<sup>49-53</sup> This flexibility in the dichalcogenoimidodiphosphinate system is one of its greatest advantages, where the EPNPE framework can be tailored to various coordination geometries desired by the central metal.<sup>51,54</sup> The large chalcogen-chalcogen separation or ‘bite’ facilitates regular coordination spheres with large central atoms.<sup>55</sup> Applications of dichalcogenoimidodiphosphinate complexes include single-source precursors for solid-state metal chalcogenide materials, as probes for stereochemically active lone pairs, lanthanide shift reagents, luminescent materials, and enzyme mimetics, as well as catalysts, and selective metal chelating agents.<sup>49-53</sup>

From an NMR standpoint, the iminobis(dialkylphosphine selenide) systems provide a wealth of interactions for investigation. The presence of phosphorus-31,  $I = \frac{1}{2}$ , N.A. 100%, directly bonded to every selenium-77,  $I = \frac{1}{2}$ , N.A. 7.63%, is expressed in

every  $^{77}\text{Se}$  NMR spectrum via indirect spin-spin coupling,  $^1J(^{77}\text{Se}, ^{31}\text{P})_{\text{iso}}$ , for each selenium environment. This indirect spin-spin coupling interaction is also available through the satellite peaks in the corresponding  $^{31}\text{P}$  NMR spectrum. As the two selenium atoms in the tetraalkyldiselenoimidodiphosphate anion are the coordinating atoms within the metal complexes, the selenium chemical shift tensor should provide a sensitive probe to the nature of the complexing metal, as well as the conformation of the six-membered  $\text{MSe}_2\text{P}_2\text{N}$  ring(s) formed. Indirect spin-spin coupling constants between selenium-77 and any NMR-active nuclides of the complexed metal center,  $^1J(\text{M}, ^{77}\text{Se})_{\text{iso}}$ , are accessible from either the  $^{77}\text{Se}$  or metal NMR spectrum. The ability to obtain  $J$ -couplings from either of the NMR-active nuclei makes multinuclear NMR investigations a valuable approach in obtaining, verifying and identifying these  $^{77}\text{Se}$  NMR parameters.

## 1.2 Overview

The principal objective of the research presented in this thesis is to provide an expanded foundation for an improved interpretation of the nuclear magnetic resonance properties of selenium containing chemical systems, particularly chemical shifts and indirect nuclear spin-spin couplings. The goal of this thesis is achieved via experimental and theoretical means through solid-state NMR spectroscopy and density functional theory, DFT, computations. These parameters provide insight into the  $^{77}\text{Se}$  NMR interactions through the comparison of experimental and calculated values with each other and, where possible, in the context of chemical concepts such as molecular geometries and electronic structures.

In Chapter 2 the current literature on solid-state  $^{77}\text{Se}$  NMR spectroscopy is reviewed, placing the research presented in this thesis into context. Chapter 3 details the basic principles, theory and techniques utilized in the conducted research contained in subsequent chapters. The pertinent interactions contained within the selenium-77 NMR Hamiltonian are covered. The experimental procedures permitting the acquisition of high-resolution solid-state  $^{77}\text{Se}$  NMR spectra are presented along with the methods of extracting the desired NMR parameters. Additionally, the theory of nuclear magnetic shielding will be discussed in the context of its computation within a DFT framework. DFT calculations including scalar and spin-orbit relativistic effects via the zeroth order regular approximation, ZORA, are addressed briefly.

Chapter 4 presents a comprehensive investigation of selenium chemical shift tensors. Experimentally determined chemical shift tensors from solid-state  $^{77}\text{Se}$  NMR spectra for several organic, organometallic, and inorganic selenium containing compounds. Selenium magnetic shielding tensors were calculated for all of the molecules investigated using ZORA DFT. The computations provide the orientations of the chemical shift tensors, as well as a test of the theory for calculating the magnetic shielding interaction for heavier elements. The ZORA DFT calculations were performed with non-relativistic, scalar relativistic, and scalar with spin-orbit relativistic levels of theory, and provide a gauge of the level of relativistic theory required to accurately reproduce the experimental trends and values.

A  $^{31}\text{P}$  and  $^{77}\text{Se}$  solid-state NMR investigation of the iminobis(dialkylphosphine chalcogenide)  $\text{HN}(\text{R}_2\text{PE})_2$  ( $\text{R} = \text{}^i\text{Pr}, \text{Ph}; \text{E} = \text{O}, \text{S}, \text{Se}$ ) systems is presented in Chapter 5. The results are related to the known  $\text{HN}(\text{R}_2\text{PE})_2$  structures. Scalar relativistic ZORA



DFT nuclear magnetic shielding tensor calculations were performed yielding the orientations of the corresponding chemical shift tensors.

Chapters 6 and 7 report the results of multinuclear magnetic resonance investigations of the metal(II) complexes of the tetraisopropyldiselenoimido-diphosphate anion,  $M[N(^iPr_2PSe)_2]_2$ . In Chapter 6, a solid-state  $^{31}P$ ,  $^{77}Se$ ,  $^{113}Cd$ , and  $^{199}Hg$  NMR study on the single-source precursors for metal-selenide materials,  $M[N(^iPr_2PSe)_2]_2$  ( $M = Zn, Cd, Hg$ ) is presented. In Chapter 7, a comparison of the square-planar complexes of Group 10 ( $Pd^{II}$ ,  $Pt^{II}$ ) and 16 ( $Se^{II}$ ,  $Te^{II}$ ) centers with  $[N(^iPr_2PSe)_2]^-$  is made based on the results of solid-state  $^{31}P$ ,  $^{77}Se$ ,  $^{125}Te$ , and  $^{195}Pt$  NMR spectroscopy. In both chapters, the experimental results are supported and assisted by discussions of corresponding ZORA DFT computations.

Chapter 8 summarizes the contributions of the research presented in this thesis made to solid-state  $^{77}Se$  NMR spectroscopy. Experimentally determined results are placed in context of the known literature of solid-state  $^{77}Se$  NMR covered in Chapter 2. Important theoretical considerations for the calculation of  $^{77}Se$  NMR parameters are revisited. Finally, system specific information from the multinuclear NMR investigations of the iminobis(dialkylphosphine selenide) systems studied is summarized.

### 1.3 References

- (1) Odom, J. D.; Dawson, W. H.; Ellis, P. D. *J. Am. Chem. Soc.* **1979**, *101*, 5815-5822.
- (2) Clive, D. L. J. *Tetrahedron* **1978**, *34*, 1049-1132.
- (3) Reich, H. J. *Acc. Chem. Res.* **1979**, *12*, 22-30.
- (4) Krief, A. *Tetrahedron* **1980**, *36*, 2531-2640.
- (5) *Chem. Eng. News* **1976**, *24*.
- (6) Oldfield, J. E. *J. Nutr.* **1987**, *117*, 2002-2008.
- (7) Rayman, M. P. *Lancet* **2000**, *356*, 233-241.
- (8) Johansson, L.; Gafvelin, G.; Arnér, E. S. J. *Biochim. Biophys. Acta* **2005**, *1726*, 1-13.
- (9) *Chem. Eng. News* **1977**, *35*.
- (10) Clark, L. C.; Combs Jr, G. F.; Turnbull, B. W.; Slate, E. H.; Chalker, D. K.; Chow, J.; Davis, L. S.; Glover, R. A.; Graham, G. F.; Gross, E. G.; Krongrad, A.; Leshner Jr, J. L.; Park, H. K.; Sanders Jr, B. B.; Smith, C. L.; Taylor, J. R. *J. Am. Med. Assoc.* **1996**, *276*, 1957-1963.
- (11) Pan, W. H.; Fackler, J. P. *J. Am. Chem. Soc.* **1978**, *100*, 5783-5789.
- (12) Iwaoka, M.; Komatsu, H.; Katsuda, T.; Tomoda, S. *J. Am. Chem. Soc.* **2004**, *126*, 5309-5317.
- (13) Böck, A.; Forchhammer, K.; Heider, J.; Leinfelder, W.; Sawers, G.; Veprek, B.; Zinoni, F. *Mol. Microbiol.* **1991**, *5*, 515-520.
- (14) Salzmann, M.; Stocking, E. M.; Silks III, L. A.; Senn, H. *Magn. Reson. Chem.* **1999**, *37*, 672-675.
- (15) Shchedrina, V. A.; Novoselov, S. V.; Malinouski, M. Y.; Gladyshev, V. N. *Proc. Natl. Acad. Sci. U. S. A.* **2007**, *104*, 13919-13924.
- (16) Drahl, C. *Chem. Eng. News* **2007**, *85*, 14.
- (17) Duddeck, H. *Prog. Nucl. Magn. Reson. Spectrosc.* **1995**, *27*, 1-323.

- (18) Bechgaard, K.; Jacobsen, C. S.; Mortensen, K.; Pedersen, H. J.; Thorup, N. *Solid State Commun.* **1980**, *33*, 1119-1125.
- (19) Jerome, D.; Mazaud, A.; Ribault, M.; Bechgaard, K. *J. Physique Lett.* **1980**, *41*, L95-L98.
- (20) Ishiguro, T.; Yamaji, K. *Organic Superconductors*; Springer-Verlag: Berlin, 1990; Vol. 88.
- (21) Krivovichev, S. V.; Kahlenber, V.; Tananaev, I. G.; Kaindl, R.; Mersdorf, E.; Myasoedov, B. F. *J. Am. Chem. Soc.* **2005**, *127*, 1072-1073.
- (22) Nath, M.; Choudhary, A.; Rao, C. N. R. *Chem. Commun.* **2004**, 2698-2699.
- (23) Li, L.; Wu, Q.-S.; Ding, Y.-P. *Nanotechnology* **2004**, *15*, 1877-1881.
- (24) Cho, K. S.; Talapin, D. V.; Gaschler, W.; Murray, C. B. *J. Am. Chem. Soc.* **2005**, *127*, 7140-7147.
- (25) Charvet, N.; Reiss, P.; Roget, A.; Dupuis, A.; Grunwald, D.; Carayon, S.; Chandezon, F.; Livache, T. *J. Mater. Chem.* **2004**, *14*, 2638-2642.
- (26) Sekar, P.; Greyson, E. C.; Barton, J. E.; Odom, T. W. *J. Am. Chem. Soc.* **2005**, *127*, 2054-2055.
- (27) Berrettini, M. G.; Braun, G.; Hu, J. G.; Strouse, G. F. *J. Am. Chem. Soc.* **2004**, *126*, 7063-7070.
- (28) Yochelis, S.; Hodes, G. *Chem. Mat.* **2004**, *16*, 2740-2744.
- (29) Han, L.; Qin, D.; Jiang, X.; Liu, Y.; Wang, L.; J., C.; Cao, Y. *Nanotechnology* **2006**, *17*, 4736-4742.
- (30) Park, K. H.; Jang, K.; Kim, S.; Kim, H. J.; Son, S. U. *J. Am. Chem. Soc.* **2006**, *128*, 14780-14781.
- (31) Tu, H.; Mogyrosi, K.; Kelley, D. F. *Phys. Rev. B: Condens. Matter* **2005**, *72*, 205306:205301-205313.
- (32) Mogyrosi, K.; Kelley, D. F. *J. Phys. Chem. C* **2007**, *111*, 579-585.
- (33) Poborchii, V. V.; Kolobov, A. V.; Oyanagi, H.; Romanov, S. G.; Tanaka, K. *Chem. Phys. Lett.* **1997**, *280*, 10-16.
- (34) Goldbach, A.; Saboungi, M.-L. *Acc. Chem. Res.* **2005**, *38*, 705-712.

- (35) Qiu, X.; Austin, L. N.; Muscarella, P. A.; Dyck, J. S.; Burda, C. *Angew. Chem., Int. Ed. Engl.* **2006**, *45*, 5656-5659.
- (36) Ota, J. R.; Roy, P.; Srivastava, S. K.; Popovitz-Biro, R.; Tenne, R. *Nanotechnology* **2006**, *17*, 1700-1705.
- (37) Milliron, D. J.; Raoux, S.; Shelby, R. M.; Jordan-Sweet, J. *Nat. Mater.* **2007**, *6*, 352-356.
- (38) Li, X.; Li, Y.; Li, S.; Zhou, W.; Chu, H.; Chen, W.; Li, I. L.; Tang, Z. *Cryst. Growth Des.* **2005**, *5*, 911-916.
- (39) Zhang, B.; Ye, X.; Dai, W.; Hou, W.; Zuo, F.; Xie, Y. *Nanotechnology* **2006**, *17*, 385-390.
- (40) Zhang, S.-Y.; Fang, C.-X.; Wei, W.; Jin, B.-K.; Tian, Y.-P.; Shen, Y.-H.; Yang, J.-X.; Gao, H.-W. *J. Phys. Chem. C* **2007**, *111*, 4168-4174.
- (41) Mayers, B.; Jiang, X.; Sunderland, D.; Cattle, B.; Xia, Y. *J. Am. Chem. Soc.* **2003**, *125*, 13364-13365.
- (42) Zhang, X.-H.; Bureau, B.; Adam, J.-L.; Lucas, J. *Verre (Paris, Fr.)* **2004**, *10*, 22-27.
- (43) Bureau, B.; Zhang, X.-H.; Smektala, F.; Adam, J.-L.; Troles, J.; Ma, H.-L.; Boussard-Plédel, C.; Lucas, J.; Lucas, P.; Le Coq, D.; Riley, M. R.; Simmons, J. H. *J. Non-Cryst. Solids* **2004**, *345 & 346*, 276-283.
- (44) Hudalla, C.; Weber, B.; Eckert, H. *J. Non-Cryst. Solids* **1998**, *224*, 69-79.
- (45) Duer, M. J. *Solid-State NMR Spectroscopy: Principles and Applications*; Blackwell Science: Oxford, 2002.
- (46) Levitt, M. H. *Spin Dynamics: Basics of Nuclear Magnetic Resonance*; John Wiley & Sons Ltd.: Chichester, 2001.
- (47) Kaupp, M.; Bühl, M.; Malkin, V. G. *Calculation of NMR and EPR Parameters*; Wiley-VCH Verlag GmbH & Co. KGaA: Weinheim, 2004.
- (48) Tossell, J. A., Ed. *Nuclear Magnetic Shieldings and Molecular Structure*; Kluwer Academic Publishers: Dordrecht, 1993.
- (49) Haiduc, I.; Silaghi-Dumitrescu, I. *Coord. Chem. Rev.* **1986**, *74*, 127-270.
- (50) Woollins, J. D. *Dalton Trans.* **1996**, 2893-2901.

- (51) Silvestru, C.; Drake, J. E. *Coord. Chem. Rev.* **2001**, *223*, 117-216.
- (52) Ly, T. Q.; Woollins, J. D. *Coord. Chem. Rev.* **1998**, *176*, 451-481.
- (53) Bhattacharyya, P.; Woollins, J. D. *Polyhedron* **1995**, *14*, 3367-3388.
- (54) Balazs, L.; Stanga, O.; Breunig, H. J.; Silvestru, C. *Dalton Trans.* **2003**, 2237-2242.
- (55) Darwin, K.; Gilby, L. M.; Hodge, P. R.; Piggott, B. *Polyhedron* **1999**, *18*, 3729-3733.

## Chapter 2

### Solid-State Selenium-77 NMR

#### 2.1 Introduction

##### 2.1.1 Selenium-77 NMR

Selenium-77 is one of the six natural isotopes of selenium and, with a natural abundance of 7.63%, it is the only NMR-active isotope of selenium possessing a nuclear spin quantum number,  $I$ , greater than zero. Early hyperfine measurements suggested that  $^{77}\text{Se}$  possessed a nuclear quadrupole moment,  $I > 1/2$ ;<sup>1</sup> however, in 1951 earlier reports<sup>2,3</sup> were confirmed supporting that  $I = 1/2$  for  $^{77}\text{Se}$ .<sup>4</sup> The resonant frequency of  $^{77}\text{Se}$  relative to that of protons is 19.07%, and has a relative receptivity of  $5.37 \times 10^{-4}$  and 3.15 with respect to hydrogen-1 and carbon-13, respectively.<sup>5</sup> Practical considerations such as longer spin-lattice relaxation times,  $T_1$ , and small observed nuclear Overhauser effects find that  $^{77}\text{Se}$  NMR is typically of comparable sensitivity to  $^{13}\text{C}$  NMR.<sup>6</sup>

Nuclear magnetic resonance has been utilized to investigate essentially every area of selenium chemistry. Selenium-77 NMR is an ideal technique for investigating selenium-containing materials as the  $^{77}\text{Se}$  chemical shift ranges over 3000 ppm<sup>6,7</sup> and is extremely sensitive to changes in molecular structure. Selenium-77 NMR in the solution phase has been thoroughly reviewed,<sup>6-12</sup> where it has been used in studies of molecular dynamics and chemical reactions in addition to molecular characterization. In 1986, Luthra and Odom originally compiled the growing  $^{77}\text{Se}$  NMR data on organoselenium compounds.<sup>9</sup> In 1995, Duddeck's comprehensive review expanded the values of  $^{77}\text{Se}$  NMR parameters for organic selenium systems to include inorganic species and metal

complexes.<sup>6</sup> In 2004, Dudgeon provided an update of his 1995 review of liquid-state <sup>77</sup>Se NMR spectroscopy.<sup>7</sup>

### 2.1.2 Solid-State <sup>77</sup>Se NMR

Solid-state <sup>77</sup>Se NMR spectroscopy provides isotropic chemical shift,  $\delta_{iso}$ , indirect spin-spin coupling constants,  $J_{iso}$ , as well as spin-lattice,  $T_1$ , and spin-spin,  $T_2$ , relaxation times. Particularly important is that solid-state <sup>77</sup>Se NMR provides access to anisotropic interactions that are generally inaccessible from solution NMR studies. The most commonly encountered anisotropic parameter in NMR is the chemical shift. There are a number of conventions for describing this anisotropy, all of which utilize the isotropic average of the principal components,  $\delta_{ii}$ , of the chemical shift tensor:

$$\delta_{iso} = \frac{1}{3}(\delta_{11} + \delta_{22} + \delta_{33}) \quad [2.1]$$

which is often used in comparison with chemical shifts obtained in solution. Haeberlen's notation defines the anisotropy,  $\Delta\sigma$ , and asymmetry,  $\eta_\sigma$ , as:

$$\Delta\sigma = \delta_{zz} - \frac{1}{2}(\delta_{xx} + \delta_{yy}) \quad [2.2]$$

$$\eta_\sigma = \frac{3}{2} \frac{(\delta_{yy} - \delta_{zz})}{\Delta\sigma} \quad [2.3]$$

where  $|\delta_{zz} - \delta_{iso}| \geq |\delta_{xx} - \delta_{iso}| \geq |\delta_{yy} - \delta_{iso}|$ .<sup>13</sup> The so-called Maryland notation replaces the anisotropy and asymmetry with the span,  $\Omega$ , and skew,  $\kappa$ :

$$\Omega = \delta_{11} - \delta_{33} \quad [2.4]$$

$$\kappa = 3 \frac{(\delta_{22} - \delta_{iso})}{\Omega} \quad [2.5]$$

where  $\delta_{11} \geq \delta_{22} \geq \delta_{33}$ .<sup>14</sup> Orientation dependencies also exist for direct dipolar and indirect spin-spin coupling interactions, which can be utilized to orient the principal axes of the various interaction tensors ( $\delta_{ii}$ ,  $J_{ii}$ , etc.) with the dipolar Se-X vector and potentially within the crystal axis frame.

In contrast to the well reviewed literature on <sup>77</sup>Se NMR in solution phases, a similarly comprehensive solid-state <sup>77</sup>Se NMR review is lacking. General <sup>77</sup>Se NMR reviews have covered solid-state <sup>77</sup>Se NMR reasonably well; however, the data is typically compiled as a lump sum of the results of the technique rather than organized by functionality as with the results of the solution <sup>77</sup>Se NMR data.<sup>6,7,10</sup> The specifically solid-state <sup>77</sup>Se NMR reviews that have appeared focus almost entirely on diamagnetic systems,<sup>15</sup> and some on only selected diamagnetic organoselenium compounds.<sup>16-18</sup>

### 2.1.3 Structure

A compilation of the literature on solid-state <sup>77</sup>Se NMR investigations to the end of 2007 is presented, with select publications from 2008. Every effort has been made to provide as complete a review as possible; however, some accounts have no doubt been missed despite these efforts. The review has been structured as follows, beginning with the solid-state <sup>77</sup>Se NMR data for elemental selenium, followed by sections on selenes



(X=Se double bonded systems), bridging selenium environments, inorganic selenium systems, and finally miscellaneous molecular structures containing selenium.

Following recent IUPAC recommendations<sup>19</sup> the three principal components of the available selenium chemical shift tensors have been tabulated, where necessary deriving them from the reported values of  $\Delta\sigma$  and  $\eta_\sigma$ , or  $\Omega$  and  $\kappa$ . However, as many authors have utilized the anisotropy and asymmetry convention of Haeberlen or the span and skew of the Maryland convention in discussions of the respective chemical shift tensors reported, in some cases their use has been retained in the body of this review. All chemical shifts have been reported with respect to dimethyl selenide. As numerous reference compounds have been utilized for reporting selenium chemical shifts, the values of  $\delta_{\text{iso}}$  used to convert the reported chemical shifts to those with respect to a neat liquid of dimethyl selenide are given in Table 2.1. Given the noted medium dependence of the selenium chemical shift,<sup>6</sup> all principal components,  $\delta_{ii}$ , as well as isotropic chemical shifts,  $\delta_{\text{iso}}$ , are reported to the nearest whole number in parts per million, ppm. This level of accuracy seems appropriate given that the selenium chemical shift range is approximately ten times that of  $^{13}\text{C}$ , whose chemical shifts are typically reported to one decimal place ( $\pm 0.1$  ppm),<sup>6</sup> and at least three times that of the lighter chalcogens  $^{17}\text{O}$  and  $^{33}\text{S}$ .<sup>20</sup>

Indirect spin-spin coupling constants,  $^1J(^{77}\text{Se}, \text{X})_{\text{iso}}$ , have been reported only in the cases where they have been obtained directly from solid-state  $^{77}\text{Se}$  NMR spectroscopy. The signs of  $^1J(^{77}\text{Se}, ^{31}\text{P})_{\text{iso}}$ <sup>21,22</sup> and  $^1J(^{199}\text{Hg}, ^{77}\text{Se})_{\text{iso}}$ <sup>23</sup> are known to be negative, and have been reported as such herein, even if they were not in the source from which they were taken.

**Table 2.1** Isotropic selenium chemical shifts of various  $^{77}\text{Se}$  NMR reference compounds.

Compound	Condition	$\delta_{\text{iso}}$
CdSe	solid	-492
Ph <sub>3</sub> PSe	chloroform	-275
Me <sub>2</sub> Se	neat	0
H <sub>2</sub> SeO <sub>4</sub>	aqueous	1001
Na <sub>2</sub> SeO <sub>3</sub>	aqueous (inf. dilute)	1253
(NH <sub>4</sub> ) <sub>2</sub> SeO <sub>4</sub>	solid	1040
H <sub>2</sub> SeO <sub>3</sub>	aqueous	1282
H <sub>2</sub> SeO <sub>3</sub>	saturated	1300

Theoretical calculation of magnetic shielding tensors,  $\sigma$ , are one of the most complementary techniques to solid-state NMR because of their connection with the experimental chemical shift tensors through the relationship

$$\delta_{ii}(\text{sample}) = \frac{\sigma_{\text{iso}}(\text{ref}) - \sigma_{ii}(\text{sample})}{1 - \sigma_{\text{iso}}(\text{ref})} \quad [2.6]$$

where  $\sigma_{\text{iso}}(\text{ref})$  is the isotropic shielding of a standard reference, here Me<sub>2</sub>Se ( $\ell$ ).

Numerous investigations of calculated selenium magnetic shielding and/or chemical shift tensors have been reported.<sup>24-31</sup> Additionally, recent theoretical computations of indirect spin-spin coupling constants involving selenium have appeared in the literature.<sup>32-34</sup> The interested reader is encouraged to pursue these references for a more detailed description of the intricacies of calculating  $^{77}\text{Se}$  NMR parameters. For the purposes of this review, only the theoretical parameters obtained in conjunction with experimental solid-state  $^{77}\text{Se}$  NMR values will be discussed in relation to the performance of the computations.

## 2.2 Solid-State $^{77}\text{Se}$ NMR

### 2.2.1 Selenium

The structure of crystalline selenium is known to possess helical chains of selenium that are oriented in a hexagonal arrangement.<sup>35</sup> Solid-state NMR investigations of elemental selenium have demonstrated the sensitivity of  $^{77}\text{Se}$  chemical shifts to minor changes in the local environment since the initial investigation of a single crystal of trigonal selenium at 77 K. This study indicated that the most shielded principal component lies nearly parallel to the direction of the helices.<sup>35-37</sup> Subsequent variable temperature experiments up to 480 K have demonstrated a general decrease in selenium shielding with increasing temperature for crystalline selenium, see Table 2.2.<sup>38-40</sup> Self-diffusion within crystalline selenium has been monitored by spin-lattice relaxation rates between 350 K and 492 K.<sup>41</sup> Additional studies of elemental selenium by solid-state NMR have been noted in conjunction with investigations of various inorganic selenides and are in agreement with the values from the above single-crystal measurements.<sup>42-44</sup>

Selenium is also known to exist in a vitreous form which consists primarily of selenium chains and  $\text{Se}_6$  rings.<sup>45</sup> The solid-state  $^{77}\text{Se}$  NMR spin-lattice relaxation of glassy selenium has been investigated in the temperature range  $200\text{ K} < T < 275\text{ K}$ , and reported that the relaxation found was dominated by paramagnetic impurities.<sup>46</sup> The  $^{77}\text{Se}$  NMR spectra of crystalline and glassy selenium have been contrasted.<sup>45,47,48</sup> The results of Bureau and coworkers,<sup>45,48</sup> along with those of Gopal and Milne,<sup>49</sup> show that the vitreous structure of glassy selenium is demonstrated with a substantially broader isotropic line width, 17 kHz at  $B_0 = 7.0\text{ T}$ .

**Table 2.2** Solid-state  $^{77}\text{Se}$  NMR chemical shifts and chemical shift tensors for elemental selenium.

Compound	T / K	$\delta_{\text{iso}}$	$\delta_{11}$	$\delta_{22}$	$\delta_{33}$	Reference
Se	77	666	896	694	408	35
	290	772	1006	797	513	38
	RT	792	1017	817	542	39
	RT	800	1025	825	550	40
	RT	793				50
	480	812	1033	844	558	38
Vitreous Se		862				45
		865				48,49
Se in orthorhombic I <sub>2</sub> (51 atom% Se)		808	1055	834	535	49
15 wt% Se in AlPO <sub>4</sub> -5		849				50
34 wt% Se in zeolite Y		712, 812, 1139				50
Rb <sub>2</sub> [Pd(Se <sub>4</sub> ) <sub>2</sub> ] $\cdot$ Se <sub>8</sub>		627	958	686	237	51
		652	1023	731	202	

Elemental selenium has also been characterized within various structures by solid-state  $^{77}\text{Se}$  NMR. Parise et al. have loaded selenium into the porous frameworks of the aluminophosphate AlPO<sub>4</sub>-5 and within zeolite Y.<sup>50</sup> When AlPO<sub>4</sub>-5 was loaded with 15% selenium by weight, a  $^{77}\text{Se}$  MAS NMR signal at 849 ppm showed significantly less chemical shift anisotropy than found in trigonal selenium.<sup>50</sup> Three  $^{77}\text{Se}$  NMR peaks were detected for 34 wt % selenium in zeolite Y; however, only two of the signals one at 712 ppm and the other at 824 ppm are attributed to elemental selenium. The peak at 1139 ppm was assigned to an oxidized selenium species.<sup>50</sup> Iodine is known to assist in the crystallization of selenium,<sup>52</sup> and Gopal and Milne have detected crystalline Se within orthorhombic iodine at the eutectic composition of 51 atom % Se:I<sub>2</sub> by solid-state  $^{77}\text{Se}$  NMR.<sup>49</sup> The Se<sub>8</sub> rings within Rb<sub>2</sub>[Pd(Se<sub>4</sub>)<sub>2</sub>] $\cdot$ Se<sub>8</sub> form infinite [Rb(Se<sub>8</sub>)<sub>x</sub>]<sup>x+</sup> columns

perpendicular to the  $[\text{Pd}(\text{Se}_4)_2]_x^{2x-}$  planes.<sup>51</sup> The selenium nuclei within the  $\text{Se}_8$  rings are more shielded than the above selenium species likely due to their interaction with  $\text{Rb}^+$ .<sup>51</sup>

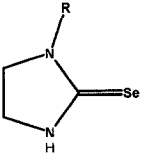
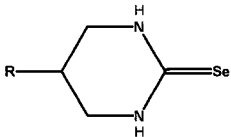
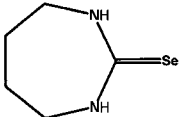
## 2.2.2 Selones

### 2.2.2.1 Seleno-Carbonyls

Of the seleno-carbonyl moieties,  $\text{C}=\text{Se}$ , one of the simplest are the ambidentate selenocyanate ligands,  $\text{SeCN}^-$ . In the solid state, the  $\text{SeCN}^-$  anion yields  $^{77}\text{Se}$  NMR powder patterns that are axially symmetric or near axially symmetric, consistent with the known linear structure of this anion. Selenium chemical shift parameters found for  $\text{ASeCN}$  ( $\text{A} = \text{K}^+, \text{NH}_4^+, \text{NMe}_4^+$ ), whose spans range from 804 – 874 ppm, which are reproduced in Table 2.3.<sup>53</sup> Ab initio calculations of the selenium chemical shift tensor for  $\text{SeCN}^-$ , at the Hartree-Fock and Møller-Plesset second-order perturbation levels, on an optimized structure yield qualitative agreement with the experimentally observed values.<sup>53</sup>

Solid-state  $^{77}\text{Se}$  NMR studies of additional seleno-carbonyl systems have, to date, focused on various derivatives functionally similar to selenourea,  $\text{Se}=\text{C}(\text{NH}_2)_2$ . Selenourea itself possesses nine non-equivalent molecules within the unit cell and the weighted average of the obtained selenium chemical shift tensors, given in Table 2.3, are reduced to the single peak at 177 ppm within the camphor inclusion compound of selenourea.<sup>54</sup> The *N,N*-dimethyl derivative,  $\text{Se}=\text{C}(\text{NH}_2)(\text{NMe}_2)$ , possesses only a single *N,N*-dimethyl selenourea molecule within the crystal structure asymmetric unit as evident by the single selenium chemical shift tensor reported.<sup>55</sup> Wazeer and coworkers have studied a variety of additional derivatives of selenourea by solid-state  $^{77}\text{Se}$  NMR.<sup>56</sup>

**Table 2.3** Solid-state  $^{77}\text{Se}$  chemical shifts and chemical shift tensors for seleno-carbonyl systems.<sup>a)</sup>

Compound	$\delta_{\text{iso}}$	$\delta_{11}$	$\delta_{22}$	$\delta_{33}$	Reference	
KSeCN	-283	25	-23	-849	53	
$\text{NH}_4\text{SeCN}$	-256	26	-15	-778	53	
$[\text{NMe}_4]\text{SeCN}$	-299	-40	-40	-814	53	
$(\text{NH}_2)_2\text{CSe}_{\text{avg}}^{\text{b)}}$	180	480	410	-349	54	
$(\text{NMe}_2)(\text{NH}_2)\text{CSe}$	213	501	260	-122	55	
	R = H	60	725	57	-604	56
	R = Me	69	471	-52	-213	56
	R = Et	72	445	-19	-210	56
	R = <sup>n</sup> Pr	31	427	-50	-284	56
		56	442	-40	-233	
	R = <sup>i</sup> Pr	57	451	-55	-225	56
	R = H	173	541	390	-412	56
	R = OH	169	496	430	-424	56
	43	601	465	-938	56	

<sup>a)</sup> Experimental temperature either room temperature or was not specified.

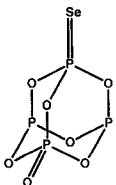
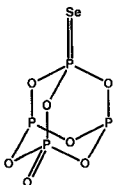
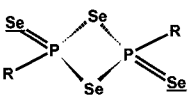
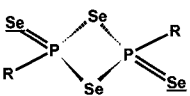
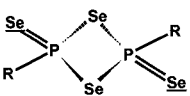
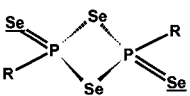
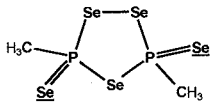
<sup>b)</sup> Weighted average of values from nine non-equivalent selenourea molecules.

The selenium chemical shift tensors of the functionalized imidazolidine-2-selones and 1,3-diazinane-2-selones as well as 1,3-diazepine-2-selone, shown in Figures 2.1a-c, serve as a good example of the sensitivity of the magnetic shielding interaction to peripheral modifications of a structural framework.<sup>56</sup>

### 2.2.2.2 Phosphine Selones

Phosphine selones are another functional group that have been used to investigate the local environment of selenium by solid-state  $^{77}\text{Se}$  NMR. As shown in Tables 2.4 and

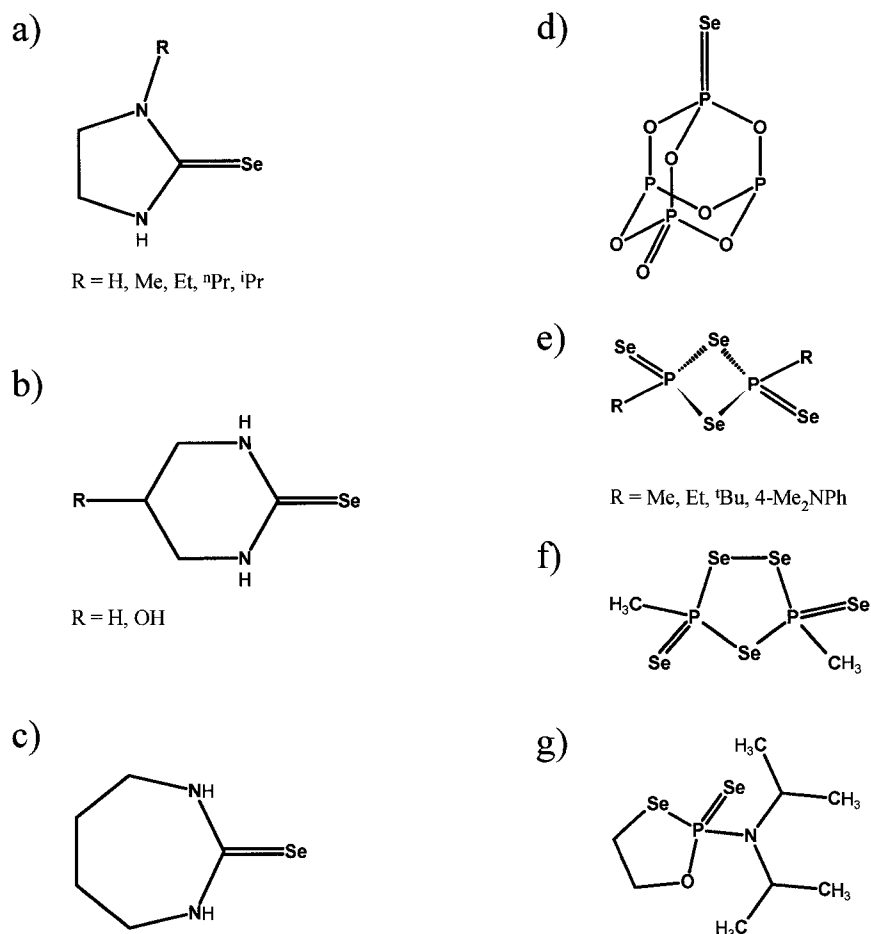
**Table 2.4** Solid-state  $^{77}\text{Se}$  chemical shifts and chemical shift tensors for phosphine selone systems.<sup>a)</sup>

Compound	$\delta_{\text{iso}}$	$\delta_{11}$	$\delta_{22}$	$\delta_{33}$	Reference
$\text{Me}_3\text{PSe}$	-200	-118	-133	-349	57
$\text{Ph}_3\text{PSe}$	-258	-122	-288	-362	57
	-243	-86	-264	-377	
	-144				58
 R = Me	312				59
 R = Et	266				59
 R = <sup>t</sup> Bu	128				59
 R = 4-Me <sub>2</sub> NPh	196				59
	161, 131				59

<sup>a)</sup> Experimental temperature either room temperature or was not specified.

2.5, the isotropic selenium chemical shifts and indirect one-bond selenium-phosphorus coupling constants,  $^1J(^{77}\text{Se}, ^{31}\text{P})_{\text{iso}}$ , in phosphine selone systems vary from -258 ppm to 312 ppm, and -656 to -1160 Hz, respectively. Grossman and coworkers have investigated the anisotropic chemical shift and indirect spin-spin coupling interactions in 70%  $^{77}\text{Se}$  enriched trimethyl- and triphenyl-phosphine selone.<sup>57</sup> For,  $\text{Me}_3\text{PSe}$ , experiments provide a mean value of the anisotropy of the phosphorus-selenium  $J$  tensor of  $\text{Me}_3\text{PSe}$ ,  $\Delta J \sim +650 \pm 200$  Hz. The experimental value is in good agreement with the value calculated, +705 Hz, using DFT.<sup>57</sup>

Solid-state  $^{77}\text{Se}$  NMR has also been utilized in the characterization of several other P=Se systems, yielding both isotropic chemical shifts and values of  $^1J(^{77}\text{Se}, ^{31}\text{P})_{\text{iso}}$ .

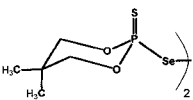
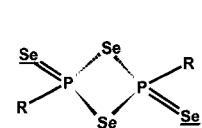
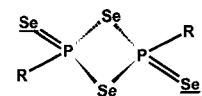
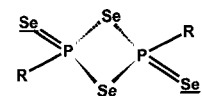
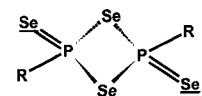
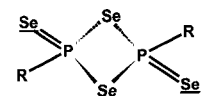
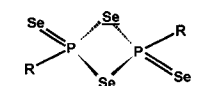
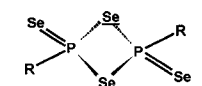
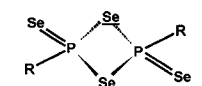
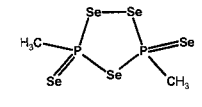
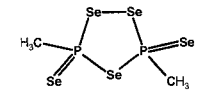
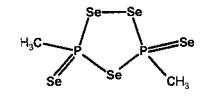
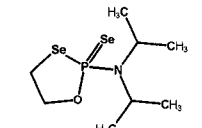
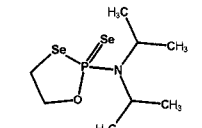



**Figure 2.1** a) imidazolidine-2-selones, b) 1,3-diazinane-2-selones, c) 1,3-diazepine-2-selone, d) tetraphosphorus heptaoxide monoselenide, e) 1,3-diselena-2,4-diphosphetane-2,4-diselones, f) 3,5-dimethyl-1,2,4-triselena-3,5-diphospholane-3,5-diselone, and g) 2-*N,N*-diisopropylamino-1,3,2 $\lambda^5$ -oxaselenaphospholane-2-selone are representative of the seleno-carbonyls (a-c) and phosphine selenes (d-g) that have been studied by solid-state  $^{77}\text{Se}$  NMR.

The inorganic adamantane-like structure of tetraphosphorus heptaoxide monoselenide,  $\text{P}_4\text{O}_7\text{Se}$ , Figure 2.1d, with  $\delta_{\text{iso}} = -144$  ppm, has the largest value of  $^1J(^{77}\text{Se}, ^{31}\text{P})_{\text{iso}}$  recorded by solid-state  $^{77}\text{Se}$  NMR, at -1160 Hz.<sup>58</sup> The magnitudes of the selenium-phosphorus coupling constants were utilized in the structural characterizations of the 1,3-diselena-



**Table 2.5** Indirect spin-spin coupling constants,  ${}^nJ({}^{77}\text{Se}, {}^m\text{X})_{\text{iso}}$  ( $m < 77$ ).<sup>a)</sup>

Compound	${}^m\text{X}(n)$	${}^nJ({}^{77}\text{Se}, \text{X})_{\text{iso}} / \text{Hz}$	References
$\text{Ag}_7\text{PSe}_6$	${}^{31}\text{P}(1)$	-430, -524	60,61
$\text{Me}_3\text{PSe}$	${}^{31}\text{P}(1)$	-656	57
$\text{Ph}_3\text{PSe}$	${}^{31}\text{P}(1)$	-733, -736	57
$[({}^i\text{Bu})(\text{Ph})\text{P}(\text{S})\text{Se}]_2$	${}^{31}\text{P}(1)$	-355	62
$[({}^i\text{PrO})_2\text{P}(\text{S})\text{Se}]_2$	${}^{31}\text{P}(1)$	-532	63
$[(\text{Me}_3\text{CCH}_2\text{O})_2\text{P}(\text{S})\text{Se}]_2$	${}^{31}\text{P}(1)$	-469, -486	64
	${}^{31}\text{P}(1)$	-418, -429	65
 · $\text{C}_6\text{H}_6$ solvate	${}^{31}\text{P}(1)$	-458, -406	65
 R = Me	${}^{31}\text{P}(1)$	-730	59
 R = Et	${}^{31}\text{P}(1)$	-730	59
 R = ${}^i\text{Bu}$	${}^{31}\text{P}(1)$	-780	59
 R = 4-Me <sub>2</sub> NPh	${}^{31}\text{P}(1)$	-700	59
 R = Me	${}^{31}\text{P}(1)$	-260	59
 R = Et	${}^{31}\text{P}(1)$	-260	59
 R = ${}^i\text{Bu}$	${}^{31}\text{P}(1)$	-260	59
 P=Se	${}^{31}\text{P}(1)$	-730, -750	59
 P-Se-P		-420	
 P-Se-Se		-340, -350	
 P=Se	${}^{31}\text{P}(1)$	-870, -892	66
 P-Se-C		-393, -465	
	${}^{31}\text{P}(1)$	-1160 Hz	58

<sup>a)</sup> Experimental temperature either room temperature or was not specified.

2,4-diphosphetane-2,4-diselones and in 3,5-dimethyl-1,2,4-triseleno-3,5-diphospholane-3,5-diselone, Figures 2.1e and 2.1f, which were able to easily differentiate the P=Se moieties,  ${}^1J({}^{77}\text{Se}, {}^{31}\text{P})_{\text{iso}} < -700 \text{ Hz}$ , from the bridging Se environments,  ${}^1J({}^{77}\text{Se}, {}^{31}\text{P})_{\text{iso}} > -350 \text{ Hz}$ , see Table 2.5.<sup>59</sup> Similarly for 2-N,N-diisopropylamino-1,3,2λ<sup>5</sup>-

oxaselenaphospholane-2-selone, Figure 2.1g, Potrzebowski et al. have differentiated the bridging C-Se-P moiety from the P=Se selenium environment using  $^{77}\text{Se}$  CP MAS spectra of based upon the magnitudes of the selenium-phosphorus coupling constants.<sup>66</sup>

### 2.2.3 Bridging Selenium Systems

Bridging selenium environments are one of the most common moieties found in selenium containing systems. Hydrogen selenide, the simplest bridging selenium system, undergoes two solid-solid phase transitions where the two highest temperature phases, solid I and II, are cubic and the low temperature phase, solid III, is non-cubic. A solid-state  $^{77}\text{Se}$  NMR study of  $\text{H}_2\text{Se}$  has yielded spin-lattice relaxation data over the entire solid I phase temperature range, the temperature dependence of the  $^{77}\text{Se}$  chemical shift for the solid I and II phases, and the traceless selenium shielding tensor in the solid III phase.<sup>67</sup> A large deuterium isotope shift in  $\delta_{\text{iso}}(\text{Se})$  of 7 ppm per deuterium from  $\text{H}_2\text{Se} \rightarrow \text{HDSe} \rightarrow \text{D}_2\text{Se}$  was also observed in the solid I phase.<sup>67</sup> Solid-state  $^{77}\text{Se}$  NMR investigations of  $\text{H}_2\text{Se}$  and  $\text{D}_2\text{Se}$  inclusion compounds found that hydrogen selenide is deshielded by approximately 30 ppm in the small cage, with respect to the large cage, of the structure I clathrate hydrate.<sup>68,69</sup>

The subsection that follows has been organized in order to review the contributions to solid-state  $^{77}\text{Se}$  NMR made on systems where selenium bridges two organic centers; i.e., those containing C-Se-C linkages. Discussion of the solid-state  $^{77}\text{Se}$  NMR investigations of selenium bridging organic and inorganic or two inorganic atoms follow.

### 2.2.3.1 Bridging Organic Centers

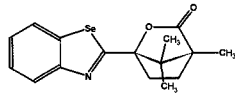

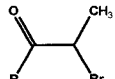
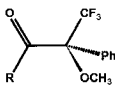
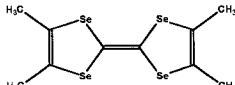
#### 2.2.3.1.1 Selenoethers

Dimethyl selenide, as the primary reference for selenium chemical shifts, holds a position of interest in solid-state  $^{77}\text{Se}$  NMR. The selenium chemical shift tensor for  $\text{Me}_2\text{Se}$ , the simplest of selenoethers, has been characterized at 77 K by Collins, Ratcliffe and Ripmeester, and is reproduced in Table 2.6.<sup>54</sup>

Selenoethers of biological relevance, such as the seleno-amino acid selenomethionine, have become an important class of selenium containing biomolecules since the recognition of selenium as an essential nutrient in mammalian systems.<sup>70</sup> Selenomethionine with selenocysteine, amino acids where sulfur has been replaced with selenium, are the primary sources of selenium in the human body.<sup>71</sup> Potrzebowski and coworkers have characterized the selenium chemical shift tensors in the L- and DL-forms of selenomethionine.<sup>72,73</sup> The slowing of the rotation of the methyl group in L-selenomethionine was shown to have a large influence on the selenium chemical shift tensor at low temperature.<sup>72</sup> Gajda et al. have also calculated the selenium chemical shift tensor in L-selenomethionine using DFT, demonstrating rough agreement with the experimental principal components and that the orientation of  $\delta_{22}$  lies perpendicular to the local  $\text{C}^\delta\text{-Se-C}^\gamma$  plane, and that  $\delta_{11}$  and  $\delta_{33}$  are coincident within this local plane.<sup>72</sup>

Selenium analogues of the crown ethers, the polyselenoethers or selenium coronands, show intriguing natural and host-guest conformations. Isotropic  $^{77}\text{Se}$  chemical shifts measured by solid-state NMR in coronands ranging from 1,5,9-triselenacyclododecane,  $12\text{Se}_3$ , to 1,5,9,13,17,21-hexaselenacyclotetracosane,  $24\text{Se}_6$ , see Figure 2.2, cover between 113 ppm and 327 ppm.<sup>74-77</sup> Through electrochemical

**Table 2.6** Solid-state  $^{77}\text{Se}$  chemical shifts and chemical shift tensors for selenium bridging organic centers.

Compound	T / K	$\delta_{\text{iso}}$	$\delta_{11}$	$\delta_{22}$	$\delta_{33}$	Reference
$\text{Me}_2\text{Se}$	77	6.7	226	141	-347	54
L-Selenomethionine	183	123	388	178	-197	72
		73	339	154	-276	
	297	123	384	181	-196	72,73
		84	311	179	-237	
	313	108	252	204	131	73
DL-Selenomethionine	297	112	369	202	-236	73
	333	114	360	205	-223	73
$[\text{8Se2}][\text{SO}_2\text{CF}_3]_2$		810	1066	1066	300	77
		768	1005	1005	292	
$12\text{Se}3^{\text{a})}$		206, 300				77
$12\text{Se}4^{\text{a})}$		130, 171, 186, 196, 203, 209				74,76
$14\text{Se}4^{\text{a})}$		220, 225				76
$16\text{Se}2\text{S}2^{\text{a})}$		136, 179, 199				77
$16\text{Se}4^{\text{a})}$		115, 118, 157, 165, 177				76
$16\text{Se}4(\text{OH})^{\text{a})}$		167	299	132	70	77
		131	264	83	47	
$16\text{Se}4(\text{OH})_2^{\text{a})}$		113, 134, 145, 155, 192				77
$[\text{16Se4}][\text{SO}_3\text{CF}_3]_2^{\text{a})}$		173, 420, 505, 737				78,79
$18\text{Se}6^{\text{a})}$		136, 188, 206, 264, 327				75,76
$24\text{Se}6^{\text{a})}$		158, 174, 194				76
		408	749	410	64	80
R = H		536	917	454	236	80
		529	915	413	259	
		591	942	443	388	80
		624	999	451	423	80
		586	956	463	340	
		600	1007	472	321	80
	RT	658	970	818	186	54
		670	982	830	198	

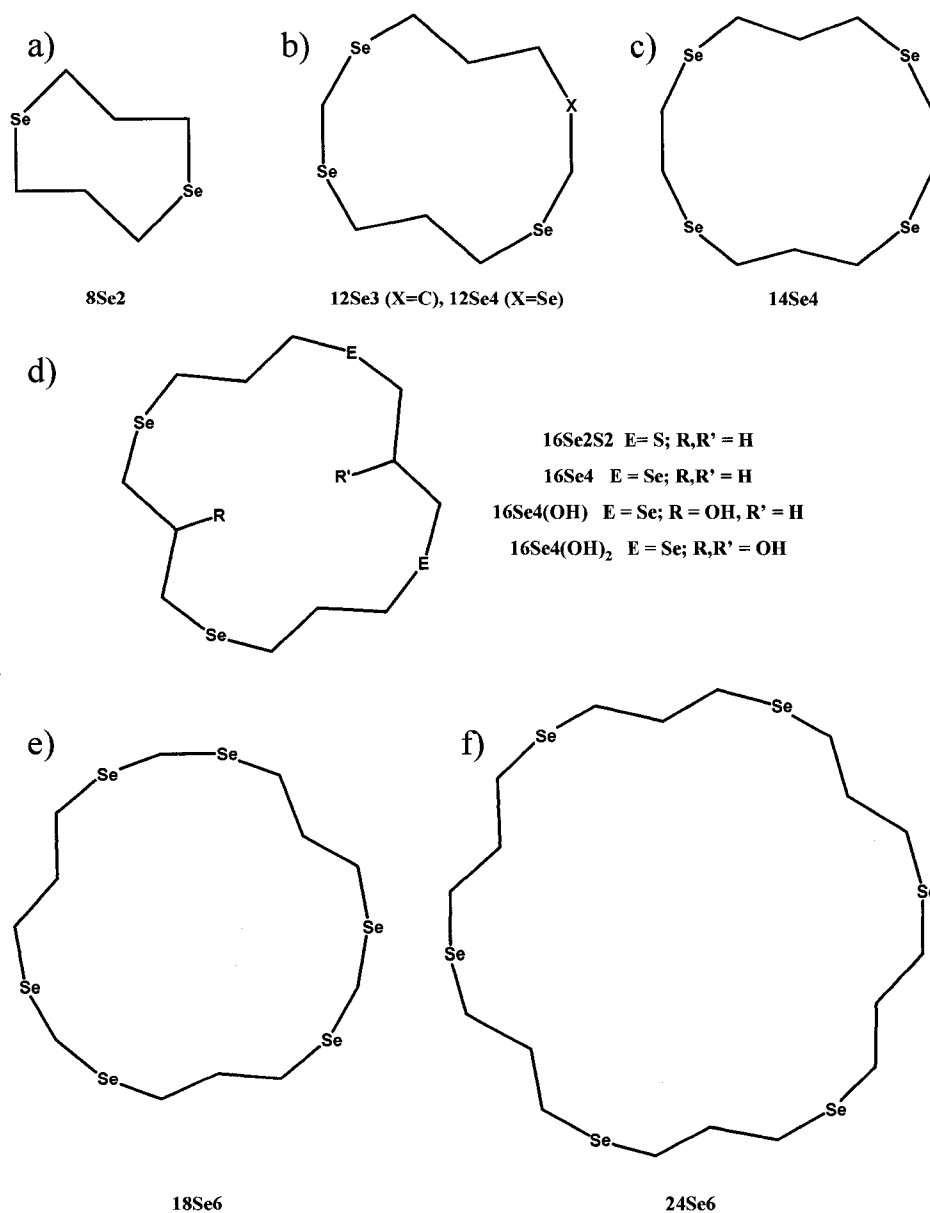
<sup>a)</sup> See Figure 2.2.

oxidation of 1,5,9,13-tetraselenahexadecane,  $16\text{Se}_4$ , the complex  $[16\text{Se}_4][\text{SO}_3\text{CF}_3]_2$  is afforded yielding four very different peaks at 173, 420, 505, and 737 ppm in the  $^{77}\text{Se}$  NMR spectrum,<sup>78,79</sup> which have been assigned to the four unique selenium atoms in the asymmetric unit based on estimated contributions to the  $^{77}\text{Se}$  line width from Se-F dipolar couplings.<sup>79</sup> To date, only two selenium chemical shift tensors involving selenium coronands, those for 1,5,9,13-tetraselenacyclohexadecan-3-ol,  $16\text{Se}_4(\text{OH})$ , have been completely characterized.<sup>77</sup>

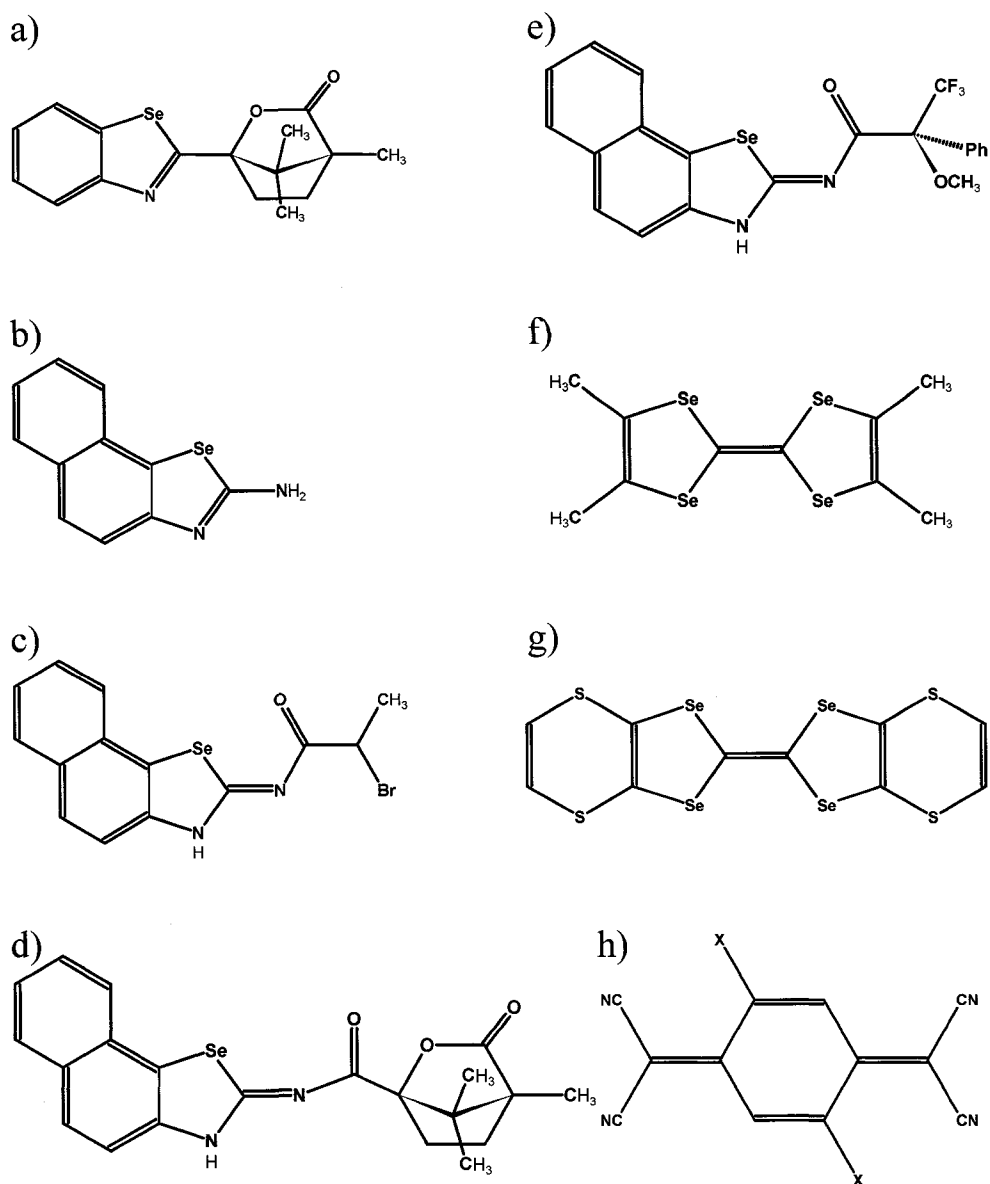
Carbon-selenium-carbon functionalities also occur within more rigid, including aromatic, structures. The selenium chemical shift tensors from solid-state  $^{77}\text{Se}$  NMR for some selenazole and selenazoline derivatives coupled with chiral moieties, Figures 2.3a-e, have been compared with their corresponding solution NMR values, where observed differences are discussed with respect to conformational variations.<sup>80</sup> Another selenoether within a rigid framework that has been studied by solid-state  $^{77}\text{Se}$  NMR is tetramethyltetraselenafulvalene, TMTSF Figure 2.3f, which is a precursor for some of the organic conducting and superconducting materials that will be discussed in the following section. The two similar selenium chemical shift tensors for the neutral TMTSF molecule in the solid state have been characterized at room temperature and are reproduced in Table 2.6.<sup>54</sup>

#### 2.2.3.1.2 Organic Conductors

Electrical conductivity in organic systems has illuminated the influence of molecular structure on organic conductivity and superconductivity.<sup>81</sup> Since their initial description,<sup>82</sup> these so-called Bechgaard salts;  $(\text{TMTSF})_2\text{X}$ , where X is a mono-valent



**Figure 2.2** The selenium coronands that have been studied by solid-state  $^{77}\text{Se}$  NMR: a) 1,5-diselenacyclooctane ( $8\text{Se}_2$ ), b) 1,5,9-triselenacyclododecane ( $12\text{Se}_3$ ) and 1,3,7,9-tetraselenacyclododecane ( $12\text{Se}_4$ ), c) 1,4,8,11-tetraselenacyclotetradecane ( $14\text{Se}_4$ ), d) 1,5-diselena-9,13-dithiacyclohexadecane ( $16\text{Se}_2\text{S}_2$ ), 1,5,9,13-tetraselenacyclohexadecane ( $16\text{Se}_4$ ), 1,5,9,13-tetraselenacyclohexadecane-3-ol ( $16\text{Se}_4(\text{OH})$ ), 1,5,9,13-tetraselenacyclohexadecane-3,11-diol ( $16\text{Se}_4(\text{OH})_2$ ), e) 1,3,7,9,13,15-hexaselenacyclooctadecane ( $18\text{Se}_6$ ), and f) 1,5,9,13,17,21-hexaselenacyclotetracosane ( $24\text{Se}_6$ ).



**Figure 2.3** Structurally rigid selenoethers that have been studied by solid-state  $^{77}\text{Se}$  NMR: selenazoles (a,b), selenazolines (c-e), and tetraselenafulvalenes (f,g). Also given, in h), is the structure of the 2,5-dihalo-tetracyanoquinodimethane,  $\text{X}_2\text{TCNQ}$  ( $\text{X} = \text{Cl}, \text{Br}$ ), anion.

anion, continue to be investigated due to the wide variety of available physical properties that depend on the choice of anion as well as environmental variables such as pressure, temperature, and applied magnetic field.<sup>83,84</sup> All members of these charge transfer salts are essentially isostructural, and thus it is the nature of the inorganic anion that largely governs the various low temperature properties observed.<sup>85</sup> At room temperature and ambient pressure, the Bechgaard salts are described as quasi one-dimensional conductors; however, at low temperature there exists a competition between two types of critical behavior.<sup>86-88</sup> Should the anion, X, possess a center of symmetry then the metal-insulator transition in the 10-20 K region is one that results in a magnetic spin density wave (SDW) state. Under pressure the metal-insulator transition is gradually depressed and above a critical pressure, typically > 6 kbar, a superconducting (SC) state is established at temperatures less than 1 K.<sup>89</sup> If X does not contain a center of symmetry, the phase diagram for these materials is complicated by an additional phase transition that occurs above the SDW/SC transition.<sup>87</sup> This new phase boundary is a structural phase transition associated with ordering the non-centrosymmetric anions.

Nuclear magnetic resonance investigations have been instrumental in both describing the nature of, and detailing the transitions between, the low temperature phases of these materials.<sup>90,91</sup> Selenium has become the preferred nucleus of interest in these solid-state NMR studies, as the selenium nuclei exhibit no rotational behavior within the rigid TMTSF framework which simplifies the analysis of the electronic origin of the <sup>77</sup>Se relaxation rates in comparison to those over the entire temperature range via <sup>1</sup>H NMR.<sup>92,93</sup> Selenium-77 nuclear spin-lattice relaxation rates,  $T_1^{-1}$ , are the most common form of NMR information utilized in the characterization of the phase



transitions in the  $(\text{TMTSF})_2\text{X}$  salts, as they reveal low frequency electronic spin dynamics occurring at or near the onset of these transitions.<sup>94</sup> The number and range of phase transitions that have been studied by solid-state  $^{77}\text{Se}$  NMR are summarized in Table 2.7.

$(\text{TMTSF})_2\text{PF}_6$  is a Bechgaard salt containing the centrosymmetric anion  $\text{PF}_6^-$ , which possesses a metal-insulator transition at  $\sim 12$  K at ambient pressure. Solid-state  $^{77}\text{Se}$  NMR evidence for this transition comes from  $T_1^{-1}$  data that exhibit a local maximum at 12.2 K under 1 bar of pressure, and at 8.7 K under 5.5 kbar (below the critical pressure of 6 kbar).<sup>89,92,95-98</sup> Applications of strong magnetic fields,  $> 15$  T, have induced an additional SDW state, a so-called field induced SDW, observed as a discontinuity in the  $T_1^{-1}$  vs T plot around 4 K and suggest that additional FISDW states could be found in the presence of even higher applied magnetic field strengths.<sup>92,99</sup> The transition to the initial insulating SDW state at ambient pressure can be suppressed with the application of pressure and metallic character is retained down to 1.2 K at pressures greater than 8 kbar.<sup>89,96,98,100</sup>  $(\text{TMTSF})_2\text{PF}_6$  is well known as the first organic molecular superconductor,<sup>101,102</sup> but the nature of the superconducting phase has only recently been investigated by solid-state  $^{77}\text{Se}$  NMR. Knight shifts of samples under 7 kbar of pressure and low magnetic field strengths,  $< 2.4$  T, were studied as a function of temperature down to 0.09 K.<sup>103-105</sup> The results were inconsistent with those predicted to arise from conventional superconductivity (spin-singlet electron pairing), and strongly support superconductivity from spin-triplet pairing. Under pressures sufficient to induce a superconductive phase transition, the SC state can be suppressed by moderate magnetic

**Table 2.7** Solid-state  $^{77}\text{Se}$  NMR monitored phase transitions in the organic conductors,  $\text{A}_2\text{X}$ .

A	X	Anion ordering	Metal-insulator			Superconducting		
		$T_{\text{AO}}$ K	$T_{\text{MI}}$ K	$P_{\text{MI}}$ kbar	$B_{0,\text{MI}}$ T	$T_{\text{c}}$ K	$P_{\text{c}}$ kbar	$B_{0,\text{c}}$ T
TMTSF	$\text{PF}_6^-$	NA	12.2	.001	-	1	10	
			8.7	5.5	-			
			4	-	> 15			
	$\text{ClO}_4^-(\text{R})$	24	> 0	-	> 4	1	.001	< 4
	$\text{ClO}_4^-(\text{Q})$	-	3.5	.001	-			
	$\text{NO}_3^-$		9	-	-			
	$\text{ReO}_4^-$	180	180	-	-			
	$\text{FSO}_3^-$	89	89	-	-			
TMDTDS F	$\text{PF}_6^-$	NA	7	-	-			
	$\text{ReO}_4^-$	163	163	-	-			
BETD- TSF	$\text{Cl}_2\text{TCNQ}^-$		20	7	-			
	$\text{Br}_2\text{TCNQ}^-$		12	.001	-			
	$\lambda\text{-FeCl}_4^-$		3.5	-	9	> 0	-	> 18
			1.6	-	11.7			

fields that recover a conducting phase. This intermediate region of applied magnetic field strengths between the suppression of the SC and onset of the FISDW states exhibit a magic angle effect, MAE, where sharp reductions in magnetoresistance can occur for certain angles of the  $(\text{TMTSF})_2\text{PF}_6$  single crystal with respect to the applied magnetic field direction.<sup>106</sup> These reductions in magnetoresistance are predicted to enhance the

FISDW phase transition temperature;<sup>107</sup> however, attempts to observe this behavior via solid-state <sup>77</sup>Se NMR have been unsuccessful to date.<sup>108,109</sup>

Modifications to the (TMTSF)<sub>2</sub>PF<sub>6</sub> system have been prepared and investigated in order to elucidate further information on the nature of the various phases of this complex. Solid-state <sup>77</sup>Se NMR studies under high pressure, 6 and 7 kbar, on (TMTSF)<sub>2</sub>PF<sub>6</sub> doped with 10% (TMTSF)<sub>2</sub>AsF<sub>6</sub> have ventured to investigate the result of introducing disorder into this system near the SC boundary.<sup>94</sup> The donor molecule tetramethyldithiadiselenafulvalene, TMDTDSF, presents a mixed sulfur-selenium system whose bis-cationic complexes with PF<sub>6</sub><sup>-</sup> show intermediate properties between those of (TMTSF)<sub>2</sub>PF<sub>6</sub> and the tetramethyltetrathiafulvalene salt, (TMTTF)<sub>2</sub>PF<sub>6</sub>.<sup>110</sup> Selenium-77 spin-lattice relaxation studies have identified the onset of a SDW state at 7 K in (TMDTDSF)<sub>2</sub>PF<sub>6</sub>.<sup>85,93</sup>

(TMTSF)<sub>2</sub>ClO<sub>4</sub> has received considerable interest as the conducting state in this salt can be maintained down to liquid helium temperatures, and it is the only Bechgaard salt that exhibits a SC state, with T<sub>c</sub> ~ 1.2 K, at ambient pressure.<sup>111</sup> As mentioned above, non-centrosymmetric anions complicate the behavior of their salts due to the presence of anion disorder. For the perchlorate salt, an anion ordering transition occurs at 24 K; however, the disorder can be frozen into the sample by rapidly cooling the sample below 40 K resulting in the so-called quenched, or Q, state. The result of retaining the disordered ClO<sub>4</sub><sup>-</sup> anions is a magnetic SDW phase is induced and stabilized below 3.5 K as evidenced by a peak in the <sup>77</sup>Se spin-lattice relaxation rate around this temperature.<sup>86,88,112</sup>

Only by slowly cooling  $(\text{TMTSF})_2\text{ClO}_4$  through its anion ordering transition does the SC state appear at low temperature and ambient pressure. While the  $^{77}\text{Se}$   $T_1^{-1}$  does not show any anomalous behavior at or near the anion ordering temperature,  $T_{\text{AO}} = 24$  K, a broad peak in the  $^{77}\text{Se}$  nuclear spin echo decay rate,  $T_2^{-1}$ , does provide evidence for this transition.<sup>113-115</sup> The initial explanation for this behavior in  $T_2^{-1}$  was slow molecular motions;<sup>113,114</sup> however, a recent investigation charges that carrier density fluctuations rather than molecular orientational fluctuations are responsible.<sup>115</sup> After slow cooling of  $(\text{TMTSF})_2\text{ClO}_4$ , within the relaxed (R) state of the perchlorate salt, a non-magnetic conducting state persists down to the SC transition at ambient pressure. Numerous solid-state  $^{77}\text{Se}$  NMR studies have shown an enhancement in spin-lattice relaxation rates as the sample is cooled towards the SC transition producing a plateau of  $T_1^{-1}$  below 25 K.<sup>86,88,112,116,117</sup> Recent solid-state  $^{77}\text{Se}$  NMR investigations of  $(\text{TMTSF})_2\text{ClO}_4$  in the superconducting state appeared consistent with spin-triplet pairing;<sup>109</sup> however, a low applied magnetic field, 1 T, and very low temperature, 100 mK, investigation suggests that the nature of the SC results from the salt in the spin-singlet state.<sup>118</sup> Applications of magnetic fields in excess of 4 T at low temperatures can suppress SC and induce a SDW state. The ability to stabilize SDW states via two methods, from retaining anion disorder by rapid cooling to the quenched state or by applying large magnetic fields on a slowly cooled relaxed state sample, demonstrates the degrees of choice and control one can exert on these systems. Solid-state  $^{77}\text{Se}$  NMR linewidth and  $T_1^{-1}$  investigations have also been utilized in diagnosing these and subsequent FISDW states at low temperatures under field strengths of up to 15 T.<sup>83,84,86,88,112,119-121</sup>

Similar to  $(\text{TMTSF})_2\text{ClO}_4$ ,  $(\text{TMTSF})_2\text{NO}_3$  is a charge transfer salt with a non-centrosymmetric anion. While the anion ordering transition is known,  $T_{\text{AO}} = 41 \text{ K}$ ,  $^{77}\text{Se}$   $T_1^{-1}$  experiments around this temperature failed to observe any anomalies; however, the SDW transition at 9 K was observed by the characteristic peak in  $T_1^{-1}$  as well as line broadening at this temperature.<sup>87</sup>

$(\text{TMTSF})_2\text{ReO}_4$  is another Bechgaard salt containing a non-centrosymmetric anion and a structural phase transition associated with the ordering of the anion; however, unlike the perchlorate and nitrate salts, the  $X = \text{ReO}_4^-$  salt is accompanied by a metal-insulator transition at its anion ordering transition,  $T_{\text{AO}} = 180 \text{ K}$ .<sup>122</sup> The temperature dependence of the solid-state  $^{77}\text{Se}$  NMR spectra between  $285 \text{ K} > T > 135 \text{ K}$  are compared with those of the related mixed S-Se system  $(\text{TMDTDSF})_2\text{ReO}_4$  ( $T_{\text{AO}} = 163 \text{ K}$ ) from  $230 \text{ K} > T > 120 \text{ K}$ .<sup>85</sup> Selenium-77 spin-lattice relaxation rates for both of these perrhenate salts show characteristic exponential drops in  $T_1^{-1}$  with decreasing temperature at  $T_{\text{AO}}$ .<sup>85,93</sup>

Recently, a Bechgaard salt containing anions with a permanent electric dipole moment has been investigated. Similar to the perrhenate salt,  $(\text{TMTSF})_2\text{FSO}_3$  possesses an anion ordering transition accompanied by a metal-insulator transition at 89 K. Solid-state  $^{77}\text{Se}$  NMR investigations have shown abrupt lineshape changes and that the Knight shift and  $T_1^{-1}$  decrease exponentially with temperature at  $T_{\text{AO}}$ .<sup>87,123</sup> Under a pressure of  $\sim 6 \text{ kbar}$ ,  $(\text{TMTSF})_2\text{FSO}_3$  becomes superconducting around 3 K.<sup>124</sup> A solid-state  $^{77}\text{Se}$  NMR investigation of  $(\text{TMTSF})_2\text{FSO}_3$  under a pressure of 6.5 kbar between  $200 \text{ K} > T > 5 \text{ K}$  has revealed lineshape broadening and a peak in the spin-spin relaxation rate at  $T_{\text{AO}}$ .<sup>123,125,126</sup>

Bis(ethylenedithio)tetraselenafulvalene, BETD-TSF Figure 2.3g, has also been utilized within 2:1 charge transfer salts similar in nature to the Bechgaard salts; however, the  $(\text{BETD-TSF})_2\text{X}$  salts are able to form quasi two-dimensional organic conductors. The first  $(\text{BETD-TSF})_2\text{X}$  systems to be investigated by solid-state  $^{77}\text{Se}$  NMR were the 2,5-dihalo-tetracyanoquinodimethane salts,  $\text{X} = \text{Cl}_2\text{TCNQ}$  and  $\text{Br}_2\text{TCNQ}$  depicted in Figure 2.3h. The two similar salts exhibit distinct phase behaviors, where at ambient pressure the  $\text{Cl}_2\text{TCNQ}$  salt is metallic to low temperatures, the  $\text{Br}_2\text{TCNQ}$  complex possesses a metal-insulator transition at  $T_{\text{MI}} = 12$  K. Solid-state  $^{77}\text{Se}$  NMR linewidth and  $T_1^{-1}$  data are able to detect the  $T_{\text{MI}}$  in the  $\text{Br}_2\text{TCNQ}$  salt,<sup>127-129</sup> and the lack of any anomalies in  $T_1^{-1}$  down to 5 K for the  $\text{Cl}_2\text{TCNQ}$  complex support that the salt is metallic at least down to this temperature.<sup>128,129</sup> With increasing pressure  $T_{\text{MI}}$  decreases for the  $\text{Br}_2\text{TCNQ}$  salt, at 3.5 kbar  $(\text{BETD-TSF})_2(\text{Cl}_2\text{TCNQ})$  becomes a superconductor at 1 K, and above 6 kbar a metal-insulator transition occurs at  $T_{\text{MI}} > 10$  K. A maximum in the  $^{77}\text{Se}$  spin-lattice relaxation rate at 20 K has been observed for  $(\text{BETD-TSF})_2(\text{Cl}_2\text{TCNQ})$  under a pressure of 7 kbar establishing  $T_{\text{MI}}$  for the complex under this pressure.<sup>130</sup>

Unlike the TMTSF analogues, the  $(\text{BETD-TSF})_2\text{X}$  salts are not isostructural with respect to variation of X and several polymorphs are known to exist. The  $(\text{BETD-TSF})_2\text{I}_3$  salts form numerous polymorphs that are particularly interesting as they possess linear  $\text{I}_3^-$  anions, and the tetrathiafulvalene derivative  $\beta$ - $(\text{BETD-TTF})_2\text{I}_3$  was the second ambient pressure superconductor to be found.<sup>131</sup> Preliminary solid-state  $^{77}\text{Se}$  NMR spectra for  $\alpha$ - $(\text{BETD-TSF})_2\text{I}_3$  between 50 K and 150 K have appeared in a recent report on charge disproportionation in organic conductors.<sup>126</sup>

In solid-state  $^{77}\text{Se}$  NMR investigations of  $(\text{BETD-TSF})_2\text{GaCl}_4$ ,  $\kappa$ - $(\text{BETD-TSF})_2\text{GaCl}_4$  has been used as a reference system as it remains metallic with no evidence for superconductivity down to 0.5 K.<sup>132</sup> Conversely  $\lambda$ - $(\text{BETD-TSF})_2\text{GaCl}_4$ , which differs from the  $\kappa$ -polymorph in the arrangement of the BETD-TSF molecules,<sup>133</sup> shows superconductivity below 6 K at ambient pressure.<sup>134</sup> Solid-state  $^{77}\text{Se}$  NMR Knight shift, linewidth and spin-lattice relaxation rate investigations on  $\lambda$ - $(\text{BETD-TSF})_2\text{GaCl}_4$  in the range  $100 \text{ K} > T > 7 \text{ K}$  have revealed the development of antiferromagnetic spin fluctuations below 30 K.<sup>135,136</sup>

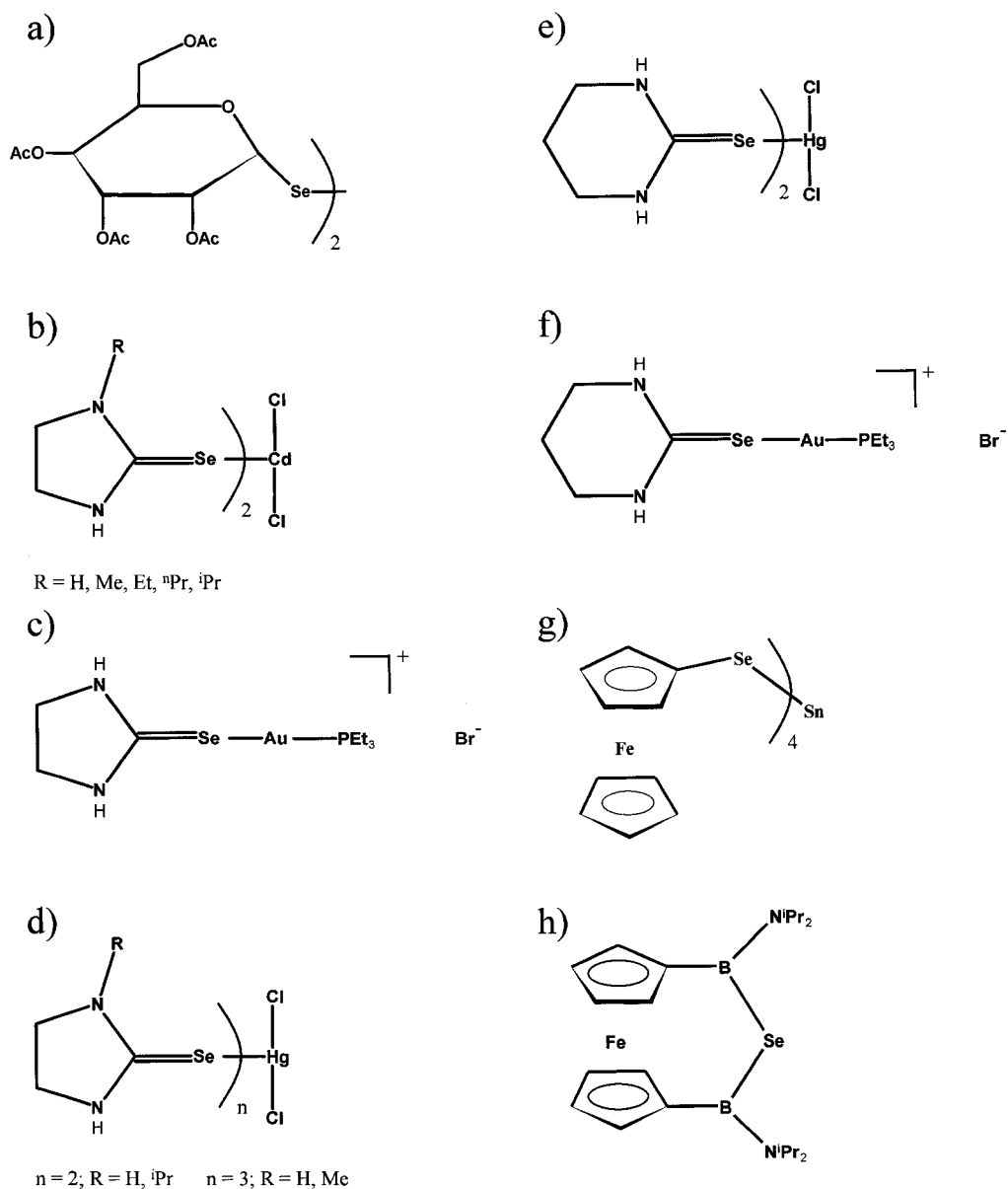
The  $(\text{BETD-TSF})_2\text{FeX}_4$  ( $X = \text{Cl, Br}$ ) salts are an interesting case as the  $\text{FeX}_4^-$  anion possesses high spin  $\text{Fe}^{3+}$ . Under ambient pressure,  $\lambda$ - $(\text{BETD-TSF})_2\text{FeCl}_4$  shows a metal-insulator transition at  $T_{\text{MI}} = 8 \text{ K}$ . External applied magnetic fields reduce  $T_{\text{MI}}$  and solid-state  $^{77}\text{Se}$  NMR evidence for this transition has been found at 3.5 K when  $B_0 = 9.0 \text{ T}$ ,<sup>137</sup> and 1.6 K when  $B_0 = 11.7 \text{ T}$ .<sup>138</sup> At fields greater than 18 T,  $\lambda$ - $(\text{BETD-TSF})_2\text{FeCl}_4$  undergoes field induced superconductivity, FISC, reaching a maximum  $T_c = 4.2 \text{ K}$  at  $B_0 = 33 \text{ T}$ , and with even greater magnetic fields  $T_c$  returns to 0 K around  $B_0 = 45 \text{ T}$ . Solid-state  $^{77}\text{Se}$  NMR measurements were able to provide the first direct evidence of strong coupling between the conduction  $\pi$  electrons and the Fe  $d$  electron spins in  $\lambda$ - $(\text{BETD-TSF})_2\text{FeCl}_4$ ,<sup>126,137,139,140</sup> and another FISC  $\kappa$ - $(\text{BETD-TSF})_2\text{FeBr}_4$ .<sup>141,142</sup> This evidence has been used to elucidate the nature of the FISC state in these materials. In 1962, Jaccarino and Peter predicted FISC when the external field is able to cancel the exchange field from the Fe moments.<sup>143</sup> The high field solid-state  $^{77}\text{Se}$  NMR studies of the  $(\text{BETD-TSF})_2\text{FeX}_4$  FISCs have been interpreted as evidence for this Jaccarino-Peter compensation mechanism.<sup>126,137,139,140,142</sup>

### 2.2.3.2 Bridging Organic and Inorganic Centers

Organic diselenides, the selenium equivalent of organic peroxides, are an intriguing functional group as they possess glutathione peroxidase-like activity.<sup>144-148</sup> The C-Se-Se environments within diphenyl diselenide have been probed by solid-state <sup>77</sup>Se NMR, noting a large difference in the most shielded principal component,  $\delta_{33}$ , between the two selenium sites in this diselenide.<sup>149</sup> IGLO calculations of the selenium chemical shift tensors of Ph<sub>2</sub>Se<sub>2</sub> were used to identify that the differences in  $\delta_{33}$  were primarily due to differences in Se-Se-C<sup>ipso</sup>-C<sup>ortho</sup> torsion angles.<sup>149</sup> Potrzebowski and coworkers have investigated the effects of polymorphism on the selenium chemical shift tensor(s) in bis(2,3,4,6-tetra-*O*-acetyl- $\beta$ -D-glucopyranosyl) diselenide shown in Figure 2.4a.<sup>150</sup> The polymorphs were identified based on the arrangements of the C-C-Se-Se-C-C backbone, where the selenium chemical shift tensors were related to the crystal structures of the *anti-syn* and *anti-anti* conformations.<sup>150</sup> The structure of a third polymorph, unable to be characterized by X-ray crystallography, was deduced to possess the *syn-syn* conformation with the assistance of solid-state <sup>77</sup>Se NMR.<sup>150</sup>

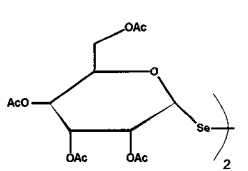
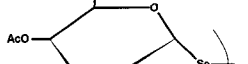
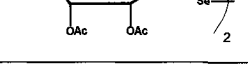
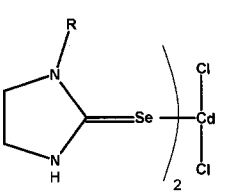
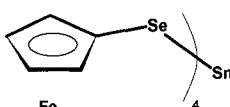
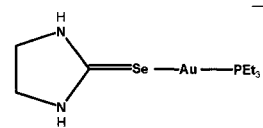
Selenium bridging organic and inorganic centers other than selenium have been characterized by solid-state <sup>77</sup>Se NMR. Of these, a large percentage includes complexes of seleno-carbonyls with group 11 or 12 late transition metal centers. Selenourea, *N,N*-dimethyl selenourea, as well as various imidazolidine-, diazinane-, and diazpine-selones have been coordinated with zinc,<sup>151</sup> silver,<sup>55</sup> cadmium,<sup>151,152</sup> gold,<sup>153,154</sup> and mercury,<sup>151,155,156</sup> see Figures 2.4b-f. For complexes with first and second row transition metals, the isotropic chemical shifts were consistently more shielded than those found for the uncoordinated seleno-carbonyl, see Tables 2.8 and 2.3, respectively.<sup>55,151,152</sup>





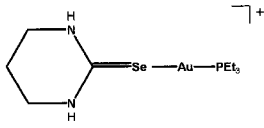
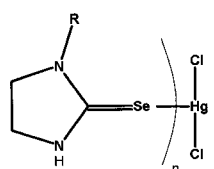
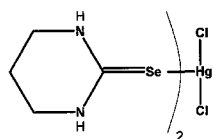
**Figure 2.4** Examples of the bridging selenium environments that have been studied by solid-state  $^{77}\text{Se}$  NMR: a) bis(2,3,4,6-tetra-*O*-acetyl- $\beta$ -D-glucopyranosyl) diselenide; imidazolidine-selone coordination complexes with b) cadmium, c) gold and d) mercury; diazinane-selone complexes with e) mercury and f) gold; as well as the ferrocenyl complexes g) tetrakis(ferrocenylselenolato)stannane and h) 1,3-dibora-2-selena-[3]ferrocenophane.

**Table 2.8** Solid-state  $^{77}\text{Se}$  chemical shifts and chemical shift tensors for selenium bridging organic and inorganic centers.<sup>a)</sup>

Compound	$\delta_{\text{iso}}$	$\delta_{11}$	$\delta_{22}$	$\delta_{33}$	Reference
$\text{Ph}_2\text{Se}_2$	350	537	510	2	149
	425	565	527	183	
 <i>anti-syn</i>	484	718	504	231	150
 <i>anti-anti</i>	367	639	484	-22	
 <i>syn-syn</i>	461	779	434	169	150
	514	844	473	225	150
	416	731	400	118	
$\text{Zn}(\text{Se}=\text{C}(\text{NH}_2)_2)_2\text{Cl}_2$	124	970	-215	-383	151
	152	1101	22	420	
$\text{Ag}[\text{Se}=\text{C}(\text{NMe}_2)(\text{NH}_2)][\text{NO}_3]$	180	382	304	-146	55
	170	398	322	-210	
$\text{Ag}[\text{Se}=\text{C}(\text{NMe}_2)(\text{NH}_2)]_2[\text{NO}_3]$	192	417	305	-146	55
	129	382	329	-325	
$\text{Cd}(\text{Se}=\text{C}(\text{NH}_2)_2)_2\text{Cl}_2$	140	801	-96	-283	151
$\text{Cd}(\text{SeC}_6\text{H}_2(\text{Pr})_3)(\text{bpy})$	-155	90	0	-559	157
	-156	107	-29	-546	
 R = H	12	804	94	-861	152
R = Me	8	670	121	-768	152
	60	881	42	-741	
R = Et	2	463	11	-468	152
	13	471	15	-446	
R = <sup>n</sup> Pr	-37	898	-28	-983	152
	-22	903	-7	-962	
R = <sup>i</sup> Pr	-27	947	-60	-968	152
	-20	1076	8	-1144	
 Fe	49, 107,				158
	113, 120				
$[\text{Me}_3\text{P}-\text{Au}-\text{Se}=\text{C}(\text{NH}_2)_2]_2[\text{Cl}]_2$	205	578	394	-361	153
 $\text{Br}^-$	69	455	159	-405	154

<sup>a)</sup> Experimental temperature either room temperature or was not specified.

**Table 2.8 Continued.**<sup>a)</sup>

Compound	$\delta_{150}$	$\delta_{11}$	$\delta_{22}$	$\delta_{33}$	Reference	
	228	620	425	360	154	
$\text{Hg}(\text{Se}=\text{C}(\text{NH}_2)_2)_2\text{Cl}_2$	207	787	6	-159	151	
	262	862	52	-127		
	R = H n = 2	102, 95			155	
	R = <sup>i</sup> Pr n = 2	13	578	443	-983	155
	R = H n = 3	112, 125, 130			155	
	R = Me n = 3	8	304	187	-468	156
		84	548	116	-413	156
		92	636	520	-878	
	124, 138				155	

<sup>a)</sup> Experimental temperature either room temperature or was not specified.

Relatively fewer inorganic complexes of selenolates,  $\text{RSe}^-$ , have been characterized by solid-state  $^{77}\text{Se}$  NMR. The single-crystal NMR of the cadmium complex,  $\text{Cd}(\text{SeC}_6\text{H}_2(\text{}^i\text{Pr})_3)_2(\text{bpy})$ , was investigated as an analogue to biologically occurring metalloproteins that coordinate by cysteine and histidine residues.<sup>157</sup> The  $^{77}\text{Se}$  CP MAS spectrum of a microcrystalline powder sample of tetrakis(ferrocenylselenolato)-stannane, Figure 2.4g, yields four isotropic chemical shift values at 49, 107, 113, and 120 ppm for the C-Se-Sn selenium environments.<sup>158</sup>

**Table 2.9** Indirect spin-spin coupling constants,  ${}^nJ({}^{77}\text{Se}, {}^m\text{X})_{\text{iso}}$  ( $m \geq 77$ ).<sup>a)</sup>

Compound	X(n)	${}^nJ({}^{77}\text{Se}, \text{X})_{\text{iso}} / \text{Hz}$	X(n)	${}^nJ({}^{77}\text{Se}, \text{X})_{\text{iso}} / \text{Hz}$	References
[NMe <sub>4</sub> ] <sub>2</sub> [Zn(Se <sub>4</sub> ) <sub>2</sub> ]	<sup>77</sup> Se(1)	150-180			159
12Se <sub>4</sub> <sup>b)</sup>	<sup>77</sup> Se(2)	31-36			76
18Se <sub>6</sub> <sup>b)</sup>	<sup>77</sup> Se(2)	128, 129			75,76
[NMe <sub>4</sub> ] <sub>2</sub> [Cd(Se <sub>4</sub> ) <sub>2</sub> ]	<sup>113</sup> Cd(1)	250-330			159
[Me <sub>2</sub> SnSe] <sub>3</sub>	<sup>119</sup> Sn(1)	1191, 1264			160
		1178, 1246, 1133			161
[NMe <sub>4</sub> ] <sub>2</sub> [Hg(Se <sub>4</sub> ) <sub>2</sub> ]	<sup>199</sup> Hg(1)	-1220 – -1480	<sup>199</sup> Hg(2)	330	159
(Hg(CN) <sub>2</sub> )(16Se <sub>4</sub> ) <sup>b)</sup>	<sup>199</sup> Hg(1)	-110, -123	<sup>77</sup> Se(2)	43	162

<sup>a)</sup> Experimental temperature either room temperature or was not specified.

<sup>b)</sup> See Figure 2.2.

### 2.2.3.3 Bridging Inorganic Centers

#### 2.2.3.3.1 Symmetric X-Se-X Linkages

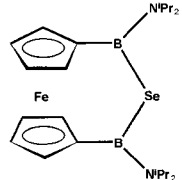
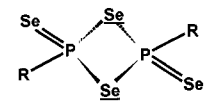
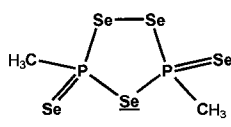
In this section, only selenium bridging two inorganic centers of the same element are considered. The B-Se-B linkage in 1,3-dibora-2-selena-[3]ferrocenophane, Figure 2.4h, gives a <sup>77</sup>Se CP MAS NMR peak at 41 ppm, quite different than that found at -40 °C in solution, 4.3 ppm.<sup>163</sup>

The N-Se-N moiety produces a broad peak at 1113 ppm in the <sup>77</sup>Se CP MAS NMR spectrum of Se[N(SiMe<sub>3</sub>)<sub>2</sub>]<sub>2</sub> due to indirect spin-spin and residual dipolar coupling from <sup>14</sup>N.<sup>164</sup> The magnitude of  ${}^1J({}^{77}\text{Se}, {}^{14}\text{N})_{\text{iso}}$  was estimated to be approximately 53 Hz in Se[N(SiMe<sub>3</sub>)<sub>2</sub>]<sub>2</sub>.<sup>164</sup> The eight-membered ring system 1,5-Se<sub>2</sub>S<sub>2</sub>N<sub>4</sub> possesses an alternating nitrogen-chalcogen pattern and the two <sup>77</sup>Se chemical shifts, 1409 and 1455 ppm, for the two N-Se-N linkages within the ring are more deshielded than found in Se[N(SiMe<sub>3</sub>)<sub>2</sub>]<sub>2</sub>, and one of the most deshielded selenium environments found by solid-state <sup>77</sup>Se NMR.<sup>165</sup>

Grossman and coworkers have synthesized a family of 1,3-diselena-2,4-diphosphetane-2,4-diselones,  $(\text{RPSe}_2)_2$  ( $\text{R} = \text{Me}, \text{Et}, \text{}^t\text{Bu}, 4\text{-Me}_2\text{NC}_6\text{H}_4$ ), Figure 2.1e, and have employed solid-state NMR in order to elucidate their structures. The isotropic  $^{77}\text{Se}$  chemical shifts and indirect spin-spin coupling constants for the two equivalent P-Se-P components, from CP MAS spectra, range from 621 ppm to 890 ppm, and all possess  $^1J(^{77}\text{Se}, ^{31}\text{P})_{\text{iso}} \sim -260 \text{ Hz}$ .<sup>59</sup> Ab initio HF and SOS-DFPT calculations of the selenium magnetic shielding tensor provide the orientation of the selenium chemical shift tensor for  $(\text{}^t\text{BuPSe}_2)_2$ , where  $\delta_{11}$  lies within the  $\text{P}_2\text{Se}_2$  ring plane, bisecting the P-Se-P angle, and that this plane bisects the  $\delta_{22}\text{-Se-}\delta_{33}$  angle.<sup>59</sup> A similar system, 3,5-dimethyl-1,2,4-triselena-3,5-diphospholane-3,5-diselone possessing only a single P-Se-P unit, Figure 2.1f, yields  $\delta_{\text{iso}}(\text{Se}) = 632 \text{ ppm}$  and  $^1J(^{77}\text{Se}, ^{31}\text{P})_{\text{iso}} \sim -420 \text{ Hz}$ .<sup>59</sup>

Inorganic polyselenides, Se-Se-Se, found in late transition metal complexes have been investigated by solid-state  $^{77}\text{Se}$  NMR. There appears to be a significant difference in the entire selenium chemical shift tensor depending on whether the Se-Se-Se moiety is found within a heterocyclic ring or as a chain between inorganic centers. The group 12 complexes  $[\text{NMe}_4]_2[\text{M}(\text{Se}_4)_2]$  ( $\text{M} = \text{Zn}, \text{Cd}, \text{Hg}$ ) form five-membered  $\text{MSe}_4$  rings and the  $^{77}\text{Se}$  peaks arising from Se-Se-Se linkages were differentiated from the M-Se-Se selenium environments due to the magnitudes of the one- and two-bond mercury-selenium couplings in  $[\text{NMe}_4]_2[\text{Hg}(\text{Se}_4)_2]$ , Table 2.9.<sup>159</sup> The Se-Se-Se  $\delta_{\text{iso}}$ 's range from 30 ppm to 142 ppm with an average span,  $\Omega$ , of 1139 ppm, Table 2.10.<sup>159</sup> The layered polyselenide,  $\text{Rb}_2[\text{Pd}(\text{Se}_4)_2] \cdot \text{Se}_8$ , possesses  $\text{Se}_4$  chains that link two Pd centers together, and the  $^{77}\text{Se}$  peak from the Se-Se-Se selenium is significantly more deshielded at 648 ppm and in a more symmetric environment,  $\Omega = 388 \text{ ppm}$ , than found in the  $\text{MSe}_4$  rings

**Table 2.10** Solid-state  $^{77}\text{Se}$  chemical shifts and chemical shift tensors for inorganic X-Se-X bridging moieties.<sup>a)</sup>

Compound	$\delta_{\text{iso}}$	$\delta_{11}$	$\delta_{22}$	$\delta_{33}$	Reference
	41				163
$\text{Se}[\text{N}(\text{SiMe}_3)_2]_2$	1113				164
$1,5\text{-Se}_2\text{S}_2\text{N}_4$	1455				165
					
R = Me	835				59
R = Et	678				59
R = <sup>t</sup> Bu	621				59
R = 4-Me <sub>2</sub> NC <sub>6</sub> H <sub>4</sub>	890				59
	632				59
$[\text{NMe}_4]_2[\text{Zn}(\text{Se}_4)_2]$	142	593	184	-350	159
	137	773	16	-379	
	122	657	135	-428	
	71	600	93	-480	
$\text{Rb}_2[\text{Pd}(\text{Se}_4)_2] \cdot \text{Se}_8$	648	826	680	438	51
$[\text{NMe}_4]_2[\text{Cd}(\text{Se}_4)_2]$	128	827	57	-501	159
	92	759	37	-519	
	71	794	-11	-571	
	63	739	-60	-490	
$[\text{NMe}_4]_2[\text{Hg}(\text{Se}_4)_2]$	101	591	111	-398	159
	90	612	77	-419	
	48	581	76	-514	
	30	552	82	-543	
$(\text{Me}_2\text{SnSe})_3$	-288	-267	-288	-309	161
	-374	-300	-361	-460	
	-266				160
	-352				

<sup>a)</sup> Experimental temperature either room temperature or was not specified.

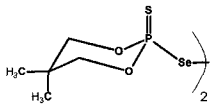
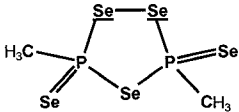
of  $[\text{NMe}_4]_2[\text{M}(\text{Se}_4)_2]$  (M = Zn, Cd, Hg).<sup>51</sup>

Dimethyl tin selenide,  $(\text{Me}_2\text{SnSe})_3$ , has a six-membered inorganic ring structure of alternating tin and selenium atoms. The crystal structure indicates that two of the three Sn-Se-Sn components are equivalent, which the solid-state  $^{77}\text{Se}$  NMR spectrum of  $(\text{Me}_2\text{SnSe})_3$  supports in displaying only two isotropic peaks with a 2:1 intensity ratio.<sup>160,161</sup> One-bond indirect spin-spin coupling constants,  $^1J(^{119}\text{Sn}, ^{77}\text{Se})_{\text{iso}}$ , are found to range in magnitude from 1133 to 1264 Hz.<sup>160,161</sup> By combining the results of solid-state  $^{77}\text{Se}$  and  $^{119}\text{Sn}$  NMR; Gay, Jones and Sharma were able to assign the selenium chemical shift tensors to specific crystallographic sites, and the values of  $^1J(^{119}\text{Sn}, ^{77}\text{Se})_{\text{iso}}$  to specific tin-selenium pairs.<sup>161</sup>

#### 2.2.3.3.2 Non-Symmetric X-Se-Y Linkages

The P-Se-Se-P linkage is one of the more common inorganic bridging moieties. A number of investigations on a series of bis(organothiophosphoryl) diselenides have been summarized.<sup>18</sup> Potrzebowski and coworkers have noted<sup>18,62</sup> a linear correlation between the span of the selenium chemical shift tensors and the Se-Se bond distance in these diselenides.<sup>62-65</sup> In another phosphorus diselenide, the two P-Se-Se selenium environments in 3,5-dimethyl-1,2,4-triseleno-3,5-diphospholane-3,5-diselone, Figure 2.1f, possess deshielded isotropic  $^{77}\text{Se}$  shifts, 636 and 649 ppm,<sup>59</sup> compared to the bis(organothiophosphoryl) diselenides, 274 – 457 ppm, Table 2.11.<sup>62</sup> The one-bond phosphorus-selenium coupling constants are similar, where -355 to -532 Hz couplings are obtained for the bis(organothiophosphoryl) diselenides,<sup>62-65</sup> and the values of  $^1J(^{77}\text{Se}, ^{31}\text{P})_{\text{iso}}$ , -340 and -350 Hz, are found in 3,5-dimethyl-1,2,4-triseleno-3,5-diphospholane-3,5-diselone,<sup>59</sup> see Table 2.5.

**Table 2.11** Solid-state  $^{77}\text{Se}$  chemical shifts and chemical shift tensors for inorganic X-Se-Y bridging moieties.<sup>a)</sup>

Compound	$\delta_{\text{iso}}$	$\delta_{11}$	$\delta_{22}$	$\delta_{33}$	Reference
$[(^i\text{Bu})(\text{Ph})\text{P}(\text{S})\text{Se}]_2$	457	722	544	106	62
$[(^i\text{PrO})_2\text{P}(\text{S})\text{Se}]_2$	288	660	350	-160	63
$[(\text{Me}_3\text{CCH}_2\text{O})_2\text{P}(\text{S})\text{Se}]_2$	276	613	394	-178	64
	274	602	410	-189	
	421	746	422	92	65
 $\cdot\text{C}_6\text{H}_6$ solvate	377	694	444	-22	
	400	688	340	173	65
	348	622	412	16	
	649				
	636				59
$[\text{NMe}_4]_2[\text{Zn}(\text{Se}_4)_2]$	670	1068	914	29	159
	657	1044	899	27	
	637	1048	809	55	
	595	1046	704	36	
$\text{Rb}_2[\text{Pd}(\text{Se}_4)_2] \cdot \text{Se}_8$	551	765	596	291	51
$[\text{NMe}_4]_2[\text{Cd}(\text{Se}_4)_2]$	662	1052	922	13	159
	642	1063	856	6	
	611	973	874	-14	
	600	952	799	49	
$[\text{NMe}_4]_2[\text{Hg}(\text{Se}_4)_2]$	693	1246	849	-15	159
	634	1086	828	-12	
	619	1089	740	29	
	527	1050	666	-135	

<sup>a)</sup> Experimental temperature either room temperature or was not specified.

The M-Se-Se linkages in the late transition metal polyselenide complexes appear significantly more similar than the Se-Se-Se moieties within the same complexes. The isotropic  $^{77}\text{Se}$  chemical shifts of the M-Se-Se selenium in  $\text{Rb}_2[\text{Pd}(\text{Se}_4)_2] \cdot \text{Se}_8$ , 551 ppm,<sup>51</sup> is within the range of  $\delta_{\text{iso}}$ 's found for  $[\text{NMe}_4]_2[\text{M}(\text{Se}_4)_2]$  (M = Zn, Cd, Hg), 527 – 670 ppm.<sup>159</sup> The approximate order of magnitude difference between  $^1J(^{113}\text{Cd}, ^{77}\text{Se})_{\text{iso}}$  and



$^1J(^{199}\text{Hg}, ^{77}\text{Se})_{\text{iso}}$  in the polyselenide complexes are consistent with trends found for Group 14 couplings.<sup>166-172</sup>

## 2.2.4 Inorganic Systems

### 2.2.4.1 *Selenium Oxides*

Solid-state  $^{77}\text{Se}$  NMR investigations of the oxides of selenium have, not surprisingly, focused on the two most commonly observed; selenites,  $\text{SeO}_3^{2-}$ , and selenates,  $\text{SeO}_4^{2-}$ . The selenium chemical shift tensor for a single crystal of selenous acid was the earliest solid-state  $^{77}\text{Se}$  NMR investigation of a selenium oxide system and is given in Table 2.12.<sup>173</sup> Since then, various mixed alkali hydrogen selenite systems have been investigated. Potassium hydrogen selenite and  $\text{RbHSeO}_3$  are isomorphous systems whose structures contain centrosymmetric  $(\text{HSeO}_3^-)_2$  dimers. Selenium-77 NMR studies of single crystals of  $\text{MHSeO}_3$  ( $M = \text{K}, \text{Rb}$ ) found that the single  $\text{HSeO}_3^-$  selenium environment had a significantly different asymmetry parameter,  $\eta_\sigma$ , than that found in  $\text{H}_2\text{SeO}_3$ .<sup>174</sup> The structures of the  $\text{MH}_3(\text{SeO}_3)_2$  salts are not as symmetric as the  $\text{MHSeO}_3$  systems and solid-state  $^{77}\text{Se}$  NMR investigations have identified two signals corresponding to  $\text{HSeO}_3^-$  and  $\text{H}_2\text{SeO}_3$  environments within the crystal structure.<sup>174-176</sup> While a large difference in  $\eta_\sigma$  was only found between the  $\text{HSeO}_3^-$  and  $\text{H}_2\text{SeO}_3$  selenium chemical shift tensors for  $M = \text{NH}_4$ , it was noted that the shielding anisotropy,  $\Delta\sigma$ , was smaller for the biselenite than in the selenous acid site for all  $\text{MH}_3(\text{SeO}_3)_2$  ( $M = \text{NH}_4, \text{K}, \text{Cs}$ ).<sup>174-176</sup> Solid-state  $^{77}\text{Se}$  NMR has also monitored the paraelectric-antiferroelectric transition in  $\text{CsH}_3(\text{SeO}_3)_2$  as evidenced by the doubling of the unit cell resulting in two

**Table 2.12** Solid-state  $^{77}\text{Se}$  chemical shifts and chemical shift tensors for selenium oxides.

Compound	T / K	$\delta_{\text{iso}}$	$\delta_{11}$	$\delta_{22}$	$\delta_{33}$	Reference	
$\text{H}_2\text{SeO}_3$		1262	1451	1334	1002	173,174	
	RT	1288	1477	1364	1017	54	
$\text{KHSeO}_3$	RT	1294	1416	1383	1082	174	
	175	1262	1416	1360	1014	174	
$\text{RbHSeO}_3$		1274	1384	1352	1082		
	RT	1293	1412	1376	1091	174	
$\text{NH}_4\text{H}_3(\text{SeO}_3)_2$	233	1269	1472	1312	1023	174,175	
		1252	1370	1316	1069		
$\text{KH}_3(\text{SeO}_3)_2$	175	1262	1416	1360	1014	174	
		1274	1384	1352	1082		
$\text{CsH}_3(\text{SeO}_3)_2$	293	1272	1410	1301	1106	176	
		1268	1352	1323	1129		
	123	1243	1431	1344	954	174,176	
		1253	1508	1355	897		
Hydrocalcite- $\text{SeO}_3$ (0-51% RH)		1245	1408	1308	1020		
		1256	1372	1341	1055		
	RT	1276	1306	1306	1215	177	
	(75% RH)	RT	1279	1288	1288	1261	177
		RT	1276	1306	1306	1215	
(84% RH)	RT	1279	1288	1288	1261	177	
	RT	1276	1306	1306	1215		
$\text{Au}_2(\text{SeO}_3)_2(\text{SeO}_4)$		1370	1568	1568	974	178	
$\text{Au}_2(\text{SeO}_3)_2(\text{SeO}_4)$		1046	1227	1227	685	178	
$\text{Li}_2\text{SeO}_4$		1024				179	
$\text{K}_2\text{SeO}_4$	300	62	80	72	34	180	
$(\text{NH}_2\text{CH}_2\text{COOH})_3\text{H}_2\text{SeO}_4$	303	1018	1055	1014	984	181	
		261	1017	1053	1016	982	181
		261	1016	1052	1016	981	
$\text{NH}_4\text{HSeO}_4$	293	1007	1144	1009	870	182	
		293	1009	1226	948	854	
		203	1006	1197	951	870	182
		203	1005	1223	952	841	
		203	1006	1223	952	843	
$\text{RbHSeO}_4$	388	1015	1163	1020	863	183	
		388	1013	1232	952	854	
		293	1016	1230	961	855	183
		293	1015	1230	959	855	
		293	1014	1227	961	855	

**Table 2.12** Continued.

Compound	T / K	$\delta_{180}$	$\delta_{11}$	$\delta_{22}$	$\delta_{33}$	Reference
$(\text{NH}_4)_2\text{SeO}_4$	RT	1040.2	1075	1038	1008	54
Hydrotalcite- $\text{SeO}_4$ (0% Rel. Humid.)	RT	1053				177
(11% Rel. Humid.)	RT	1053	1057	1057	1051	177
(33% Rel. Humid.)	RT	1053	1057	1057	1051	177
(51% Rel. Humid.)	RT	1049	1057	1057	1045	177
Hydrotalcite- $\text{SeO}_4$ (paste)	233	1053	1061	1061	1038	177
Hydrotalcite- $\text{SeO}_4$ (paste)	371	1050	1056	1048	1048	177
$\text{Na}_{12}(\text{SeO}_6)(\text{SeO}_4)_3$		1045, 1044				184
		1033				
$\text{Na}_{12}(\text{SeO}_6)(\text{SeO}_4)_3$		667				184
$\text{Li}_4\text{SeO}_5$		876	1046	971	611	179

$\text{HSeO}_3^-$  and two  $\text{H}_2\text{SeO}_3$  selenium chemical shift tensors, as given in Table 2.12.<sup>176</sup> Hou and Kirkpatrick have investigated  $\text{SeO}_3^{2-}$  located within the layers of hydrotalcite-like compounds as a function of relative humidity, RH, by solid-state  $^{77}\text{Se}$  stationary and MAS NMR.<sup>177</sup> Their findings show a RH-independent  $^{77}\text{Se}$  NMR signal due to interlayer located selenite, and a RH-dependent signal that arises at high RH due to  $\text{SeO}_3^{2-}$  on the exterior surfaces of the material.<sup>177</sup>

Recently, a mixed selenite-selenate gold complex,  $\text{Au}_2(\text{SeO}_3)_2(\text{SeO}_4)$  was synthesized and characterized by solid-state  $^{77}\text{Se}$  NMR.<sup>178</sup> The  $^{77}\text{Se}$  MAS NMR spectrum of  $\text{Au}_2(\text{SeO}_3)_2(\text{SeO}_4)$  displays two peaks in approximate 2:1 intensity ratio, and determination of the two selenium chemical shift tensors indicates that the  $\text{SeO}_4^{2-}$  anion is a highly distorted tetrahedron.<sup>178</sup>

Ammonium hydrogen selenate,  $\text{NH}_4\text{HSeO}_4$ , has been the most reported on selenium oxide system studied by solid-state  $^{77}\text{Se}$  NMR, which is primarily due to its complex phase behavior.<sup>182</sup> Above 98 K the sample is found in a ferroelectric phase,

which persists until 250 K where the salt possesses an incommensurate antiferroelectric phase. At 262 K,  $\text{NH}_4\text{HSeO}_4$  becomes paraelectric until at 417 K a superionic phase transition occurs before the sample decomposes at 427 K. Solid-state  $^{77}\text{Se}$  NMR has been a useful tool in the investigation of nearly all of these phases and their transitions. The first ferroelectric phase transition followed by  $^{77}\text{Se}$  NMR was performed on a related system triglycine selenate,  $(\text{NH}_2\text{CH}_2\text{COOH})_3\text{H}_2\text{SeO}_4$ , about the 295 K transition temperature.<sup>181</sup> Initial investigations of the selenium chemical shift tensors around the ferroelectric phase transitions in  $\text{MHSeO}_4$  ( $\text{M} = \text{NH}_4$ ,<sup>185,186</sup>  $\text{Rb}$ <sup>183,186</sup>) were consistent with the known structures and provided evidence that proton ordering of specific hydrogen bonds occur at this transition; however, an additional study was required to follow the triplication of the unit cell that occurs at low temperatures within the ferroelectric phase, which was observed by the triplication in the number of  $^{77}\text{Se}$  NMR signals between 213 K and 248 K.<sup>187</sup> Aleksandrova and coworkers studies of the  $^{77}\text{Se}$  NMR spectra of  $\text{NH}_4\text{HSeO}_4$  within the incommensurate region revealed that the phase is metastable.<sup>188-190</sup> Replacement of the hydrogen atoms in  $\text{NH}_4\text{HSeO}_4$  with deuterium via  $\text{D}_2\text{O}$  exchange introduces a metastable structural phase transition within the paraelectric phase. Solid-state  $^{77}\text{Se}$  NMR has revealed that the stable monoclinic structure of  $\text{NH}_4\text{HSeO}_4$  can be returned to the metastable orthorhombic  $\text{ND}_4\text{DSeO}_4$  by slow cooling the sample from above 329 K.<sup>191,192</sup> An investigation of the  $^{77}\text{Se}$  NMR properties of the high temperature phase transition within ammonium and rubidium hydrogen selenate demonstrated the ability to characterize the superionic phase transition in these two similar salts.<sup>193</sup> Variable temperature  $^{77}\text{Se}$  spin-lattice relaxation measurements on  $\text{CsHSeO}_4$  have noted an anomaly in the  $T_1^{-1}$ , associated with  $\text{SeO}_4$  tetrahedron fluctuations, below the

superionic phase transition as well as a discontinuity in the  $T_1^{-1}$  vs T at the transition temperature.<sup>194</sup>

Ammonium selenate,  $(\text{NH}_4)_2\text{SeO}_4$ , has been recommended as a convenient setup sample for cross polarization solid-state  $^{77}\text{Se}$  NMR.<sup>195</sup> The selenium chemical shift tensor for  $(\text{NH}_4)_2\text{SeO}_4$  has been determined and is reproduced in Table 2.12.<sup>54</sup> A solid-state  $^{77}\text{Se}$  NMR investigation of  $\text{K}_2\text{SeO}_4$  provides the tabulated chemical shift tensor for the paraelectric phase and evidence for the ferroelectric phase transition; however, the study was unable to detect the incommensurate phase transition in this sample.<sup>180</sup>

Static and MAS  $^{77}\text{Se}$  NMR spectra of  $\text{SeO}_4^{2-}$  within hydrotalcite-like compounds as a function of RH suggest significant changes in hydrogen bonding occur within the interlayer  $\text{SeO}_4^{2-}$  between 33% and 51% RH.<sup>177</sup> Variable temperature  $^{77}\text{Se}$  NMR spectra of stationary pastes between 193 K and 371 K indicate increasing motional averaging of the selenium chemical shift tensor.<sup>177</sup>

Haas and Jansen have been utilizing solid-state  $^{77}\text{Se}$  NMR in the characterization of some novel selenium oxide systems. The  $^{77}\text{Se}$  MAS NMR spectrum of  $\text{Na}_{12}(\text{SeO}_6)(\text{SeO}_4)_3$  was able to clearly resolve the three peaks, 1045, 1044, and 1033 ppm, due to the three crystallographically non-equivalent  $\text{SeO}_4^{2-}$  anions from the single  $^{77}\text{Se}$  resonance at 667 ppm arising from  $\text{SeO}_6^{6-}$ .<sup>184</sup> The single selenium chemical shift tensor for  $\text{Li}_4\text{SeO}_5$ , given in Table 2.12, was characterized and is consistent with the reported crystal structure.<sup>179</sup>

## 2.2.4.2 Inorganic Mono-, Di-, and Poly-selenides

### 2.2.4.2.1 Inorganic Monoselenides

The earliest inorganic selenide studied by solid-state  $^{77}\text{Se}$  NMR spectroscopy was the paramagnetic insulator  $\alpha$ -MnSe. The investigations were undertaken to probe the thermal behavior of the material, which was suggested to undergo transformations from  $\alpha$ -MnSe's rock salt structure to the zinc blende structure of  $\beta$ -MnSe and/or the wurtzite structure of the  $\gamma$ -polymorph.<sup>196</sup> Variable temperature solid-state  $^{77}\text{Se}$  NMR experiments between 150 and 300 K were undertaken; however, they were unable to prove or disprove the emergence of  $\beta$ - or  $\gamma$ -MnSe phases in  $\alpha$ -MnSe. Temperature dependent NMR frequency shifts, with respect to the  $^{27}\text{Al}$  NMR signal of a saturated solution of  $\text{Al}_2(\text{SO}_4)_3$ , were found with a room temperature value of 8.07%.<sup>197,198</sup> By assuming Curie-Weiss behavior, Jones was able to determine the value of the hyperfine coupling constant,  $A = 21.6$  MHz, in  $\alpha$ -MnSe.<sup>197,198</sup>

The class of II-VI semiconductors are one of the best known groups of semiconducting materials. Selenium-77 Knight shifts of CdSe, as well as CdSe doped with  $\sim 10^{20}$  indium atoms per cubic centimeter of CdSe were initially reported by Setty.<sup>43</sup> Solid-state  $^{77}\text{Se}$  NMR investigations of the Group 12 metal selenide materials MSe (M = Zn, Cd, Hg), along with PbSe, were undertaken in 1978,<sup>199</sup> and the results are detailed in Table 2.13. Only CdSe possessed an anisotropic chemical shift tensor due to its hexagonal structure; whereas, the site symmetry within ZnSe and HgSe (zinc blende structures) as well as PbSe (rock salt structure) produced only isotropic  $^{77}\text{Se}$  NMR peaks.<sup>199</sup> Selenium-77 NMR linewidths have been reported for ZnSe in a multinuclear NMR study of zinc chalcogenides.<sup>200,201</sup> Moran et al. have investigated ZnSe and CdSe

**Table 2.13** Solid-state  $^{77}\text{Se}$  chemical shifts and chemical shift tensors for inorganic selenium systems.

Compound	T / K	$\delta_{\text{iso}}$	$\delta_{11}$	$\delta_{22}$	$\delta_{33}$	Reference
[NMe <sub>4</sub> ]SeO <sub>2</sub> Cl	RT	1371	1783	1652	678	54
Li <sub>7</sub> PSe <sub>6</sub>		-736				202
		-843				
$\beta$ -Ag <sub>7</sub> PSe <sub>6</sub>	293	619	935	789	132	203
	293	610	918	795	118	
	293	-817	-945	-902	-604	
	293	-1274				
		612				60
		-818				
		-1271				
		612				61
		624				
$\gamma$ -Ag <sub>7</sub> PSe <sub>6</sub>	500	751	1033	903	318	203
	500	-882				
	500	-1170				
[(C <sub>5</sub> H <sub>5</sub> )CrSe] <sub>4</sub>	303	1079				204
		1018				
ZnSe	RT	-369	-369	-369	-369	199
Ga <sub>x</sub> Zn <sub>8-x</sub> P <sub>x</sub> Se <sub>2-x</sub> [BO <sub>2</sub> ] <sub>12</sub> (x = 0, 0.5, 1)		-824				205
[NMe <sub>4</sub> ] <sub>2</sub> Se <sub>5</sub>		389	629	629	91	206
		366	661	661	224	
		564	997	882	183	
		566	999	884	185	
		864	1218	920	455	
[NMe <sub>4</sub> ] <sub>2</sub> Se <sub>6</sub>		463	904	654	169	206
		662	1190	917	121	
		890				
As <sub>2</sub> Se <sub>3</sub>		210				48
		309				
		327				
Mo <sub>6</sub> Se <sub>8</sub>		3691	3871	3851	3351	207
		4531	4056	4492	5044	
CdSe	RT	-490	-475	-475	-519	199
		-476	-461	-461	-505	208
CdS <sub>0.4</sub> Se <sub>0.6</sub>		-481				208
HgSe	RT	-112	-112	-112	-112	199
PbSe	RT	-631	-631	-631	-631	199

inclusion complexes within sodalite frameworks.<sup>205,209</sup> The  $^{77}\text{Se}$  MAS NMR signal of  $\text{Zn}_8\text{Se}_2(\text{BO}_2)_{12}$  is approximately 400 ppm more shielded than bulk ZnSe, and that of  $\text{Cd}_8\text{Se}_2(\text{BeSiO}_4)_6 \sim 500$  ppm more shielded than bulk CdSe.<sup>209</sup> The effect of doping GaP to produce the mixed ZnSe/GaP semiconductor in  $\text{Ga}_x\text{Zn}_{8-x}\text{P}_x\text{Se}_{2-x}[\text{BO}_2]_{12}$  was found to have no detectable influence on the  $^{77}\text{Se}$  MAS spectrum for values of  $x = 0, 0.5, 1$ .<sup>205</sup> Molecular clusters of CdSe, between 12-35 Å, were readily discerned from bulk CdSe by their  $^{77}\text{Se}$  NMR spectra.<sup>210</sup> Recently, solid-state  $^{77}\text{Se}$  NMR has again been called upon to characterize CdSe nanoparticles. Ratcliffe et al. have observed an increase by nearly an order of magnitude in the linewidth in the solid-state  $^{77}\text{Se}$  NMR spectra of sulfur doped  $\text{CdS}_{0.4}\text{Se}_{0.6}$  relative to CdSe.<sup>208</sup> Strouse and coworkers have utilized solid-state NMR to investigate the surface of hexadecylamine-capped 2 nm CdSe nanocrystals by taking advantage of  $^1\text{H}$ - $^{77}\text{Se}$  CP MAS.<sup>211</sup> Their results were able to identify surface selenium environments at edges, vertices and within facets, as well as tetrahedral selenium sites one layer below the surface.<sup>211</sup> Additionally,  $^{77}\text{Se}$  HETCOR measurements indicate that the selenium sites are in close proximity with the methylene groups from hexydecylamine and not the  $\text{NH}_2$  indicating that this head group is most likely attached at Cd sites.<sup>211</sup>

Recently, Babu et al. utilized solid-state  $^{77}\text{Se}$  NMR to characterize the interaction between selenium and ruthenium in Ru-Se catalysts at Ru:Se concentrations of 3.3:1 and 2:1.<sup>44</sup> A large Knight shift and an apparent Korringa relationship of the spin-lattice relaxation rate, indicate that the selenium environment(s) attain metallic character when bound to ruthenium.<sup>44</sup>

The remaining inorganic monoselenide materials investigated by solid-state  $^{77}\text{Se}$  NMR contain *f*-block elements. Cerium selenide, an antiferromagnet, has been studied as



a function of temperature above its Néel temperature. The  $^{77}\text{Se}$  Knight shift as a function of temperature possesses Curie-Weiss behavior and suggests a localized behavior of the Ce  $4f$  moments.<sup>212</sup> Variable temperature solid-state  $^{77}\text{Se}$  NMR investigations were also performed on sulfur doped samarium selenide,  $\text{SmS}_x\text{Se}_{1-x}$  ( $x = 0, 0.1, 0.2, 0.3, 0.4, 0.5$ ), due to similarities in magnetic and electronic properties with  $\text{EuSe}$ .<sup>213</sup> The  $^{77}\text{Se}$  NMR shift was found to be linear with respect to sulfur concentration at both 77 and 300 K.<sup>213</sup> Europium selenide is ferrimagnetic below 2.8 K, and a number of solid-state  $^{77}\text{Se}$  NMR investigations have been undertaken on this ferrimagnetic phase. Suzuki and coworkers reported the disappearance of the  $^{77}\text{Se}$  NMR signal above 2.9 K, at the boundary between the ferrimagnetic and antiferromagnetic phases.<sup>214</sup> Budnick et al. have investigated the effect of 1 % and 10 % doping of gadolinium into the rock salt structure of  $\text{EuSe}$  at 1.3 K, noting a significant  $^{77}\text{Se}$  NMR shift to higher frequencies in  $\text{Eu}_{0.99}\text{Gd}_{0.01}\text{Se}$  and  $\text{Eu}_{0.90}\text{Gd}_{0.10}\text{Se}$ .<sup>215</sup> Kawakami noted the onset of ferromagnetic phases within  $\text{EuSe}$  at 1.3 K with magnetic fields in excess of 1 T.<sup>216</sup> Small changes in the composition of  $\text{UAsSe}$  have been observed within solid-state  $^{77}\text{Se}$  NMR spectra. As the arsenic:selenium ratio is decreased from  $\text{UAs}_{1.0}\text{Se}$  towards  $\text{UAs}_{0.9}\text{Se}$ , the  $^{77}\text{Se}$  NMR linewidths are found to increase indicating increasing disorder within this metallic system.<sup>217</sup>

#### 2.2.4.2.2 Inorganic Diselenides

The structures of the early transition metal diselenides possess numerous electronic properties of interest that are dominated by the two dimensional geometry of these layered systems. For example, the Group 5 diselenides are found as metals ( $\text{VSe}_2$ ), semiconductors ( $\text{TaSe}_2$ ), and superconductors ( $\text{NbSe}_2$ ).<sup>42</sup> The varying polytypes within

these layered structures are labeled according to the type of coordination found for the transition metal. Octahedral coordination is designated by  $1T$ ; whereas, trigonal prismatic coordinated transition metal systems of different stacking structures are indicated by the symbols  $2H$ ,  $3R$ , and  $4H$ .<sup>42</sup> Selenium-77 Knight shifts of the layered Group 4, 5 and 6 diselenides were presented by Silbernagel and Gamble.<sup>42</sup> Their results show a general decrease in the  $^{77}\text{Se}$  Knight shift with increasing period for all compounds of the same polytype within a given group, and similarities in the Knight shifts of the  $1T$  structures of Group 4 and 5 transition metal diselenides of the same row (i.e.,  $\text{TiSe}_2$  and  $\text{VSe}_2$ ,  $\text{HfSe}_2$  and  $\text{TaSe}_2$ ).<sup>42</sup>

Variable temperature solid-state  $^{77}\text{Se}$  NMR studies on  $1T$ - $\text{TiSe}_2$  have shown a large change in the Knight shift at the second-order structural transition temperature, 202 K.<sup>218</sup> The majority of solid-state  $^{77}\text{Se}$  NMR investigations have primarily focused on the Group 5 diselenides. Vanadium diselenide,  $1T$ - $\text{VSe}_2$ , possesses a structural phase transition accompanied by charge density waves (CDWs) at 110 K, and  $^{77}\text{Se}$  NMR has shown both a local maximum in the Knight shift,<sup>219,220</sup> as well as an increase in linewidth with decreasing temperature below this transition temperature.<sup>220</sup> Like  $1T$ - $\text{VSe}_2$ ,  $2H$ - $\text{NbSe}_2$  has a structural phase transition accompanied by CDWs that can be detected by  $^{77}\text{Se}$  NMR line broadening below the transition temperature; however, the transition occurs at a temperature of 31 K.<sup>220,221</sup> Unlike  $1T$ - $\text{VSe}_2$ ,  $2H$ - $\text{NbSe}_2$  becomes superconducting below 7 K, and evidence for this transition from  $^{77}\text{Se}$  NMR comes from a sharp decrease in the Knight shift and an exponential increase in  $T_1$  as  $T$  decreases below  $T_c = 7$  K.<sup>222</sup> The  $2H$  polytype of tantalum diselenide is an ordinary metal above 122 K; however,  $2H$ - $\text{TaSe}_2$  undergoes transitions to an incommensurate CDW state

below 120 K, and to a commensurate CDW state below 90 K. An initial solid-state  $^{77}\text{Se}$  NMR investigation was unsuccessful in observing any anomalies in the Knight shift or linewidth in the temperature range  $20\text{ K} < T < 300\text{ K}$ .<sup>223</sup> Subsequent  $^{77}\text{Se}$  NMR studies have observed significant changes in linewidth, lineshape, and number of resonances occurring at or around the two CDW transitions.<sup>221,224-226</sup> Suits, Couturié and Slichter have also shown that their  $^{77}\text{Se}$  NMR results<sup>225,226</sup> in the incommensurate CDW state are consistent with McMillan's description of discommensurations (separate commensurate regions within the structure that produce an incommensurate material on average).<sup>227,228</sup>

Intercalation of lithium within the layered structures of the early transition metal diselenides produces little or no noticeable structural modifications to the host material. Silbernagel has shown that solid-state  $^{77}\text{Se}$  NMR parameters are sensitive to intercalation in  $\text{Li}_{1.00}\text{MSe}_2$  ( $\text{M} = \text{Group 4 and 5 metals}$ ).<sup>229</sup> The reported  $^{77}\text{Se}$  Knight shifts for intercalated diselenides are significantly more similar than those of the parent unintercalated materials.<sup>229</sup> Dramatic changes in spin-lattice relaxation rate are also found for the Group 4 and 5 diselenides before and after intercalation, which are interpreted to be consistent with their respective electronic band properties.<sup>229</sup> Subsequent solid-state  $^{77}\text{Se}$  NMR studies on intercalated diselenides have been reported for  $\text{Li}_x\text{ZrSe}_2$ , which have potential application in lithium secondary cells. For compositions  $x < 0.40$ ,  $\text{Li}_x\text{ZrSe}_2$  is a semiconductor, and for  $x > 0.40$ , the intercalation compound becomes metallic. The semiconductor-metal transition has been monitored where  $\text{Li}_x\text{ZrSe}_2$  possessing a semiconducting composition show a constant Knight shift; however, the Knight shift decreases linearly with increasing  $x$  above  $x = 0.40$ .<sup>230,231</sup> Evidence for lithium ordering in semiconducting and metallic  $\text{Li}_x\text{ZrSe}_2$  have also been

observed in solid-state  $^{77}\text{Se}$  NMR measurements. Variable temperature  $^{77}\text{Se}$  NMR spectra as well as spin-spin relaxation rates on semiconducting  $\text{Li}_{0.29}\text{ZrSe}_2$  indicate lithium ordering occurs around 205 K;<sup>232</sup> whereas, in metallic  $\text{Li}_x\text{ZrSe}_2$  ( $x = 0.51, 0.70$ ) similar measurements show ordering of lithium ions near 250 K.<sup>232-234</sup>

Selenium has been substituted for sulfur in order to study the sulfided cobalt-molybdenum catalyst, which transforms petroleum phases containing thiols and aromatic sulfides into hydrocarbons and  $\text{H}_2\text{S}$ , by solid-state  $^{77}\text{Se}$  NMR. Molybdenum disulfide is known to be the active catalyst; however, the presence of cobalt sulfides can enhance the activity by an order of magnitude. Spin-lattice relaxation measurements have indicated the presence of two different  $\text{MoSe}_2$  environments corresponding to selenium at the edges of the particles having very different  $T_1$ s than the other selenium sites, and that the relative ratio of these edge Se environments to other Se sites is larger in the  $\text{CoMoSe}_2$  silica-supported catalyst than is found in bulk  $\text{MoSe}_2$ .<sup>235</sup> From solid-state  $^{77}\text{Se}$  NMR measurements before and after reaction of the catalyst with thiophene, a reduction in relative intensity of the edge Se sites was found as sulfur replaces selenium at the edge sites.<sup>235</sup> This study has shown that the edge environments are the active sites of the catalyst, and that inclusion of cobalt increases the number of these edge sites.

The later transition metal diselenides that have been investigated by solid-state  $^{77}\text{Se}$  NMR spectroscopy,  $\text{CoSe}_2$  and  $\text{NiSe}_2$ , possess the pyrite structure. The  $^{77}\text{Se}$  Knight shift for  $\text{CoSe}_x$  ( $1.95 < x < 2.20$ ) as a function of temperature shows a maximum around 50 K.<sup>236,237</sup> Panissod et al. have interpreted their results as evidence of structural instability,<sup>236,237</sup> which is consistent with the extra reflections detected in neutron diffraction experiments on  $\text{CoSe}_2$  at low temperature.<sup>238</sup> Nickel diselenide is a

paramagnetic metal, which appears to have a similar  $^{77}\text{Se}$  hyperfine interaction mechanism as  $\text{CoSe}_2$ .<sup>239</sup> However,  $\text{NiS}_{2-x}\text{Se}_x$  possesses electronic properties as a function of  $x$ . For  $x < 0.5$ ,  $\text{NiS}_{2-x}\text{Se}_x$  is a semiconductor, between  $0.5 < x < 1.0$  the compound is an antiferromagnetic metal at low temperatures, and at  $x > 1.0$   $\text{NiS}_{2-x}\text{Se}_x$  the magnetic ordering is suppressed and the sample remains paramagnetic.<sup>240</sup> Antiferromagnetic ordering in  $\text{NiS}_{2-x}\text{Se}_x$  ( $0.5 < x < 1.0$ ) was first reported by Krill and coworkers,<sup>241</sup> and recent solid-state  $^{77}\text{Se}$  NMR measurements on  $x = 0.76$  and  $0.96$  compounds have been contrasted with  $x = 1.25$  and  $2.00$  samples.<sup>242</sup> Anomalies in the  $(T_1T)^{-1}$  vs.  $T$  plots for the  $x = 0.76$  and  $0.96$  near their respective Néel temperatures clearly differentiate these compounds from  $x = 1.25, 2.00$  paramagnetic metal plots that show little variation down to low temperatures.<sup>242</sup>

#### 2.2.4.2.3 Inorganic Polyselenides

The most commonly studied inorganic polyselenides by solid-state  $^{77}\text{Se}$  NMR are the ferromagnetic chromium selenide spinels,  $\text{MCr}_2\text{Se}_4$ . A  $77\text{ K}$  study of  $\text{CuCr}_2\text{Se}_4$  was able to extract a  $^{77}\text{Se}$  hyperfine field of  $7.14\text{ T}$ , and extrapolated a value of  $7.30\text{ T}$  at  $0\text{ K}$ .<sup>243</sup> Subsequent investigations have focused on the anisotropic hyperfine interactions in  $\text{MCr}_2\text{Se}_4$  ( $\text{M} = \text{Cd}, \text{Hg}$ ). Anti-parallel hyperfine fields were found to increase in magnitude for both  $\text{CdCr}_2\text{Se}_4$  and  $\text{HgCr}_2\text{Se}_4$  spinels at  $77\text{ K}$ ,<sup>244</sup>  $4.2\text{ K}$ ,<sup>244-247</sup> and  $1.4\text{ K}$ .<sup>248</sup> Small amounts of doping of copper<sup>247</sup> or indium<sup>246</sup> into  $\text{Cd}_{1-x}\text{M}_x\text{Cr}_2\text{Se}_4$  ( $\text{M} = \text{Cu}, \text{In}; x \leq 0.07$ ) have shown significant changes in their respective NMR spectra.

The solid-state  $^{77}\text{Se}$  MAS NMR spectrum of crystalline arsenic selenide,  $\text{As}_2\text{Se}_3$ , has been obtained at  $15\text{ kHz}$ . Three resonances at  $210, 309,$  and  $327\text{ ppm}$  are observed

and possess considerably more narrow line widths than the single peak observed at  $\sim 380$  ppm in amorphous  $\text{As}_2\text{Se}_3$  (vide infra).<sup>48</sup>

Németh and coworkers have investigated the quasi one-dimensional conductor  $(\text{TaSe}_4)_2\text{I}$  by solid-state  $^{77}\text{Se}$  NMR in the temperature region  $150 \text{ K} < T < 320 \text{ K}$ . The initial results of Knight shifts and spin-lattice relaxation rates were unable to monitor the transition into a CDW state at  $265 \text{ K}$ ;<sup>249</sup> however, an increase in  $^{77}\text{Se}$  NMR linewidth was noticed around this transition temperature and an ensuing investigation into this line broadening with decreasing temperature below  $265 \text{ K}$  was found along with a local minimum in  $T_2^{-1}$  at the transition temperature.<sup>249,250</sup>

Mixed valence cations in  $\text{M}_3\text{Se}_4$  systems typically demonstrate a 1:2 ratio of  $\text{M}^{2+}:\text{M}^{3+}$ . Bastow has attempted to observe the solid-state  $^{77}\text{Se}$  MAS NMR in metallic  $\text{Mo}_3\text{Se}_4$ ; however, the sample that contained both  $\text{Mo}_3\text{Se}_4$  and  $\text{MoSe}_2$  by  $^{95}\text{Mo}$  NMR revealed only a single  $^{77}\text{Se}$  peak consistent with  $\text{MoSe}_2$ .<sup>251</sup> Unlike  $\text{Mo}_3\text{Se}_4$ , which is expected to give three  $^{77}\text{Se}$  NMR peaks from three non-equivalent selenium environments, in  $\text{Sm}_3\text{Se}_4$  all selenium sites are equivalent despite the 1:2  $\text{Sm}^{2+}:\text{Sm}^{3+}$  ratio. Takagi and coworkers have found that the  $^{77}\text{Se}$  Knight shift in  $\text{Sm}_3\text{Se}_4$  lies in between those of  $\text{SmSe}$  ( $\text{Sm}^{2+}$ ) and  $\text{Sm}_2\text{Se}_3$  ( $\text{Sm}^{3+}$ ) throughout the temperature range  $110 \text{ K} < T < 300 \text{ K}$ ,<sup>252,253</sup> and have shown evidence for the temperature activation of valence fluctuation,  $\text{Sm}^{2+} \leftrightarrow \text{Sm}^{3+}$ , in  $\text{Sm}_3\text{Se}_4$  between  $140\text{-}160 \text{ K}$  from spin-spin lattice relaxation measurements.<sup>253,254</sup>

The binary and pseudo-binary Chevrel phase compounds,  $\text{Mo}_6\text{Se}_{8-x}\text{Q}_x$  ( $\text{Q} = \text{Te}, \text{I}$ ), are an interesting class of high field superconductors.<sup>255</sup> The very deshielded selenium chemical shift tensors for the axial and peripheral selenium environments found in the

binary  $\text{Mo}_6\text{Se}_8$  have been characterized and are tabulated in Table 2.13.<sup>207</sup> Solid-state  $^{77}\text{Se}$  NMR investigations of the pseudo-binary  $\text{Mo}_6\text{Se}_{8-x}\text{Te}_x$  ( $0.0 < x < 7.5$ ) have shown that selenium is preferentially located at the axial sites before occupying the peripheral chalcogen environments in these solid solutions.<sup>207,256</sup> The pseudo-binary Chevrel phase compounds,  $\text{Mo}_6\text{Se}_{8-x}\text{I}_x$  ( $0.0 < x < 2.0$ ), have been investigated as a function of temperature and found that the occupancy of iodine at either axial or peripheral locations appears temperature dependent.<sup>257</sup>

#### 2.2.4.3 Vitreous Systems

The study of chalcogenide glasses has recently been reviewed and highlights solid-state  $^{77}\text{Se}$  NMR as a useful probe of the local selenium environment within inorganic selenide glasses.<sup>258,259</sup> Binary phosphorus-selenium compositions form glasses up to 52 atom % P, and 5.0, 12.5, and 20.0 atom % P systems have been investigated by  $^{31}\text{P}$ - $^{77}\text{Se}$  spin echo double resonance (SEDOR) NMR where the results indicate that the number of selenium atoms bonded to more than one phosphorus significantly increases between 12.5 and 20.0 atom % P.<sup>260</sup> Variable temperature  $^{77}\text{Se}$  NMR measurements on P-Se glasses from 0 to 40 atom % P have been obtained through the glass transition temperature,  $T_g$ , of these systems and significant narrowing of the  $^{77}\text{Se}$  NMR signal is found to occur approximately 100 K above  $T_g$ .<sup>261,262</sup> The use of cross polarization from  $^{31}\text{P}$  to  $^{77}\text{Se}$  has been demonstrated in the inorganic glass,  $\beta\text{-P}_4\text{Se}_3$ ; however, it has not been utilized in establishing P-Se connectivity in subsequent studies of either crystalline or amorphous P-Se systems.<sup>263</sup>

**Table 2.14** Solid-state  $^{77}\text{Se}$  chemical shifts found in vitreous selenium systems.

Compound	$\delta_{\text{iso}}$	Reference
Se, 40 atom % P	1314	261,262
	1105	
$\text{Ge}_x\text{Se}_{1-x}$ x = 0.11	863, 435	45
x = 0.14	865, 435	45
x = 0.20	860, 445	45
x = 0.25	860, 445	45
x = 0.29	820, 430	45
x = 0.33	410	45
$\text{As}_x\text{Se}_{1-x}$ x = 0.10	865, 570	48
x = 0.18	850, 550	48
x = 0.23	850, 525	48
x = 0.40	380	48
$\text{Te}_x\text{Se}_{1-x}$ x = 0.10	880, 700	40
x = 0.20	880, 700, 510	40
x = 0.25	880, 700, 500	40
x = 0.33	860, 690, 500	40
x = 0.50	900, 710, 510	40

Amorphous germanium selenide is of interest for applications in infrared optics. Bureau and coworkers have investigated  $\text{Ge}_x\text{Se}_{1-x}$  in the range of composition  $0.00 < x < 0.33$  (i.e., from vitreous selenium to  $\text{GeSe}_2$ ) by solid-state  $^{77}\text{Se}$  NMR.<sup>39,45</sup> The results, reproduced in Table 2.14, suggest the presence of clusters of selenium rings and/or chains (Se-Se-Se species) with chemical shifts greater than 820 ppm along with  $\text{GeSe}_4$  tetrahedra (Ge-Se-Ge species),  $410 \text{ ppm} < \delta < 445 \text{ ppm}$ .<sup>39,45</sup> The number of  $^{77}\text{Se}$  peaks are in contrast to the chain-crossing model that consists of homogeneously distributed Ge throughout the glasses, which would be expected to lead to a third resonance due to Ge-Se-Se species.

Arsenic selenide glasses,  $\text{As}_x\text{Se}_{1-x}$  ( $0.00 < x < 0.40$ ; i.e., from glassy selenium to  $\text{As}_2\text{Se}_3$ ), have been the most studied vitreous system by solid-state  $^{77}\text{Se}$  NMR. Bishop



and Taylor were the first to report the chemical shift difference between glassy Se and vitreous  $\text{As}_2\text{Se}_3$ .<sup>47</sup> Unlike the germanium selenide glasses,  $\text{As}_x\text{Se}_{1-x}$  shows three distinct  $^{77}\text{Se}$  signals at  $\sim 850$  ppm,  $\sim 550$  ppm, and 380 ppm consistent with Se-Se-Se, As-Se-Se, and As-Se-As selenium environments, respectively, as predicted by the chain-crossing model of evenly distributed  $\text{AsSe}_3$  pyramids.<sup>39,48,264</sup> The effect of doping amorphous  $\text{As}_2\text{Se}_3$  ( $x = 0.40$ ) with Cu, Ag, Tl, I, and Ge have also been investigated by solid-state  $^{77}\text{Se}$  NMR.<sup>265</sup> A general increase in chemical shift and linewidth was found when increasing Cu content in  $\text{Cu}_z(\text{As}_{0.40}\text{Se}_{0.60})_{1-z}$  for  $z < 0.25$ .<sup>265,266</sup>

Solid-state  $^{77}\text{Se}$  NMR studies of vitreous  $\text{Te}_x\text{Se}_{1-x}$  systems in the concentration range  $0.0 < x < 0.50$  (i.e., from vitreous Se to TeSe) are able to discern three chemical shift regions about 880 ppm, 710 ppm, and 510 ppm corresponding to Se-Se-Se, Te-Se-Se, and Te-Se-Te selenium environments, respectively; however, the results are not entirely consistent with the chain-crossing model.<sup>40</sup>

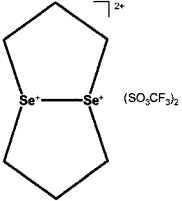
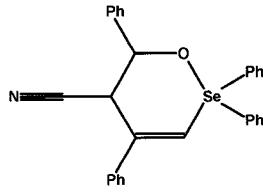
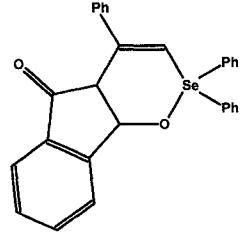
## 2.2.5 Miscellaneous Selenium Systems

### 2.2.5.1 Miscellaneous Organoselenium Systems

The  $^{77}\text{Se}$  NMR spectrum of a stationary sample of solid  $[\text{NMe}_4]\text{SeH}$ , which possesses  $\text{SeH}^-$  anions at a crystallographic four-fold rotation axis, with and without proton decoupling indicate that the  $\text{HSe}^-$  moiety undergoes significant anisotropic molecular motions.<sup>267</sup>

Trisorganoselenonium salts,  $\text{R}_3\text{Se}^+$ , are commonly isolated in organoselenium chemistry, and a number of these species have been characterized by solid-state  $^{77}\text{Se}$  NMR. Collins, Ratcliffe and Ripmeester characterized the selenium chemical shift tensor

**Table 2.15** Solid-state  $^{77}\text{Se}$  chemical shifts and chemical shift tensors for miscellaneous organoselenium systems.<sup>a)</sup>

Compound	$\delta_{180}$	$\delta_{11}$	$\delta_{22}$	$\delta_{33}$	Reference
$[\text{NMe}_4]\text{SeH}$	-465				267
$\text{Me}_2\text{Se}$ in HZSM-5	0				268
$\text{MeSeH}$ in HZSM-5	-130				268
$\text{Me}_3\text{Se}^+$ in HZSM-5	245				268
$\text{Me}_3\text{SeI}$	256	355.1	216.8	196.4	54
$[\text{PhC}\equiv\text{CSePh}_2][\text{OTf}]$	468				269
	810 768	1066 1005	1066 1005	300 292	77
$[\text{Cu}(16\text{Se}4)][\text{SO}_3\text{CF}_3]^{b)}$	112 159				162
$(\text{Hg}(\text{CN})_2)(16\text{Se}4)^{b)}$	127 202				162
10.95-Å kaolinite : $\text{Me}_2\text{SeO}$	758				270
11.26-Å kaolinite : $\text{Me}_2\text{SeO}$	785				270
11.38-Å kaolinite : $\text{Me}_2\text{SeO}$	788				270
	454				269
	451				269

<sup>a)</sup> Experimental temperature either room temperature or was not specified.

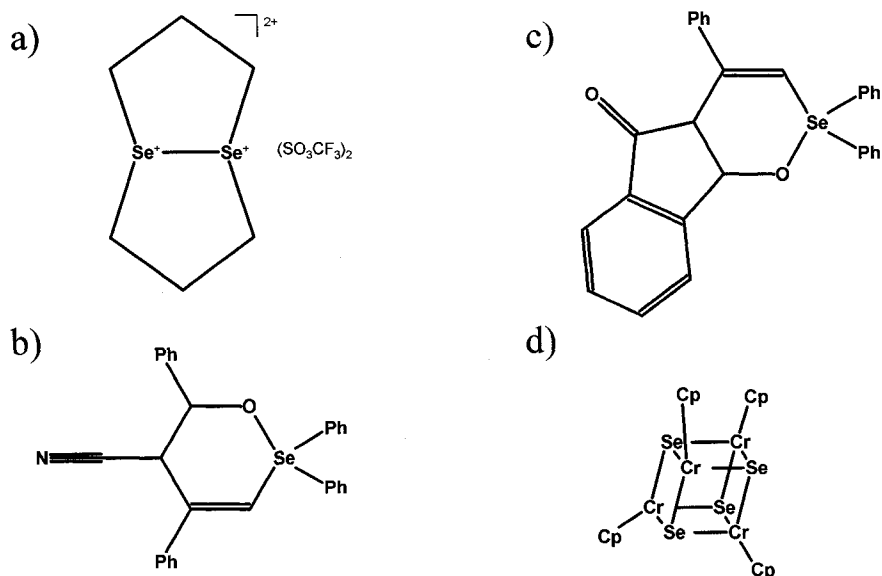
<sup>b)</sup> See Figure 2.2.

of trimethylselenonium iodide as part of their investigation of numerous selenium containing compounds.<sup>54</sup> Diphenyl(phenylethynyl)selenonium triflate,

[PhC≡CSePh<sub>2</sub>][OTf], was prepared from the reaction of diphenylselenoxide, Ph<sub>2</sub>SeO, and phenylethynyl trimethylsilane, PhC≡CSiMe<sub>3</sub>, and the value of  $\delta_{\text{iso}}$ , 468 ppm, is consistent with other hypervalent organoselenium compounds found in Table 2.15.<sup>269</sup>

Dicationic 1,5-diselenacyclooctane trifluoromethane sulfonate, Figure 2.5a, possesses two three-coordinate selenonium environments that, not surprisingly, show very similar selenium chemical shift tensor principal components.<sup>77</sup> Similarly, the selenium coronand complexes with copper and mercury demonstrate three-coordinate selenium species with at least a partial positive charge. The Cu(I) ion in 1,5,9,13-tetraselenacyclohexadecanecopper(I) trifluoromethane sulfonate is pseudo-tetrahedrally coordinated to four 16Se4 selenium coronands and gives rise to two broad <sup>77</sup>Se NMR peaks at 112 and 159 ppm.<sup>162</sup> The mercury dicyanide complex with 16Se4 is similarly surrounded by four selenium coronands and yields two selenium chemical shifts at 127 and 202 ppm.<sup>162</sup> The fairly long Hg-Se distances, 3.38 and 3.44 Å, are likely part of the reason for the relatively small values of  $^1J(^{199}\text{Hg}, ^{77}\text{Se})_{\text{iso}}$ , 110 and 123 Hz; however, two-bond Se-Hg-Se coupling,  $^2J(^{77}\text{Se}, ^{77}\text{Se})_{\text{iso}} = 43$  Hz, appear to arise between seleniums on different coronands that are oriented *cis* with respect to the approximately linear Hg(CN)<sub>2</sub> molecules.<sup>162</sup>

Solid-state <sup>77</sup>Se NMR has been utilized to follow the reactivity of dimethyl selenide within the zeolite catalyst HZSM-5, and was able to provide clear evidence for the formation of trimethylselenonium, Me<sub>3</sub>Se<sup>+</sup>, and methane selenol within the porous system.<sup>268</sup> Another study of organoselenium species as inclusion compounds within porous frameworks demonstrates the sensitivity of the <sup>77</sup>Se chemical shift of



**Figure 2.5** Miscellaneous structures that have been studied by solid-state  $^{77}\text{Se}$  NMR: a) 1,5-diselenacyclooctane trifluoromethane sulfonate, b) and c) four-coordinate selenuranes, and d)  $[(\text{C}_5\text{H}_5)\text{CrSe}]_4$ .

dimethylselenoxide to changes in kaolinite structures with various basal dimensions, see Table 2.15.<sup>270</sup>

Kataoka and coworkers have prepared two four-coordinate organoselenium compounds by reaction of  $[\text{PhC}\equiv\text{CSePh}_2][\text{OTf}]$  with ketones of the form  $\text{R}_1\text{CH}_2\text{C}(\text{O})\text{R}_2$ .<sup>269</sup> The isotropic selenium chemical shifts for the compounds, 454 and 451 ppm for Figures 2.5b and 2.5c, respectively, are not altogether very different from that of the reactant  $[\text{PhC}\equiv\text{CSePh}_2][\text{OTf}]$ , 468 ppm.<sup>269</sup>

### 2.2.5.2 Miscellaneous Inorganic Systems

The  $^{77}\text{Se}$  CP MAS spectrum of the  $\text{SeO}_2\text{Cl}^-$  ion in  $[\text{NMe}_4]\text{SeO}_2\text{Cl}$  displays variable fine structure within the spinning sideband manifold.<sup>54</sup> Non-equivalent crystallographic selenium sites and/or residual dipolar coupling from  $^{35/37}\text{Cl}$  were deduced as the likely sources of this fine structure.<sup>54</sup>

The nature of the selenium species in solid  $\text{Li}_7\text{PSe}_6$  has been elucidated by  $^{77}\text{Se}$  NMR. Two peaks, at -736 and -843 ppm, are assigned to distinct  $\text{Se}^{2-}$  species due to their similarity to that of  $\text{Li}_2\text{Se}$ , -760 ppm, and a broad spinning sideband manifold between 0 and 1000 ppm that was uncharacterized was associated to selenophosphate sites.<sup>202</sup> Similarly,  $\text{Se}^{2-}$  and  $\text{PSe}_4^{3-}$  selenium environments were identified in the  $^{77}\text{Se}$  MAS spectra of the  $\beta$ - and  $\gamma$ -phases of  $\text{Ag}_7\text{PSe}_6$ .<sup>60,61,203</sup>

The nearly axially symmetric selenium chemical shift tensors of the tridentate selenium environments in  $[\text{CpCrSe}]_4$  are consistent with the proposed structure, where Se and Cr form the corners of a distorted cube and each selenium is coordinated to three chromium atoms, Figure 2.5d; however, an assignment of the two selenium resonances, at 1018 and 1079 ppm to selenium sites within the same  $[\text{CpCrSe}]_4$  structure or within two crystallographically distinct structures, could not be made.<sup>204</sup>

The study of the tetramethylammonium salts of five- and six-membered polyselenide chains by solid-state NMR offers insight into the nature of these isolated polyselenide systems. The terminal selenium sites are the most shielded environments for both the  $\text{Se}_5^{2-}$ , 366 and 389 ppm, and the  $\text{Se}_6^{2-}$ , 463 ppm, chains.<sup>206</sup> The next selenium atoms in the chain possess bridging  $\text{Se}-\underline{\text{Se}}-\text{Se}$  environments and are more deshielded than the terminal sites, see Table 2.13.<sup>206</sup> The most internal selenium

environments in the polyselenide chains possess selenium resonances at 864 ppm ( $\text{Se}_5^{2-}$ ) and 890 ppm ( $\text{Se}_6^{2-}$ ), in the region where elemental selenium is found, see Tables 2.2 and 2.13.<sup>206</sup>

### 2.3 Summary

Solid-state  $^{77}\text{Se}$  NMR spectroscopy has developed not only as a complementary tool to  $^{77}\text{Se}$  NMR of corresponding solution phases, but as a comparable method to other solid-state techniques for the characterization of solid selenium containing materials. The range of isotropic selenium chemical shifts in solution, approximately 3300 ppm,<sup>6,7</sup> has been expanded at both extremes by solid-state  $^{77}\text{Se}$  NMR. At the high frequency end  $\text{Mo}_6\text{Se}_8$  gives two very deshielded values of  $\delta_{\text{iso}}$ , 3691 and 4531 ppm,<sup>207</sup> replacing the previously known limit of 2434 ppm where some selenoaldehydes, molybdenum selenides and cationic selenium containing heterocycles are found.<sup>6,7</sup> Similarly, the low frequency limit was expanded from the isotropic chemical shifts found in selenium bridging moieties in some tungsten complexes,  $\delta_{\text{iso}} \sim -900$  ppm, to the  $\text{Se}^{2-}$  sites in  $\text{Ag}_7\text{PSe}_6$  that are found as far as  $\delta_{\text{iso}} = -1274$  ppm.<sup>60,203</sup> Together, the isotropic chemical shifts for  $^{77}\text{Se}$  in solids range over 5800 ppm.

Knowledge of the indirect spin-spin coupling constants involving  $^{77}\text{Se}$  have also benefited from solid-state  $^{77}\text{Se}$  NMR investigations. The one-bond selenium-phosphorus couplings in solid-state  $^{77}\text{Se}$  NMR studies, Table 2.5, cover most of the known ranges of  $^1J(^{77}\text{Se}, ^{31}\text{P})_{\text{iso}}$  for phosphine selones, -650 Hz to -1200 Hz, and phosphorus-selenium single bonded systems, -200 Hz to -620 Hz.<sup>6,7</sup> One- and two-bond selenium-selenium couplings,  $^nJ(^{77}\text{Se}, ^{77}\text{Se})_{\text{iso}}$ , found in solid-state  $^{77}\text{Se}$  NMR are also consistent with those

found in solution phases,<sup>6,7</sup> Similarly consistent values of one-bond coupling constants between  $^{77}\text{Se}$  and  $^{113}\text{Cd}$ ,  $^{119}\text{Sn}$ , or  $^{199}\text{Hg}$  are found between solid-state  $^{77}\text{Se}$  NMR spectra, Table 2.9, and solution  $^{77}\text{Se}$  NMR.<sup>6</sup>

From organic systems, compounds and conductors, to inorganic materials, complexes and glasses, solid-state  $^{77}\text{Se}$  NMR is clearly an important tool in identifying and characterizing many areas of selenium chemistry. It would appear that as interest in selenium chemistry continues to expand, the utility and applicability of selenium-77 NMR in general, and in turn solid-state  $^{77}\text{Se}$  NMR, will assist in facilitating this rapidly developing field.

## 2.4 References

- (1) Mack, J. E.; Arroe, O. H. *Phys. Rev.* **1949**, 76, 173.
- (2) Strandberg, M. W. P.; Wentink Jr, T.; Hill, A. G. *Phys. Rev.* **1949**, 75, 827-832.
- (3) Geschwind, S.; Minden, H.; Townes, C. H. *Phys. Rev.* **1950**, 78, 174-175.
- (4) Davis, S. P.; Jenkins, F. A. *Phys. Rev.* **1951**, 83, 1269-1269.
- (5) Harris, R. K.; Becker, E. D.; Crabral de Menezes, S. M.; Goodfellow, R.; Granger, P. *Pure Appl. Chem.* **2001**, 73, 1795-1818.
- (6) Duddeck, H. *Prog. Nucl. Magn. Reson. Spectrosc.* **1995**, 27, 1-323.
- (7) Duddeck, H. *Annu. Rep. NMR Spectrosc.* **2004**, 52, 105-166.
- (8) Rodger, C.; Sheppard, N.; McFarlane, H. C. E.; McFarlane, W. In *NMR and the Periodic Table*; Harris, R. K., Mann, B. E., Eds.; Academic Press: London, 1978, pp 402-412.
- (9) Luthra, N. P.; Odom, J. D. In *The Chemistry of Organic Selenium and Tellurium Compounds*; Patai, S., Rappoport, Z., Eds.; John Wiley & Sons: New York, 1986; Vol. 1, pp 189-241.
- (10) Duddeck, H. In *Encyclopedia of Nuclear Magnetic Resonance*; Grant, D. M., Harris, R. K., Eds.; John Wiley & Sons: Chichester, 1996; Vol. 7, pp 4623-4635.
- (11) Klapötke, T. M.; Broschag, M. *Compilation of Reported <sup>77</sup>Se NMR Chemical Shifts: Up to the Year 1994*; Wiley: Chichester, 1996.
- (12) Duddeck, H. *Chemical Shifts and Coupling Constants for Selenium-77*; Springer: Berlin, Heidelberg, New York, 2004; Vol. III/35G.
- (13) Haeberlen, U. *Advances in Magnetic Resonance, Suppl. 1: High Resolution NMR in Solids: Selective Averaging*; Academic Press: New York, 1976.
- (14) Mason, J. *Solid State Nucl. Magn. Reson.* **1993**, 2, 285-288.
- (15) Sebald, A. *NMR Basic Princ. & Prog.* **1994**, 31, 119-121.
- (16) Granger, P. *Phosphorus Sulfur Silicon Relat. Elem.* **1998**, 136, 137 & 138, 373-376.
- (17) Potrzebowski, M. J. *Phosphorus Sulfur Silicon Relat. Elem.* **1998**, 136, 137 & 138, 423-426.



- (18) Potrzebowski, M. J. *Bull. Pol. Acad. Sci., Chem.* **1998**, *46*, 61-74.
- (19) Harris, R. K.; Becker, E. D.; Cabral de Menezes, S. M.; Granger, P.; Hoffman, R. E.; Zilm, K. W. *Pure Appl. Chem.* **2008**, *80*, 59-84.
- (20) Wasylshen, R. E.; Connor, C.; Friedrich, J. O. *Can. J. Chem.* **1984**, *62*, 981-985.
- (21) Jameson, C. J. In *Multinuclear NMR*; Mason, J., Ed.; Plenum Press: New York, 1987, pp 89-131.
- (22) Jameson, C. J. In *Phosphorus-31 NMR Spectroscopy in Stereochemical Analysis. Organic Compounds and Metal Complexes*; Verkade, J. G., Quin, L. D., Eds.; VCH Publishers, Inc.: Deerfield Beach, 1987; Vol. 8, pp 205-230.
- (23) Colquhoun, I. J.; McFarlane, W. *Dalton Trans.* **1981**, 658-660.
- (24) Magyarfalvi, G.; Pulay, P. *Chem. Phys. Lett.* **1994**, *225*, 280-284.
- (25) Malkin, V. G.; Malkina, O. L.; Casida, M. E.; Salahub, D. R. *J. Am. Chem. Soc.* **1994**, *116*, 5898-5908.
- (26) Bühl, M.; Gauss, J.; Stanton, J. F. *Chem. Phys. Lett.* **1995**, *241*, 248-252.
- (27) Bühl, M.; Thiel, W.; Fleischer, U.; Kutzelnigg, W. *J. Phys. Chem.* **1995**, *99*, 4000-4007.
- (28) Schreckenbach, G.; Ruiz-Morales, Y.; Ziegler, T. *J. Chem. Phys.* **1996**, *104*, 8605-8612.
- (29) Wilson, P. J. *Mol. Phys.* **2001**, *99*, 363-367.
- (30) Keal, T. W.; Tozer, D. J. *Mol. Phys.* **2005**, *103*, 1007-1011.
- (31) Nakanishi, W.; Hayashi, S.; Shimizu, D.; Hada, M. *Chem. Eur. J.* **2006**, *12*, 3829-3846.
- (32) Jokisaari, J.; Autschbach, J. *Phys. Chem. Chem. Phys.* **2003**, *5*, 4551-4555.
- (33) Wrackmeyer, B. *Struct. Chem.* **2005**, *16*, 67-71.
- (34) Wrackmeyer, B.; García Hernandez, Z.; Herberhold, M. *Magn. Reson. Chem.* **2007**, *45*, 198-204.
- (35) Koma, A.; Tanaka, S. *Solid State Commun.* **1972**, *10*, 823-827.

- (36) Koma, A. *Phys. Status Solidi B* **1973**, *56*, 655-664.
- (37) Koma, A. *Phys. Status Solidi B* **1973**, *57*, 299-306.
- (38) Günther, B.; Kanert, O. *Phys. Rev. B* **1985**, *31*, 20-33.
- (39) Bureau, B.; Troles, J.; Le Floch, M.; Smektala, F.; Lucas, J. *J. Non-Cryst. Solids* **2003**, *326*, 58-63.
- (40) Bureau, B.; Boussard-Plédel, C.; Le Floch, M.; Troles, J.; Smektala, F.; Lucas, J. *J. Phys. Chem. B* **2005**, *109*, 6130-6135.
- (41) Günther, B.; Kanert, O.; Wolf, D. *Solid State Commun.* **1983**, *47*, 409-413.
- (42) Silbernagel, B. G.; Gamble, F. R. In *Low Temp. Phys.-LT 13, Proc. Int. Conf. Low Temp. Phys., 13th*; Timmerhaus, K. D., O'Sullivan, W. J., Hammel, E. F., Eds.; Plenum, 1974; Vol. 3, pp 438-441.
- (43) Setty, D. L. R. *Indian J. Pure Appl. Phys.* **1977**, *15*, 806-808.
- (44) Babu, P. K.; Lewera, A.; Chung, J. H.; Hunger, R.; Jaegermann, W.; Alonso-Vante, N.; Wieckowski, A.; Oldfield, E. *J. Am. Chem. Soc.* **2007**, *129*, 15140-15141.
- (45) Bureau, B.; Troles, J.; Le Floch, M.; Guenot, P.; Smektala, F.; Lucas, J. *J. Non-Cryst. Solids* **2003**, *319*, 145-153.
- (46) Gladden, L. F.; Elliott, S. R. *J. Non-Cryst. Solids* **1987**, *97 & 98*, 1175-1178.
- (47) Bishop, S. G.; Taylor, P. C. *Solid State Commun.* **1972**, *11*, 1323-1326.
- (48) Bureau, B.; Troles, J.; Le Floch, M.; Smektala, F.; Silly, G.; Lucas, J. *Solid State Sci.* **2003**, *5*, 219-224.
- (49) Gopal, M.; Milne, J. *Inorg. Chem.* **1992**, *31*, 4530-4533.
- (50) Parise, J. B.; MacDougall, J. E.; Herron, N.; Farlee, R.; Sleight, A. W.; Wang, Y.; Bein, T.; Moller, K.; Moroney, L. M. *Inorg. Chem.* **1988**, *27*, 221-228.
- (51) Goldbach, A.; Fayon, F.; Vosegaard, T.; Wachhold, M.; Kanatzidis, M. G.; Massiot, D.; Saboungi, M.-L. *Inorg. Chem.* **2003**, *42*, 6996-7000.
- (52) *Gmelin's Handbuch der Anorganischen Chemie*; 8th ed.; Springer Verlag: Berlin, 1980; Vol. A2.

- (53) Bernard, G. M.; Eichele, K.; Wu, G.; Kirby, C. W.; Wasylshen, R. E. *Can. J. Chem.* **2000**, *78*, 614-625.
- (54) Collins, M. J.; Ratcliffe, C. I.; Ripmeester, J. A. *J. Magn. Reson.* **1986**, *68*, 172-179.
- (55) Wazeer, M. I. M.; Isab, A. A.; Ahmad, S. *Can. J. Anal. Sci. Spectrosc.* **2006**, *51*, 43-48.
- (56) Wazeer, M. I. M.; Isab, A. A.; Perzanowski, H. P. *Magn. Reson. Chem.* **2003**, *41*, 1026-1029.
- (57) Grossmann, G.; Potrzebowski, M. J.; Fleischer, U.; Krüger, K.; Malkina, O. L.; Ciesielski, W. *Solid State Nucl. Magn. Reson.* **1998**, *13*, 71-85.
- (58) Clade, J.; Jansen, M. Z. *Anorg. Allg. Chem.* **1997**, *623*, 1407-1412.
- (59) Grossmann, G.; Ohms, G.; Kruger, K.; Karaghiosoff, K.; Eckstein, K.; Hahn, J.; Hopp, A.; Malkina, O. L.; Hrobarik, P. *Z. Anorg. Allg. Chem.* **2001**, *627*, 1269-1278.
- (60) Maxwell, R.; Lathrop, D.; Franke, D.; Eckert, H. *Angew. Chem., Int. Ed. Engl.* **1990**, *29*, 882-884.
- (61) Franke, D.; Hudalla, C.; Eckert, H. *Solid State Nucl. Magn. Reson.* **1992**, *1*, 33-40.
- (62) Potrzebowski, M. J.; Blaszczyk, J.; Wieczorek, M. W.; Klinowski, J. *J. Phys. Chem. A* **1997**, *101*, 8077-8084.
- (63) Potrzebowski, M. J.; Blaszczyk, J.; Majzner, W. R.; Wieczorek, M. W.; Baraniak, J.; Stec, W. J. *Solid State Nucl. Magn. Reson.* **1998**, *11*, 215-224.
- (64) Potrzebowski, M. J. *Magn. Reson. Chem.* **1995**, *33*, 8-14.
- (65) Potrzebowski, M. J.; Grossmann, G.; Blaszczyk, J.; Wieczorek, M. W.; Sieler, J.; Knopik, P.; Komber, H. *Inorg. Chem.* **1994**, *33*, 4688-4695.
- (66) Potrzebowski, M. J.; Blaszczyk, J.; Wieczorek, M. W.; Misiura, K.; Stec, W. J. *J. Chem. Soc., Perkin Trans. 2* **1997**, 163-168.
- (67) Facey, G.; Wasylshen, R. E.; Collins, M. J.; Ratcliffe, C. I.; Ripmeester, J. A. *J. Phys. Chem.* **1986**, *90*, 2047-2052.
- (68) Collins, M. J.; Davidson, D. W.; Ratcliffe, C. I.; Ripmeester, J. A. *Stud. Phys. Theor. Chem.* **1987**, *46*, 497-503.

- (69) Collins, M. J.; Ratcliffe, C. I.; Ripmeester, J. A. *J. Phys. Chem.* **1990**, *94*, 157-162.
- (70) Oldfield, J. E. *J. Nutr.* **1987**, *117*, 2002-2008.
- (71) Johansson, L.; Gafvelin, G.; Arnér, E. S. J. *Biochim. Biophys. Acta* **2005**, *1726*, 1-13.
- (72) Gajda, J.; Pacholczyk, J.; Bujacz, A.; Bartoszak-Adamska, E.; Bujacz, G.; Ciesielski, W.; Potrzebowski, M. J. *J. Phys. Chem. B* **2006**, *110*, 25692-25701.
- (73) Potrzebowski, M. J.; Katarzynski, R.; Ciesielski, W. *Magn. Reson. Chem.* **1999**, *37*, 173-181.
- (74) Pinto, B. M.; Johnston, B. D.; Batchelor, R. J.; Einstein, F. W. B.; Gay, I. D. *Can. J. Chem.* **1988**, *66*, 2956-2958.
- (75) Pinto, B. M.; Batchelor, R. J.; Johnston, B. D.; Einstein, F. W. B.; Gay, I. D. *J. Am. Chem. Soc.* **1988**, *110*, 2990-2991.
- (76) Batchelor, R. J.; Einstein, F. W. B.; Gay, I. D.; Gu, J.-H.; Johnston, B. D.; Pinto, B. M. *J. Am. Chem. Soc.* **1989**, *111*, 6582-6591.
- (77) Batchelor, R. J.; Einstein, F. W. B.; Gay, I. D.; Gu, J.-H.; Mehta, S.; Pinto, B. M.; Zhou, X.-M. *Inorg. Chem.* **2000**, *39*, 2558-2571.
- (78) Batchelor, R. J.; Einstein, F. W. B.; Gay, I. D.; Gu, J.-H.; Pinto, B. M.; Zhou, X.-M. *J. Am. Chem. Soc.* **1990**, *112*, 3706-3707.
- (79) Batchelor, R. J.; Einstein, F. W. B.; Gay, I. D.; Gu, J.-H.; Pinto, B. M.; Zhou, X.-M. *Can. J. Chem.* **2000**, *78*, 598-613.
- (80) Duddeck, H.; Bradenahl, R.; Stefaniak, L.; Jazwinski, J.; Kamienski, B. *Magn. Reson. Chem.* **2001**, *39*, 709-713.
- (81) Ishiguro, T.; Yamaji, K. *Organic Superconductors*; Springer-Verlag: Berlin, 1990; Vol. 88.
- (82) Bechgaard, K.; Jacobsen, C. S.; Mortensen, K.; Pedersen, H. J.; Thorup, N. *Solid State Commun.* **1980**, *33*, 1119-1125.
- (83) Carretta, P.; Berthier, C.; Horvatic, M.; Fagot-Revurat, Y.; Segransan, P.; Jerome, D.; Bourbonnais, C. In *Physical Phenomena at High Magnetic Fields-II*; Fisk, Z., Ed.; World Scientific, Singapore: Tallahassee, 1996, pp 328-333.

- (84) Azevedo, L. J.; Williams, J. M.; Compton, S. J. *Phys. Rev. B: Condens. Matter* **1983**, *28*, 6600-6602.
- (85) Gotschy, B.; Auban-Senzier, P.; Farrall, A.; Bourbonnais, C.; Jerome, D.; Canadell, E.; Henriques, R. T.; Johansen, I.; Bechgaard, K. *J. Phys. I* **1992**, *2*, 677-694.
- (86) Takahashi, T.; Jerome, D.; Bechgaard, K. *J. Phys. Colloques* **1983**, *44*, 805-811.
- (87) Hiraki, K.; Nemoto, T.; Takahashi, T.; Kang, H.; Jo, Y.; Kang, W.; Cung, O.-H. *Synth. Met.* **2003**, *135-136*, 691-692.
- (88) Takahashi, T.; Jerome, D.; Bechgaard, K. *J. Physique Lett.* **1982**, *43*, 565-573.
- (89) Wzietek, P.; Creuzet, F.; Bourbonnais, C.; Jerome, D.; Bechgaard, K.; Batail, P. *J. Phys. I* **1993**, *3*, 171-201.
- (90) Kanoda, K. *Hyperfine Interact.* **1997**, *104*, 235-249.
- (91) Miyagawa, K.; Kanoda, K.; Kawamoto, A. *Chem. Rev.* **2004**, *104*, 5635-5653.
- (92) Valfells, S.; Kuhns, P.; Kleinhammes, A.; Brooks, J. S.; Moulton, W.; Takasaki, S.; Yamada, J.; Anzai, H. *Phys. Rev. B: Condens. Matter* **1997**, *56*, 2585-2593.
- (93) Auban-Senzier, P.; Gotschy, B.; Farrall, A.; Bourbonnais, C.; Jerome, D.; Henriques, R. T.; Johansen, I.; Bechgaard, K. *Synth. Met.* **1993**, *55*, 654-659.
- (94) Brown, S. E.; Yu, W.; Zomborsky, F.; Alavi, B. *Synth. Met.* **2003**, *137*, 1299-1301.
- (95) Andrieux, A.; Jerome, D.; Bechgaard, K. *J. Physique Lett.* **1981**, *42*, 87-90.
- (96) Creuzet, F.; Bourbonnais, C.; Caron, L. G.; Jerome, D.; Moradpour, A. *Synth. Met.* **1987**, *19*, 277-282.
- (97) Bourbonnais, C.; Wzietek, P.; Creuzet, F.; Jerome, D.; Batail, P.; Bechgaard, K. *Phys. Rev. Lett.* **1989**, *62*, 1532-1535.
- (98) Wzietek, P.; Bourbonnais, C.; Creuzet, F.; Jerome, D.; Bechgaard, K.; Batail, P. *Synth. Met.* **1991**, *41-43*, 2435-2438.
- (99) Valfells, S.; Kuhns, P.; Kleinhammes, A.; Moulton, W.; Brooks, J. S.; Takasaki, S.; Yamada, J.; Anzai, H.; Uji, S. *Synth. Met.* **1997**, *86*, 2109-2110.
- (100) Azevedo, L. J.; Schirber, J. E.; Engler, E. M. *Phys. Rev. B* **1983**, *27*, 5842-5845.

- (101) Jerome, D.; Mazaud, A.; Ribault, M.; Bechgaard, K. *J. Physique Lett.* **1980**, *41*, L95-L98.
- (102) Ribault, M.; Benedek, G.; Jerome, D.; Bechgaard, K. *J. Physique Lett.* **1980**, *41*, L397-L399.
- (103) Lee, I. J.; Brown, S. E.; Clark, W. G.; Kang, W.; Naughton, M. J.; Chaikin, P. M. *Synth. Met.* **2003**, *133-134*, 33-36.
- (104) Lee, I. J.; Brown, S. E.; Clark, W. G.; Strouse, M. J.; Naughton, M. J.; Kang, W.; Chaikin, P. M. *Phys. Rev. Lett.* **2002**, *88*, 017004.
- (105) Lee, I. J.; Chow, D. S.; Clark, W. G.; Strouse, M. J.; Naughton, M. J.; Chaikin, P. M.; Brown, S. E. *Phys. Rev. B: Condens. Matter* **2003**, *68*, 092510.
- (106) Kang, W.; Hannahs, S. T.; Chaikin, P. M. *Phys. Rev. Lett.* **1992**, *69*, 2827-2830.
- (107) Lebed, A. G.; Bak, P. *Phys. Rev. Lett.* **1989**, *63*, 1315-1317.
- (108) Wu, W.; Chaikin, P. M.; Kang, W.; Shinagawa, J.; Yu, W.; Brown, S. E. *Phys. Rev. Lett.* **2005**, *94*, 097004.
- (109) Shinagawa, J.; Wu, W.; Chaikin, P. M.; Kang, W.; Yu, W.; Zhang, F.; Kurosaki, Y.; Parker, C.; Brown, S. E. *J. Low Temp. Phys.* **2006**, *142*, 227-232.
- (110) Auban, P.; Jerome, D.; Lerstrup, K.; Johannsen, I.; Jorgensen, M.; Bechgaard, K. *J. Phys.* **1989**, *50*, 2727-2739.
- (111) Bechgaard, K.; Carneiro, K.; Rasmussen, F. B.; Olsen, M.; Rindorf, G.; Jacobsen, C. S.; Pedersen, H. J.; Scott, J. C. *J. Am. Chem. Soc.* **1981**, *103*, 2440-2442.
- (112) Takahashi, T.; Jerome, D.; Bechgaard, K. *J. Phys.* **1984**, *45*, 945-952.
- (113) Takigawa, M.; Saito, G. *J. Phys. Soc. Jpn.* **1986**, *55*, 1233-1243.
- (114) Takigawa, M.; Saito, G. *Phys. B (Amsterdam, Neth.)* **1986**, *143*, 497-499.
- (115) Zhang, F.; Kurosaki, Y.; Shinagawa, J.; Alavi, B.; Brown, S. E. *Phys. Rev. B: Condens. Matter* **2005**, *72*, 060501.
- (116) Bourbonnais, C.; Creuzet, F.; Jerome, D.; Bechgaard, K.; Moradpour, A. *J. Physique Lett.* **1984**, *45*, 755-765.
- (117) Creuzet, F.; Bourbonnais, C.; Jerome, D.; Bechgaard, K.; Moradpour, A. *Mol. Cryst. Liq. Cryst.* **1985**, *119*, 45-51.

- (118) Shinagawa, J.; Kurosaki, Y.; Zhang, F.; Parker, C.; Brown, S. E.; Jerome, D.; Christensen, J. B.; Bechgaard, K. *Phys. Rev. Lett.* **2007**, *98*, 147002.
- (119) Takahashi, T. *Mol. Cryst. Liq. Cryst.* **1985**, *119*, 113-116.
- (120) Creuzet, F.; Jerome, D.; Bourbonnais, C.; Moradpour, A. *J. Phys. C: Solid State Phys.* **1985**, *18*, L821-L828.
- (121) Takigawa, M.; Saito, G. *Phys. B (Amsterdam, Neth.)* **1986**, *143*, 422-424.
- (122) Jacobsen, C. S.; Pedersen, H. J.; Mortensen, K.; Rindorf, G.; Thorup, N.; Torrance, J. B.; Bechgaard, K. *J. Phys. C: Solid State Phys.* **1982**, *15*, 2651-2663.
- (123) Hiraki, K.; Kang, H.; Nemoto, T.; Satsukawa, H.; Takahashi, T.; Jo, Y. J.; Kang, W.; Chung, O. H. *J. Phys. IV* **2004**, *114*, 103-105.
- (124) Jo, Y. J.; Choi, E. S.; Kang, H.; Kang, W.; Seo, I. S.; Chung, O.-H. *Phys. Rev. B* **2003**, *67*, 014516.
- (125) Satsukawa, H.; Kang, H.; Hiraki, K.; Takahashi, T.; Jo, Y.; Kang, W.; Chung, O.-H. *Synth. Met.* **2005**, *153*, 417-420.
- (126) Takahashi, T.; Hiraki, K.; Moroto, S.; Tajima, N.; Takano, Y.; Kubo, Y.; Satsukawa, H.; Chiba, R.; Yamamoto, H. M.; Kato, R.; Naito, T. *J. Phys. IV* **2005**, *131*, 3-8.
- (127) Hiraki, K.; Takahashi, T.; Kondo, R.; Kagoshima, S.; Hasegawa, T.; Mochida, T.; Iwasa, Y. *Synth. Met.* **2001**, *120*, 917-918.
- (128) Hiraki, K.; Takahashi, T.; Kondo, R.; Kagoshima, S.; Hasegawa, T.; Mochida, T.; Iwasa, Y. *J. Phys. Chem. Solids* **2001**, *62*, 401-403.
- (129) Hiraki, K.; Furuta, S.; Takahashi, T.; Kondo, R.; Kagoshima, S.; Hasegawa, T.; Mochida, T.; Iwasa, Y. *Phys. Rev. B* **2002**, *66*, 035104.
- (130) Takano, Y.; Hiraki, K.; Takahashi, T.; Kondo, R.; Kagoshima, S.; Hasegawa, T.; Mochida, T.; Iwasa, Y. *J. Low Temp. Phys.* **2006**, *143*, 647-650.
- (131) Yagubskii, É. B.; Shchegolev, I. F.; Laukhin, V. N.; Kononovich, P. A.; Karatsovnik, M. V.; Zvarykina, A. V.; Buravov, L. I. *JETP Lett.* **1984**, *39*, 12-16.
- (132) Uozaki, H.; Endo, S.; Matsui, H.; Ueda, K.; Sugimoto, T.; Toyota, N. *Synth. Met.* **1999**, *103*, 1983.

- (133) Kobayashi, A.; Udagawa, T.; Tomita, H.; Naito, T.; Kobayashi, H. *Chem. Lett.* **1993**, 2179-2182.
- (134) Kobayashi, H.; Udagawa, T.; Tomita, H.; Bun, K.; Naito, T.; Kobayashi, A. *Chem. Lett.* **1993**, 1559-1562.
- (135) Takagi, S.; Maruta, D.; Sasaki, H.; Uozaki, H.; Tsuchiya, H.; Abe, Y.; Ishizaki, Y.; Negishi, E.; Matsui, H.; Endo, S.; Toyota, N. *Synth. Met.* **2003**, *137*, 1297-1298.
- (136) Takagi, S.; Maruta, D.; Sasaki, H.-I.; Uozaki, H.; Tsuchiya, H.; Abe, Y.; Ishizaki, Y.; Negishi, E.; Matsui, H.; Endo, S.; Toyota, N. *J. Phys. Soc. Jpn.* **2003**, *72*, 483-486.
- (137) Wu, G.; Clark, W. G.; Brown, S. E.; Brooks, J. S.; Kobayashi, A.; Kobayashi, H. *Phys. Rev. B* **2007**, *76*, 132510.
- (138) Endo, S.; Goto, T.; Fukase, T.; Matsui, H.; Uozaki, H.; Tsuchiya, H.; Negishi, E.; Ishizaki, Y.; Abe, Y.; Toyota, N. *Synth. Met.* **2003**, *133-134*, 557-558.
- (139) Hiraki, K.; Mayaffre, H.; Horvatic, M.; Berthier, C.; Tanaka, H.; Kobayashi, A.; Kobayashi, H.; Takahashi, T. *J. Low Temp. Phys.* **2006**, *142*, 185-190.
- (140) Hiraki, K.; Mayaffre, H.; Horvatic, M.; Berthier, C.; Uji, S.; Yamaguchi, T.; Tanaka, H.; Kobayashi, A.; Kobayashi, H.; Takahashi, T. *J. Phys. Soc. Jpn.* **2007**, *76*, 124708.
- (141) Fujiyama, S.; Takigawa, M.; Kikuchi, J.; Kodama, K.; Nakamura, T.; Fujiwara, E.; Fujiwara, H.; Cui, H.; Kobayashi, H. *Synth. Met.* **2005**, *154*, 253-256.
- (142) Fujiyama, S.; Takigawa, M.; Kikuchi, J.; Cui, H.-B.; Fujiwara, H.; Kobayashi, H. *Phys. Rev. Lett.* **2006**, *96*, 217001.
- (143) Jaccarino, V.; Peter, M. *Phys. Rev. Lett.* **1962**, *9*, 290-292.
- (144) Jacques-Silva, M. C.; Nogueira, C. W.; Broch, L. C.; Flores, É. M. M.; Rocha, J. B. T. *Pharmacol. Toxicol.* **2001**, *88*, 119-125.
- (145) Rossato, J. I.; Ketzer, L. A.; Centurião, F. B.; Silva, S. J. N.; Lüdtke, D. S.; Zeni, G.; Braga, A. L.; Rubin, M. A.; Rocha, J. B. T. *Neurochem. Res.* **2002**, *27*, 297-303.
- (146) Maciel, E. N.; Flores, É. M. M.; Rocha, J. B. T.; Folmer, V. *Bull. Environ. Contam. Toxicol.* **2003**, *70*, 470-476.
- (147) Wirth, T. *Molecules* **1998**, *3*, 164-166.



- (148) Wilson, S. R.; Zucker, P. A.; Huang, R.-R. C.; Spector, A. *J. Am. Chem. Soc.* **1989**, *111*, 5936-5939.
- (149) Balzer, G.; Duddeck, H.; Fleischer, U.; Röhr, F. *Fresenius J. Anal. Chem.* **1997**, *357*, 473-476.
- (150) Potrzebowski, M. J.; Michalska, M.; Blaszczyk, J.; Wieczorek, M. W.; Ciesielski, W.; Kazmierski, S.; Pluskowski, J. *J. Org. Chem.* **1995**, *60*, 3139-3148.
- (151) Isab, A. A.; Wazeer, M. I. M. *J. Coord. Chem.* **2005**, *58*, 529-537.
- (152) Wazeer, M. I. M.; Isab, A. A. *Spectrochim. Acta, Part A* **2005**, *62*, 880-885.
- (153) Fettouhi, M.; Wazeer, M. I. M.; Ahmad, S.; Isab, A. A. *Polyhedron* **2004**, *23*, 1-4.
- (154) Wazeer, M. I. M.; Isab, A. A.; Ahmad, S. *J. Coord. Chem.* **2005**, *58*, 391-398.
- (155) Isab, A. A.; Wazeer, M. I. M.; Fettouhi, M.; Ahmad, S.; Ashraf, W. *Polyhedron* **2006**, *25*, 2629-2636.
- (156) Al-Amri, A.-H. D.; Fettouhi, M.; Wazeer, M. I. M.; Isab, A. A. *Inorg. Chem. Commun.* **2005**, *8*, 1109-1112.
- (157) Subramanian, R.; Govindaswamy, N.; Santos, R. A.; Koch, S. A.; Harbison, G. S. *Inorg. Chem.* **1998**, *37*, 4929-4933.
- (158) Herberhold, M.; Hübner, M.; Wrackmeyer, B. *Z. Naturforsch., B: Chem. Sci.* **1993**, *48*, 940-950.
- (159) Barrie, P. J.; Clark, R. J. H.; Withnall, R.; Chung, D.-Y.; Kim, K.-W.; Kanatzidis, M. G. *Inorg. Chem.* **1994**, *33*, 1212-1216.
- (160) Harris, R. K.; Sebald, A. *Magn. Reson. Chem.* **1987**, *25*, 1058-1062.
- (161) Gay, I. D.; Jones, C. H. W.; Sharma, R. D. *J. Magn. Reson.* **1989**, *84*, 501-514.
- (162) Batchelor, R. J.; Einstein, F. W. B.; Gay, I. D.; Gu, J.-H.; Pinto, B. M. *J. Organomet. Chem.* **1991**, *411*, 147-157.
- (163) Herberhold, M.; Dörfler, U.; Milius, W.; Wrackmeyer, B. *J. Organomet. Chem.* **1995**, *492*, 59-63.
- (164) Wrackmeyer, B.; Distler, B.; Gerstmann, S.; Herberhold, M. *Z. Naturforsch., B: Chem. Sci.* **1993**, *48*, 1307-1314.

- (165) Maaninen, A.; Ahlgren, M.; Ingman, P.; Laitinen, R. S. *Phosphorus Sulfur Silicon Relat. Elem.* **2001**, *169*, 161-164.
- (166) Dreeskamp, H.; Stegmeier, G. *Z. Naturforsch., A* **1967**, *22*, 1458-1464.
- (167) Kennedy, J. D.; McFarlane, W.; Pyne, G. S.; Wrackmeyer, B. *Dalton Trans.* **1975**, 386-390.
- (168) Kennedy, J. D.; McFarlane, W.; Wrackmeyer, B. *Inorg. Chem.* **1976**, *16*, 1299-1302.
- (169) Wrackmeyer, B.; Horchler, K. *Magn. Reson. Chem.* **1990**, *28*, 56-61.
- (170) Wrackmeyer, B.; Zhou, H. *Magn. Reson. Chem.* **1990**, *28*, 1066-1069.
- (171) Christendat, D.; Butler, I. S.; Gilson, D. F. R.; Morin, F. G. *Can. J. Chem.* **1999**, *77*, 1892-1898.
- (172) Willans, M. J.; Demko, B. A.; Wasylshen, R. E. *Phys. Chem. Chem. Phys.* **2006**, *8*, 2733-2743.
- (173) Lundin, A. G.; Moskvich, Y. N.; Sukhovskii, A. A. *Pis'ma Zh. Eksp. Teor. Fiz.* **1978**, *27*, 623-625.
- (174) Vinogradova, I. S.; Sukhovskii, A. A.; Khizbullin, F. F. *J. Solid State Chem.* **1989**, *78*, 209-214.
- (175) Krieger, A. I.; Lundin, A. G.; Moskvich, Y. N.; Sukhovskii, A. A. *Phys. Status Solidi A* **1980**, *58*, K81-K84.
- (176) Krieger, A. I.; Moskvich, Y. N.; Sukhovskii, A. A.; Faleev, O. V. *Phys. Status Solidi A* **1982**, *69*, 455-466.
- (177) Hou, X.; Kirkpatrick, R. J. *Chem. Mat.* **2000**, *12*, 1890-1897.
- (178) Wickleder, M. S.; Buchner, O.; Wickleder, C.; el Sheik, S.; Brunklaus, G.; Eckert, H. *Inorg. Chem.* **2004**, *43*, 5860-5864.
- (179) Haas, H.; Jansen, M. *Z. Anorg. Allg. Chem.* **2000**, *626*, 1174-1178.
- (180) Topic, B.; Vonkienlin, A.; Golzhauser, A.; Haeberlen, U.; Blinc, R. *Phys. Rev. B* **1988**, *38*, 8625-8632.
- (181) Moskvich, Y. N.; Sukhovskii, A. A.; Sorokin, A. A.; Lundin, A. G. *Fiz. Tverd. Tela (Leningrad)* **1980**, *22*, 232-235.

- (182) Aleksandrova, I. P.; Moskvich, Y. N.; Rozanov, O. V.; Sadreev, A. F.; Seryukova, I. V.; Sukhovskiy, A. A. *Ferroelectrics* **1986**, *67*, 63-84.
- (183) Rozanov, O. V.; Moskvich, Y. N.; Sukhovskii, A. A. *Fiz. Tverd. Tela (Leningrad)* **1983**, *25*, 376-380.
- (184) Haas, A.; Jansen, M. Z. *Anorg. Allg. Chem.* **2001**, *627*, 1313-1318.
- (185) Aleksandrova, I. P.; Rozanov, O. V.; Sukhovskii, A. A.; Moskvich, Y. N. *Fiz. Tverd. Tela (Leningrad)* **1982**, *24*, 1677-1680.
- (186) Rozanov, O. V.; Moskvich, Y. N.; Sukhovskii, A. A.; Aleksandrova, I. P. *Izv. Akad. Nauk SSSR, Ser. Khim.* **1983**, *47*, 719-722.
- (187) Sukhovskii, A. A.; Aleksandrova, I. P.; Moskvich, Y. N. *Phys. Status Solidi A* **1989**, *111*, 477-483.
- (188) Aleksandrova, I. P.; Rosanov, O. V.; Sukhovskiy, A. A.; Moskvich, Y. N. *Phys. Lett. A* **1983**, *95*, 339-342.
- (189) Aleksandrova, I. P.; Moskvich, Y. N.; Rozanov, O. V.; Sukhovskiy, A. A. *Ferroelectr., Lett. Sect.* **1984**, *1*, 131-134.
- (190) Aleksandrova, I. P.; Moskvich, Y. N.; Razanov, O. V.; Sadreev, A. F.; Seryukova, I. V.; Sukhovskiy, A. A. *Jpn. J. Appl. Phys., Part 1* **1985**, *24*, 856-858.
- (191) Sukhovskiy, A. A.; Moskvich, Y. N.; Rozanov, O. V.; Aleksandrova, I. P. *Ferroelectr., Lett. Sect.* **1984**, *3*, 45-52.
- (192) Sukhovskii, A. A.; Moskvich, Y. N.; Rozanov, O. V.; Aleksandrova, I. P. *Fiz. Tverd. Tela (Leningrad)* **1986**, *28*, 3368-3373.
- (193) Moskvich, Y. N.; Rozanov, O. V.; Sukhovskiy, A. A.; Aleksandrova, I. P. *Ferroelectrics* **1985**, *63*, 83-89.
- (194) Yoshida, Y.; Matsuo, Y.; Ikehata, S. *Solid State Ionics* **2005**, *176*, 2457-2460.
- (195) Bryce, D. L.; Bernard, G. M.; Gee, M.; Lumsden, M.; Eichele, K.; Wasylshen, R. E. *Can. J. Anal. Sci. Spectrosc.* **2001**, *46*, 46-82.
- (196) Lindsay, R. *Phys. Rev.* **1951**, *84*, 569-571.
- (197) Jones, E. D. *Phys. Lett.* **1965**, *18*, 98-99.
- (198) Jones, E. D. *Phys. Rev.* **1966**, *151*, 315-324.

- (199) Koch, W.; Lutz, O.; Nolle, A. *Z. Phys. A: Hadrons Nucl.* **1978**, *289*, 17-20.
- (200) Bastow, T. J. *Mater. Australasia* **1987**, *19*, 12.
- (201) Bastow, T. J.; Stuart, S. N. *Phys. Status Solidi B* **1988**, *145*, 719-728.
- (202) Francisco, R. H. P.; Tepe, T.; Eckert, H. *J. Solid State Chem.* **1993**, *107*, 452-459.
- (203) Gaudin, E.; Boucher, F.; Evain, M.; Taulelle, F. *Chem. Mat.* **2000**, *12*, 1715-1720.
- (204) Dean, P. A. W.; Goh, L. Y.; Gay, I. D.; Sharma, R. D. *J. Organomet. Chem.* **1997**, *533*, 1-5.
- (205) Moran, K. L.; Gier, T. E.; Harrison, W. T. A.; Stucky, G. D.; Eckert, H.; Eichele, K.; Wasylshen, R. E. *J. Am. Chem. Soc.* **1993**, *115*, 10553-10558.
- (206) Barrie, P. J.; Clark, R. J. H.; Chung, D. Y.; Chakrabarty, D.; Kanatzidis, M. G. *Inorg. Chem.* **1995**, *34*, 4299-4304.
- (207) Hamard, C.; Auffret, V.; Peña, O.; Le Floch, M.; Nowak, B.; Wojakowski, A. *Phys. B (Amsterdam, Neth.)* **2000**, *291*, 339-349.
- (208) Ratcliffe, C. I.; Yu, K.; Ripmeester, J. A.; Zaman, M. B.; Badarau, C.; Singh, S. *Phys. Chem. Chem. Phys.* **2006**, *8*, 3510-3519.
- (209) Moran, K. L.; Ott, A. W.; Gier, T. E.; Harrison, W. T. A.; Eckert, H.; Stucky, G. *D. Mater. Res. Soc. Symp. Proc.* **1992**, *242*, 249-254.
- (210) Thayer, A. M.; Steigerwald, M. L.; Duncan, T. M.; Douglass, D. C. *Phys. Rev. Lett.* **1988**, *60*, 2673-2676.
- (211) Berrettini, M. G.; Braun, G.; Hu, J. G.; Strouse, G. F. *J. Am. Chem. Soc.* **2004**, *126*, 7063-7070.
- (212) Hiraoka, K.; Kojima, K.; Shinohara, T.; Hihara, T.; Wachter, P. *Phys. B (Amsterdam, Neth.)* **1997**, *230-232*, 133-135.
- (213) Brog, K. C.; Kenan, R. P. *Phys. Rev. B* **1973**, *8*, 1492-1499.
- (214) Suzuki, H.; Komaru, T.; Hihara, T.; Koi, Y. *J. Phys. Soc. Jpn.* **1971**, *30*, 288.
- (215) Budnick, J. I.; Raj, K.; Burch, T. J.; Holtzberg, F. *J. Phys. Colloques* **1971**, *32*, 763-765.
- (216) Kawakami, M. *J. Magn. Magn. Mater.* **1985**, *52*, 446-448.

- (217) Cichorek, T.; Michalak, R.; Kromer, F.; Müller, J.; Steglich, F.; Wojakowski, A.; Henkie, Z. *Acta Phys. Pol., B* **2001**, *32*, 3399-3403.
- (218) Dupree, R.; Warren, W. W.; DiSalvo, F. J. *Phys. Rev. B: Condens. Matter* **1977**, *16*, 1001-1007.
- (219) Thompson, A. H.; Silbernagel, B. G. *Phys. Rev. B* **1979**, *19*, 3420-3426.
- (220) Skripov, A. V.; Sibirtsev, D. S.; Cherpanov, Y. G.; Aleksashin, B. A. *J. Phys.: Condens. Matter* **1995**, *7*, 4479-4487.
- (221) Borsa, F.; Torgeson, D. R.; Shanks, H. R. *Phys. Rev. B: Condens. Matter* **1977**, *15*, 4576-4579.
- (222) Wada, S. *J. Phys. Soc. Jpn.* **1977**, *42*, 764-769.
- (223) Ehrenfreund, E.; Gossard, A. C.; Gamble, F. R.; Geballe, T. H. *J. Appl. Phys.* **1971**, *42*, 1491-1493.
- (224) Pfeiffer, L.; Walstedt, R. W.; Bell, R. F.; Kovacs, T. *Phys. Rev. Lett.* **1982**, *49*, 1162-1165.
- (225) Suits, B. H.; Couturié, S.; Slichter, C. P. *Phys. Rev. Lett.* **1980**, *45*, 194-197.
- (226) Suits, B. H.; Couturié, S.; Slichter, C. P. *Phys. Rev. B: Condens. Matter* **1981**, *23*, 5142-5151.
- (227) McMillan, W. L. *Phys. Rev. B* **1975**, *12*, 1187-1196.
- (228) McMillan, W. L. *Phys. Rev. B* **1976**, *14*, 1496-1502.
- (229) Silbernagel, B. G. *Solid State Commun.* **1975**, *17*, 361-365.
- (230) Berthier, C.; Chabre, Y.; Segransan, P. *Phys. B (Amsterdam, Neth.)* **1980**, *99*, 107-116.
- (231) Berthier, C.; Chabre, Y.; Segransan, P.; Chevalier, P.; Trichet, L.; Le Mehaute, A. *Solid State Ionics* **1981**, *5*, 379-382.
- (232) Chabre, Y.; Berthier, C.; Segransan, P.; Trichet, L.; Deniard, P. *Solid State Ionics* **1983**, *9 & 10*, 467-470.
- (233) Chabre, Y.; Berthier, C.; Segransan, P. *J. Physique Lett.* **1983**, *44*, L619-L624.
- (234) Chabre, Y. *Mater. Res. Soc. Symp. Proc.* **1989**, *135*, 265-270.

- (235) Ledoux, M. J.; GSegura, Y.; Panissod, P. *Prepr. - Am. Chem. Soc., Div. Pet. Chem.* **1990**, *35*, 217-220.
- (236) Panissod, P.; Krill, G.; Lahrichi, M.; Lapierre, M. F. *Phys. Lett. A* **1976**, *59*, 221-222.
- (237) Panissod, P.; Larhichi, M.; Lapierre-Ravet, M. F. *Solid State Commun.* **1979**, *31*, 273-276.
- (238) Adachi, K.; Sato, K.; Takeda, M. *J. Phys. Soc. Jpn.* **1969**, *26*, 631-638.
- (239) Inoue, N.; Yasuoka, H.; Ogawa, S. *J. Phys. Soc. Jpn.* **1980**, *48*, 850-856.
- (240) Gautier, F.; Krill, G.; Lapierre, M. F.; Panissod, P.; Robert, C.; Czjzek, G.; Fink, J.; Schmidt, H. *Phys. Lett.* **1975**, *53A*, 31-33.
- (241) Krill, G.; Panissod, P.; Lapierre, M. F.; Gautier, F.; Robert, C.; Czjzek, G.; Fink, J.; Schmidt, H.; Kuentzler, R. *J. Phys. Colloques* **1976**, *37*, 23-27.
- (242) Hamada, K.; Takagi, S.; Maruta, D.; Matsuura, M.; Hiraka, H.; Yamada, K.; Endoh, Y. *Phys. B (Amsterdam, Neth.)* **2000**, *281 & 282*, 641-643.
- (243) Yokoyama, H.; Watanabe, R.; Chiba, S. *J. Phys. Soc. Jpn.* **1967**, *23*, 450.
- (244) Stauss, G. H.; Rubinstein, M.; Feinleib, J.; Dwight, K.; Menyuk, N.; Wold, A. J. *Appl. Phys.* **1968**, *39*, 667-668.
- (245) Berger, S. B.; Budnick, J. I.; Burch, T. J. *J. Appl. Phys.* **1968**, *39*, 658-660.
- (246) Moskvina, A. S.; Shemyakov, A. A.; Prokopenko, V. K. *Fiz. Tverd. Tela (Leningrad)* **1989**, *31*, 293-296.
- (247) Kovtun, N. M.; Prokopenko, V. K.; Shemyakov, A. A.; Aminov, T. G.; Shabunina, G. G. *Fiz. Tverd. Tela (Leningrad)* **1982**, *24*, 2814-2815.
- (248) Berger, S. B.; Budnick, J. I.; Burch, T. J. *Phys. Rev.* **1969**, *179*, 272-274.
- (249) Németh, L.; Matus, P.; Kriza, G.; Alavi, B. *Synth. Met.* **2001**, *120*, 1007-1008.
- (250) Németh, L.; Kriza, G.; Matus, P.; Alavi, B. *J. Phys. IV* **2005**, *131*, 357-358.
- (251) Bastow, T. J. *Solid State Nucl. Magn. Reson.* **1998**, *12*, 191-199.
- (252) Takagi, S.; Suzuki, H.; Ochiai, A.; Suzuki, T. *J. Magn. Magn. Mater.* **1992**, *116*, 77-79.

- (253) Takagi, S.; Suzuki, H.; Ochiai, A.; Suzuki, T. *J. Phys. Soc. Jpn.* **1993**, *62*, 2861-2868.
- (254) Takagi, S.; Suzuki, H.; Ochiai, A.; Suzuki, T.; Amato, A.; Feyerherm, R.; Gygax, F. N.; Schenck, A. *Phys. B (Amsterdam, Neth.)* **1993**, *186-188*, 422-424.
- (255) Fischer, Ø. *Appl. Phys.* **1978**, *16*, 1-28.
- (256) Hamard, C.; Le Floch, M.; Peña, O.; Wojakowski, A. *Phys. B (Amsterdam, Neth.)* **1999**.
- (257) Knoll, R.; Goren, S. D.; Korn, C.; Shames, A.; Perrin, C.; Privalov, A.; Vieth, H. *M. Phys. B (Amsterdam, Neth.)* **2002**, *324*, 157-166.
- (258) Zhang, X.-H.; Bureau, B.; Adam, J.-L.; Lucas, J. *Verre (Paris, Fr.)* **2004**, *10*, 22-27.
- (259) Bureau, B.; Zhang, X.-H.; Smektala, F.; Adam, J.-L.; Troles, J.; Ma, H.-L.; Boussard-Plédel, C.; Lucas, J.; Lucas, P.; Le Coq, D.; Riley, M. R.; Simmons, J. H. *J. Non-Cryst. Solids* **2004**, *345 & 346*, 276-283.
- (260) Lathrop, D.; Eckert, H. *J. Am. Chem. Soc.* **1990**, *112*, 9017-9019.
- (261) Maxwell, R.; Eckert, H. *J. Am. Chem. Soc.* **1994**, *116*, 682-689.
- (262) Maxwell, R.; Lathrop, D.; Eckert, H. *J. Non-Cryst. Solids* **1995**, *180*, 244-250.
- (263) Pietrass, T.; Seydoux, R.; Roth, R. E.; Eckert, H.; Pines, A. *Solid State Nucl. Magn. Reson.* **1997**, *8*, 265-267.
- (264) Golovchak, R.; Shpotyuk, O.; Kozdras, A.; Bureau, B.; Vlcek, M.; Ganjoo, A.; Jain, H. *Philos. Mag.* **2007**, *87*, 4323-4334.
- (265) Ueda, S.; Shimizu, T. *Phys. Status Solidi B* **1979**, *95*, 279-282.
- (266) Ueda, S.; Shimizu, T. *Phys. Status Solidi B* **1978**, *88*, K1-K3.
- (267) Batchelor, R. J.; Einstein, F. W. B.; Gay, I. D.; Jones, C. H. W.; Sharma, R. D. *Inorg. Chem.* **1993**, *32*, 4378-4383.
- (268) Munson, E. J.; Kheir, A. A.; Haw, J. F. *J. Phys. Chem.* **1993**, *97*, 7321-7327.
- (269) Kataoka, T.; Watanabe, S.-I.; Yamamoto, K.; Yoshimatsu, M.; Tanabe, G.; Muraoka, O. *J. Org. Chem.* **1998**, *63*, 6382-6386.

(270) Raupach, M.; Barron, P. F.; Thompson, J. G. *Clays Clay Miner.* **1987**, *35*, 208-219.



## Chapter 3

### Theory and Methods

#### 3.1 NMR Interactions

The solid-state NMR Hamiltonian relevant to the systems investigated in this thesis may be written as

$$\hat{\mathcal{H}} = \hat{\mathcal{H}}_Z + \hat{\mathcal{H}}_\sigma + \hat{\mathcal{H}}_D + \hat{\mathcal{H}}_J + \hat{\mathcal{H}}_Q \quad [3.1]$$

where the contributing terms in equation 3.1 describe the Zeeman, nuclear magnetic shielding, direct dipolar, indirect spin-spin, and quadrupolar interactions, respectively.<sup>1-4</sup>

The Zeeman interaction details the interaction of the nuclear spins with the static externally applied magnetic field,  $\mathbf{B}_0$ , while the remaining terms are one- and two-spin internal Hamiltonians that are derived from the explicit nuclear magnetic properties of the system.

In Cartesian form, all of the above NMR spin interactions may be written in the following structure

$$\hat{\mathcal{H}}_A = c \mathbf{I} \cdot \mathbf{A} \cdot \mathbf{S} = c \begin{bmatrix} I_x & I_y & I_z \end{bmatrix} \begin{bmatrix} A_{xx} & A_{xy} & A_{xz} \\ A_{yx} & A_{yy} & A_{yz} \\ A_{zx} & A_{zy} & A_{zz} \end{bmatrix} \begin{bmatrix} S_x \\ S_y \\ S_z \end{bmatrix} \quad [3.2]$$

where the constant  $c$  depends on the nature of the interaction and may or may not be equal to unity,  $\mathbf{I}$  is a nuclear spin operator,  $\mathbf{A}$  is a second-rank interaction tensor, and  $\mathbf{S}$  is a vector that may be a second spin operator or, for example, an applied magnetic field. In the following sub-sections each of the above mentioned NMR interactions will be discussed in detail.

### 3.1.1 The Zeeman Interaction

The fundamental interaction giving rise to nuclear magnetic resonance is the Zeeman interaction. The corresponding Zeeman Hamiltonian describes the interaction of the nuclear spin,  $\mathbf{I}$ , and an external applied magnetic field,  $\mathbf{B}_0$ :

$$\hat{\mathcal{H}}_Z = \hbar \mathbf{I} \cdot \mathbf{Z} \cdot \mathbf{B}_0 \quad [3.3]$$

where  $\mathbf{Z}$  represents the magnetogyric ratio of spin  $\mathbf{I}$  and is equal to  $-\gamma_1 \mathbf{1}$ , where  $\mathbf{1}$  corresponds to the unit tensor. The vector  $(B_x, B_y, B_z)$  describes the Cartesian representation of  $\mathbf{B}_0$ ; however, one is typically only concerned with the largest component of the  $\mathbf{B}_0$  vector. When this magnetic field is chosen to be along the z-direction the resultant Zeeman Hamiltonian becomes

$$\hat{\mathcal{H}}_Z = -\gamma_1 \hbar I_z B_z \quad [3.4]$$

where the z-component of the  $\mathbf{B}_0$  field is commonly referred to as  $B_0$ . Under the application of such a magnetic field, for a spin- $1/2$  nucleus, equation 3.4 yields two possible states with different energies:

$$E_{Z,m_I} = -\gamma_1 \hbar m_I B_0 \quad [3.5]$$

It is possible to induce transitions between these spin states via the application of electromagnetic radiation of the appropriate frequency. The energy difference between the states, in frequency units, is given by the Larmor equation:

$$\nu_L = \frac{|\gamma_1| B_0}{2\pi} \quad [3.6]$$

where  $\nu_L$  is referred to as the Larmor frequency.

### 3.1.2 The Nuclear Magnetic Shielding Interaction

One of the primary sources of chemical information arising from nuclear magnetic resonance stems from the nuclear magnetic shielding interaction. The external applied magnetic field induces currents in the electrons surrounding the nuclei that result in induced magnetic fields, which are proportional to  $\mathbf{B}_0$ , at the nuclei themselves.<sup>3</sup> The corresponding Hamiltonian may be represented by

$$\hat{\mathcal{H}}_{\sigma} = \hbar\gamma_{\text{I}} \mathbf{I} \cdot \boldsymbol{\sigma} \cdot \mathbf{B}_0 \quad [3.7]$$

where  $\gamma_{\text{I}}$ ,  $\mathbf{I}$ , and  $\mathbf{B}_0$  are the magnetogyric ratio of nucleus  $\text{I}$ , its nuclear spin operator, and the external applied magnetic field, as mentioned previously. The nuclear magnetic shielding tensor,  $\boldsymbol{\sigma}$ , can be described by a second-rank tensor defined by:

$$\boldsymbol{\sigma} = \begin{bmatrix} \sigma_{xx} & \sigma_{xy} & \sigma_{xz} \\ \sigma_{yx} & \sigma_{yy} & \sigma_{yz} \\ \sigma_{zx} & \sigma_{zy} & \sigma_{zz} \end{bmatrix} \quad [3.8]$$

In general, any second-rank tensor can be separated into symmetric and antisymmetric components, of which those of the nuclear magnetic shielding tensor are:

$$\boldsymbol{\sigma}^{\text{sym}} = \frac{1}{2}(\boldsymbol{\sigma} + \boldsymbol{\sigma}^{\text{T}}) = \frac{1}{2} \begin{bmatrix} 2\sigma_{xx} & \sigma_{xy} + \sigma_{yx} & \sigma_{xz} + \sigma_{zx} \\ \sigma_{yx} + \sigma_{xy} & 2\sigma_{yy} & \sigma_{yz} + \sigma_{zy} \\ \sigma_{zx} + \sigma_{xz} & \sigma_{zy} + \sigma_{yz} & 2\sigma_{zz} \end{bmatrix} \quad [3.9]$$

$$\boldsymbol{\sigma}^{\text{antisym}} = \frac{1}{2}(\boldsymbol{\sigma} - \boldsymbol{\sigma}^{\text{T}}) = \frac{1}{2} \begin{bmatrix} 0 & \sigma_{xy} - \sigma_{yx} & \sigma_{xz} - \sigma_{zx} \\ \sigma_{yx} - \sigma_{xy} & 0 & \sigma_{yz} - \sigma_{zy} \\ \sigma_{zx} - \sigma_{xz} & \sigma_{zy} - \sigma_{yz} & 0 \end{bmatrix} \quad [3.10]$$

where  $\boldsymbol{\sigma}^{\text{T}}$  is the transpose of  $\boldsymbol{\sigma}$ .<sup>5</sup> In the zeroth order approximation, the line shapes in the NMR spectra of solids do not depend on  $\boldsymbol{\sigma}^{\text{antisym}}$ , and the antisymmetric components are

not considered further.<sup>1,6</sup> Hereafter, the nuclear magnetic shielding tensor refers explicitly to the symmetric component of the nuclear magnetic shielding tensor. In the principal axis system, PAS, of  $\sigma^{\text{sym}}$  the nuclear magnetic shielding tensor attains a diagonal tensor with all off-diagonal components equal to zero.

$$\sigma^{\text{sym}} = \frac{1}{2} \begin{bmatrix} 2\sigma_{xx} & \sigma_{xy} + \sigma_{yx} & \sigma_{xz} + \sigma_{zx} \\ \sigma_{yx} + \sigma_{xy} & 2\sigma_{yy} & \sigma_{yz} + \sigma_{zy} \\ \sigma_{zx} + \sigma_{xz} & \sigma_{zy} + \sigma_{yz} & 2\sigma_{zz} \end{bmatrix} \xrightarrow[\text{PAS}]{\text{transform}} \begin{bmatrix} \sigma_{11} & 0 & 0 \\ 0 & \sigma_{22} & 0 \\ 0 & 0 & \sigma_{33} \end{bmatrix} \quad [3.11]$$

The diagonal ‘principal’ components, designated  $\sigma_{11}$ ,  $\sigma_{22}$ , and  $\sigma_{33}$ , are ordered by convention such that  $\sigma_{11} \leq \sigma_{22} \leq \sigma_{33}$ .<sup>7</sup> The isotropic average of the nuclear magnetic shielding tensor is given by

$$\sigma_{\text{iso}} = \frac{1}{3} \text{Tr}(\sigma) = \frac{1}{3} \text{Tr}(\sigma^{\text{sym}}) = \frac{\sigma_{11} + \sigma_{22} + \sigma_{33}}{3} \quad [3.12]$$

where  $\sigma_{\text{iso}}$  is the nuclear magnetic shielding constant and describes the shielding experienced by a nucleus in an isotropic medium, such as the rapid tumbling experienced in solution. If the charge distribution about the nucleus is spherically symmetric, the induced field at the nucleus,  $B_{\text{ind}}$ , opposes the applied magnetic field, such that

$$B_{\text{ind}} = -\sigma_{\text{iso}} B_0 \quad [3.13]$$

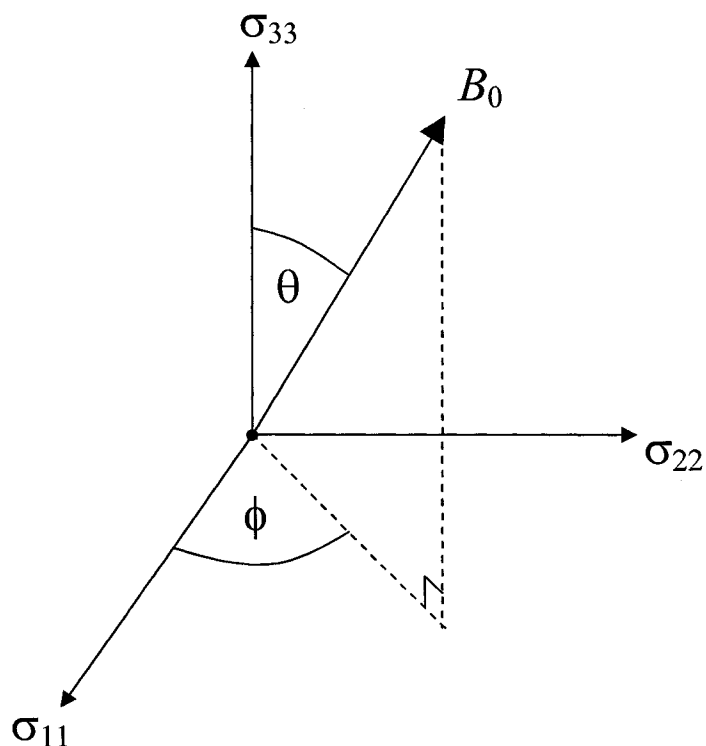
which implies that the local magnetic field experienced by the nucleus is described by:

$$B_{\text{loc}} = (1 - \sigma_{\text{iso}}) B_0 \quad [3.14]$$

Considering the nuclear magnetic shielding tensor,  $\sigma$ , the resonance frequency given in equation 3.6 may be modified to include the nuclear magnetic shielding interaction:

$$\nu(\theta, \phi) = \nu_L \left[ 1 - (\sigma_{11} \sin^2 \theta \cos^2 \phi + \sigma_{22} \sin^2 \theta \sin^2 \phi + \sigma_{33} \cos^2 \theta) \right] \quad [3.15]$$

where the angles  $\theta$  and  $\phi$  define the orientation dependence of the PAS of  $\sigma$  with respect to  $B_0$ , Figure 3.1. Equation 3.15 emphasizes that nuclear magnetic shielding is an orientation-dependent property such that the shielding of a nucleus in a molecule depends on the relative orientation of that molecule with respect to the external applied magnetic field.



**Figure 3.1** Diagram illustrating the orientation of the external applied magnetic field, as defined by the polar angles  $\theta$  and  $\phi$ , with respect to the nuclear magnetic shielding tensor.

Nuclear magnetic shielding is directly related to the experimentally observable property, the chemical shift. The chemical shift,  $\delta$ , is related to magnetic shielding by

$$\delta = \frac{\sigma_{\text{ref}} - \sigma}{1 - \sigma_{\text{ref}}} \quad [3.16]$$

where  $\sigma_{\text{ref}}$  is the shielding of a chosen reference compound. Given that  $\sigma_{\text{ref}}$  is on the order of hundreds of parts per million; i.e.,  $10^{-4}$ , the denominator of equation 3.16 is often approximated by unity such that the chemical shift is nearly equivalent to the difference in nuclear magnetic shielding between the chosen reference compound and that of the chemical species of interest.

Experimentally, one measures the change in frequency of the compound with respect to the resonance frequency of the chosen reference:

$$\delta = \frac{\nu - \nu_{\text{ref}}}{\nu_{\text{ref}}} \times 10^6 \quad [3.17]$$

The principal components of the chemical shift tensor correspond directly to those of the nuclear magnetic shielding tensor; i.e.,  $\delta_{11}$  corresponds to  $\sigma_{11}$ ,  $\delta_{22}$  with  $\sigma_{22}$ , and  $\delta_{33}$  to  $\sigma_{33}$ .<sup>7</sup>

### 3.1.3 The Direct Dipolar Interaction

The direct dipolar coupling experienced between two nuclei is analogous to the classical interaction between two magnetic dipoles.<sup>3,8</sup> The direct dipolar Hamiltonian may be written as

$$\hat{\mathcal{H}}_D = h \mathbf{I} \cdot \mathbf{D} \cdot \mathbf{S} \quad [3.18]$$

where  $\mathbf{I}$  and  $\mathbf{S}$  are the nuclear spin operators corresponding to the two nuclei involved, and  $\mathbf{D}$  is the symmetric and traceless direct dipolar coupling tensor. In its PAS with the internuclear vector,  $r_{\text{IS}}$ , along the z-direction,  $\mathbf{D}$  is diagonal:

$$\mathbf{D} = R_{DD} \begin{bmatrix} 1 & 0 & 0 \\ 0 & 1 & 0 \\ 0 & 0 & -2 \end{bmatrix} \quad [3.19]$$

The direct dipolar coupling constant,  $R_{DD}$ , is given by

$$R_{DD} = \left( \frac{\mu_0}{4\pi} \right) \left( \frac{\hbar}{2\pi} \right) \left( \frac{\gamma_I \gamma_S}{\langle r_{IS}^3 \rangle} \right) \quad [3.20]$$

where  $\mu_0$  is the permeability of a vacuum,  $\gamma_I$  and  $\gamma_S$  are the magnetogyric ratios of the coupled spins,  $I$  and  $S$ , and  $\langle r_{IS}^3 \rangle$  is the motionally-averaged cube of the distance between the coupled nuclei. Measurements of the direct dipolar coupling constant can be used to infer internuclear distances in rigid systems; however, motional averaging results in a reduction in  $R_{DD}$  and a corresponding apparent increase in  $r_{IS}$ .<sup>9</sup>

### 3.1.4 The Indirect Nuclear Spin-Spin Interaction

An additional form of coupling between nuclear spins arises from the electron-mediated interaction between two nuclear magnetic moments.<sup>8</sup> The indirect spin-spin coupling interaction may be represented by the Hamiltonian

$$\hat{\mathcal{H}}_J = h \mathbf{I} \cdot \mathbf{J} \cdot \mathbf{S} \quad [3.21]$$

where  $\mathbf{J}$  is the indirect spin-spin coupling tensor.<sup>1,3</sup> Similar to the nuclear magnetic shielding tensor, in general,  $\mathbf{J}$  contains up to nine independent elements. However, one is typically only concerned with the symmetric portion that, in its PAS, takes the form:

$$\mathbf{J} = \begin{bmatrix} J_{11} & 0 & 0 \\ 0 & J_{22} & 0 \\ 0 & 0 & J_{33} \end{bmatrix} \quad [3.22]$$

The isotropic average of the indirect spin-spin coupling tensor is given by

$$J_{iso} = \frac{1}{3} Tr(\mathbf{J}) = \frac{J_{11} + J_{22} + J_{33}}{3} \quad [3.23]$$

where  $J_{iso}$  is the indirect spin-spin coupling constant and describes the coupling experienced in an isotropic medium. Unlike the direct dipolar interaction the trace of  $\mathbf{J}$  is not zero, and  $J_{iso}$  is manifested in both solution and solid-state NMR spectra.<sup>8</sup> The  $\mathbf{J}$  tensor may be defined by its principal components, which are ordered such that  $|J_{33} - J_{iso}| \geq |J_{11} - J_{iso}| \geq |J_{22} - J_{iso}|$ , or by the derived quantities;  $J_{iso}$  given in equation 3.23 above, the anisotropy,  $\Delta J$ ,

$$\Delta J = J_{33} - \frac{J_{11} + J_{22}}{2} \quad [3.24]$$

and the asymmetry,  $\eta_J = (J_{22} - J_{11})/(J_{33} - J_{iso})$ .

Contributions to the NMR line shape from  $\Delta J$  share an identical orientation dependence with the direct dipolar coupling tensor.<sup>8</sup> Experimentally, one is unable to separate the two and  $R_{DD}$  and  $\Delta J$  must be considered together as an effective direct dipolar coupling constant,  $R_{eff}$ ,

$$R_{eff} = R_{DD} - \frac{\Delta J}{3} \quad [3.25]$$

where  $R_{DD}$  is given in equation 3.20.



### 3.1.5 The Quadrupolar Interaction

Nuclei with spin  $I > \frac{1}{2}$  possess a nuclear quadrupole moment,  $Q$ , as a result of a non-spherical nuclear charge distribution. Nuclear electric quadrupolar interactions are important when considering NMR with these quadrupolar nuclei, as well as for spin- $\frac{1}{2}$  nuclei that are spin-spin coupled to quadrupolar nuclei. The nuclear quadrupole moment interacts with the electric field gradient, EFG, at the nucleus.<sup>10,11</sup> The Hamiltonian describing this interaction may be given by

$$\hat{H}_Q = \frac{eQ}{6I(2I-1)} \mathbf{I} \cdot \mathbf{V} \cdot \mathbf{I} \quad [3.26]$$

where  $\mathbf{V}$  describes the EFG tensor, which is symmetric and traceless. In its PAS, the EFG tensor may be characterized by two parameters consisting of the largest principal component  $eq_{zz} = V_{zz} = \partial^2 V / \partial z^2$ , where  $V$  is the electric potential, and the asymmetry parameter  $\eta_Q = (V_{xx} - V_{yy}) / V_{zz}$ . The product of the nuclear quadrupole moment and the largest principal component of the EFG tensor is known as the nuclear quadrupolar coupling constant,  $C_Q$ ,

$$C_Q = \frac{e^2 Q q_{zz}}{h} \quad [3.27]$$

where  $C_Q$  is expressed in frequency units.

Should the Zeeman interaction not greatly exceed that of the quadrupolar interaction, the energy levels of the quadrupolar nucleus will be quantized by both the applied magnetic field as well as the EFG.<sup>12-14</sup> Under such circumstances, dipolar

coupling between the quadrupolar nucleus and a spin- $\frac{1}{2}$  nucleus may be manifested in NMR spectra, even those from experiments designed to remove direct dipolar couplings such as magic angle spinning (vide infra).

### **3.2 Experimental Techniques in Solid-State NMR**

As mentioned in Chapter 1, NMR of solids is complicated with respect to solution phases by anisotropic contributions to the familiar chemical shift and indirect spin-spin coupling, by additional interactions such as direct dipolar and quadrupolar coupling that are also anisotropic, and commonly by slower nuclear magnetic relaxation rates. These qualities are predominantly the result of highly restricted motion in solids, which allows for much of the information contained in the second-rank interaction tensors to be extracted by the experimentalist. However, in many cases the anisotropic interactions can often produce broad and sometimes featureless line shapes in the corresponding NMR spectrum.

Solid-state NMR spectroscopists often seek ‘solution-like’ spectra of their solid samples, while leaving as much of the orientation-dependent tensorial information available as possible. Theoretical and practical considerations in performing routine solid-state NMR spectroscopy are well reported, of which only a select few are given here.<sup>2,15-17</sup> The combination of magic angle spinning, high-power heteronuclear decoupling, and cross polarization,<sup>18</sup> used predominantly throughout the experiments documented in this thesis, is one of the more common approaches utilized in attaining solid-state NMR spectra of dilute or rare spin- $\frac{1}{2}$  nuclei.

### 3.2.1 Magic Angle Spinning

In many of the NMR Hamiltonians described previously, a common angular dependency of the form

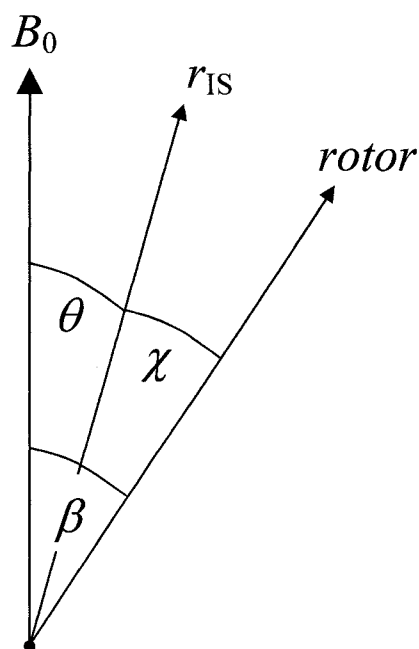
$$(3 \cos^2 \theta - 1) \quad [3.28]$$

is encountered when the interaction is expanded and expressed in polar coordinates. For example, in the direct dipolar Hamiltonian the angle  $\theta$  defines the angle between the internuclear vector,  $r_{IS}$ , and the external applied magnetic field,  $B_0$ . For the time average of equation 3.28 for a sample spinning mechanically about an axis of arbitrary orientation with respect to  $B_0$ , it may be shown<sup>16</sup> that

$$\langle 3 \cos^2 \theta - 1 \rangle = \frac{1}{2} (3 \cos^2 \beta - 1) \langle 3 \cos^2 \chi - 1 \rangle \quad [3.29]$$

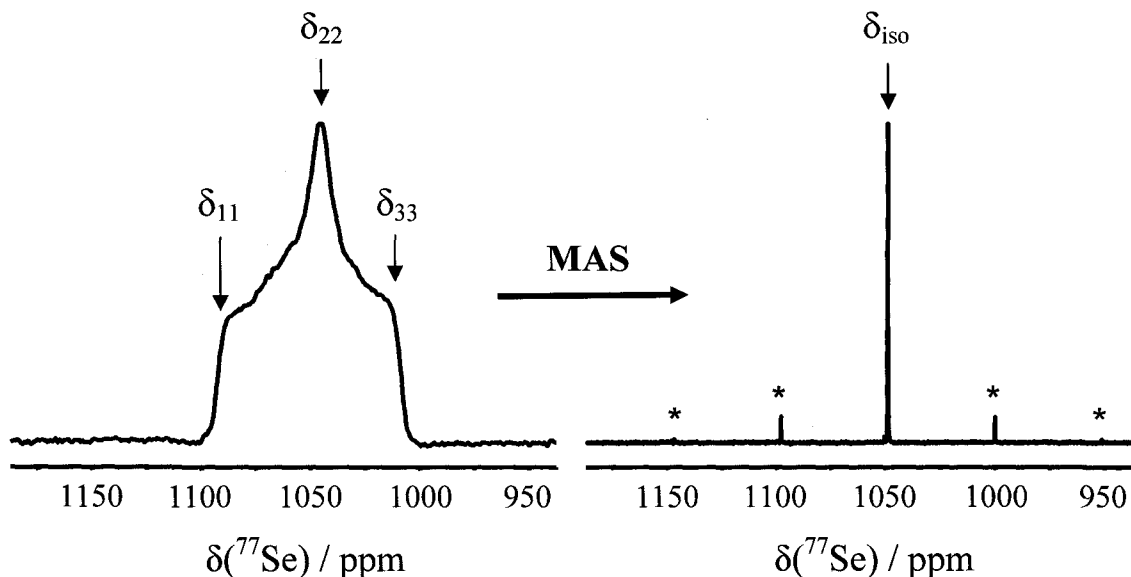
where  $\beta$  corresponds to the arbitrary angle between  $B_0$  and the axis of sample rotation, and  $\chi$  describes the angle between  $r_{IS}$  and the sample rotor axis, Figure 3.2. While the angles  $\theta$  and  $\chi$  are outside the realm of control for the experimentalist,  $\beta$  can be set to any desirable orientation. When  $\beta$  is set to  $54.74^\circ$ ; i.e., the root of  $(3 \cos^2 \beta - 1)$ , the time average of equation 3.28 becomes equal to zero. At this ‘magic’ angle, average isotropic values will be obtained for the various anisotropic interaction(s) of interest; i.e., direct dipolar coupling, anisotropic magnetic shielding, first-order quadrupolar coupling.

Singular, narrow line shapes can be achieved by this so-called magic angle spinning, MAS, only when the rate of sample rotation is significantly greater than the magnitude of the interaction being averaged. Should the rotor spinning frequency,  $\nu_{\text{rot}}$ ,



**Figure 3.2** Relative angles describing the orientation of the external applied magnetic field,  $B_0$ , internuclear vector,  $r_{IS}$ , and the sample rotation, rotor, axes.

be of comparable, or smaller, magnitude than the breadth of the anisotropic interaction then the MAS NMR spectrum will exhibit a series of spinning sidebands flanking either side of the isotropic peak(s), Figure 3.3. These spinning sidebands, collectively referred to as the spinning sideband manifold, are located at integer multiples of the spinning frequency away from their respective isotropic peak. For manifolds resultant from anisotropic magnetic shielding, the positions and relative intensities of the spinning sidebands may be analyzed to yield the principal components of the chemical shift tensor.<sup>19,20</sup> For this reason, slow spinning MAS NMR experiments are often employed to extract information about the anisotropic magnetic shielding interaction, yet remove anisotropies smaller than  $\nu_{rot}$  in magnitude.



**Figure 3.3** The effect of MAS at  $\nu_{\text{rot}} = 3.0$  kHz on the  $^{77}\text{Se}$  NMR spectrum of  $(\text{NH}_4)_2\text{SeO}_4$ . Spinning sidebands are denoted with asterisks.

### 3.2.2 High-Power Heteronuclear Decoupling

High-power decoupling in solid-state NMR primarily refers to the suppression of large direct dipolar interactions between abundant nuclei, such as  $^1\text{H}$  or  $^{19}\text{F}$ , and dilute nuclei, such as  $^{13}\text{C}$  or  $^{77}\text{Se}$ .<sup>21</sup> These heteronuclear direct dipolar couplings are typically too large to be suppressed by MAS alone. Decoupling has the additional effect of removing indirect spin-spin coupling interactions between the abundant and dilute nuclei. For the experiments presented in this thesis the abundant spins being decoupled are always protons. Proton decoupling is accomplished via the application of an rf field, at or near the  $^1\text{H}$  Larmor frequency, during the acquisition of the dilute spin free induction decay, FID.

In comparison to solution NMR spectroscopy, decoupling of the abundant spins in solids requires much more power. Decoupling fields involving protons are on the order of 60-100 kHz, which correspond to power outputs in the range of hundreds of watts.

The efficiency of the decoupling achieved depends largely on the magnitude of the decoupling field with respect to the heteronuclear direct dipolar interaction, and this efficiency is typically measured in the widths of the NMR peaks in the spectrum of the dilute nucleus. Traditional decoupling in the solid state is attained via continuous wave, CW, decoupling; however more advanced decoupling procedures are an active area of research. One such decoupling sequence, which has become a benchmark approach, involves a series of rf pulses of alternating phase. This so-called two-pulse phase-modulated, TPPM,<sup>21</sup> decoupling has the effect as if one were using a higher CW decoupling field.<sup>15</sup>

### 3.2.3 Cross Polarization

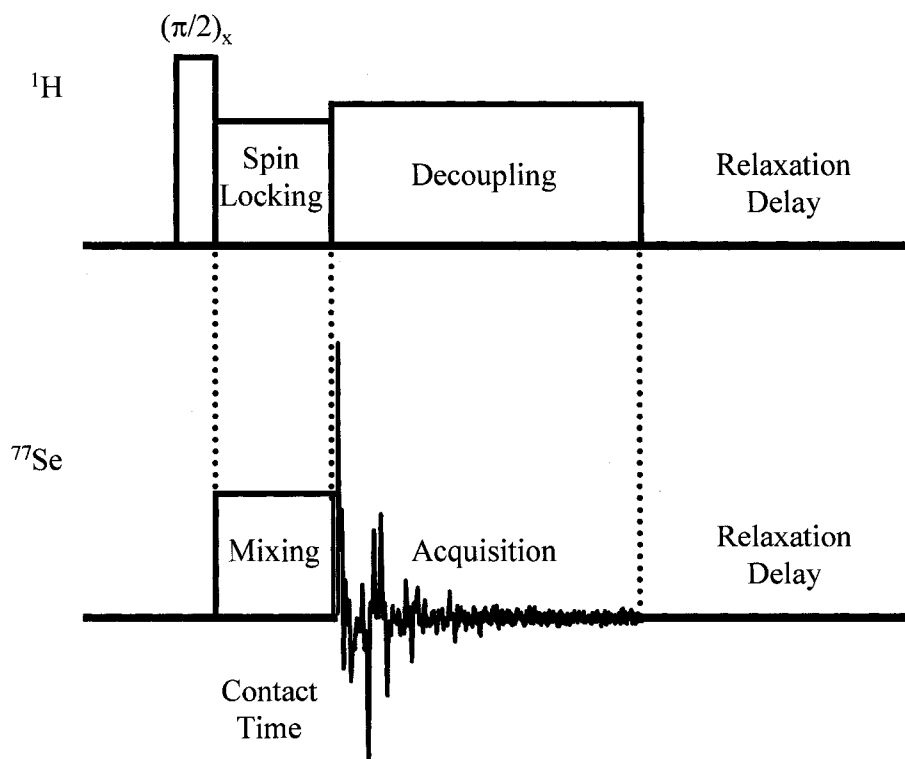
Cross polarization, CP, is an NMR technique where spin polarization of abundant spin nuclei is transferred to dilute spins in cases where the abundant and dilute spins are direct dipolar coupled. The first of two benefits for utilizing CP results in a signal enhancement by a maximum factor of  $\gamma_{\text{abund}}/\gamma_{\text{dilute}}$ , where the magnitude of the enhanced signal is dependent on the nature of the direct dipolar interaction. In principle, <sup>1</sup>H CP to <sup>77</sup>Se can result in a signal intensity gain of

$$\gamma_{^1\text{H}} / \gamma_{^{77}\text{Se}} \cong 5.17 \quad [3.30]$$

However, significant enhancements are rarely encountered for selenium in practice.<sup>22</sup>

The second, and for the purposes of this thesis more important, benefit is the recycle delays for a CP experiment are determined by the  $T_1$  of the abundant spin rather than the dilute spin. As the  $T_1$  values of dilute spin- $\frac{1}{2}$  nuclei are typically much larger than those of protons, this reduction in relaxation time allows for an increase in the signal-to-noise

ratio when using the CP experiment for a dilute spin nucleus for a given period of experiment time.



**Figure 3.4** Typical cross polarization pulse sequence.

The general form of the CP pulse sequence is depicted for  $^1\text{H}$  CP to  $^{77}\text{Se}$  in Figure 3.4. In the rotating frame, the  $(\pi/2)_x$  pulse tips the  $^1\text{H}$  magnetization along the y-direction, along which it is subsequently held or spin locked. While the  $^1\text{H}$  magnetization is spin locked another rf pulse is applied on the  $^{77}\text{Se}$  channel for a period known as the contact time, which is typically on the order of milliseconds. In the most common form of CP, called Hartmann-Hahn CP, the  $^1\text{H}$  and  $^{77}\text{Se}$  rf fields are matched to where their frequencies in the rotating frame are equivalent, such that

$$\gamma_{^1H} B_{1,^1H} = \gamma_{^{77}Se} B_{1,^{77}Se} \quad [3.31]$$

which is known as the Hartmann-Hahn condition.<sup>23</sup> It is during the contact time where spin polarization is transferred from the protons to the selenium nuclei.

Under MAS conditions where homo- and hetero-nuclear dipolar couplings are on the order of the rotor spinning frequency, the Hartmann-Hahn match condition attains a spinning speed dependence. A simple but effective remedy involves a minor modification of the mixing pulse shown in Figure 3.4. Instead of a flat, constant  $B_1$  field on the  $^{77}\text{Se}$  channel, an rf field following a linear amplitude ramp in intensity is employed. This ramped-amplitude cross polarization, RACP,<sup>24</sup> provides a broad range of Hartmann-Hahn match conditions eliminating the need to re-optimize rf field strengths when changing spinning frequencies.

### 3.3 Quantum Chemical Calculation of NMR Parameters

The quantum chemical calculations performed on systems investigated in this thesis were computed on isolated molecules or molecular ions with rigid structures. As a result, when compared to experimental NMR results from solid materials the computations must be considered in the context of their neglect of molecular vibrations and effects resultant from crystal packing forces.

The theory of nuclear magnetic shielding and indirect spin-spin coupling was initially advanced by Ramsey.<sup>25,26</sup> While computational programs do not utilize these formalisms in the quantum chemical computation of the respective NMR parameters, often the results are reported in a form consistent with the original theory. For nuclear



magnetic shielding, Ramsey decomposed the total shielding into diamagnetic and paramagnetic components

$$\sigma = \sigma^d + \sigma^p \quad [3.32]$$

where the diamagnetic term depends only on the ground electronic state of the molecule, and  $\sigma^p$  contains a summation over excited electronic states.<sup>25</sup> The utility of the magnetic shielding tensor is rooted in this connection with the electronic structure of the molecule of interest. Thus insight into local electronic structure about nuclei is possible via the measurement of chemical shift tensors.<sup>27</sup>

Indirect spin-spin coupling in a qualitative fashion involves the polarization of the electronic network by one nucleus that is subsequently transferred to a second nucleus. Three mechanisms by which the polarization can be transferred constitute Ramsey's original non-relativistic theory.<sup>26</sup> First, the spin-dipolar mechanism describes how one nuclear magnetic moment can induce electron spin polarization via a dipolar interaction with the electron spins. Second, the spin-orbit mechanism arises from electronic currents induced by the magnetic field produced by one nuclear magnetic dipole, which then influences the second nucleus. Finally, the Fermi-contact mechanism details the interaction between the nuclear magnetic moment and the electrons that have a finite probability of being located at the nucleus.

### 3.3.1 Density Functional Theory

Density functional theory, DFT, provides a favorable balance between accuracy and computational effort. Due to the size and nature of the systems investigated in this thesis, DFT has been utilized as the theoretical foundation for the computation of the

sought after NMR parameters. The Amsterdam Density Functional, ADF,<sup>28</sup> program package was employed for all of the DFT calculations performed as it offers access to relativistic corrections via the zeroth order regular approximation, which will be discussed in the following section. As a detailed description of the theory and implementation of DFT is beyond the scope of this thesis, the purpose of this section is to identify the concepts necessary to understand and evaluate DFT calculations of NMR parameters.

The fundamental tenet of DFT stems from the derivation<sup>29</sup> of the total energy of a molecular system as a functional of the electron density,  $\rho(\mathbf{r})$ ,

$$E = E[\rho(\mathbf{r})] \quad [3.33]$$

where  $\rho(\mathbf{r})$  is constructed, within Kohn-Sham DFT, from a set of molecular orbitals,  $\chi$ ,

$$\rho(\mathbf{r}) = \sum_{a=1}^{n_e} |\chi_a(\mathbf{r})|^2 \quad [3.34]$$

and the total energy may be written as

$$E[\rho(\mathbf{r})] = T + V_n + V_e + E_{xc} \quad [3.35]$$

where  $T$  is the kinetic energy as derived from the Kohn-Sham orbitals,  $V_n$  and  $V_e$  are the classical electron-nuclear and electron-electron Coulomb energies, respectively, and  $E_{xc}$  is referred to as the exchange-correlation functional. As the first three terms of  $E[\rho(\mathbf{r})]$  in equation 3.35 can be defined explicitly,  $E_{xc}$  is the only functional that need be developed. As implied by its name, the exchange-correlation functional contains the exchange and correlation energies; however,  $E_{xc}$  also serves as a depository for terms not accounted for in the kinetic and Coulomb energy terms. The specific functionals employed in the

calculations performed in the subsequent chapters use both the local density as well as the local gradient of the density in their definitions.

As mentioned earlier, modern computational programs do not calculate nuclear magnetic shielding and indirect spin-spin coupling according to the equations derived by Ramsey.<sup>25,26</sup> The components of the nuclear magnetic shielding tensor may be equivalently arrived at by taking the second derivative of the energy with respect to the magnetic moment of the nucleus,  $\mu$ , and the external applied magnetic field,  $B_0$ .<sup>30-32</sup>

$$\sigma_{ij} = \left[ \frac{\partial^2 E}{\partial \mu_i \partial B_{0,j}} \right]_{\mu, B_0=0} \quad i, j = x, y, z \quad [3.36]$$

One of the original problems concerning the computation of the nuclear magnetic shielding, and other properties arising from the effect of  $B_0$ , was that the results depended on the origin of the vector potential of the external applied magnetic field. As a molecular property, the nuclear magnetic shielding must be independent of the calculation origin; however, an obviously impractical solution to this so-called gauge origin problem is the use of a complete basis set. The gauge origin problem is addressed in ADF with the use of gauge including atomic orbitals, GIAOs, which defines the vector potential with local gauge origins at the center of each orbital.<sup>33,34</sup> The use of GIAOs has the additional benefit of a more rapid basis set convergence.<sup>32</sup>

While calculations of indirect spin-spin coupling have not been performed on the specific systems investigated, primarily a result of the considerable computational effort required, the method by which  $\mathbf{J}$  is computed is included here for completeness. Indirect

spin-spin coupling is calculated in a similar manner by taking the second derivative of the energy with respect to the nuclear magnetic moments of the coupled nuclei

$$K_{ij} = \left[ \frac{\partial^2 E}{\partial \mu_{I,i} \partial \mu_{S,j}} \right]_{\mu_I, \mu_S=0} \quad i, j = x, y, z \quad [3.37]$$

where  $\mathbf{K}$  is the reduced indirect spin-spin coupling tensor, with units of  $T^2 J^{-1}$ , and is related to  $\mathbf{J}$  by:

$$\mathbf{J}_{I,S} = \gamma_I \gamma_S \frac{h}{4\pi^2} \mathbf{K}_{I,S} \quad [3.38]$$

Thus,  $\mathbf{K}$  is independent of the magnitudes of the nuclear magnetic moments and is particularly useful when comparing indirect spin-spin couplings between different spin pairs.

### 3.3.2 The Zeroth Order Regular Approximation

From the liquid standard state of mercury to the color of gold, relativistic effects are well known contributors to the properties of heavy elements.<sup>35</sup> Relativistic effects are manifested in the calculation of NMR parameters via the mass-velocity and Darwin terms, together referred to as scalar relativistic effects, as well as by the effects of spin-orbit coupling. Scalar relativistic effects typically increase the calculated nuclear magnetic shielding, relative to a non-relativistic computation, via the diamagnetic contribution as a result of the contraction of the inner shells. However, since the contraction of core orbitals is essentially identical for every nucleus, regardless of the

chemical environment, this effect cancels in the calculation of relative chemical shifts, see equation 3.16.<sup>36</sup> Thus, scalar relativistic effects primarily impact calculated chemical shifts through stabilization and/or destabilization of the energy levels of the valence occupied and virtual orbitals, resulting in potentially significant paramagnetic contributions. Spin-orbit relativistic effects produce additional core and valence contributions to the calculated nuclear magnetic shielding. The former of which is also typically negated when determining relative chemical shifts. The spin-orbit induced spin polarization in both cases influences nuclear magnetic shieldings through a Fermi-contact mechanism.<sup>36</sup>

Theoretical treatment of relativistic effects is generally approached via the four component Dirac Hamiltonian. However, while not inherently more complex than non-relativistic computations, fully relativistic calculations require a more complicated mathematics as well as additional basis functions.<sup>37</sup> In addition, the size of the secular equation arising from a four component Hamiltonian results in fully relativistic computations that are prohibitively time consuming for any but the smallest of systems. A common approach in simplifying the Dirac equation involves transforming the Dirac Hamiltonian into a two component form utilizing  $2 \times 2$  Pauli spin-matrices. After such a transformation, the Dirac equation may be written in terms of the upper two and lower two components referred to as the large and small components, respectively. The large and small components are not independent of each other, that is one may be written in terms of the other. In this way, the original four component Hamiltonian may be written in a two component form and approximate solutions of the Dirac equation may then be sought. When the relationship between the large and small components is expanded to

zeroth order in  $(E-V)/2m_e c^2$ , where  $m_e$  is the electron mass and  $c$  is the speed of light, one arrives at the well known Pauli Hamiltonian.<sup>35</sup> However, an expansion of this form is not valid for particles in a Coulomb potential as the expansion parameter is not small near the nucleus.<sup>37</sup>

Expansion in powers of  $E/(2m_e c^2 - V)$  instead results in an operator that is, unlike the Pauli Hamiltonian, regular everywhere and bounded from below such that variational computations are stable.<sup>37</sup> To zeroth order the most important relativistic effects, including an accurate description of spin-orbit coupling, are already present.<sup>37-40</sup> This so-called zeroth order regular approximation, ZORA, produces eigenvalues and densities that are accurate approximations to those of full four component Dirac calculations.<sup>37</sup> Additionally, as a two component theory, the ZORA Hamiltonian can utilize smaller basis sets, thus reducing the computational effort required to achieve relativistic corrections to calculated molecular properties such as nuclear magnetic shielding and indirect spin-spin coupling.

### 3.4 References

- (1) Haeberlen, U. *Advances in Magnetic Resonance, Suppl. 1: High Resolution NMR in Solids: Selective Averaging*; Academic Press: New York, 1976.
- (2) Fyfe, C. A. *Solid-State NMR for Chemists*; C.F.C. Press: Guelph, 1983.
- (3) Mehring, M. *Principles of High Resolution NMR in Solids*; 2<sup>nd</sup> ed.; Springer-Verlag: Berlin, 1983.
- (4) Abragam, A. *The Principles of Nuclear Magnetism*; Clarendon Press: Oxford, 1986.
- (5) Anet, F. A. L.; O'Leary, D. J. *Concepts Magn. Reson.* **1991**, *3*, 193-214.
- (6) Anet, F. A. L.; O'Leary, D. J. *Concepts Magn. Reson.* **1992**, *4*, 35-52.
- (7) Mason, J. *Solid State Nucl. Magn. Reson.* **1993**, *2*, 285-288.
- (8) Wasylshen, R. E. In *Encyclopedia of Nuclear Magnetic Resonance*; Grant, D. M., Harris, R. K., Eds.; John Wiley and Sons, Ltd.: Chichester, 1996, pp 1685-1695.
- (9) Ishii, Y.; Terao, T.; Hayashi, S. *J. Chem. Phys.* **1997**, *107*, 2760-2774.
- (10) Man, P. P. In *Encyclopedia of Nuclear Magnetic Resonance*; Grant, D. M., Harris, R. K., Eds.; John Wiley and Sons, Ltd.: Chichester, 1996, pp 3838-3848.
- (11) Vega, A. J. In *Encyclopedia of Nuclear Magnetic Resonance*; Grant, D. M., Harris, R. K., Eds.; John Wiley and Sons, Ltd.: Chichester, 1996, pp 3869-3889.
- (12) Olivieri, A. C. *J. Magn. Reson.* **1989**, *81*, 201-205.
- (13) Zumbulyadis, N.; Henrichs, P. M.; Young, R. H. *J. Chem. Phys.* **1981**, *75*, 1603-1611.
- (14) Hexem, J. G.; Frey, M. H.; Opella, S. J. *J. Chem. Phys.* **1982**, *77*, 3847-3856.
- (15) Bryce, D. L.; Bernard, G. M.; Gee, M.; Lumsden, M.; Eichele, K.; Wasylshen, R. E. *Can. J. Anal. Sci. Spectrosc.* **2001**, *46*, 46-82.
- (16) Harris, R. K. *Nuclear Magnetic Resonance Spectroscopy*; Longman Group UK Limited, 1987.
- (17) Duer, M. J. *Solid-State NMR Spectroscopy: Principles and Applications*; Blackwell Science: Oxford, 2002.

- (18) Schaefer, J.; Stejskal, E. O. *J. Am. Chem. Soc.* **1976**, *98*, 1031-1032.
- (19) Maricq, M. M.; Waugh, J. S. *J. Chem. Phys.* **1979**, *70*, 3300-3316.
- (20) Herzfeld, J.; Berger, A. E. *J. Chem. Phys.* **1980**, *73*, 6021-6030.
- (21) Bennett, A. E.; Rienstra, C. M.; Auger, M.; Lakshmi, K. V.; Griffin, R. G. *J. Chem. Phys.* **1995**, *103*, 6951-6958.
- (22) Duddeck, H. *Prog. Nucl. Magn. Reson. Spectrosc.* **1995**, *27*, 1-323.
- (23) Hartmann, S. R.; Hahn, E. L. *Phys. Rev.* **1962**, *128*, 2042-2053.
- (24) Metz, G.; Wu, X.; Smith, S. O. *J. Magn. Reson. Ser. A* **1994**, *110*, 219-227.
- (25) Ramsey, N. F. *Phys. Rev.* **1950**, *78*, 699-703.
- (26) Ramsey, N. F. *Phys. Rev.* **1953**, *91*, 303-307.
- (27) Jameson, C. J.; Mason, J. In *Multinuclear NMR*; Mason, J., Ed.; Plenum Press: New York, 1987, pp 51-88.
- (28) Theoretical Chemistry, Vrije Universiteit, Amsterdam, <http://www.scm.com>.
- (29) Hohenberg, P.; Kohn, W. *Phys. Rev.* **1964**, *136*, B864-B871.
- (30) Helgaker, T.; Jaszunski, M.; Ruud, K. *Chem. Rev.* **1999**, *99*, 293-352.
- (31) Facelli, J. C. *Concepts Magn. Reson.* **2004**, *20A*, 42-69.
- (32) Vaara, J. *Phys. Chem. Chem. Phys.* **2007**, *9*, 5399-5418.
- (33) Ditchfield, R. *J. Chem. Phys.* **1972**, *56*, 5688-5691.
- (34) Wolinski, K.; Hinton, J. F.; Pulay, P. *J. Am. Chem. Soc.* **1990**, *112*, 8251-8260.
- (35) Autschbach, J.; Ziegler, T. In *Encyclopedia of Nuclear Magnetic Resonance*; Grant, D. M., Harris, R. K., Eds.; John Wiley and Sons, Ltd.: Chichester, U.K., 2002; Vol. 9, pp 306-323.
- (36) Schreckenbach, G. *Inorg. Chem.* **2002**, *41*, 6560-6572.
- (37) van Lenthe, E.; van Leeuwen, R.; Baerends, E. J.; Snijders, J. G. *Int. J. Quantum Chem.* **1996**, *57*, 281-293.



- (38) Chang, C.; Pelissier, M.; Durand, P. *Phys. Scr.* **1986**, *34*, 394-404.
- (39) van Lenthe, E.; Baerends, E. J.; Snijders, J. G. *J. Chem. Phys.* **1993**, *99*, 4597-4610.
- (40) van Lenthe, E.; Baerends, E. J.; Snijders, J. G. *J. Chem. Phys.* **1994**, *101*, 9783-9792.

## Chapter 4

# A Combined Experimental and Quantum Chemistry Study of Selenium Chemical Shift Tensors<sup>†</sup>

### 4.1 Introduction

Selenium is playing an increasingly important role in chemistry, particularly in materials chemistry. For example, selenium has been utilized in the structure of various nanoparticles, nanowires, and nanotubules.<sup>1-4</sup> Applications have also been reported where selenium is incorporated within the channels of porous materials.<sup>5-10</sup> Interest in selenium chemistry has not seen such growth since it was recognized that selenium is an essential nutrient in mammalian systems.<sup>11</sup> The discovery that the TGA codon directs the incorporation of selenium has ultimately led to the acceptance of selenocysteine as the 21<sup>st</sup> amino acid.<sup>12,13</sup>

Nuclear magnetic resonance (NMR) has been utilized to investigate a limited number of selenium-containing nano-composites;<sup>14-17</sup> however, fewer studies have focused on the selenium nucleus itself.<sup>16,17</sup> Selenium-77 NMR is an ideal technique for investigating selenium-containing materials as the <sup>77</sup>Se chemical shift ranges over 3000 ppm<sup>18,19</sup> and is extremely sensitive to changes in molecular structure. Clearly, it is desirable to have a sound understanding of the structural features that influence <sup>77</sup>Se NMR parameters.

Theoretical calculation of NMR parameters, particularly for selenium where empirical interpretations are more difficult than those extracted from <sup>1</sup>H or <sup>13</sup>C NMR

---

<sup>†</sup> A version of this chapter has been published: B.A. Demko, K. Eichele, and R.E. Wasylishen, *Journal of Physical Chemistry A*, **2006**, *110*, 13537-13550.

spectra, has become increasingly useful for spectroscopists.<sup>20</sup> Selenium-77 NMR studies of isotropic liquids, specifically isotropic chemical shifts and indirect spin-spin coupling constants, is a well developed area of research.<sup>18,19,21-24</sup> The comparison of calculated isotropic chemical shifts with experimental values has recently been criticized as a poor method for determining the accuracy of a given quantum chemical approach given that the fundamental parameter, the magnetic shielding interaction, is characterized by a second-rank tensor containing nine components in general versus the single value obtained from NMR studies of isotropic solutions.<sup>25</sup> Solid-state NMR, which can yield the symmetric part of the chemical shift tensor, is potentially more informative than its solution counterpart,<sup>26,27</sup> however, the literature and scope of solid-state <sup>77</sup>Se NMR investigations has been relatively limited.<sup>18,19</sup> Magnetic resonance experiments on heavier nuclei are known to present challenges both experimentally and theoretically,<sup>28</sup> and the question of whether or not relativistic effects are important for the calculation of <sup>77</sup>Se NMR parameters remains a topic of some debate.<sup>28-41</sup>

The aim of the present investigation is to probe a wide variety of selenium-containing solid compounds, covering the known isotropic chemical shift range of selenium, using solid-state NMR spectroscopy and computational chemistry. Specifically, we have used solid-state <sup>77</sup>Se NMR spectroscopy to provide the principal components of the chemical shift tensor for a number of organic, organophosphorus, and inorganic selenium compounds. Due to the inherent ability and success of density functional theory (DFT) in addressing electron correlation, which allows the investigation of larger systems and/or those containing heavy atoms, DFT was employed to calculate the corresponding selenium magnetic shielding tensors. The DFT calculations were

performed at varying levels of inclusion of both scalar and spin-orbit relativistic effects via the zeroth order regular approximation (ZORA) formalism.<sup>42-45</sup> The calculated magnetic shielding tensors when transformed into chemical shift tensors and compared with the experimental values allow insight into the level of relativistic theory required to accurately describe the observed magnetic shielding.

## 4.2 Background Theory

The magnetic shielding experienced by a nucleus in a molecule generally depends on the orientation of that molecule with respect to the external magnetic field,  $\mathbf{B}_0$ . This results from induced magnetic fields about the nucleus due to the circulation of electrons, which slightly alters the NMR resonance condition. To completely describe this shielding, a second-rank tensor, containing up to nine unique components may be required. In the magnetic shielding tensor's principal axis system (PAS), the symmetric part of the tensor is diagonal, and only three orthogonal components ( $\sigma_{11} \leq \sigma_{22} \leq \sigma_{33}$ ), and three Euler angles ( $\alpha, \beta, \gamma$ ), which relate the orientation of the PAS to the molecular frame, are required to properly describe the interaction tensor. The span of the shielding tensor is defined as  $\Omega = \sigma_{33} - \sigma_{11}$ , and represents the maximum orientation dependence of the shielding experienced by the nucleus in a given molecule. The isotropic shielding,  $\sigma_{iso}$ , is one-third the trace of the shielding tensor;  $\sigma_{iso} = (\sigma_{11} + \sigma_{22} + \sigma_{33})/3$ . The NMR spectrum of a powdered sample containing an 'isolated spin' yields the principal components of the chemical shift tensor, whose values are related to the magnetic shielding tensor by:

$$\delta_{ii}(sample) = \frac{\sigma_{iso}(ref) - \sigma_{ii}(sample)}{1 - \sigma_{iso}(ref)} \quad [4.1]$$

where  $\sigma_{iso}(ref)$  is the isotropic shielding of a standard reference and  $\delta_{11} \geq \delta_{22} \geq \delta_{33}$ . Solid-state NMR can also provide the Euler angles; however, single crystals of sufficient size and quality are usually required for their determination,<sup>46-50</sup> and as a consequence Euler angles are less commonly reported than the principal components which are readily obtained from powdered samples.

The non-relativistic theory of nuclear magnetic shielding was developed by Ramsey,<sup>51,52</sup> and is recognized as among the most influential papers in 20<sup>th</sup> century quantum chemistry.<sup>53</sup> The significance of relativistic effects in the calculation of nuclear magnetic shieldings for heavy nuclei has attracted great interest since its initial description,<sup>54-57</sup> and a few representative references of its discussion are given here.<sup>54-63</sup>

Specifically for the organophosphine selenides, due to the presence of <sup>31</sup>P (100% natural abundance), it is prudent to discuss the theory of spin-spin coupling. The concept of direct dipolar and indirect spin-spin coupling is well covered in the literature.<sup>64-69</sup> The direct dipolar, **D**, tensor is of second-rank and is traceless, while the indirect spin-spin, **J**, tensor is a general 2<sup>nd</sup>-rank tensor with a non-zero trace. The average of the principal components of **J** ( $J_{11}$ ,  $J_{22}$ ,  $J_{33}$ ) provides the isotropic indirect spin-spin coupling constant,  $J_{iso}$ . For directly bonded selenium-77 and phosphorus-31 spin pairs,  $^1J(^{77}\text{Se}, ^{31}\text{P})$  values are known to be negative.<sup>65,70</sup> The anisotropy of the **J**-tensor is defined as  $\Delta J = J_{33} - (J_{11} + J_{22})/2$ , and is inherently linked with the direct dipolar coupling constant,  $R_{DD}$ ;  $R_{DD}$  and  $\Delta J$  can not be separated and an effective direct dipolar coupling constant,  $R_{eff}$ , is obtained experimentally:

$$R_{eff} = R_{DD} - \Delta J / 3 \quad [4.2]$$

and

$$R_{DD} = \left( \frac{\mu_0}{4\pi} \right) \left( \frac{\hbar}{2\pi} \right) \left( \frac{\gamma_I \gamma_S}{\langle r_{IS}^3 \rangle} \right) \quad [4.3]$$

where  $\mu_0$  is the permeability of a vacuum,  $\gamma_I$  and  $\gamma_S$  are the magnetogyric ratios of the coupled spins,  $I$  and  $S$ , and  $\langle r_{IS}^3 \rangle$  is the motionally-averaged cube of the distance between the coupled nuclei. When the value of  $R_{eff}$  can be determined from an experimental spectrum,  $\Delta J$  can be estimated from equation 4.2 provided  $r_{IS}$  is known (equation 4.3). Previously, we have shown that the dipolar-splitting-ratio method can provide information on the orientation of the internuclear dipolar vector with respect to the chemical shift tensor principal components in powder samples containing an isolated spin-pair.<sup>71</sup>

### 4.3 Experimental

Representations of compounds **1-16** investigated in this study are given in Figure 4.1. The following samples were acquired from commercial sources and used without further purification: *N,N*-dimethylselenourea (**1**) and diphenylselenium dichloride (**3**) from Strem; *N*-methylbenzothiazole-2-selone (**2**), tetramethyltetraselenafulvalene (**5**) and diphenyl diselenide (**6**) from Aldrich; seleno-DL-methionine (**4**) from Sigma; ammonium selenate (**14**) and ammonium selenotungstate (**15**) from Alfa. The organophosphine selenides (**7 – 13**) were prepared from the appropriate phosphine and KSeCN, according to the procedure outlined in the literature.<sup>72</sup>

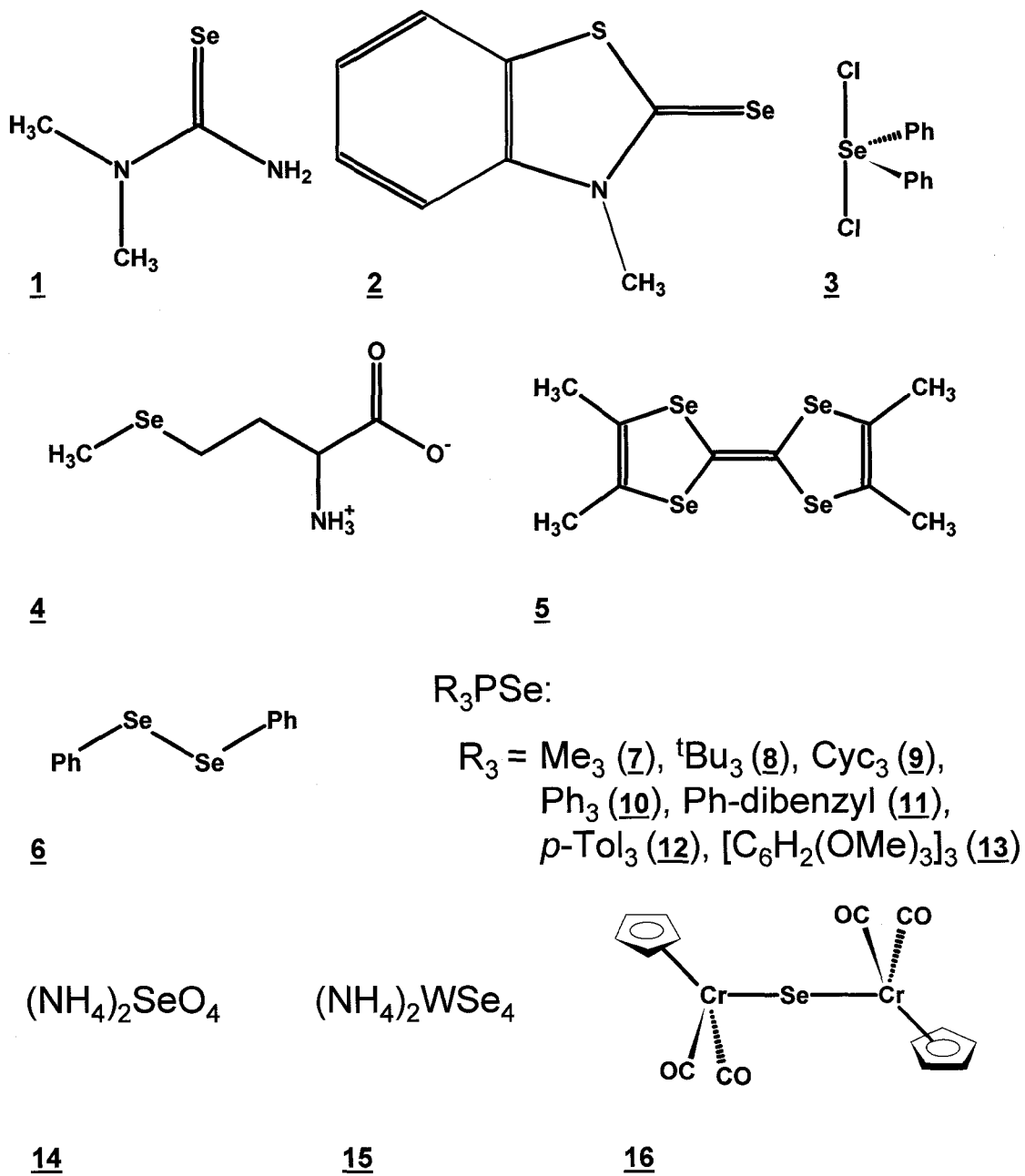


Figure 4.1 Compounds 1-16, investigated in this study.

Selenium-77 NMR spectra were recorded at 38.154 and 76.277 MHz on Bruker MSL-200 and AMX-400 NMR spectrometers ( $B_0 = 4.7$  and  $9.4$  T), respectively. The samples were packed into 7 mm o.d. zirconium oxide rotors, and spun at magic angle spinning (MAS) frequencies ( $\nu_{\text{rot}}$ ) between 1.5 and 6.2 kHz. Standard cross polarization (CP), or ramped-amplitude CP (RACP), and high-power  $^1\text{H}$  decoupling were employed in acquiring all NMR spectra, except for cases where CP was so inefficient that improved results were obtained after a single pulse with  $^1\text{H}$  decoupling and long recycle delays. Selenium chemical shifts were referenced to a neat liquid of dimethyl selenide ( $\text{Me}_2\text{Se}$ ) at  $23$  °C by setting the isotropic NMR peak of solid  $(\text{NH}_4)_2\text{SeO}_4$  to  $+1040.2$  ppm.<sup>73,74</sup> Isotropic chemical shifts were identified by varying the spinning frequency. The principal components of the chemical shift tensors,  $\delta_{ii}$ , were determined via the method of Herzfeld and Berger<sup>75</sup> except those for  $(\text{NH}_4)_2\text{SeO}_4$ , which were determined from the discontinuities in the spectrum of a stationary sample, and all spectra were simulated using the determined values with the program WSOLIDS<sup>76</sup> in order to assess the quality of the parameters obtained. This procedure results in errors of  $\pm 0.2$  ppm in the isotropic chemical shifts, and errors in the principal components on the order of 1-3% of the span of the respective chemical shift tensor.

Quantum chemistry calculations of magnetic shielding tensors were carried out using the NMR module<sup>77-79</sup> of the Amsterdam Density Functional (ADF) program package.<sup>80-84</sup> The Vosko-Wilk-Nusair<sup>85</sup> local density approximation with the Becke88-Perdew86<sup>86-88</sup> generalized gradient approximation were used for the exchange-correlation functional. Non-relativistic (NR), scalar relativistic (SR) and scalar with spin-orbit relativistic (SO) calculations were performed in order to gauge the importance of



relativistic effects for the calculation of NMR parameters involving selenium. The relativistic corrections carried out are based on the implementation of the ZORA formalism.<sup>42-45</sup> Triple- $\zeta$  doubly polarized, TZ2P, Slater-type ZORA basis sets were used for all atoms except for hydrogen, which received double- $\zeta$  quality, DZ, basis functions. The calculations were performed on a Linux-based cluster with either dual AMD MP 1800+ Athlon processor nodes or two AMD XP 1800+ Athlon processors operating in parallel.

The crystal structures for compounds **1** to **16** have previously been determined by X-ray diffraction (XRD).<sup>89-104</sup> The atomic coordinates for compound **12** could not be generated from the report in the literature,<sup>100</sup> and were determined from a non-relativistic geometry optimization using ADF basis sets of similar quality to those used in the magnetic shielding tensor calculations. All DFT calculations were carried out on isolated molecules using the non-hydrogen atomic coordinates, determined from the crystal structures where possible. For the ionic compounds **14** and **15**,  $\text{NH}_4^+$  cations within 5.0 Å of the central atom in the anionic tetrahedron,  $\text{SeO}_4^{2-}$  or  $\text{WSe}_4^{2-}$ , were included in the calculations. Hydrogen atoms were placed at idealized positions ( $r_{\text{CH}} = 1.09$  Å (alkyl) or 1.08 Å (aryl),  $r_{\text{NH}} = 1.02$  Å). Herein, we use the labels ‘a’, ‘b’, etc. to designate the difference between multiple sites, and a calculated value was assigned to the site that minimized the difference between the calculated and experimental values. The molecules were translated so that the selenium atoms were located at the origin in order to minimize a gauge variance for the calculation of the off-diagonal components of the magnetic shielding tensors within ADF 2004.01 and earlier versions.<sup>‡80</sup> Since the calculations were performed on isolated molecules, intermolecular interactions were not included.

---

<sup>‡</sup> This issue has recently been rectified in ADF 2005.01.

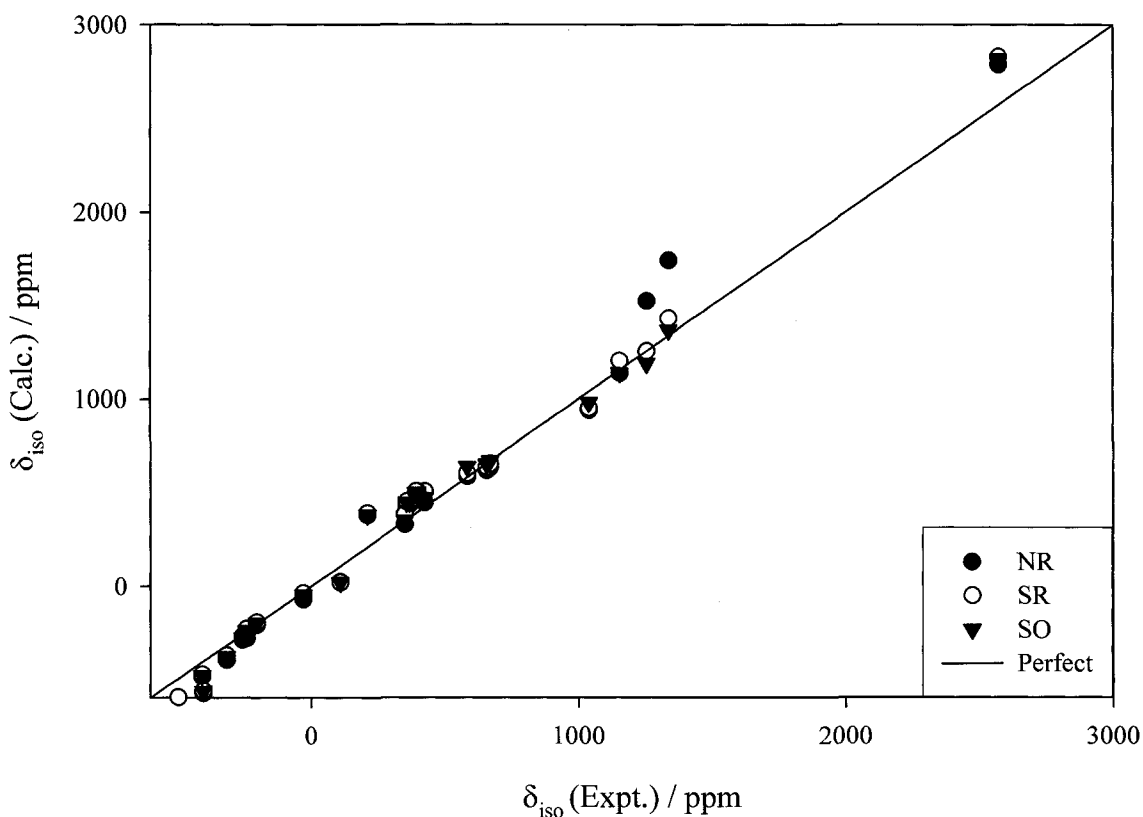
Solvent effects are known to affect the chemical shift for selenium compounds,<sup>18,22,105,106</sup> and have been observed to vary by up to 50 ppm in organoselenium species.<sup>22,107</sup> Changes of phase are also known to influence selenium magnetic shielding tensors; for example,  $\sigma_{\text{iso}}(^{77}\text{Se})$  for  $\text{H}_2\text{Se}$  decreases by  $126.6 \pm 0.5$  ppm when gaseous hydrogen selenide (5 atm) undergoes liquefaction, and decreases further by  $11.4 \pm 0.2$  ppm when liquid  $\text{H}_2\text{Se}$  freezes.<sup>108</sup> These potential effects must be considered when comparing calculated values to experimental solution and solid-state parameters.

The chemical shift tensors were determined from the calculated magnetic shielding tensors and the value of  $\sigma_{\text{iso}}(\text{Me}_2\text{Se})$ , calculated at the same level of theory, according to equation 4.1. Due to the lack of an experimentally determined structure, the geometry of  $\text{Me}_2\text{Se}$  was optimized, and converged with a staggered-staggered orientation of the molecule consistent with previous investigations.<sup>28,30-32</sup> The calculated NR, SR, and SO values used for the isotropic shielding of dimethyl selenide were 1627.8, 1580.0, and 1745.2 ppm, respectively. These values are in agreement with those previously reported by other authors.<sup>28,30-33,35,38,41,109-112</sup>

## 4.4 Results and Discussion

### 4.4.1 Comparison of Observed and Calculated Selenium Chemical Shift Tensors

Experimental and computational results in this investigation are summarized in Tables 4.1 – 4.3. The successes of the DFT computations in reproducing the experimental results obtained are illustrated in Figures 4.2 – 4.4. The linear regression parameters; slope and intercept, along with the mean absolute deviation for the plots in Figures 4.2 – 4.4 have been tabulated in Appendix A. A plot of calculated versus



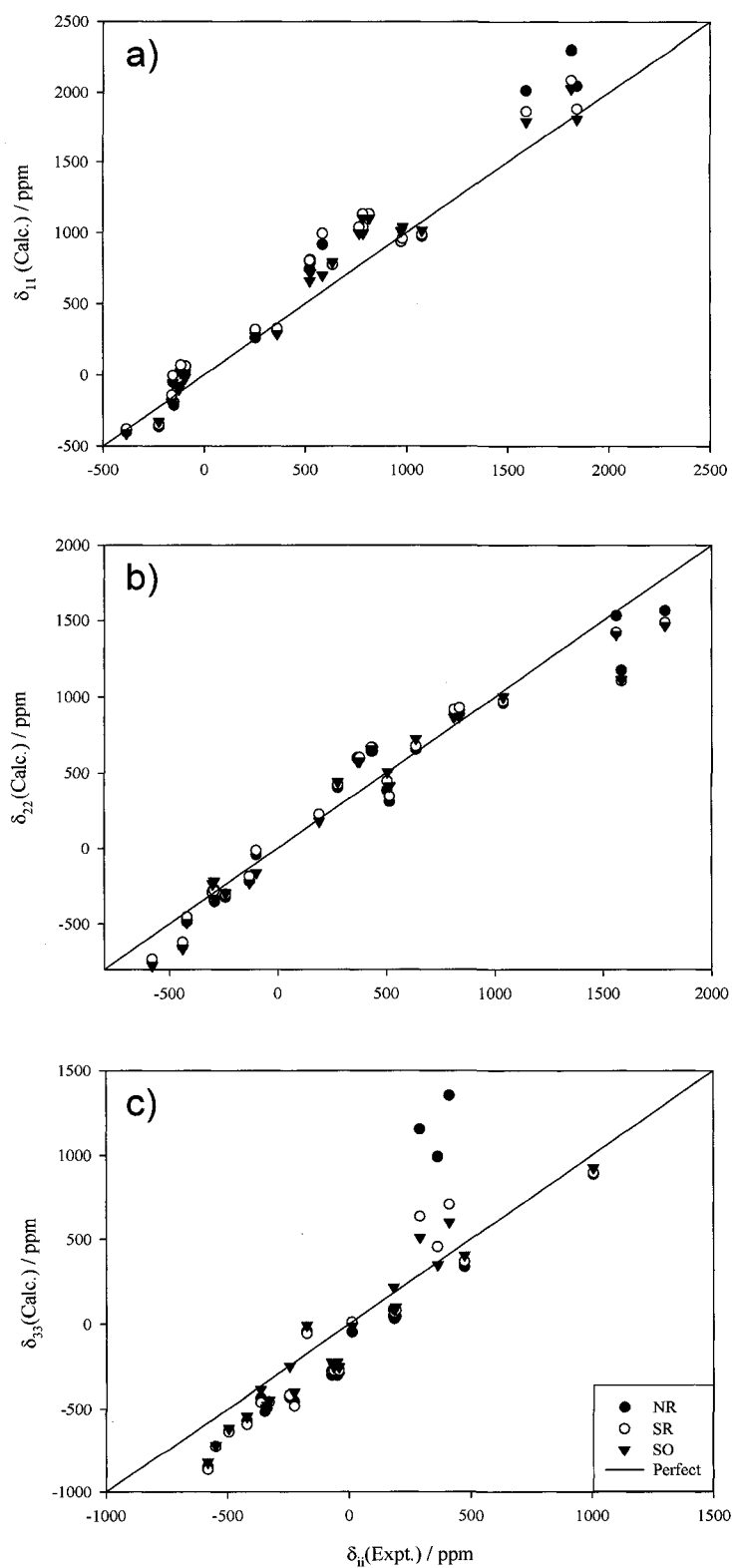
**Figure 4.2** Experimental vs. calculated isotropic chemical shifts,  $\delta_{\text{iso}}$ , for the selenium-containing compounds investigated, **1-16**; the solid diagonal line indicates perfect agreement between calculated and experimental results.

experimental isotropic chemical shifts for all of the compounds investigated is given in Figure 4.2. All theoretical methods employed perform very well in reproducing  $\delta_{\text{iso}}$  as evidenced by the small deviation of the individual points from the solid line that represents perfect agreement between experiment and theory. The agreement was expected as numerous approaches have been successful in reproducing isotropic selenium chemical shifts.<sup>25,28,30-33,35,37-41,110</sup> The largest discrepancy observed appears for the values of  $\delta_{\text{iso}}(\text{NR})$  calculated for two of the isotropic chemical shifts for ammonium selenotungstate, **15a** and **15b**.

Plots of theoretical versus experimental values for the individual principal components,  $\delta_{ii}$ , of the selenium chemical shift tensors investigated are given in Figure 4.3. From Figure 4.3a, it is clear that the calculated values for  $\delta_{11}$  reproduce the trend observed in the values of  $\delta_{11}(\text{Expt.})$ . The deviations of the individual points from the idealized line of perfect agreement are noticeably larger in magnitude than those found for the comparison of isotropic values. The plot emphasizes that the majority of the calculations tend to underestimate the magnitude of the shielding for this component, which leads to an overestimation of the value of  $\delta_{11}(\text{Calc.})$  with respect to the corresponding experimental value; however, the inclusion of relativistic effects lead to better results in general.

Figure 4.3b displays a plot of calculated versus experimental values of  $\delta_{22}$ . The trend observed in all of the experimentally determined intermediate principal components is well reproduced by  $\delta_{22}(\text{Calc.})$ . Unlike the  $\delta_{11}$  component, there exists more balance in the instances of over- and underestimation of the calculated shielding in  $\delta_{22}$  throughout the chemical shift tensors investigated, and relativistic effects do not appear to improve the agreement with experiment. The differences in magnitude between the individual points and the line of perfect agreement are generally larger than those observed for  $\delta_{\text{iso}}(\text{Calc.})$  in Figure 4.2.

When the experimental and calculated values of  $\delta_{33}$  are plotted against each other (Figure 4.3c) there are a couple points worth noting. First, the largest single deviation of any  $\delta_{ii}(\text{Calc.})$  from its corresponding experimental value is observed in the calculation of  $\delta_{33}$  for one of the three sites of  $(\text{NH}_4)_2\text{WSe}_4$ , **15a**. The values of  $\delta_{33}(\text{NR})$  for each of the

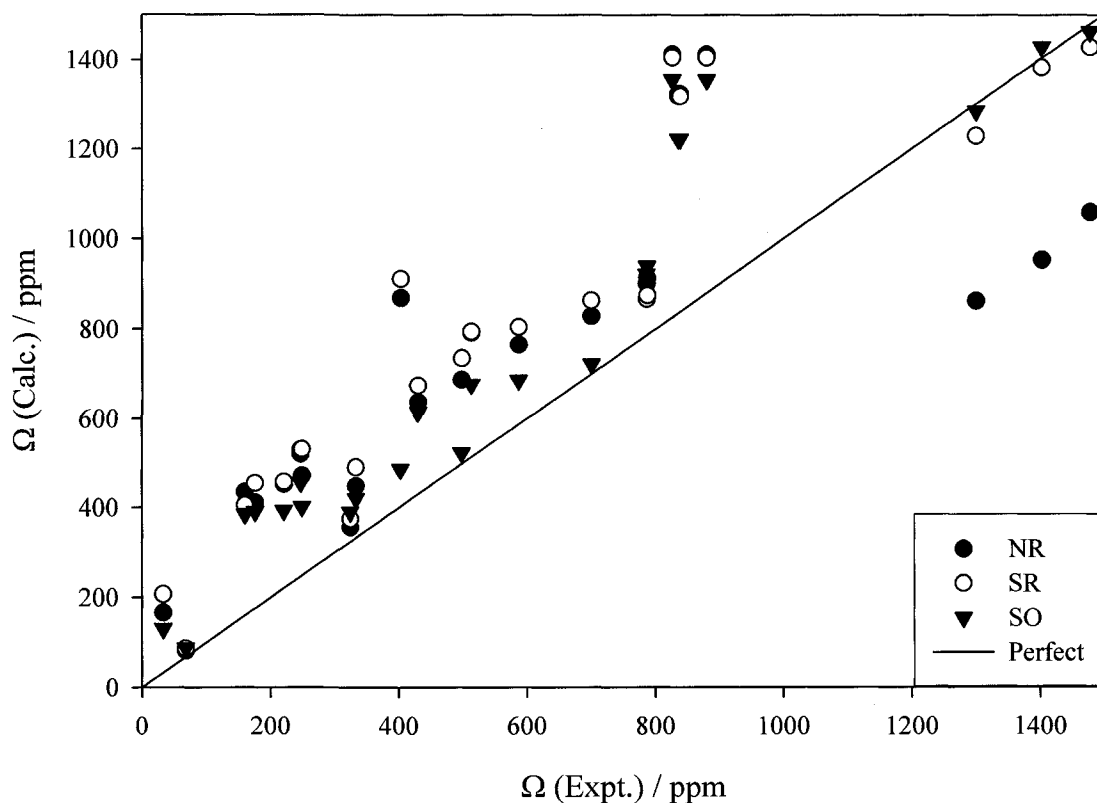


**Figure 4.3** Experimental vs. calculated values for (a)  $\delta_{11}$ , (b)  $\delta_{22}$ , and (c)  $\delta_{33}$  for the selenium-containing compounds investigated, **1-15**; the solid diagonal line indicates perfect agreement between calculated and experimental results.

three crystallographically non-equivalent selenium environments of ammonium selenotungstate, **15**, display substantially large deviations from their corresponding experimentally determined principal component. Secondly, aside from the  $\delta_{33}(\text{Calc.})$  values for  $(\text{NH}_4)_2\text{WSe}_4$  and a few other exceptions, the majority of the  $\delta_{33}$  components are calculated to be more shielded, resulting in smaller values of  $\delta_{33}$ , than is found experimentally.

Magnifying the accuracy of the calculations for the most and least shielded principal components, the experimentally determined spans of all of the compounds investigated are compared with their theoretical counterparts in Figure 4.4. For the most part, the spans are overestimated except for the non-relativistic calculation of the three chemical shift tensors of  $(\text{NH}_4)_2\text{WSe}_4$ . This observation was expected given the generally observed overestimation of  $\delta_{11}$  and underestimation of  $\delta_{33}$  by the calculations (Figure 4.3). On the other hand, these errors cancel each other in their combined effect on  $\delta_{\text{iso}}$ , leading to apparent agreement between theoretical and calculated values (Figure 4.2).

The results presented, and illustrated in Figures 4.2 to 4.4, indicate that the overall agreement between all of the DFT calculations and experiment is good, given the fact that the computations are performed on isolated molecules and that the experiments are performed on solid materials. In the following subsections we shall focus, highlighting the exceptions to the general trends observed for the calculations, on the three classes of compounds investigated: 1) organoselenium compounds **1 - 6**, 2) organophosphine selenides **7 - 13**, and 3) inorganic selenium compounds **14 - 16**.

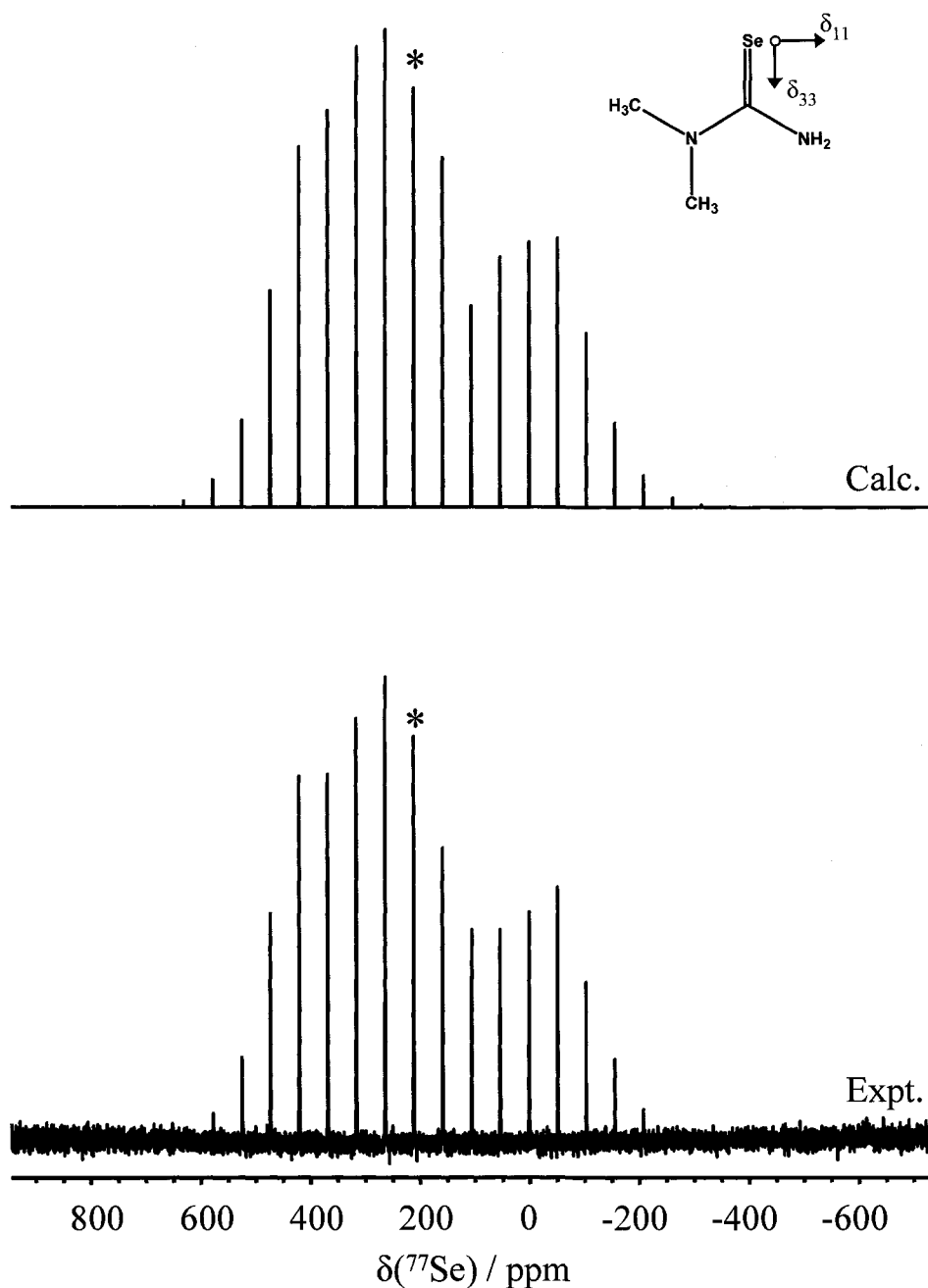


**Figure 4.4** Experimental vs. calculated spans,  $\Omega = \delta_{11} - \delta_{33}$ , for the selenium-containing compounds investigated, **1-15**; the solid diagonal line indicates perfect agreement between calculated and experimental results.

#### 4.4.2 Organoselenium Compounds

The range of molecular environments that selenium can be found in for organoselenium compounds is vast. The diversity of selenium environments in the representative compounds investigated provides a good test of the theoretical methods employed.

**1.** *N,N*-dimethylselenourea is a relatively simple seleno-carbonyl, or selone, compound for solid-state NMR investigation. The experimental and simulated spectra for **1** are given in Figure 4.5. The experimental spectrum was simulated using the parameters from a Herzfeld-Berger analysis and are given in Table 4.1. The chemical shift



**Figure 4.5** Simulated and experimental CP MAS  $^{77}\text{Se}$  NMR spectra of *N,N*-dimethylselenourea (**1**), acquired at 9.4 T, after 48 transients, spinning at 4.0 kHz, with 50 Hz of line broadening, a contact time of 10.0 ms, and a 30 s pulse delay. The isotropic peak is labeled with an asterisk (\*). Inset is a schematic of compound **1** showing the orientation of the selenium chemical shift tensor calculated at the scalar with spin-orbit relativistic level of theory.



**Table 4.1** Experimental and Theoretical Chemical Shift Tensors<sup>a)</sup> for Organoselenium Compounds.

		$\delta_{iso}$	$\delta_{11}$	$\delta_{22}$	$\delta_{33}$	$\Omega$
<b>1</b>	Expt. <sup>b)</sup>	211	527	279	-173	700
	<sup>c)</sup>	147				
	NR	384	787	407	-42	829
	SR	392	808	425	-56	864
	SO	383	715	442	-7	722
<b>2a</b>	Expt. <sup>b)</sup>	368	786	368	-50	836
	<sup>c)</sup>	357	767	377	-72	839
	NR	438	1022	594	-301	1323
	SR	455	1040	602	-278	1318
	SO	449	997	576	-225	1222
<b>2b</b>	Expt. <sup>b)</sup>	396	817	435	-64	881
	<sup>c)</sup>	392	785	430	-42	827
	NR	496	1128	645	-285	1413
	SR	508	1131	668	-274	1405
	SO	501	1102	655	-253	1355
<b>3</b>	Expt. <sup>b)</sup>	584	635	635	475	160
	<sup>d)</sup>	574.9				
	NR	588	773	654	338	435
	SR	605	773	675	368	405
	SO	640	791	723	405	386
<b>4</b>	Expt. <sup>b)</sup>	109	361	192	-226	587
	<sup>e)</sup>	112	369	202	-236	605
	NR	26	312	221	-454	766
	SR	23	325	224	-480	805
	SO	21	287	176	-399	686
<b>5a</b>	Expt. <sup>b)</sup>	657	973	811	187	786
	<sup>f)</sup>	657.5	969.5	817.5	185.5	784
	NR	621	934	898	32	902
	SR	639	934	916	66	868
	SO	653	1009	864	86	923
<b>5b</b>	Expt. <sup>b)</sup>	669	980	835	193	787
	<sup>f)</sup>	669.7	981.7	829.7	197.7	784
	NR	636	956	909	42	914
	SR	655	956	928	80	876
	SO	668	1038	867	99	939
<b>6a</b>	Expt. <sup>b)</sup>	350	524	516	11	513
	<sup>g)</sup>	350	537	510	2	535
	NR	333	742	308	-50	792
	SR	385	803	345	8	795
	SO	352	661	412	-16	677
<b>6b</b>	Expt. <sup>b)</sup>	425	586	505	183	403
	<sup>g)</sup>	425	565	527	183	382
	NR	449	916	385	46	870
	SR	507	994	444	83	911
	SO	474	701	505	215	486

a) Chemical shifts in ppm with respect to external Me<sub>2</sub>Se.

b) This Work.

c) Ref. <sup>113</sup>

d) Ref. <sup>114</sup>

e) Ref. <sup>115</sup>

f) Ref. <sup>73</sup>

g) Ref. <sup>111</sup>

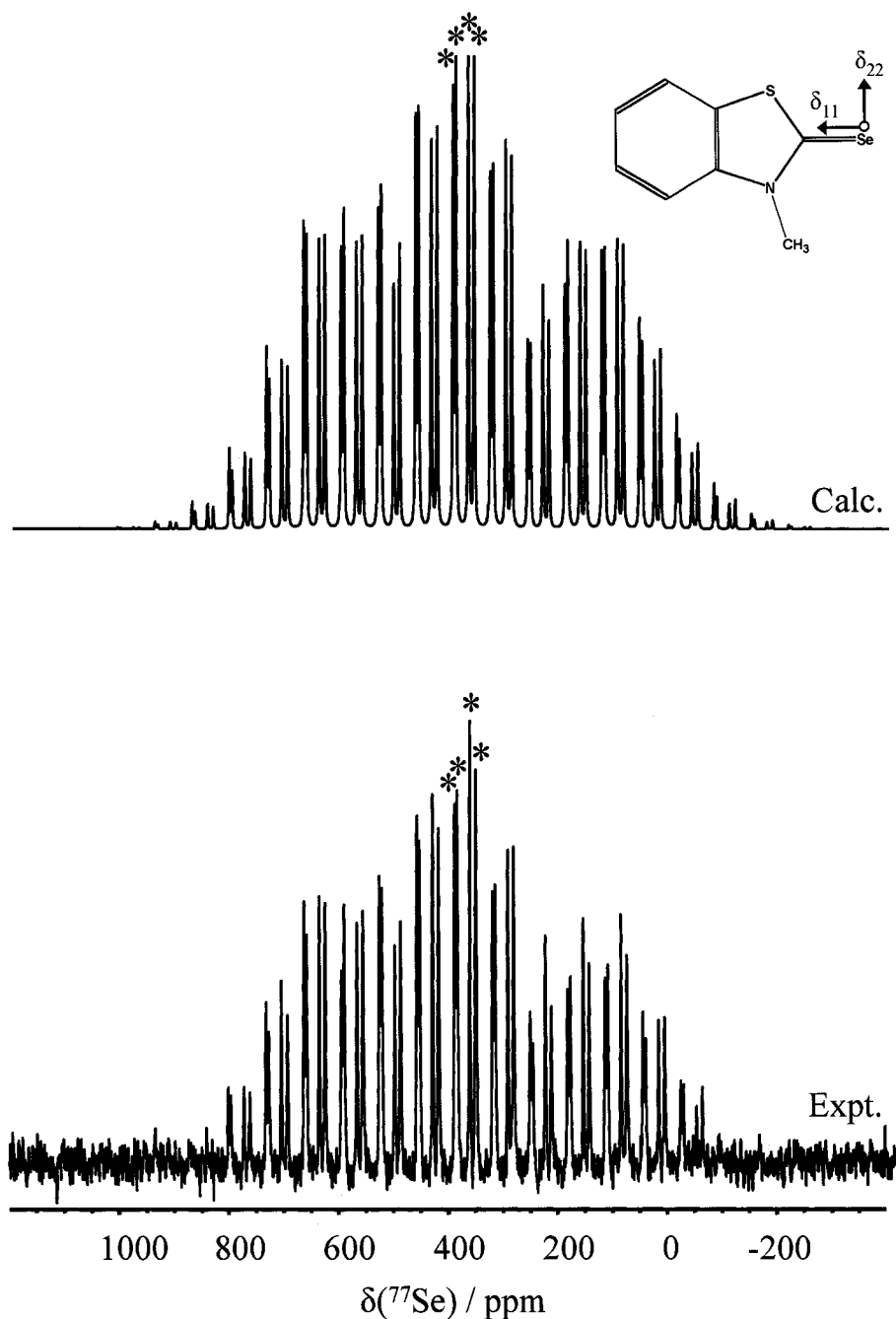
tensor for selenium in this compound has not previously been reported; however, some solution  $^{77}\text{Se}$  NMR has been performed.<sup>113</sup> The isotropic chemical shift for the solid, 211 ppm, is somewhat deshielded relative to the solution value of 147 ppm,<sup>113</sup> both of which are common values for seleno-carbonyls possessing nitrogen substituents. The difference between the two shifts is not surprising given the effect of intermolecular interactions.<sup>18</sup>

The calculated isotropic selenium chemical shifts for **1** using the NR, SR, and SO methods are in reasonable agreement with each other (Table 4.1); however all three methods overestimate the experimental value of 211 ppm. Unlike the majority of the compounds investigated herein, the value of  $\delta_{33}(\text{Calc.})$  is not underestimated by the calculations, but is one of the few that slightly overestimates this component. The span of the chemical shift tensor is overestimated at both the non-relativistic and scalar relativistic levels of theory; however, the spin-orbit relativistic calculation accurately reproduces the experimental value of  $\Omega$ . Thus, the value of  $\delta_{33}(\text{Calc.})$  does not balance the corresponding overestimated value of  $\delta_{11}(\text{Calc.})$  to obtain a calculated isotropic chemical shift that is in good agreement with the experimental value of **1**, as with the majority of the compounds investigated.

The orientations of the principal components calculated at all levels of theory are consistent in determining that the direction of greatest shielding,  $\delta_{33}$ , lies approximately along the C-Se vector, the intermediate principal component,  $\delta_{22}$ , is directed nearly perpendicular to the N-C-Se plane, and  $\delta_{11}$  orthogonal to the others, is slightly removed from coinciding with the N-C-Se plane (inset Figure 4.5). For comparison purposes, the orientation of the  $^{17}\text{O}$  chemical shift tensor in urea has  $\delta_{11}$  within the N-C-O plane, perpendicular to the C-O vector which is similar to the selenium homologue; however it

is the  $\delta_{22}$ , and not the  $\delta_{33}$  component that is oriented parallel to the chalcogen-carbon vector in urea.<sup>116</sup> The difference between the two orientations is likely a result of a larger paramagnetic (deshielding) effect in the N-C-Se plane of **1** than in the N-C-O plane of urea. This results in a larger principal component directed perpendicular to the respective plane than parallel to the carbon-chalcogen vector in the selenium species.

**2.** *N*-methylbenzothiazole-2-selone is a nearly planar molecule containing an aromatic ring with a seleno-carbonyl functional group (see Figure 4.1). This appears to be the first reported <sup>77</sup>Se NMR investigation of this compound. The <sup>77</sup>Se NMR spectrum of **2**, Figure 4.6, acquired with MAS clearly shows four isotropic peaks, and four unique <sup>77</sup>Se chemical shift tensors are recorded for the as-received sample in Table 4.1. The crystal structure for *N*-methylbenzothiazole-2-selone suggests only two non-equivalent selenium atoms are present in the unit cell.<sup>90</sup> The XRD identification was performed on only one of the two crystalline forms from a methylene chloride recrystallization of the sample, stating that the other form was not suitable for X-ray investigation.<sup>90</sup> The isotropic chemical shifts for all four of the tensors for this sample are very similar, and in agreement with related compounds containing the C=Se moiety in which the carbon is bonded to one or more nitrogen atoms.<sup>18</sup> A study of <sup>77</sup>Se  $T_1$  relaxation mechanisms of several selones in solution indicated chemical shift anisotropies on the order of 3000-6000 ppm,<sup>117</sup> which appear overestimated given the data for **1** and **2**. However, the same study reported a chemical shift anisotropy of 400 ppm for **6**, which is in line with our findings (vide infra).

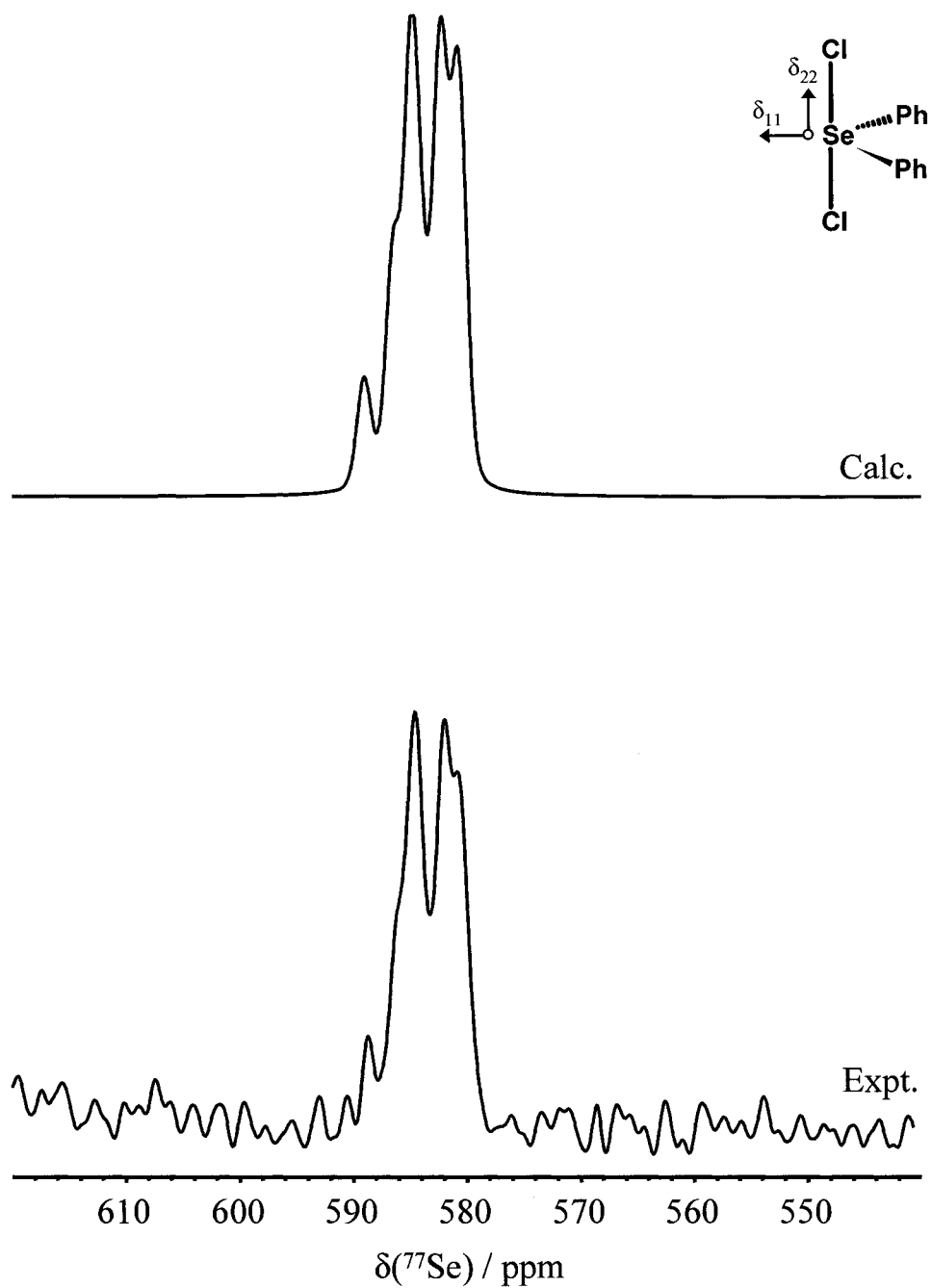


**Figure 4.6** RACP MAS  $^{77}\text{Se}$  NMR spectrum and the simulated spectrum of *N*-methylbenzothiazole-2-selone (**2**). Experimental parameters: 9.4 T, 1868 scans, 5.2 kHz MAS, with line broadening of 50 Hz applied, a 10.0 ms contact time, and a 20 s recycle delay. The isotropic peaks are labeled with an asterisk (\*). Inset is a schematic of compound **2** showing the orientation of the selenium chemical shift tensor calculated at the scalar with spin-orbit relativistic level of theory.

There are a pair of chemical shift tensors, however, that might be distinguishable from the other via calculation of their respective magnetic shielding tensors, and these pairs have been identified as **2a** and **2b** corresponding to the tensors with the two smallest and two largest isotropic chemical shifts, respectively. Each of the two selenium magnetic shielding tensors calculated from the crystal structure of **2** are compared with the pair of experimental selenium chemical shift tensors that they correspond most closely with. While this assignment is arbitrary it is noted that for all calculations the site with the smaller isotropic  $^{77}\text{Se}$  chemical shift also has a smaller span, and the larger  $\delta_{\text{iso}}(\text{Calc.})$  was found from the trace of a tensor with a broader extent of shielding. The attributes of these calculated chemical shift tensors are mimicked in the distinctions between the pairs of experimental tensors labeled **2a** and **2b**. The differences between the calculated isotropic values of sites **2a** and **2b** at all levels of theory are similar to those between the pairs of experimental tensors. The general trends observed for the majority of the calculations in Figures 4.2 – 4.4 hold for both calculated chemical shift tensors in **2**. Identical orientations for the calculated shielding tensors are obtained, regardless of the level of theory employed. The direction of  $\delta_{11}$  lies nearly coincident with the C-Se vector, and  $\delta_{33}$  is perpendicular to the molecular plane, as illustrated inset within Figure 4.6. The orientations for **2** are different from both the orientations for  $^{77}\text{Se}$  in **1** and for  $^{17}\text{O}$  in urea;<sup>116</sup> however the calculated  $^{77}\text{Se}$  chemical shift tensors for **2** are oriented nearly identically to the  $^{17}\text{O}$  chemical shift tensor determined for benzamide.<sup>118</sup> The similarities and differences between the orientations of  $^{17}\text{O}$  and  $^{77}\text{Se}$  chemical shift tensors in ketones and selenones suggests that the shielding interaction in seleno-carbonyl

compounds is at least as complicated as their oxygen counterparts, and is very sensitive to the environment of this functional group.

**3.** Diphenylselenium dichloride provides a four-coordinate environment around the selenium in which the molecule adopts a seesaw configuration with a Cl-Se-Cl angle of approximately  $180(5)^\circ$ .<sup>91</sup> The calculated and experimental isotropic  $^{77}\text{Se}$  NMR spectra for **3** are given in Figure 4.7. The selenium nucleus experiences residual dipolar coupling<sup>119-127</sup> from the quadrupolar chlorine nuclei ( $^{35/37}\text{Cl}$ ), with a residual dipolar coupling constant of 41 Hz at 9.4 T. Based on the  $^{35}\text{Cl}$  NQR frequency of 23.076 MHz provided by an NQR study for **3**,<sup>128,129</sup> and the Se-Cl distance of 2.30 Å,<sup>91</sup> a residual dipolar coupling constant of 65 Hz was anticipated. An indirect spin-spin coupling constant,  $^1J(^{77}\text{Se}, ^{35}\text{Cl})_{\text{iso}}$ , of 110 Hz is observed, and appears to be the first reported coupling between selenium and chlorine. Indirect spin-spin coupling has previously been reported between tellurium-125 and chlorine-35 in  $\text{Me}_3\text{TeCl}\cdot\text{H}_2\text{O}$ ,<sup>130</sup> in which the  $^{125}\text{Te}$  is coupled to two  $^{35}\text{Cl}$  nuclei similar to the environment observed in **3**. Scaling of  $^1J(^{125}\text{Te}, ^{35}\text{Cl})_{\text{iso}}$  by  $4\pi^2/h\gamma_{\text{Te}}\gamma_{\text{Cl}}$  to yield the reduced coupling constant,  $^1K(\text{Te}, \text{Cl})$ ,  $283 \times 10^{19} \text{ T}^2 \text{ J}^{-1}$  indicates that the corresponding value of  $487 \times 10^{19} \text{ T}^2 \text{ J}^{-1}$  for  $^1K(\text{Se}, \text{Cl})$  in **3** is of an appropriate magnitude. The principal components,  $\delta_{ii}$  (Table 4.1), determined in the simulation indicate an axially symmetric chemical shift tensor. There are however, no symmetry reasons for the chemical shift tensor to attain this axial symmetry. It is known that methods for obtaining the principal components of the chemical shift tensor from spectra of MAS samples have the greatest difficulty with axially or near axially symmetric species.<sup>131</sup> The isotropic chemical shift,  $\delta_{\text{iso}} = 584 \text{ ppm}$ , agrees well with the value for **3** in a chloroform solution,  $\delta_{\text{iso}} = 575 \text{ ppm}$ .<sup>114</sup>



**Figure 4.7** Selenium-77 RACP MAS NMR center band (spinning sidebands summed in) spectrum of compound **3**:  $\text{Ph}_2\text{SeCl}_2$  (9.4 T, 972 scans,  $\nu_{\text{rot}} = 4.0$  kHz, 50 Hz line broadening, 10.0 ms contact time, 60 s pulse delay), and its simulation. Inset is a schematic of compound **3** showing the orientation of the selenium chemical shift tensor calculated at the scalar with spin-orbit relativistic level of theory.

All of the calculated principal components of the  $^{77}\text{Se}$  chemical shift tensor, given in Table 4.1, fail to reproduce the observed axial symmetry and the small span for  $\text{Ph}_2\text{SeCl}_2$  experimentally. The orientations determined from each of the calculations were in agreement with each other. The direction of  $\delta_{11}$  is predicted to bisect the  $\text{C}_{\text{ipso}}\text{-Se-C}'_{\text{ipso}}$  angle, i.e., corresponds to the direction of the formal 'lone pair'. The intermediate principal component,  $\delta_{22}$ , is parallel to the approximately linear Cl-Se-Cl vector, and  $\delta_{33}$  perpendicular to the other two components lies in the  $\text{C}_{\text{ipso}}\text{-Se-C}'_{\text{ipso}}$  plane (inset Figure 4.7).

4. Seleno-DL-methionine is a seleno-amino acid where the sulfur in methionine has been replaced with selenium (Figure 4.1). A solid-state  $^{77}\text{Se}$  NMR investigation of this compound has been reported by Potrzebowski et al.,<sup>115</sup> and our parameters agree very well with those obtained in their investigation (Table 4.1). For selenium in a similar dialkyl environment, a selenium coronand, Batchelor et al. reported isotropic chemical shifts from 173 to 737 ppm for the four crystallographically non-equivalent selenium atoms, with spans ranging from less than 370 to 771 ppm.<sup>132</sup>

The NR, SR, and SO calculations of the chemical shift tensor principal components for seleno-DL-methionine are in very good agreement with the experimental results (Table 4.1). Deviating from the general trend observed for the calculations in Figure 4.3a, the shielding along the  $\delta_{11}$  direction is in reasonable agreement with the experimental value, if not slightly overestimated. The magnetic shielding tensor's calculated orientation, by all methods, is such that  $\delta_{11}$  lies approximately along the Se- $\text{C}_{\text{terminal}}$  bond axis,  $\delta_{22}$  is directed perpendicular to the  $\text{C}_{\gamma}\text{-Se-C}_{\text{terminal}}$  plane, and the smallest principal component of the chemical shift tensor,  $\delta_{33}$ , is nearly parallel to the



bond axis between the  $\gamma$ -carbon and selenium. Potrzebowski et al. did not perform any theoretical calculation of the selenium chemical shift tensor in **4**;<sup>115</sup> however, the orientation that they assumed is in accord with those determined by our DFT calculations.

**5.** Similar to the sulfur analogues,<sup>133</sup> tetraselenafulvalenes are precursors for conducting and superconducting materials.<sup>93</sup> The crystal structure of **5** contains an inversion center within the molecule such that only two of the selenium atoms within the molecule are expected to give rise to unique chemical shift tensors.<sup>93</sup> The values for the two sets of principal components observed are in very good agreement with a previous solid-state <sup>77</sup>Se NMR investigation of this compound by Collins et al. (Table 4.1).<sup>73</sup> The chemical shift tensors are nearly identical indicating that the electronic environments of the magnetically non-equivalent selenium atoms are very similar. Comparable isotropic chemical shifts, 408-624 ppm, and spans, 554-687 ppm, have been reported for a series of 1,3-selenazoles which possess selenium in a similar environment to the tetraselenafulvalenes.<sup>134</sup>

All theoretical methods perform equally well in reproducing the experimentally determined principal components for **5a** and **5b** (Table 4.1). The calculated orientations of the chemical shift tensors are predicted to be the same for both **5a** and **5b**, and are consistent across all of the methods employed. The direction of  $\delta_{11}$  is predicted to bisect the C-Se-C angle,  $\delta_{22}$  is oriented perpendicular to the molecular plane, and  $\delta_{33}$  is calculated to be within the skeletal molecular plane, directed close to the Se-C vector of the Se-C-Se component of the molecule.

**6.** Diselenides, the selenium equivalent of organic peroxides, are an intriguing functional group as they possess glutathione peroxidase-like activity.<sup>135-139</sup> The Bloch decay

spectrum (not shown) indicates two selenium environments with distinct chemical shift tensors. The number of sites and their parameters agree well with a previous solid-state  $^{77}\text{Se}$  CP MAS investigation of compound **6**,<sup>111</sup> specifically in the large difference in the most shielded component,  $\delta_{33}$ , of the two tensors **6a** and **6b** (Table 4.1).

The spin-orbit calculation produces a more accurate value of the span for **6b** due to an increased accuracy in the values for both  $\delta_{11}$  and  $\delta_{33}$ . The more accurate values of  $\delta_{ii}$ (Calc.) from the SO calculation indicates a contribution from spin-orbit coupling, likely in part from the presence of the directly bonded selenium. The calculated orientations for the two selenium shielding tensors in diphenyl diselenide are nearly identical. The direction of greatest shielding,  $\delta_{33}$ , most closely approaches a parallel direction to the Se-Se bond vector,  $\delta_{22}$  bisects the Se-Se-C<sub>ipso</sub> angle, and the largest principal component of the chemical shift tensor,  $\delta_{11}$ , is oriented perpendicular to the Se-Se-C<sub>ipso</sub> plane. Theoretical studies<sup>111</sup> have indicated that the differences in the chemical shift anisotropy mainly result from a  $\beta$ -effect of the torsional angle for the phenyl group at the next selenium, not the directly bonded selenium.

The chemical shift tensors investigated for compounds **1** – **6** are shown to represent the chemical diversity of these organoselenium species, and are calculated similarly with and without the consideration of relativistic effects.

#### 4.4.3 Organophosphine Selenides

The organophosphine selenides, R<sub>3</sub>PSe, provide an opportunity to investigate a number of peripheral modifications to one specific functional group.

**Table 4.2** Experimental and Theoretical Chemical Shift Tensors<sup>a)</sup> for Tris-Organophosphine Selenides.

		$\delta_{180}$	$\delta_{11}$	$\delta_{22}$	$\delta_{33}$	$\Omega$
<b>7</b>	Expt. <sup>b)</sup>	-204	-116	-130	-365	249
	<sup>c)</sup>	-199.6	-117.7	-131.7	-349.3	231.6
	NR	-207	35	-219	-437	472
	SR	-193	70	-188	-461	531
	SO	-200	17	-231	-385	402
<b>8</b>	Expt. <sup>b)</sup>	-408	-386	-419	-419	33
	<sup>d)</sup>	-414.5				
	NR	-485	-401	-486	-568	167
	SR	-475	-381	-455	-589	208
	SO	-481	-410	-493	-541	131
<b>9</b>	Expt. <sup>b)</sup>	-437	-150	-580	-580	430
	<sup>e)</sup>	-466.4				
	NR	-603	-213	-745	-850	637
	SR	-598	-193	-732	-868	675
	SO	-602	-208	-776	-823	615
<b>10a</b>	Expt. <sup>b)</sup>	-257	-124	-300	-345	221
	<sup>c)</sup>	-257.5	-122.5	-288.4	-361.5	239.0
	NR	-286	-59	-288	-512	453
	SR	-267	-20	-303	-478	458
	SO	-277	-100	-238	-494	394
<b>10b</b>	Expt. <sup>b)</sup>	-242	-93	-293	-340	247
	<sup>c)</sup>	-242.6	-86.2	-264.1	-377.4	291.2
	NR	-249	22	-270	-498	520
	SR	-228	63	-281	-467	530
	SO	-239	-20	-220	-476	456
<b>11a</b>	Expt. <sup>b)</sup>	-316	-161	-292	-494	333
	<sup>f)</sup>	-364.7				
	NR	-396	-178	-352	-627	449
	SR	-370	-142	-336	-633	491
	SO	-379	-191	-334	-611	420
<b>11b</b>	Expt. <sup>b)</sup>	-403	-224	-438	-548	324
	<sup>f)</sup>	-364.7				
	NR	-576	-363	-646	-720	357
	SR	-563	-347	-620	-723	376
	SO	-567	-324	-661	-715	391
<b>12</b>	Expt. <sup>b)</sup>	-242	-155	-241	-331	176
	<sup>g)</sup>	-264				
	NR	-277	-49	-322	-460	411
	SR	-256	-4	-306	-458	454
	SO	-267	-57	-297	-448	391
<b>13</b>	Expt. <sup>b)</sup>	-30	253	-98	-245	498
	<sup>g)</sup>	-28.4				
	NR	-70	260	-42	-428	688
	SR	-37	318	-12	-417	735
	SO	-46	273	-163	-249	522

a) Chemical shifts in ppm with respect to external Me<sub>2</sub>Se.

b) This Work.

c) Ref. <sup>27</sup>

d) Ref. <sup>140</sup>

e) Ref. <sup>141</sup>

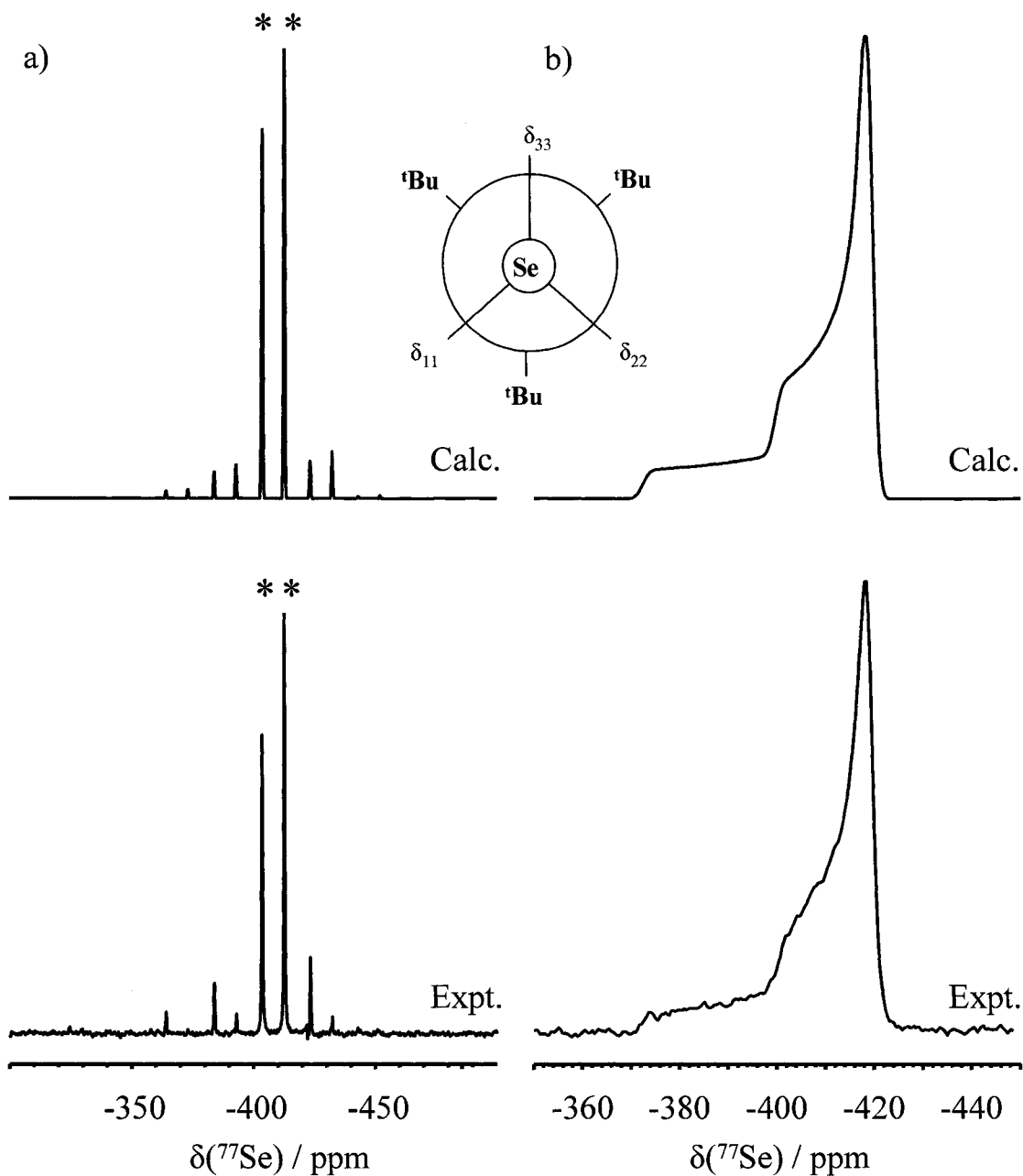
f) Ref. <sup>142</sup>

g) Ref. <sup>143</sup>

7. The selenium chemical shift tensor principal components of Me<sub>3</sub>PSe, from Herzfeld-Berger analysis of the MAS spectrum (not shown), and indirect spin-spin coupling parameters,  $J_{\text{iso}}$  and  $\Delta J$ , are in good agreement with those of an investigation by Grossmann et al. on 70% <sup>77</sup>Se enriched **7** (see Table 4.2).<sup>27</sup> There exists a single selenium environment that is coupled to the phosphorus with an indirect spin-spin coupling constant,  $^1J(^{77}\text{Se},^{31}\text{P})_{\text{iso}}$ , of -656 Hz, and a direct dipolar coupling constant of 990 Hz (calculated from  $r_{\text{PSe}} = 2.111 \text{ \AA}^{95}$ ), which results in a value of 700 Hz for  $\Delta J$  (equation 4.2).

The crystal structure for **7** does not possess a  $C_3$  symmetry axis along the P-Se bond,<sup>95</sup> and thus three distinct principal components are calculated consistent with the non-axially symmetric chemical shift tensor observed experimentally. The calculated chemical shift tensors at the NR, SR, and SO levels of theory are compared in Table 4.2 with the experimental values obtained herein, and by Grossmann et al.<sup>27</sup> for solid Me<sub>3</sub>PSe. The deviation in the calculations of the individual principal components manifests itself in larger spans. All of the calculations produce similarly oriented tensors, predicting that  $\delta_{33}$  lies approximately along the P-Se vector. This is in agreement with the simulation of the <sup>77</sup>Se NMR spectrum of a stationary sample (not shown) and based on a dipolar-splitting-ratio method investigation of this compound.<sup>27</sup>

8. Figure 4.8 shows the calculated and experimental spectra for tris-(*tert*-butyl)phosphine selenide (<sup>t</sup>Bu<sub>3</sub>PSe) under MAS and stationary conditions. The MAS spectrum yields the components of the selenium chemical shift tensor, as well as the isotropic spin-spin coupling constant,  $^1J(^{77}\text{Se},^{31}\text{P})_{\text{iso}}$ , -693 Hz. The principal components of the chemical shift tensor given in Table 4.2 are the first to be reported for compound **8**. The solid-state



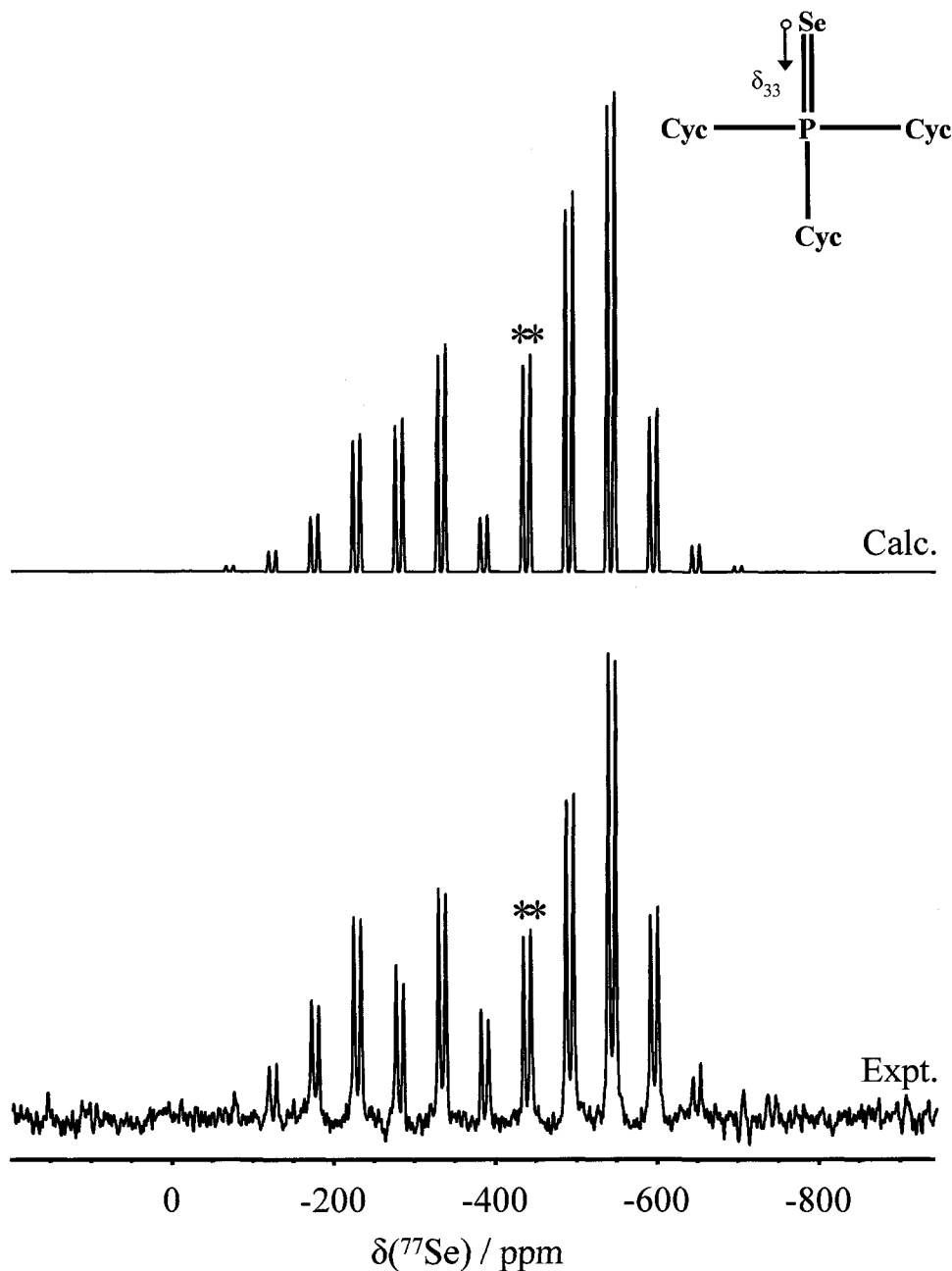
**Figure 4.8** (a) CP MAS  $^{77}\text{Se}$  NMR spectrum, and its simulation, of  $t\text{Bu}_3\text{PSe}$  (**8**) at 9.4 T, after 88 scans, 1.5 kHz MAS, 30 Hz of line broadening, a contact time of 4.0 ms, and a recycle delay of 4 s. The  $J$ -coupled isotropic peaks are labeled with asterisks (\*). (b) Experimental and simulated CP  $^{77}\text{Se}$  NMR spectra of stationary **8**. Experimental conditions: 9.4 T, 6116 transients, 200 Hz line broadening, a 4.0 ms contact time, and a 10 s pulse delay. Inset is a Newman projection along the P-Se bond of compound **8** showing the orientation of the selenium chemical shift tensor calculated at the scalar with spin-orbit relativistic level of theory.

values of  $\delta_{\text{iso}}$  and  $^1J(^{77}\text{Se}, ^{31}\text{P})_{\text{iso}}$  agree well with the values from  $^{31}\text{P}$  and  $^{77}\text{Se}$  solution NMR.<sup>140</sup> The spectrum of a stationary sample, together with the information from the MAS spectrum, yields the effective dipolar coupling constant,  $R_{\text{eff}}$ , 660 Hz. The dipolar coupling constant,  $R_{\text{DD}}$ , is calculated to be 960 Hz ( $r_{\text{PSe}} = 2.133 \text{ \AA}^{96}$ ) requiring a  $\Delta J$  of 900 Hz (equation 4.2).

The  $\delta_{\text{ii}}$  values from the ZORA DFT calculations for  $^t\text{Bu}_3\text{PSe}$  do not reproduce the experimental values or their orientations, which is not surprising considering the extremely small span observed,  $\Omega(\text{Expt.})$ , 33 ppm. From the dipolar-splitting-ratio analysis of the spectrum of a stationary sample (Figure 4.8b) and the known molecular environment, the unique component of shielding,  $\delta_{11}$ , should lie along the direction of the P-Se bond. The NR and SR calculations incorrectly predict that  $\delta_{33}$  is closest to the P-Se vector, and the SO calculation determines that all of the principal components are approximately equidistant from the internuclear vector (inset Figure 4.8).

**9.** The calculated and experimental spectra of MAS samples for tri-cyclohexylphosphine selenide ( $\text{Cyc}_3\text{PSe}$ ) are given in Figure 4.9. Due to the length of time required to obtain the MAS spectrum, the corresponding spectrum of a stationary sample for **9** was not acquired. The principal components of the chemical shift tensor are given in Table 4.2, and the isotropic chemical shift agrees well with the solution value previously reported.<sup>141</sup> A value of -682 Hz for  $^1J(^{77}\text{Se}, ^{31}\text{P})_{\text{iso}}$  was obtained, which compares very well with the values from a solution and solid-state  $^{31}\text{P}$  NMR investigation.<sup>97</sup>

The majority of the generally observed trends for the calculations are upheld in the calculation of the chemical shift tensor for **9**. A specific exception occurs for



**Figure 4.9** Selenium-77 RACP MAS NMR and calculated spectra for  $\text{Cyc}_3\text{PSe}$  (**9**). Experimental conditions: 9.4 T, 4912 scans, spinning at 4.0 kHz, 300 Hz of line broadening, a 1.0 ms contact time, and a 20 s recycle delay. The  $J$ -coupled isotropic peaks are labeled with asterisks (\*). Inset is a schematic of compound **9** showing the orientation of the selenium chemical shift tensor calculated at the scalar with spin-orbit relativistic level of theory.

$\delta_{11}$ (Calc.) where the shielding is overestimated compared to the experimentally determined value. Despite this, the larger than experimentally observed values of  $\Omega$ (Calc.) are a result of the small calculated values of  $\delta_{33}$ . All calculations predict that the  $\delta_{33}$  component is closest to the P-Se vector, as shown inset in Figure 4.9.

**10.** There are two non-equivalent  $\text{Ph}_3\text{PSe}$  molecules in the unit cell.<sup>98</sup> The chemical shift tensors have been labeled in the same manner as in a previous investigation of **10** by Grossmann et al.,<sup>27</sup> and our values obtained at natural abundance agree well with those from their investigation on 70%  $^{77}\text{Se}$  enriched **10**. The isotropic spin-spin coupling constants, -733 and -736 Hz for **10a** and **10b**, are also in agreement with values reported earlier.

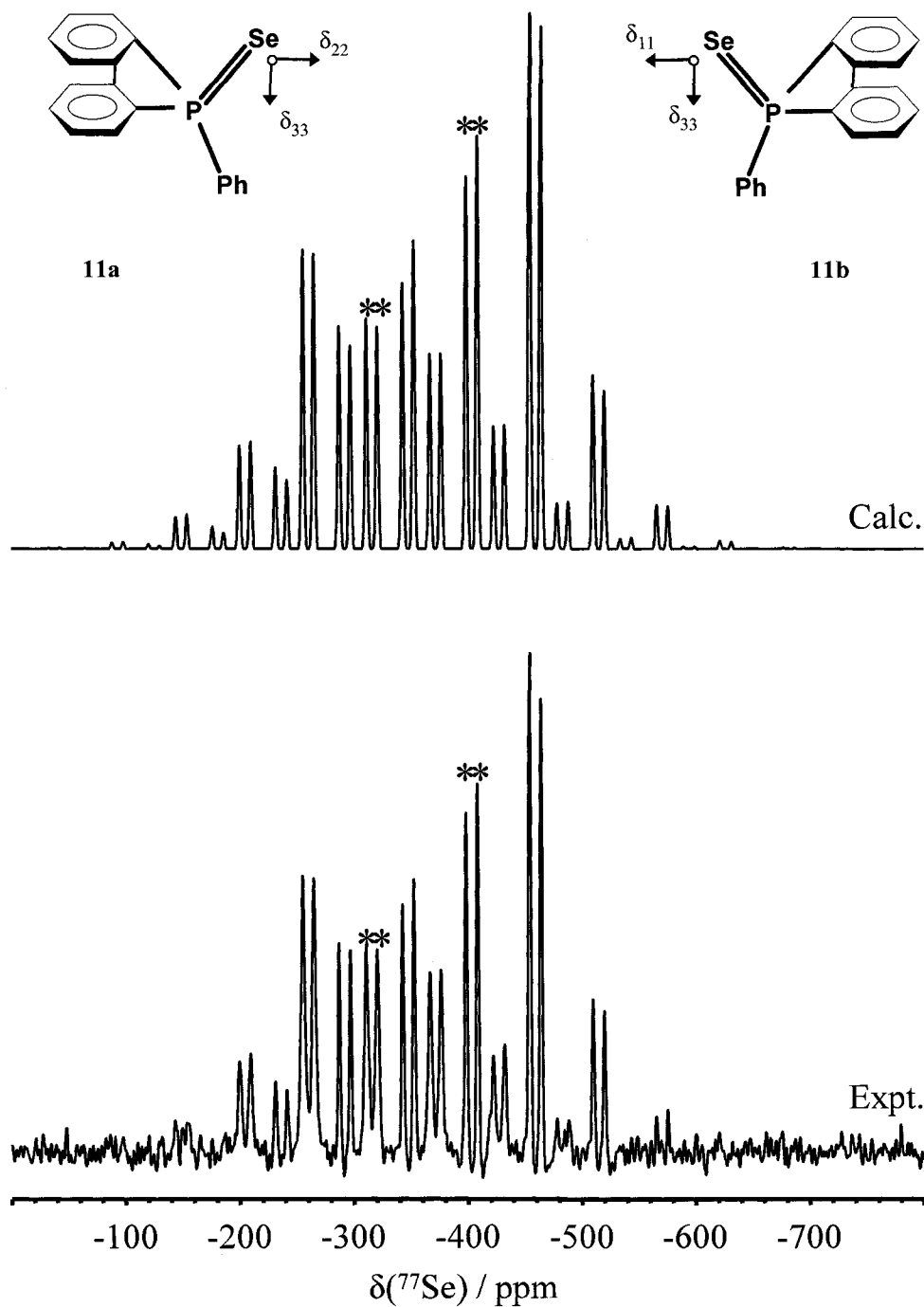
The calculations for the two non-equivalent selenium environments, **10a** and **10b**, given in Table 4.2 show slight variation between the computational methods employed, and adhere to the general trends shown in Figures 4.2 – 4.4. The calculated orientations for the chemical shift tensors for the selenium atoms in **10a** and **10b** are unique to the organophosphine selenides investigated in that it is  $\delta_{22}$  that lies approximately along the P-Se direction, and this is consistent with the orientation from a dipolar-splitting-ratio method investigation of 70% enriched  $\text{Ph}_3\text{P}^{77}\text{Se}$ .<sup>27</sup> The orientation shows some parallels with the  $^{17}\text{O}$  chemical shift tensors in the monoclinic and orthorhombic forms of  $\text{Ph}_3\text{PO}$ , where both crystallographic forms have  $\delta_{11}$  oriented along the P-O vector.<sup>144</sup> With  $\delta_{11}$  along the P-O direction in  $\text{Ph}_3\text{PO}$  it was inferred from the value of the shielding that the bonding environment is more appropriately represented by  $\text{Ph}_3\text{P}^+-\text{O}^-$  according to Ramsey's theory of nuclear magnetic shielding.<sup>51,52</sup> In both chemical shift tensors for **10**,  $\delta_{22}$  lies along the P-Se vector, and indicates that a similarly small deshielding occurs



along this direction consistent with a polarized,  $\text{Ph}_3\text{P}^+-\text{Se}^-$ , description of the phosphorus-selenium bond.

**11.** The spectrum of an MAS sample for 5-phenyldibenzophosphine 5-selenide, and its best-fit simulation are given in Figure 4.10. While similar in skeletal structure and number of molecules in the asymmetric unit to **10**, **11** possesses a dibenzophosphole moiety (inset of Figure 4.10). A spectrum of a stationary sample could not be obtained in a reasonable amount of time to afford sufficient analysis. The isotropic chemical shifts, -316 and -403 ppm, and indirect spin-spin coupling constants, -733 and -768 Hz, for **11a** and **11b** respectively, are in reasonable agreement with the corresponding motionally averaged values found in a  $\text{CDCl}_3$  solution,<sup>142</sup> as well as the  $^1J(^{77}\text{Se}, ^{31}\text{P})_{\text{iso}}$  values from a solid-state phosphorus-31 NMR investigation.<sup>145</sup>

The values of  $\delta_{ii}(\text{Calc.})$  for **11a** and **11b** are compared with the experimentally determined values in Table 4.2. The relatively accurate values of  $\Omega(\text{Calc.})$  by all methods results from the lack of overestimation for the values of  $\delta_{11}(\text{Calc.})$  as generally observed for the chemical shift tensors calculated in this investigation. The orientations calculated for compound **11** are the only ones investigated in this study that display significant differences between the two selenium environments **a** and **b**. All DFT calculations indicate that the selenium chemical shift tensor for **11a** is oriented such that  $\delta_{11}$  is perpendicular to the Se-P vector, and that this vector bisects the  $\delta_{22}\text{-Se-}\delta_{33}$  angle. While similar to that determined for **11a**,  $\delta_{22}$  for **11b** is perpendicular to the Se-P bond, and it is the  $\delta_{11}\text{-Se-}\delta_{33}$  angle that is bisected by the bond vector. As for **11a** the calculated orientations for **11b** are consistent regardless of the level of theory employed.

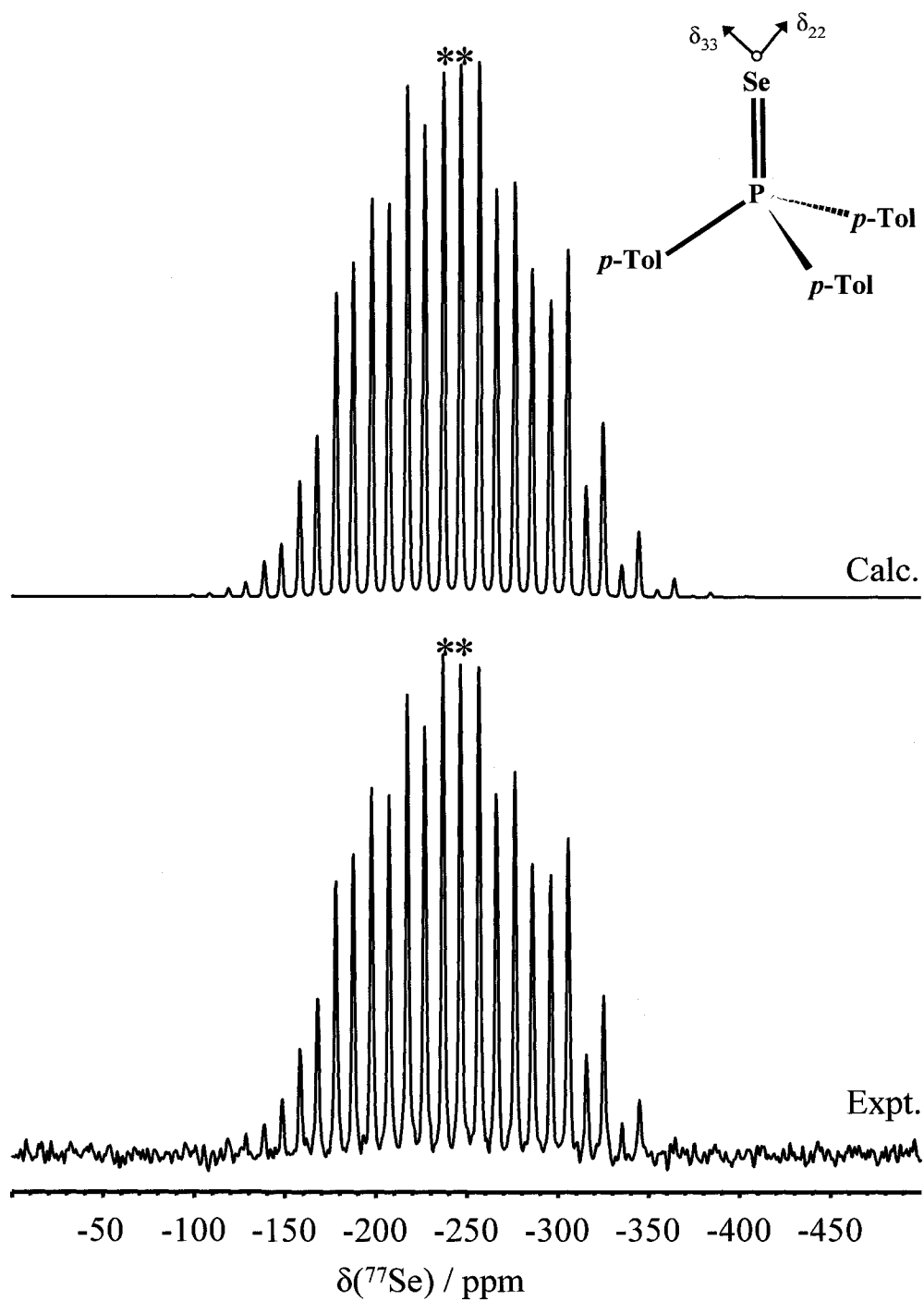


**Figure 4.10** 5-phenyldibenzophosphine 5-selenide (**11**) simulated and experimental RACP MAS  $^{77}\text{Se}$  spectra obtained at 9.4 T, 2906 scans, 4.2 kHz MAS, line broadened to 80 Hz, a 15.0 ms contact time, and a pulse delay of 60 s. The  $J$ -coupled isotropic peaks are labeled with asterisks (\*). Inset are schematics of compounds **11a** and **11b** showing the orientation of the selenium chemical shift tensors calculated at the scalar with spin-orbit relativistic level of theory.

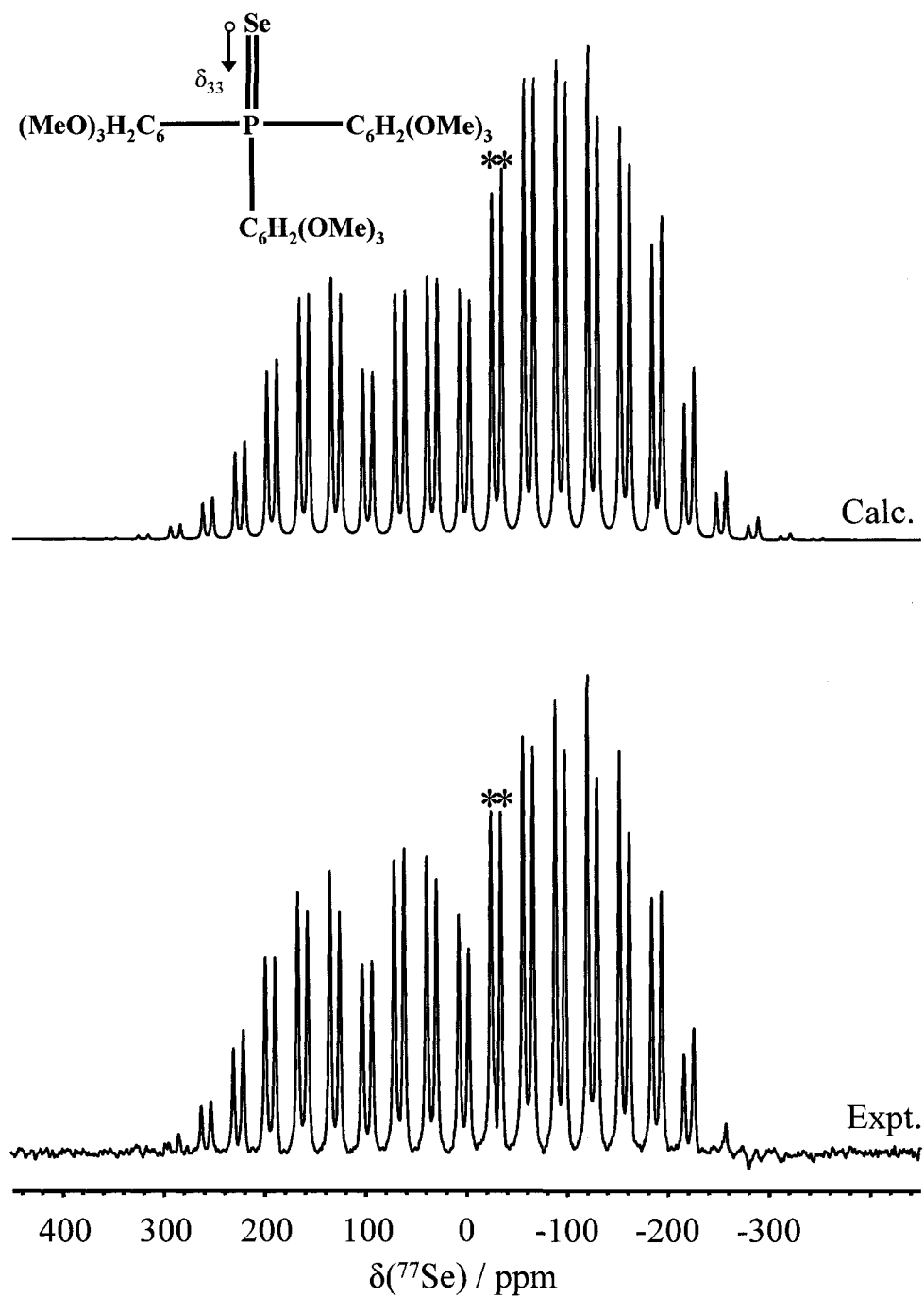
**12.** The calculated and experimental spectra for tri-*para*-tolylphosphine selenide (*p*-Tol<sub>3</sub>PSe) under MAS conditions are given in Figure 4.11. A spectrum of a stationary sample was not recorded. The experimental values of  $\delta_{\text{iso}}$ , -242 ppm, and  $^1J(^{77}\text{Se}, ^{31}\text{P})_{\text{iso}}$ , -732 Hz, compare well with the corresponding solution  $^{77}\text{Se}$  NMR values previously reported.<sup>143</sup> The principal components of the chemical shift tensor for **12** are reported in Table 4.2.

The calculated chemical shift tensor for selenium in *p*-Tol<sub>3</sub>PSe was obtained with the NR, SR, and SO calculations. The value of  $\delta_{\text{iso}}(\text{Expt.})$  is well reproduced, and the individual principal components achieve slightly poorer agreement by all methods, as expected. Each of the calculations arrive at similarly oriented selenium chemical shift tensors. The Se-P vector is directed perpendicular to  $\delta_{11}$ , and bisects the  $\delta_{22}$ -Se- $\delta_{33}$  angle (inset Figure 4.11). Despite structure similarities with **10**, the orientation of the chemical shift tensor PAS for **12** is different; however, orientations can differ when relatively small spans are encountered.

**13.** The experimental and simulated spectra for tris-2,4,6-trimethoxyphenylphosphine selenide (TTMPSe) are given in Figure 4.12. A spectrum for stationary **13** was not acquired. The principal components of the chemical shift tensor of **13** are given in Table 4.2. The span of the tensor is the largest observed of the organophosphine selenides investigated. The isotropic chemical shift, -30 ppm, and indirect spin-spin coupling constant, -735 Hz, are in excellent agreement with previously reported solution  $^{77}\text{Se}$  NMR values.<sup>143</sup>



**Figure 4.11** CP MAS  $^{77}\text{Se}$  NMR spectrum and the calculated spectrum for *p*-Tol<sub>3</sub>PSe (**12**). Experimental parameters: 9.4 T, 642 transients, 1.5 kHz MAS, 30 Hz line broadening, a contact time of 15.0 ms, and a 30 s recycle delay. The *J*-coupled isotropic peaks are labeled with asterisks (\*). Inset is a schematic of compound **12** showing the orientation of the selenium chemical shift tensor calculated at the scalar with spin-orbit relativistic level of theory.



**Figure 4.12** Experimental  $^{77}\text{Se}$  CP MAS NMR and calculated spectra for TTMPSe (**13**) at 9.4 T. Experimental parameters: 15212 scans, spinning at 2.4 kHz, 100 Hz of line broadening, a 10.0 ms contact time, and a 4 s pulse delay. The  $J$ -coupled isotropic peaks are labeled with asterisks (\*). Inset is a schematic of compound **13** showing the orientation of the selenium chemical shift tensor calculated at the scalar with spin-orbit relativistic level of theory.

It is apparent from Table 4.2 that the NR and SR calculations have the greatest difficulty in reproducing the experimental value of  $\delta_{33}$ . However, the SO calculation accurately reproduces the experimental value of  $\delta_{33}$ , and subsequently reproduces the entire chemical shift tensor for selenium to a greater extent in **13**. This improvement in calculating the entire chemical shift tensor is reflected in a more accurate value of  $\Omega(\text{Calc.})$  with respect to  $\Omega(\text{Expt.})$  (Table 4.2); however, the origin of the spin-orbit coupling effect for **13** is unclear in relation to the apparent lack of such a contribution for compounds **7** – **12**. All levels of theory predict that  $\delta_{33}$  lies closest to the P-Se bond, as depicted inset in Figure 4.12.

Upon review of compounds **7** – **13**, it is apparent that even minor peripheral modifications to the phosphine selenide functional group can produce differences in the magnitude and orientation of the principal components of the selenium chemical shift tensor. All of the selenium chemical shift tensor principal components for the organophosphine selenides investigated show relatively small deshieldings along the direction of the P-Se bond indicating that the bonding environment is most appropriately described by a polarized,  $\text{R}_3\text{P}^+\text{-Se}^-$ , representation. In general the computations perform well regardless of the level of inclusion of relativistic effects.

#### 4.4.4 Inorganic Selenium Compounds

While selenium will likely find itself in as many, if not more, different inorganic molecular environments as found in organoselenium compounds, the most likely to occur include selenium in a highly coordinated environment, selenium as a terminal moiety and selenium as a bridging nucleus between inorganic nuclei. Thus, we investigated

**Table 4.3** Experimental and Theoretical Chemical Shift Tensors<sup>a)</sup> for Inorganic Selenium Compounds.

		$\delta_{\text{iso}}$	$\delta_{11}$	$\delta_{22}$	$\delta_{33}$	$\Omega$
<b>14</b>	Expt. <sup>b)</sup>	1040.2	1076	1038	1008	68
	<sup>c)</sup>	1040.2	1074.8	1037.8	1008.0	66.8
	NR	941	973	959	891	82
	SR	952	985	973	899	86
	SO	981	1015	1001	928	87
<b>15a</b>	Expt. <sup>b)</sup>	1338	1815	1787	412	1403
	NR	1742	2306	1567	1353	953
	SR	1430	2092	1488	710	1382
	SO	1367	2030	1468	602	1428
<b>15b</b>	Expt. <sup>b)</sup>	1256	1842	1561	364	1478
	NR	1525	2049	1533	992	1057
	SR	1254	1882	1423	456	1426
	SO	1188	1808	1410	347	1461
<b>15c</b>	Expt. <sup>b)</sup>	1155	1591	1584	291	1300
	NR	1449	2016	1177	1153	863
	SR	1204	1866	1107	638	1228
	SO	1139	1793	1114	509	1284
<b>16</b>	Expt. <sup>d)</sup>	2572.3				
	NR	2789	4273	3951	142	4131
	SR	2828	4331	4045	108	4223
	SO	2817	4254	4204	-8	4262

a) Chemical shifts in ppm with respect to external  $\text{Me}_2\text{Se}$ .

b) This Work.

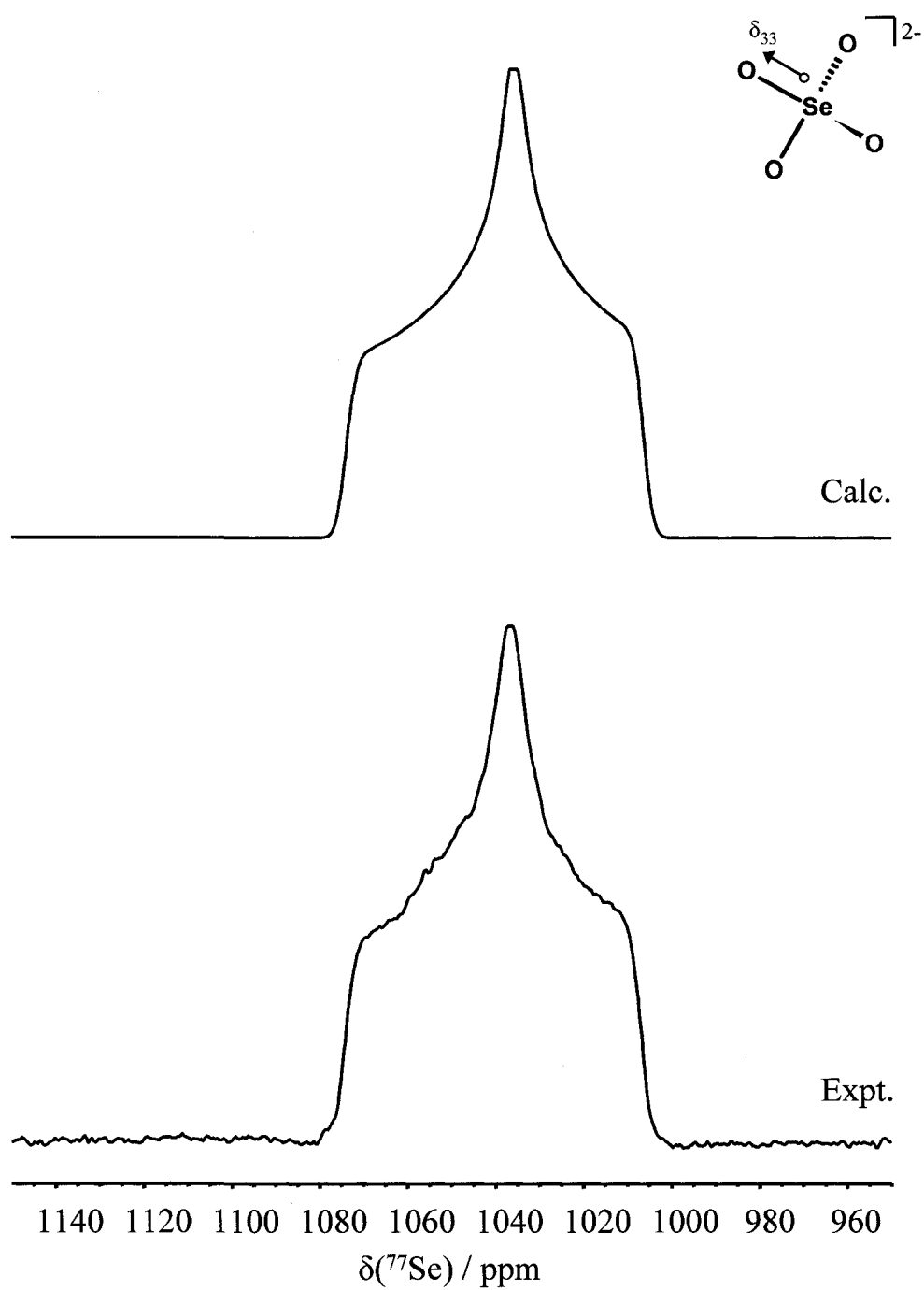
c) Ref. <sup>73</sup>

d) Ref. <sup>146</sup>

compounds **14** – **16** as representative examples.

**14.** Selenate anions are common oxidation products in selenium chemistry. Figure 4.13 shows the  $^{77}\text{Se}$  NMR spectrum of stationary  $(\text{NH}_4)_2\text{SeO}_4$ , along with its simulation. The principal components of the chemical shift tensor are compared with the earlier values of Collins et al. <sup>73</sup> in Table 4.3. The agreement is excellent for all components noting that, as ammonium selenate was employed as the secondary reference its isotropic shift was set to that reported previously, perfect agreement in  $\delta_{\text{iso}}$  is obviously achieved. <sup>73</sup>

The agreement between the calculated and experimental chemical shift tensors results in well reproduced values of  $\delta_{\text{iso}}$  and  $\Omega$  (Table 4.3). The orientations calculated by



**figure 4.13** CP static  $^{77}\text{Se}$  NMR and calculated spectra for  $(\text{NH}_4)_2\text{SeO}_4$  (**14**) acquired at 9.4 T, requiring 188 transients, 100 Hz of line broadening, a contact time of 10.0 ms, and a recycle delay of 4 s. Inset is a schematic of compound **14** showing the orientation of the selenium chemical shift tensor calculated at the scalar with spin-orbit relativistic level of theory.



all of the theoretical methods employed agree in their determination, and that  $\delta_{33}$  is parallel with a Se-O vector, as shown inset within Figure 4.13.

**15.** Selenotungstates have recently been utilized as selenium transfer agents in the preparation of organic diselenides.<sup>147</sup> The calculated and experimental spectra for  $(\text{NH}_4)_2\text{WSe}_4$  are given in Figure 4.14. The tungsten sits on a mirror plane that contains two of the selenium atoms.<sup>103</sup> This yields three distinct chemical shift tensors for the four selenium atoms, whose principal components are given in Table 4.3, where **15a** corresponds to the two crystallographically equivalent selenium atoms. All of the chemical shift tensors for the selenium nuclei of  $(\text{NH}_4)_2\text{WSe}_4$  have very large spans, and **15b** has the largest experimental span observed for all of the compounds investigated in this study.

A number of distinctions occur for compound **15** from the general observations in the calculations of the chemical shift tensors for the majority of the compounds investigated herein. While the  $\delta_{11}(\text{Calc.})$  values from all three methods for **15a**, and **15c** overestimate the corresponding experimental values, the calculations do not underestimate  $\delta_{33}$ . The non-relativistic calculations for all three chemical shift tensors for **15** significantly overestimate the value of  $\delta_{33}$  (Table 4.3). Both relativistic calculations come much closer to reproducing  $\delta_{33}(\text{Expt.})$ , and as a consequence of this achieve more accurate values of the span than the NR calculations (Table 4.3 and Figure 4.4). Thus a significant difference between the computation methods employed on the compounds investigated in this study occurs between the non-relativistic and the two relativistic calculations for all of the chemical shift tensors for **15**. All levels of theory indicate that

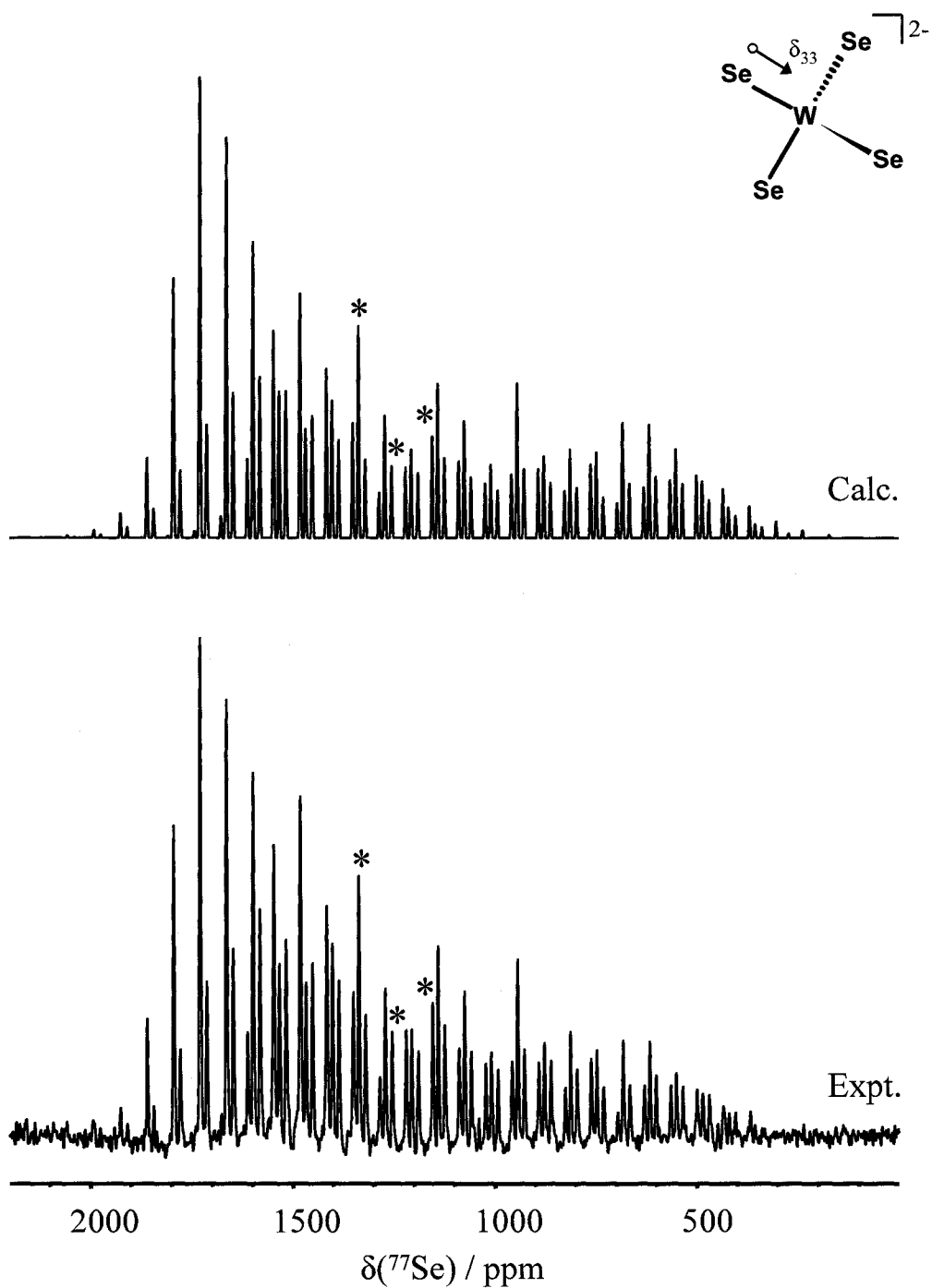


Figure 14. Experimental  $^{77}\text{Se}$  CP MAS and simulated spectra for  $(\text{NH}_4)_2\text{WSe}_4$  (**15**). Experimental conditions at 9.4 T: 1868 scans,  $\nu_{\text{rot}} = 5.0$  kHz, line broadened to 200 Hz, a contact time of 15.0 ms, and a 16 s pulse delay. Isotropic peaks are labeled with asterisks (\*). Inset is a schematic of compound **15** showing the orientation of the selenium chemical shift tensor calculated at the scalar with spin-orbit relativistic level of theory.

the orientation of the chemical shift tensors for **15a**, **15b**, and **15c** are such that the direction of  $\delta_{33}$  is directed along the Se-W vector (inset Figure 4.14).

**16.** The molecular environment within  $[\text{CpCr}(\text{CO})_2]_2\text{Se}$  possesses a bridging selenium between the two chromium centers. Such an environment, similar to the organic dialkyl selenides, can be found commonly in inorganic selenium compounds. Unfortunately, we were unable to characterize the selenium chemical shift tensor of this compound experimentally. Given the accuracy and predictive capability of the DFT calculations in the previous compounds investigated, the magnetic shielding tensor was calculated. The crystal structure of this compound has previously been reported, and indicates the presence of a single selenium atom in the asymmetric unit.<sup>104</sup> Thus only one magnetic shielding tensor was calculated, and the isotropic shift of the corresponding chemical shift tensor could then be compared with a solution value determined by Dean and coworkers (see Table 4.3).<sup>146</sup> The calculated values of  $\delta_{11}$  and  $\delta_{22}$  are approximately of the same magnitude, and are extremely deshielded with respect to the reference. The  $\delta_{33}(\text{Calc.})$  direction is significantly more shielded than the previous two principal components. The large difference between  $\delta_{11}$  and  $\delta_{33}$  yields a tensor with the largest value of  $\Omega$  calculated in this study. The large span may be the cause of the difficulty in observing the chemical shift tensor experimentally. Due to the lack of experimental values of  $\delta_{ii}$ , the only point of comparison available is with the solution value of  $\delta_{\text{iso}}$ . The large deshielded isotropic resonance observed experimentally is adequately reproduced considering the potential of solvent effects and solid to solution shifts that may affect the bridging selenium in this compound. The calculated orientation of the chemical shift tensors are in agreement, regardless of the method employed, and  $\delta_{33}$  is parallel with the

approximately linear Cr-Se-Cr vector. The plane normal to this vector containing the selenium is composed by the two extremely deshielded components,  $\delta_{11}$  and  $\delta_{22}$ .

#### 4.5 Summary

Selenium chemical shift tensors for a wide variety of compounds were investigated representing the entire known isotropic chemical shift range of selenium. ZORA DFT calculations complement the experimental work and suggest that the orientation of the selenium chemical shift tensor is not only sensitive to what is directly bonded to the selenium atom, but also to the next nearest neighbors and beyond. The calculations were carried out with varying degrees of relativistic corrections applied in an effort to assess the importance of relativistic effects. Isotropic chemical shifts were found to be calculated approximately equally well by all methods. Generally, the values of  $\delta_{33}$  were underestimated by the calculations, and coupled with the overestimations for  $\delta_{11}$ (Calc.); overestimated calculated spans often resulted. The large underestimation of  $\Omega$ (NR) for  $(\text{NH}_4)_2\text{WSe}_4$  is unique out of all of the spans obtained. This results from the failure of the NR calculation to reproduce  $\delta_{33}$ (Expt.), noting that the direction of this principal component is predicted by the calculations to coincide with the direction of the Se-W bond. Tungsten is the heaviest element ( $Z = 74$ ) in all of the compounds investigated, and it is not surprising that relativistic calculations are required to properly describe the magnetic shielding interaction for selenium in ammonium selenotungstate. Considering all of the selenium chemical shift tensors investigated in this study the scalar with spin-orbit relativistic calculations generally performed better, if only slightly, than the non-relativistic and scalar relativistic calculations. The size of a given selenium containing

system will determine whether or not the additional computational time required for the relativistic calculations are feasible. Should the selenium atom find itself bonded to a heavier element, such as tungsten, the need for the inclusion of relativistic effects becomes warranted.

## 4.6 References

- (1) Alivisatos, A. P. *Science* **1996**, *271*, 933-937.
- (2) Xu, R.; Husmann, A.; Rosenbaum, T. F.; Saboungi, M.-L.; Enderby, J. E.; Littlewood, P. B. *Nature* **1997**, *390*, 57-60.
- (3) Johnson, J. A.; Saboungi, M.-L.; Thiyagarajan, P.; Csencsits, R.; Meisel, D. *J. Phys. Chem. B* **1999**, *103*, 59-63.
- (4) Mayers, B.; Jiang, X.; Sunderland, D.; Cattle, B.; Xia, Y. *J. Am. Chem. Soc.* **2003**, *125*, 13364-13365.
- (5) Terasaki, O.; Yamazaki, K.; Thomas, J. M.; Ohsuna, T.; Watanabe, D.; Sanders, J. V.; Barry, J. C. *Nature* **1987**, *330*, 58-60.
- (6) Endo, H.; Inui, M.; Yao, M.; Tamura, K.; Hoshino, H.; Katayama, Y.; Maruyama, K. *Z. Phys. Chem. Neue Folge* **1988**, *156*, 507-511.
- (7) Parise, J. B.; MacDougall, J. E.; Herron, N.; Farlee, R.; Sleight, A. W.; Wang, Y.; Bein, T.; Moller, K.; Moroney, L. M. *Inorg. Chem.* **1988**, *27*, 221-228.
- (8) Nozue, Y.; Kodaira, T.; Terasaki, O.; Yamazaki, K.; Goto, T.; Watanabe, D.; Thomas, J. M. *J. Phys.: Condens. Matter* **1990**, *2*, 5209-5217.
- (9) Goldbach, A.; Iton, L. E.; Saboungi, M.-L. *Chem. Phys. Lett.* **1997**, *281*, 69-73.
- (10) Goldbach, A.; Saboungi, M.-L. *Acc. Chem. Res.* **2005**, *38*, 705-712.
- (11) Oldfield, J. E. *J. Nutr.* **1987**, *117*, 2002-2008.
- (12) Böck, A.; Forchhammer, K.; Heider, J.; Leinfelder, W.; Sawers, G.; Veprek, B.; Zinoni, F. *Mol. Microbiol.* **1991**, *5*, 515-520.
- (13) Salzmann, M.; Stocking, E. M.; Silks III, L. A.; Senn, H. *Magn. Reson. Chem.* **1999**, *37*, 672-675.
- (14) Mikulec, F. V.; Kuno, M.; Bennati, M.; Hall, D. A.; Griffin, R. G.; Bawendi, M. *G. J. Am. Chem. Soc.* **2000**, *122*, 2532 - 2540.
- (15) Liu, Y.; Li, L.; Fan, Z.; Zhang, H.-Y.; Wu, X.; Guan, X.-D.; Liu, S.-X. *Nano Lett.* **2002**, *2*, 257-261.
- (16) Zelakiewicz, B. S.; Yonezawa, T.; Tong, Y.-Y. *J. Am. Chem. Soc.* **2004**, *126*, 8112-8113.

- (17) Berrettini, M. G.; Braun, G.; Hu, J. G.; Strouse, G. F. *J. Am. Chem. Soc.* **2004**, *126*, 7063-7070.
- (18) Duddeck, H. *Prog. Nucl. Magn. Reson. Spectrosc.* **1995**, *27*, 1-323.
- (19) Duddeck, H. *Annu. Rep. NMR Spectrosc.* **2004**, *52*, 105-166.
- (20) Pulay, P. In *Calculation of NMR and EPR Parameters*; Kaupp, M., Bühl, M., Malkin, V. G., Eds.; Wiley-VCH Verlag GmbH & Co. KGaA: Weinheim, 2004, p XIII.
- (21) McFarlane, H. C. E.; McFarlane, W. In *NMR of Newly Accessible Nuclei*; Laszlo, P., Ed.; Academic Press: New York, 1983; Vol. 2, pp 275-299.
- (22) Luthra, N. P.; Odom, J. D. In *The Chemistry of Organic Selenium and Tellurium Compounds*; Patai, S., Rappoport, Z., Eds.; John Wiley & Sons: New York, 1986; Vol. 1, pp 189-241.
- (23) McFarlane, H. C. E.; McFarlane, W. In *Multinuclear NMR*; Mason, J., Ed.; Plenum Press: New York, 1987, pp 417-435.
- (24) Klapötke, T. M.; Broschag, M. *Compilation of Reported <sup>77</sup>Se NMR Chemical Shifts: Up to the Year 1994*; Wiley: Chichester, 1996.
- (25) Sefzik, T. H.; Turco, D.; Iuliucci, R. J.; Facelli, J. C. *J. Phys. Chem. A* **2005**, *109*, 1180-1187.
- (26) Veeman, W.S. *Philos. Trans. R. Soc. London, A* **1981**, *299*, 629-641.
- (27) Grossmann, G.; Potrzebowski, M. J.; Fleischer, U.; Krüger, K.; Malkina, O. L.; Ciesielski, W. *Solid State Nuclear Magnetic Resonance* **1998**, *13*, 71-85.
- (28) Yates, J. R.; Pickard, C. J.; Payne, M. C.; Mauri, F. *J. Chem. Phys.* **2003**, *118*, 5746-5753.
- (29) Tossell, J. A.; Lazzeretti, P. *J. Magn. Reson.* **1988**, *80*, 39-44.
- (30) Magyarfalvi, G.; Pulay, P. *Chem. Phys. Lett.* **1994**, *225*, 280-284.
- (31) Bühl, M.; Thiel, W.; Fleischer, U.; Kutzelnigg, W. *J. Phys. Chem.* **1995**, *99*, 4000-4007.
- (32) Schreckenbach, G.; Ruiz-Morales, Y.; Ziegler, T. *J. Chem. Phys.* **1996**, *104*, 8605-8612.
- (33) Nakanishi, W.; Hayashi, S. *Chem. Lett.* **1998**, 523-524.

- (34) Hayashi, S.; Nakanishi, W. *J. Org. Chem.* **1999**, *64*, 6688-6696.
- (35) Bernard, G. M.; Eichele, K.; Wu, G.; Kirby, C. W.; Wasylshen, R. E. *Can. J. Chem.* **2000**, *78*, 614-625.
- (36) Campbell, J.; Mercier, H. P. A.; Santry, D. P.; Suontamo, R. J.; Borrmann, H.; Schrobilgen, G. J. *Inorg. Chem.* **2001**, *40*, 233-254.
- (37) Tattershall, B. W.; Sandham, E. L. *J. Chem. Soc.-Dalton Trans.* **2001**, 1834-1840.
- (38) Wilson, P. J. *Mol. Phys.* **2001**, *99*, 363-367.
- (39) Bayse, C. A. *Inorg. Chem.* **2004**, *43*, 1208-1210.
- (40) Chesnut, D. B. *Chem. Phys.* **2004**, *305*, 237-241.
- (41) Bayse, C. A. *J. Chem. Theory Comput.* **2005**, *1*, 1119-1127.
- (42) Chang, C.; Pelissier, M.; Durand, P. *Phys. Scr.* **1986**, *34*, 394-404.
- (43) van Lenthe, E.; Baerends, E. J.; Snijders, J. G. *J. Chem. Phys.* **1993**, *99*, 4597-4610.
- (44) van Lenthe, E.; Baerends, E. J.; Snijders, J. G. *J. Chem. Phys.* **1994**, *101*, 9783-9792.
- (45) van Lenthe, E.; van Leeuwen, R.; Baerends, E. J.; Snijders, J. G. *Int. J. Quantum Chem.* **1996**, *57*, 281-293.
- (46) Kennedy, M. A.; Ellis, P. D. *Concepts Magn. Reson.* **1989**, *1*, 35-47.
- (47) Kennedy, M. A.; Ellis, P. D. *Concepts Magn. Reson.* **1989**, *1*, 109-129.
- (48) Power, W. P.; Mooibroek, S.; Wasylshen, R. E.; Cameron, T. S. *J. Phys. Chem.* **1994**, *98*, 1552-1560.
- (49) Eichele, K.; Wu, G.; Wasylshen, R. E.; Britten, J. F. *J. Phys. Chem.* **1995**, *99*, 1030-1037.
- (50) Eichele, K.; Wasylshen, R. E.; Corrigan, J. F.; Taylor, N. J.; Carty, A. J.; Feindel, K. W.; Bernard, G. M. *J. Am. Chem. Soc.* **2002**, *124*, 1541-1552.
- (51) Ramsey, N. F. *Molecular Beams*; Oxford University Press: London, 1956.
- (52) Ramsey, N. F. *Phys. Rev.* **1950**, *78*, 699-703.



- (53) Pyykkö, P. *Theor. Chem. Acc.* **2000**, *103*, 214-216.
- (54) Pyper, N. C. *Chem. Phys. Lett.* **1983**, *96*, 204-210.
- (55) Pyper, N. C. *Chem. Phys. Lett.* **1983**, *96*, 211-217.
- (56) Pyykkö, P. *Chem. Phys.* **1983**, *74*, 1-7.
- (57) Zhang, Z. C.; Webb, G. A. *J. Mol. Struct.* **1983**, *104*, 439-444.
- (58) Kolb, D.; Johnson, W. R.; Shorer, P. *Phys. Rev. A* **1982**, *26*, 19-31.
- (59) Kutzelnigg, W. *J. Comput. Chem.* **1999**, *20*, 1199-1219.
- (60) Vaara, J.; Malkina, O. L.; Stoll, H.; Malkin, V. G.; Kaupp, M. *J. Chem. Phys.* **2001**, *114*, 61-71.
- (61) Autschbach, J.; Ziegler, T. In *Encyclopedia of Nuclear Magnetic Resonance*; Grant, D. M., Harris, R. K., Eds.; John Wiley and Sons, Ltd.: Chichester, U.K., 2002; Vol. 9, pp 306-323.
- (62) Manninen, P.; Lantto, P.; Vaara, J.; Ruud, K. *J. Chem. Phys.* **2003**, *119*, 2623-2637.
- (63) Pyykkö, P. In *Calculation of NMR and EPR Parameters*; Kaupp, M., Bühl, M., Malkin, V. G., Eds.; Wiley-VCH Verlag GmbH & Co. KGaA: Weinheim, 2004, pp 7-19.
- (64) Ramsey, N. F. *Phys. Rev.* **1953**, *91*, 303-307.
- (65) Jameson, C. J. In *Multinuclear NMR*; Mason, J., Ed.; Plenum Press: New York, 1987, pp 89-131.
- (66) Fukui, H. *Prog. Nucl. Magn. Reson. Spectrosc.* **1999**, *35*, 267-294.
- (67) Contreras, R. H.; Peralta, J. E.; Giribet, C. G.; De Azua, M. C.; Facelli, J. C. *Annu. Rep. NMR Spectrosc.* **2000**, *41*, 55-184.
- (68) Vaara, J.; Jokisaari, J.; Wasylishen, R. E.; Bryce, D. L. *Prog. Nucl. Magn. Reson. Spectrosc.* **2002**, *41*, 233-304.
- (69) Wasylishen, R. E. In *Encyclopedia of Nuclear Magnetic Resonance*; Grant, D. M., Harris, R. K., Eds.; John Wiley and Sons, Ltd.: Chichester, 2002; Vol. 9, pp 274-282.
- (70) Jameson, C. J. In *Phosphorus-31 NMR Spectroscopy in Stereochemical Analysis*.

*Organic Compounds and Metal Complexes*; Verkade, J. G., Quin, L. D., Eds.; VCH Publishers, Inc.: Deerfield Beach, 1987; Vol. 8, pp 205-230.

- (71) Eichele, K.; Wasylshen, R. E. *J. Magn. Reson. Ser. A* **1994**, *106*, 46-56.
- (72) Nicpon, P.; Meek, D. W. *Inorg. Synth.* **1967**, *10*, 157-159.
- (73) Collins, M. J.; Ratcliffe, C. I.; Ripmeester, J. A. *J. Magn. Reson.* **1986**, *68*, 172-179.
- (74) Bryce, D. L.; Bernard, G. M.; Gee, M.; Lumsden, M.; Eichele, K.; Wasylshen, R. *E. Can. J. Anal. Sci. Spectrosc.* **2001**, *46*, 46-82.
- (75) Herzfeld, J.; Berger, A. E. *J. Chem. Phys.* **1980**, *73*, 6021-6030.
- (76) Eichele, K.; Wasylshen, R. E.; 1.17.30 ed., 2001.
- (77) Schreckenbach, G.; Ziegler, T. *J. Phys. Chem.* **1995**, *99*, 606-616.
- (78) Schreckenbach, G.; Ziegler, T. *Int. J. Quantum Chem.* **1997**, *61*, 899-918.
- (79) Wolff, S. K.; Ziegler, T. *J. Chem. Phys.* **1998**, *109*, 895-905.
- (80) Theoretical Chemistry, Vrije Universiteit, Amsterdam, <http://www.scm.com>.
- (81) Baerends, E. J.; Ellis, D. E.; Ros, P. *Chem. Phys.* **1973**, *2*, 41-51.
- (82) Versluis, L.; Ziegler, T. *J. Chem. Phys.* **1988**, *88*, 322-328.
- (83) te Velde, G.; Baerends, E. J. *J. Comput. Phys.* **1992**, *99*, 84-98.
- (84) Fonseca Guerra, C.; Snijders, J. G.; te Velde, G.; Baerends, E. J. *Theor. Chem. Acc.* **1998**, *99*, 391-403.
- (85) Vosko, S. H.; Wilk, L.; Nusair, M. *Can. J. Phys.* **1980**, *58*, 1200-1211.
- (86) Becke, A. D. *Phys. Rev. A* **1988**, *38*, 3098-3100.
- (87) Perdew, J. P. *Phys. Rev. B* **1986**, *33*, 8822-8824.
- (88) Perdew, J. P. *Phys. Rev. B* **1986**, *34*, 7406.
- (89) Pathirana, H. M. K. K.; Weiss, T. J.; Reibenspies, J. H.; Zingaro, R. A.; Meyers, E. A. *Z. Kristallogr.* **1994**, *209*, 697.

- (90) Husebye, S.; Lindeman, S. V.; Rudd, M. D. *Acta Crystallogr. Sect. C-Cryst. Struct. Commun.* **1997**, *53*, 809-811.
- (91) McCullough, J. D.; Hamburger, G. *J. Am. Chem. Soc.* **1942**, *64*, 508-513.
- (92) Rajeswaran, M.; Parthasarathy, R. *Acta Crystallogr. Sect. C-Cryst. Struct. Commun.* **1984**, *40*, 647-650.
- (93) Kistenmacher, T. J.; Emge, T. J.; Shu, P.; Cowan, D. O. *Acta Crystallogr., Sect. B: Struct. Sci.* **1979**, *35*, 772-775.
- (94) Marsh, R. E. *Acta Crystallogr.* **1952**, *5*, 458-462.
- (95) Cogne, A.; Grand, A.; Laugier, J.; Robert, J. B.; Wiesenfeld, L. *J. Am. Chem. Soc.* **1980**, *102*, 2238-2242.
- (96) Steinberger, H.-U.; Ziemer, B.; Meisel, M. *Acta Crystallogr. Sect. C-Cryst. Struct. Commun.* **2001**, *57*, 323-324.
- (97) Davies, J. A.; Dutremez, S.; Pinkerton, A. A. *Inorg. Chem.* **1991**, *30*, 2380-2387.
- (98) Jones, P. G.; Kienitz, C.; Thone, C. *Z. Kristallogr.* **1994**, *209*, 80-81.
- (99) Alyea, E. C.; Ferguson, G.; Malito, J.; Ruhl, B. L. *Acta Crystallogr. Sect. C-Cryst. Struct. Commun.* **1986**, *42*, 882-884.
- (100) Zhdanov, G. S.; Pospelov, V. A.; Umanskii, M. M.; Glushkova, V. P. *Dokl. Akad. Nauk SSSR* **1953**, *92*, 983-985.
- (101) Allen, D. W.; Bell, N. A.; March, L. A.; Nowell, I. W. *Polyhedron* **1990**, *9*, 681-685.
- (102) Carter, R. L.; Koerntgen, C.; Margulis, T. N. *Acta Crystallogr., Sect. B: Struct. Sci.* **1977**, *33*, 592-593.
- (103) Müller, A.; Krebs, B.; Beyer, H. *Z. Naturforsch.* **1968**, *23B*, 1537-1538.
- (104) Goh, L. Y.; Wei, C.; Sinn, E. *Chem. Commun.* **1985**, 462-464.
- (105) Valeev, R. B.; Kalabin, G. A.; Kushnarev, D. F. *Zh. Org. Khim.* **1980**, *16*, 2482-2486.
- (106) Luthra, N. P.; Dunlap, R. B.; Odom, J. D. *J. Magn. Reson.* **1983**, *52*, 318-322.
- (107) Carr, S. W.; Colton, R. *Aust. J. Chem.* **1981**, *34*, 35-44.

- (108) Facey, G.; Wasylshen, R. E.; Collins, M. J.; Ratcliffe, C. I.; Ripmeester, J. A. *J. Phys. Chem.* **1986**, *90*, 2047-2052.
- (109) Jameson, C. J.; Jameson, A. K. *Chem. Phys. Lett.* **1987**, *135*, 254-259.
- (110) Bühl, M.; Gauss, J.; Stanton, J. F. *Chem. Phys. Lett.* **1995**, *241*, 248-252.
- (111) Balzer, G.; Duddeck, H.; Fleischer, U.; Röhr, F. *Fresenius J. Anal. Chem.* **1997**, *357*, 473-476.
- (112) Nakanishi, W.; Hayashi, S. *J. Phys. Chem. A* **1999**, *103*, 6074-6081.
- (113) Odom, J. D.; Dawson, W. H.; Ellis, P. D. *J. Am. Chem. Soc.* **1979**, *101*, 5815-5822.
- (114) Drabowicz, J.; Luczak, J.; Mikolajczyk, M. *J. Org. Chem.* **1998**, *63*, 9565-9568.
- (115) Potrzebowski, M. J.; Katarzynski, R.; Ciesielski, W. *Magn. Reson. Chem.* **1999**, *37*, 173-181.
- (116) Dong, S.; Ida, R.; Wu, G. *J. Phys. Chem. A* **2000**, *104*, 11194-11202.
- (117) Wong, T. C.; Ang, T. T.; Guziec, F. S.; Moustakis, C. A. *J. Magn. Reson.* **1984**, *57*, 463-470.
- (118) Dong, S.; Yamada, K.; Wu, G. *Z. Naturforsch., A* **2000**, *55*, 21-28.
- (119) Opella, S. J.; Frey, M. H.; Cross, T. A. *J. Am. Chem. Soc.* **1979**, *101*, 5856-5857.
- (120) Zumbulyadis, N.; Henrichs, P. M.; Young, R. H. *J. Chem. Phys.* **1981**, *75*, 1603-1611.
- (121) Hexem, J. G.; Frey, M. H.; Opella, S. J. *J. Chem. Phys.* **1982**, *77*, 3847-3856.
- (122) Menger, E. M.; Veeman, W. S. *J. Magn. Reson.* **1982**, *46*, 257-268.
- (123) Böhm, J.; Fenzke, D.; Pfeifer, H. *J. Magn. Reson.* **1983**, *55*, 197-204.
- (124) Olivieri, A. C.; Frydman, L.; Diaz, L. E. *J. Magn. Reson.* **1987**, *75*, 50-62.
- (125) Alarcón, S. H.; Olivieri, A. C.; Harris, R. K. *Solid State Nucl. Magn. Reson.* **1993**, *2*, 325-334.
- (126) Grondona, P.; Olivieri, A. C. *Concepts Magn. Reson.* **1993**, *5*, 319-339.

- (127) Harris, R. K.; Olivieri, A. C. *Prog. Nucl. Magn. Reson. Spectrosc.* **1992**, *24*, 435 - 456.
- (128) Saatsazov, V. V.; Khotsyanova, T. L.; Magdesieva, N. N.; Kuznetsov, S. I.; Alymov, I. M.; Kyandzhetsian, R. A.; Bryukhova, E. V. *Izv. Akad. Nauk SSSR, Ser. Khim.* **1974**, *12*, 2850-2851.
- (129) Saatsazov, V. V.; Khotsyanova, T. L.; Kazakov, V. P.; Bryukhova, E. V. *Izv. Akad. Nauk SSSR, Ser. Fiz.* **1975**, *39*, 2535-2536.
- (130) Collins, M. J.; Ripmeester, J. A. *J. Am. Chem. Soc.* **1987**, *109*, 4113-4115.
- (131) Clayden, N. J.; Dobson, C. M.; Lian, L.-Y.; Smith, D. J. *J. Magn. Reson.* **1986**, *69*, 476-487.
- (132) Batchelor, R. J.; Einstein, F. W. B.; Gay, I. D.; Gu, J.-H.; Pinto, B. M.; Zhou, X.-M. *Can. J. Chem.* **2000**, *78*, 598-613.
- (133) Frère, P.; Skabara, P. J. *Chem. Soc. Rev.* **2005**, *34*, 69-98.
- (134) Duddeck, H.; Bradenahl, R.; Stefaniak, L.; Jazwinski, J.; Kamienski, B. *Magn. Reson. Chem.* **2001**, *39*, 709-713.
- (135) Jacques-Silva, M. C.; Nogueira, C. W.; Broch, L. C.; Flores, É. M. M.; Rocha, J. B. T. *Pharmacol. Toxicol.* **2001**, *88*, 119-125.
- (136) Rossato, J. I.; Ketzer, L. A.; Centurião, F. B.; Silva, S. J. N.; Lüdtke, D. S.; Zeni, G.; Braga, A. L.; Rubin, M. A.; Rocha, J. B. T. *Neurochem. Res.* **2002**, *27*, 297-303.
- (137) Maciel, E. N.; Flores, É. M. M.; Rocha, J. B. T.; Folmer, V. *Bull. Environ. Contam. Toxicol.* **2003**, *70*, 470-476.
- (138) Wirth, T. *Molecules* **1998**, *3*, 164-166.
- (139) Wilson, S. R.; Zucker, P. A.; Huang, R.-R. C.; Spector, A. *J. Am. Chem. Soc.* **1989**, *111*, 5936-5939.
- (140) du Mont, W.-W. *Z. Naturforsch.* **1985**, *40B*, 1453-1456.
- (141) Rajalingam, U.; Dean, P. A. W.; Jenkins, H. A. *Can. J. Chem.* **2000**, *78*, 590-597.
- (142) Allen, D. W.; Taylor, B. F. *J. Chem. Res.-S* **1986**, 392-393.
- (143) Allen, D. W.; Nowell, I. W.; Taylor, B. F. *J. Chem. Soc.-Dalton Trans.* **1985**, 2505-2508.

- (144) Bryce, D. L.; Eichele, K.; Wasylshen, R. E. *Inorg. Chem.* **2003**, *42*, 5085-5096.
- (145) Eichele, K.; Wasylshen, R. E.; Kessler, J. M.; Solujic, L.; Nelson, J. H. *Inorg. Chem.* **1996**, *35*, 3904-3912.
- (146) Dean, P. A. W.; Goh, L. Y.; Gay, I. D.; Sharma, R. D. *J. Organomet. Chem.* **1997**, *533*, 1-5.
- (147) Saravanan, V.; Porhiel, E.; Chandrasekaran, S. *Tetrahedron Lett.* **2003**, *44*, 2257-2260.

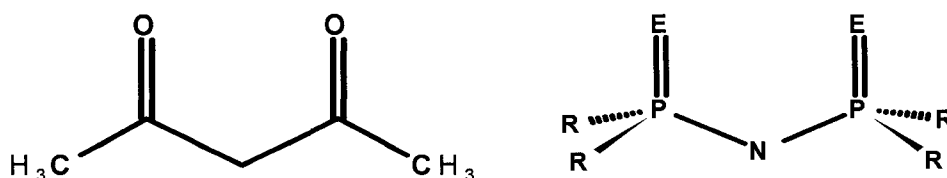
## Chapter 5

# Probing Solid Iminobis(dialkylphosphine chalcogenide) Systems with Multinuclear Magnetic Resonance

### 5.1 Introduction

The coordination of monoanionic bidentate ligands toward metal and non-metal centers continues to provide a vast area of research interest. Acetylacetonate (*acac*) and its  $\beta$ -diketonate derivatives represent the ideological figurehead of monoanionic bidentate coordination chemistry.<sup>1</sup> Recently,  $\beta$ -diketonate precursors have been utilized in the fabrication of metal oxide thin films,<sup>2</sup> and other chemical vapor deposition applications.<sup>3</sup> Interest in related metal chalcogenide materials has spurred the investigation of monoanionic bidentate ligands possessing the corresponding elements of Group 16. Some sulfur- and selenium-containing ligands such as dialkyldichalcogenophosphates, dialkyldichalcogenophosphinates, and dialkyldichalcogenocarbamates have appeared in the literature;<sup>4-6</sup> however, their small ‘bites’, chalcogen-chalcogen interatomic distances, form complexes primarily in an anisobidentate fashion.<sup>7</sup> The iminobis(dialkylphosphine chalcogenide) compounds, the so-called non-carbon (main group) analogues of acetylacetonate, offer the opportunity to vary the donor chalcogen atom and variation of the alkyl group is more easily accessible than for the organic analogues.<sup>8</sup> The fine-tuning available for specific metal complexation permits comparisons between the bonding in organic and inorganic analogues, knowledge widely sought throughout chemistry.<sup>9</sup> While not isoelectronic, *acac* and dichalcogenoimidodiphosphinate systems are closely related, Scheme 5.1. An early example of the Group 10 complexes of  $[\text{N}(\text{Ph}_2\text{PSe})_2]^-$

contained heterocyclic  $MSe_2P_2N$  rings that were puckered,<sup>10</sup> unlike those of acetylacetonate which contain planar six-membered rings.<sup>11,12</sup> The difference reflects the dichalcogenoimidodiphosphinate ligands ability to form delocalized systems without requiring planar rings due to the presence of low lying *d* orbitals.<sup>10,13,14</sup> Binding geometries of these ligands are known to depend on the choice of chalcogen, alkyl group, and metal,<sup>13,15-22</sup> allowing the formation of chelate rings and often resulting in symmetrical coordination patterns through the donor chalcogen atoms.<sup>8,23</sup>



**Scheme 5.1** Similarities between the structures of acetylacetonate, left, and the iminobis(dialkylphosphine chalcogenide), right, systems.

Dichalcogenoimidodiphosphinate anions are versatile ligands with a strong tendency to form inorganic chelate rings, and numerous reviews of their complexes exist in the literature.<sup>15,24-26</sup> In addition to applications as single-source precursors for solid-state metal chalcogenide materials,<sup>4-6,23,26-40</sup> these bidentate ligands have found uses in the search for stereochemically active lone pairs,<sup>10,19-21,41-52</sup> in catalysis,<sup>53-55</sup> and in metal extraction processes,<sup>15,49,56-63</sup> as lanthanide shift reagents,<sup>49,64-68</sup> luminescent materials,<sup>69</sup> and as enzyme mimetics.<sup>70-72</sup>

Despite the considerable interest in the properties and chemistry of the complexes of dichalcogenoimidodiphosphinate ligands, relatively little is known about the neutral



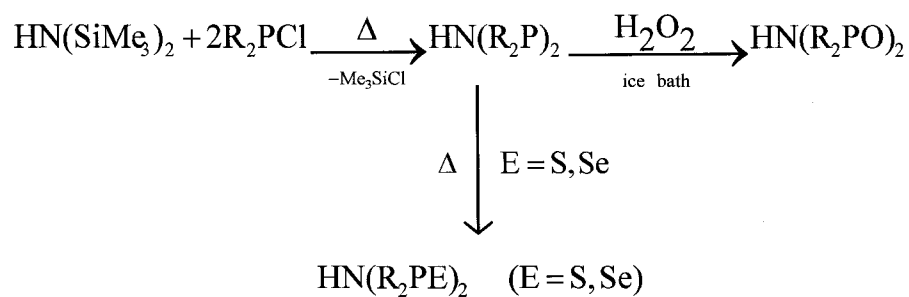
iminobis(dialkylphosphine chalcogenide),  $\text{HN}(\text{R}_2\text{PE})_2$ .<sup>73</sup> Characterization of these systems has predominantly been performed by X-ray crystallography,<sup>10,43,44,74-79</sup> often supported by infrared,<sup>44,80-83</sup> Raman,<sup>82,83</sup> and/or solution NMR spectroscopy.<sup>10,43,44,80,84</sup> Solid-state NMR, being potentially more informative than solution NMR spectroscopy, would appear to be an appropriate technique for characterizing the  $\text{HN}(\text{R}_2\text{PE})_2$  ligands. Herein we present a solid-state  $^{31}\text{P}$  and  $^{77}\text{Se}$  NMR investigation of the  $\text{HN}(\text{R}_2\text{PE})_2$  (E = O, S, Se; R = Ph,  $^i\text{Pr}$ ) systems representing the first solid-state NMR investigation of the iminobis(dialkylphosphine chalcogenides).

## 5.2 Experimental

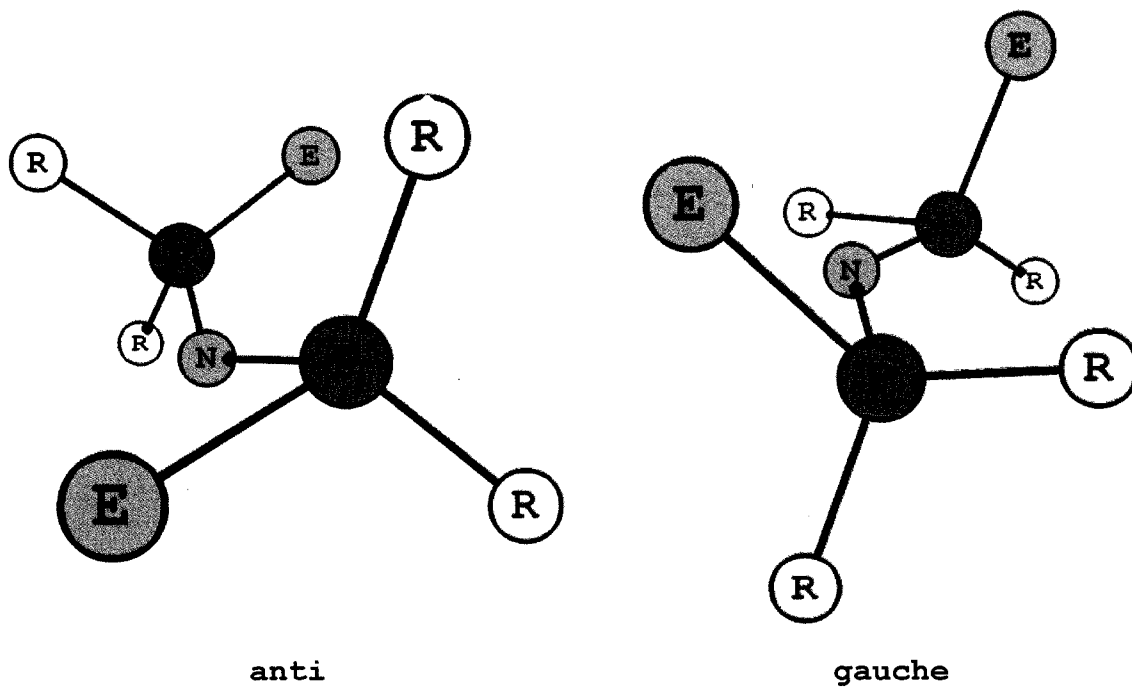
### 5.2.1 Sample Preparation

The phenyl and isopropyl derivatives of bis(dialkylphosphino)amine,  $\text{HN}(\text{R}_2\text{P})_2$  were prepared via the condensation reaction between hexamethyldisilazane,  $\text{HN}(\text{SiMe}_3)_2$  (Aldrich), and the appropriate chlorodialkylphosphine,  $\text{R}_2\text{P}\text{Cl}$  (Aldrich).<sup>81,85</sup> Briefly,  $\text{R}_2\text{P}\text{Cl}$  in toluene is added drop wise to a hot toluene solution of  $\text{HN}(\text{SiMe}_3)_2$  and is maintained above 80 °C for at least two hours in order to remove the chlorotrimethylsilane byproduct by distillation. Oxidation to the corresponding iminobis(dialkylphosphine chalcogenide) was achieved from the subsequent reaction with hydrogen peroxide (Sigma-Aldrich) in an ice bath,<sup>81,86</sup> or via reflux with elemental sulfur (Fisher),<sup>81</sup> or elemental selenium (Aldrich),<sup>10,23</sup> see Scheme 5.2. Literature X-ray crystal structures have been determined for all of the investigated iminobis-(dialkylphosphine chalcogenide) systems,  $\text{HN}(\text{R}_2\text{PE})_2$  (E = O; R = Ph<sup>76</sup> and  $^i\text{Pr}$ <sup>44</sup>, E = S; R = Ph<sup>76-78</sup> and  $^i\text{Pr}$ <sup>43</sup>, E = Se; R = Ph<sup>10</sup> and  $^i\text{Pr}$ <sup>44</sup>). A common difference between the R =

Ph and R = <sup>i</sup>Pr structures of the HN(R<sub>2</sub>PE)<sub>2</sub> systems is that while the EPNPE backbones in iminobis(diphenylphosphine chalcogenide) species are oriented *anti*, the HN(<sup>i</sup>Pr<sub>2</sub>PE)<sub>2</sub> (E = O, S, Se) molecules all possess *gauche* conformations, see Figure 5.1.



**Scheme 5.2** Iminobis(dialkylphosphine chalcogenide) preparation.



**Figure 5.1** Common conformations encountered in iminobis(dialkylphosphine chalcogenide), HN(R<sub>2</sub>PE)<sub>2</sub> (E = O, S, Se), systems.

### 5.2.2 NMR Experiments

Solid-state NMR investigations of powdered samples of  $\text{HN}(\text{R}_2\text{PE})_2$  ( $\text{E} = \text{O}, \text{S}, \text{Se}$ ;  $\text{R} = \text{Ph}, {}^i\text{Pr}$ ) were obtained on 4.7 T, 7.0 T and 11.7 T NMR spectrometers. The samples were packed in 4 mm (7.0 T and 11.7 T) and 7.5 mm (4.7 T) o.d. zirconium oxide rotors and were placed within probes suitable for magic angle spinning, MAS, NMR experiments. A ramped amplitude cross polarization, RACP, pulse sequence was used to acquire all spectra.<sup>87</sup> Proton decoupling fields of approximately 60 kHz were achieved via two-pulse phase-modulation, TPPM.<sup>88</sup> The  ${}^{31}\text{P}$  NMR spectra were referenced with respect to 85%  $\text{H}_3\text{PO}_4$  (*aq*) by setting the isotropic  ${}^{31}\text{P}$  NMR peak of solid  $(\text{NH}_4)\text{H}_2\text{PO}_4$  to 0.81 ppm.<sup>89</sup> Selenium-77 NMR spectra were referenced to  $\text{Me}_2\text{Se}$  (*l*) by setting the isotropic peak of solid ammonium selenate,  $(\text{NH}_4)_2\text{SeO}_4$ , to 1040.2 ppm.<sup>89,90</sup>

Solid-state  ${}^{31}\text{P}$  NMR experiments were performed at Larmor frequencies of 81.0, 121.6 and 202.5 MHz, and at spinning frequencies ranging from 3.0 to 7.2 kHz. A total of between 64 and 128 scans were acquired per spectrum. Contact times between 1.5 and 6.5 ms, and pulse delays between 600 and 840 s for  $\text{HN}(\text{Ph}_2\text{PE})_2$  systems and between 7 and 18 s for  $\text{HN}({}^i\text{Pr}_2\text{PE})_2$  were employed.

Solid-state  ${}^{77}\text{Se}$  NMR measurements were performed at Larmor frequencies of 38.2, 57.3 and 95.4 MHz, and at spinning frequencies ranging from 2.0 to 14.0 kHz. A total of between 384 and 16384 scans were acquired per spectrum. Contact times between 6.5 and 10.0 ms, and pulse delays between 600 and 840 s for  $\text{HN}(\text{Ph}_2\text{PE})_2$  species and between 5 and 14 s for  $\text{HN}({}^i\text{Pr}_2\text{PE})_2$  were employed.

The principal components of the respective phosphorus and selenium chemical shift tensors,  $\delta_{11} \geq \delta_{22} \geq \delta_{33}$ , were determined from the experimental spectra via the procedure of Herzfeld and Berger.<sup>91,92</sup> All experimental solid-state NMR spectra were simulated using the determined values with the program WSOLIDS<sup>93</sup> to assess the quality of the obtained parameters. This procedure results in errors of  $\pm 0.2$  ppm in the isotropic chemical shift,  $\delta_{\text{iso}} = (1/3)(\delta_{11} + \delta_{22} + \delta_{33})$ , and errors in the principal components about 1 – 3% of the span,  $\Omega = \delta_{11} - \delta_{33}$ , of the respective chemical shift tensor. Another useful quantity for describing the appearance of chemical shift powder patterns is the skew,  $\kappa = 3(\delta_{22} - \delta_{\text{iso}})/\Omega$ , where axial symmetry is described by  $\kappa = +1$  or  $-1$ .<sup>94</sup>

### 5.2.3 DFT Computations

Theoretical calculations of NMR parameters were performed on isolated molecules generated from the reported crystal structures. Magnetic shielding tensors,  $\sigma$ , were calculated using the NMR module<sup>95-97</sup> of the Amsterdam Density Functional, ADF, program package.<sup>98-102</sup> The Vosko-Wilk-Nusair<sup>103</sup> local density approximation with the Becke88-Perdew86<sup>104-106</sup> generalized gradient approximation were used for the exchange-correlation functional. Scalar relativistic corrections were carried out based on the implementation of the zeroth order regular approximation, ZORA, formalism.<sup>107-110</sup> Triple- $\zeta$  doubly polarized, TZ2P, Slater-type ZORA basis sets were used for all atoms except for hydrogen, where double- $\zeta$  quality, DZ, basis functions were utilized. The corresponding phosphorus and selenium chemical shift tensors were calculated from the magnetic shielding tensors using the relationship:

$$\delta_{ii}(sample) = \frac{\sigma_{iso}(ref) - \sigma_{ii}(sample)}{1 - \sigma_{iso}(ref)} \quad [5.1]$$

where  $\sigma_{iso}(ref)$  is the isotropic shielding of a standard reference. The absolute shielding scale for  $^{31}\text{P}$  has been determined, and the value of  $\sigma_{iso}(85\% \text{H}_3\text{PO}_4(aq))$  has been established to be 328.35 ppm.<sup>111</sup> We have previously investigated the selenium chemical shift tensors in a wide range of selenium containing compounds, and we have subsequently used the value of 1580 ppm determined therein for the reference shielding of a neat liquid of dimethyl selenide at 23 °C.<sup>112</sup>

### 5.3 Results & Discussion

All of the literature structures for the iminobis(dialkylphosphine chalcogenide) species investigated possess a single  $\text{HN}(\text{R}_2\text{PE})_2$  molecule in the asymmetric unit. There exists no symmetry elements within the molecule providing chemical equivalence between the two phosphorus (or two selenium) atoms, thus, two distinct phosphorus (or selenium) chemical shift tensors are expected in the experimental NMR spectra. The phosphorus chemical shift tensors for the iminobis(dialkylphosphine chalcogenide) systems are presented first, followed by the results of a solid-state  $^{77}\text{Se}$  NMR study on  $\text{HN}(\text{R}_2\text{PSe})_2$  ( $\text{R} = \text{Ph}, ^i\text{Pr}$ ). As the syntheses of the phenyl-derivatized species were reported prior to the isopropyl variants, the results for  $\text{HN}(\text{Ph}_2\text{PE})_2$  will precede those for  $\text{HN}(^i\text{Pr}_2\text{PE})_2$ . The extracted NMR parameters are discussed in terms of the known molecular structures, highlighting the impact in the choice of alkyl group and/or chalcogen where applicable. DFT computations of the phosphorus and selenium nuclear magnetic shielding tensors

provide the orientations of the corresponding chemical shift tensors, while the calculated principal components,  $\delta_{ii}$ , of the respective  $^{31}\text{P}$  and  $^{77}\text{Se}$  chemical shift tensors are tabulated in Appendix B.

### 5.3.1 Solid-State $^{31}\text{P}$ NMR

The  $^{31}\text{P}$  NMR parameters for all of the  $\text{HN}(\text{R}_2\text{PE})_2$  ( $\text{E} = \text{O}, \text{S}, \text{Se}$ ;  $\text{R} = \text{Ph}, \text{}^i\text{Pr}$ ) samples investigated are given in Table 5.1. Experimental solid-state  $^{31}\text{P}$  NMR spectra for  $\text{HN}(\text{R}_2\text{PO})_2$ ,  $\text{HN}(\text{R}_2\text{PS})_2$ , and  $\text{HN}(\text{R}_2\text{PSe})_2$  are given in Figures 5.2, 5.3, and 5.4, respectively. Theoretical calculations of the phosphorus chemical shift tensors are presented in Table B1.

#### 5.3.1.1 $\text{HN}(\text{R}_2\text{PO})_2$ ( $\text{R} = \text{Ph}, \text{}^i\text{Pr}$ )

Contrary to initial formulations,<sup>74,75</sup> prior to the solution of its X-ray structure,  $\text{HN}(\text{Ph}_2\text{PO})_2$  does not possess an acidic N-H proton. Rather, it is more accurately depicted as the imidodiphosphinic acid tautomer,  $\text{Ph}_2\text{P}(\text{OH})\text{NP}(\text{O})\text{Ph}_2$ .<sup>76</sup> As a result,  $\text{Ph}_2\text{P}(\text{OH})\text{NP}(\text{O})\text{Ph}_2$  has a considerably different structure than the other iminobis(dialkylphosphine chalcogenide) systems investigated. Similar to the  $\text{HN}(\text{Ph}_2\text{PE})_2$  ( $\text{E} = \text{S}, \text{Se}$ ) molecules that possess a solid state structure in which the EPNPE backbone adopts an *anti* conformation,  $\text{Ph}_2\text{P}(\text{OH})\text{NP}(\text{O})\text{Ph}_2$  is *trans* with an O-P...P-O 'torsion' angle of  $180^\circ$ .<sup>76</sup> However, unique to the  $\text{Ph}_2\text{P}(\text{OH})\text{NP}(\text{O})\text{Ph}_2$  system is a linear P-N-P angle of  $180^\circ$ .<sup>76</sup> The solid-state  $^{31}\text{P}$  NMR spectrum is given, along with its simulation, in Figure 5.2a. The two phosphorus chemical shift tensors extracted,

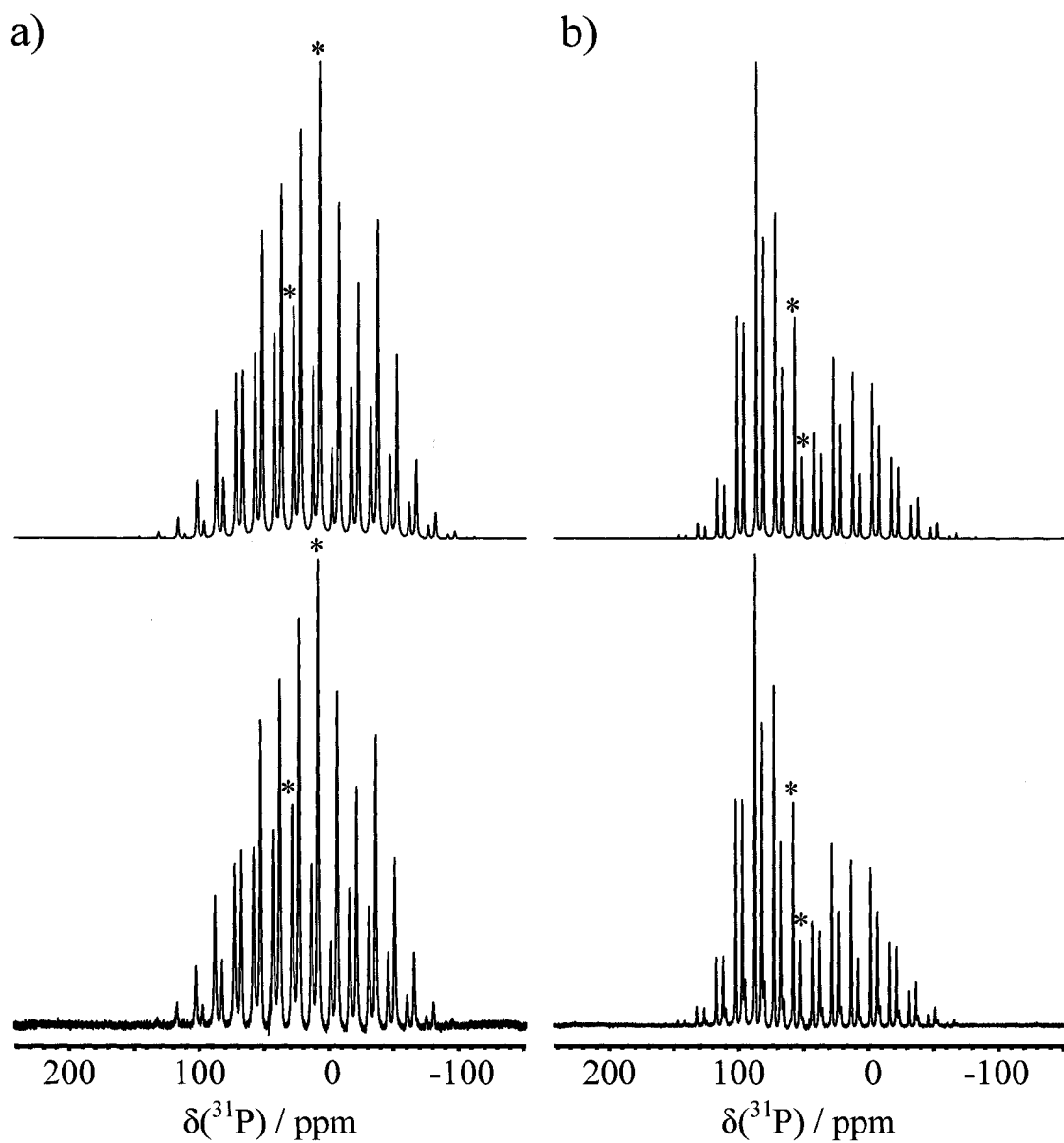
**Table 5.1** Solid-state  $^{31}\text{P}$  NMR parameters for  $\text{HN}(\text{R}_2\text{PE})_2$  (E = O, S, Se; R = Ph,  $^i\text{Pr}$ ).

E	R	$\delta_{\text{iso}}$ ppm	$\delta_{11}$ ppm	$\delta_{22}$ ppm	$\delta_{33}$ ppm	$\Omega$ ppm	$\kappa$	$^1J(\text{Se},\text{P})_{\text{iso}}^{\text{a}}$ Hz
O	Ph	8.2	79.6	13.3	-68.2	147.8	0.10	
		28.4	109.5	38.6	-62.8	172.3	0.18	
	$^i\text{Pr}$	52.5	101.8	101.8	-46.0	147.8	1.00	
		57.7	112.7	89.2	-28.8	141.5	0.67	
S	Ph	54.7	155.7	77.5	-69.2	224.9	0.30	
		57.1	164.0	92.7	-85.5	249.5	0.43	
	$^i\text{Pr}$	89.1	155.0	121.7	-9.4	164.4	0.60	
		90.6	163.0	118.5	-9.7	172.7	0.48	
Se	Ph	48.9	149.5	62.5	-65.2	214.7	0.19	-720
		52.4	160.4	79.9	-83.1	243.5	0.34	-740
	$^i\text{Pr}$	88.8	152.0	113.7	0.7	151.3	0.49	-740
		91.1	160.4	110.3	2.6	157.8	0.36	-735

<sup>a</sup> For directly bonded selenium-77 and phosphorus-31 spin pairs, signs of  $^1J(^{77}\text{Se}, ^{31}\text{P})_{\text{iso}}$  are known to be negative for numerous analogous systems.<sup>113,114</sup>

Table 5.1, possess isotropic chemical shifts and spans that differ by more than 20 ppm, despite the two tensors possessing similarly small positive skews.

Theoretical phosphorus chemical shift tensors from the DFT computations, Appendix B, produce comparable values of  $\delta_{\text{iso}}$ ,  $\delta_{\text{ii}}$ ,  $\Omega$ , and  $\kappa$  with the experimentally determined parameters; however, they do not calculate an equally large difference between the two respective isotropic chemical shifts. Additionally, the computations indicate that the phosphorus bearing the hydroxyl group is more shielded than the P=O phosphorus in  $\text{Ph}_2\text{P}(\text{OH})\text{NP}(\text{O})\text{Ph}_2$ . The calculated orientations of the two phosphorus chemical shift tensors are also different. The computed P-OH phosphorus chemical shift tensor orients  $\delta_{11}$  perpendicular to the local O-P-N plane, and  $\delta_{33}$  approximately parallel to the P-N vector with  $\delta_{22}$  within the O-P-N plane and perpendicular to P-N. The calculated P=O phosphorus chemical tensor places  $\delta_{11}$  perpendicular to the local O-P-N plane, while in contrast  $\delta_{33}$  is oriented nearly parallel to the P-O vector with  $\delta_{22}$  within the O-P-N plane



**Figure 5.2** (a) RACP MAS  $^{31}\text{P}$  NMR spectrum (lower trace) for  $\text{Ph}_2\text{P}(\text{OH})\text{NP}(\text{O})\text{Ph}_2$  and its simulation (upper trace). Experimental conditions: 11.7 T, 64 scans, MAS at 3.0 kHz, 10 Hz of line broadening, a 3.0 ms contact time, and a 900 s recycle delay. (b) RACP MAS  $^{31}\text{P}$  NMR spectrum (lower trace) for  $\text{HN}(\text{iPr}_2\text{PO})_2$  and its simulation (upper trace). Experimental conditions: 11.7 T, 128 scans, MAS at 3.0 kHz, 10 Hz of line broadening, a 3.0 ms contact time, and a 18 s recycle delay. The isotropic peaks are marked with an asterisk (\*).



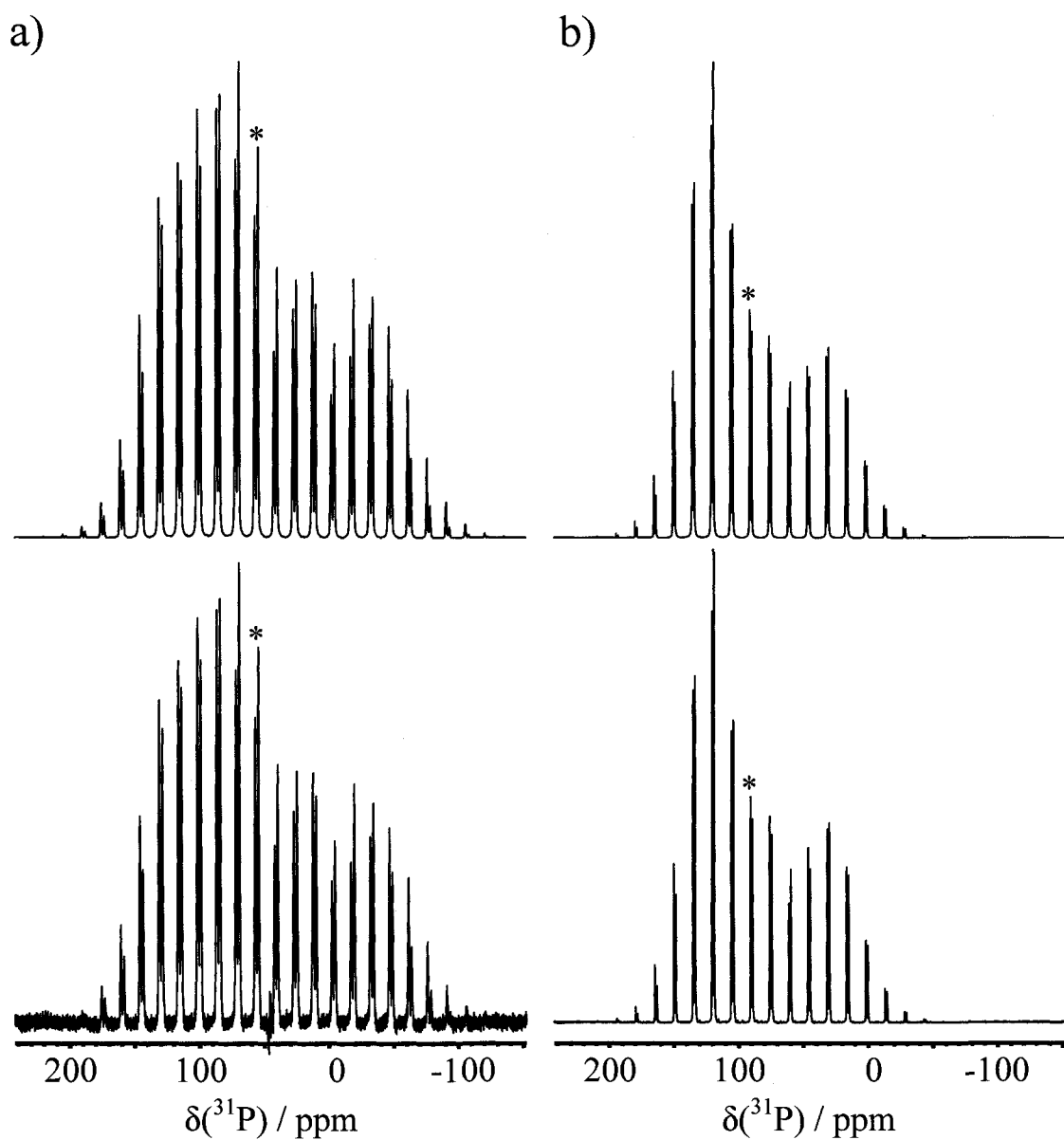
and perpendicular to P-O. Both orientations differ significantly from those calculated for the monoclinic and orthorhombic forms of  $\text{Ph}_3\text{PO}$ , where both polymorphs orient  $\delta_{11}$  along the P-O vector.<sup>115</sup>

One of the largest differences between iminobis(diisopropylphosphine oxide) and  $\text{Ph}_2\text{P}(\text{OH})\text{NP}(\text{O})\text{Ph}_2$  is that  $\text{HN}(\text{}^i\text{Pr}_2\text{PO})_2$  possesses an acidic N-H proton leading to a P-N-P angle of  $130^\circ$ .<sup>44</sup> The *gauche* conformation of iminobis(diisopropylphosphine oxide), reflected in a  $52^\circ$  O-P...P-O 'torsion' angle, yields a chain-like arrangement of  $\text{HN}(\text{}^i\text{Pr}_2\text{PO})_2$  units in its solid state structure.<sup>44</sup> The X-ray structure of  $\text{HN}(\text{}^i\text{Pr}_2\text{PO})_2$  displays some disorder in that one methyl carbon on one isopropyl group possesses two 50% occupancy sites.<sup>44</sup> There exists three discernable signals in the  $^{31}\text{P}$  MAS spectrum of  $\text{HN}(\text{}^i\text{Pr}_2\text{PO})_2$  given in Figure 5.2b; however, as one of the three signals is significantly less intense than the other two it is considered to be a minor impurity in the sample rather than resulting from disorder in the structure. The two isotropic phosphorus chemical shifts, Table 5.1, are in good agreement with the  $^{31}\text{P}$  NMR value from a chloroform solution of  $\text{HN}(\text{}^i\text{Pr}_2\text{PO})_2$ , 55.5 ppm.<sup>44</sup> The phosphorus chemical shift tensors are deshielded with respect to those of  $\text{Ph}_2\text{P}(\text{OH})\text{NP}(\text{O})\text{Ph}_2$ , as well as possess slightly smaller spans and larger positive skews. The steric or electronic source of this difference will be discussed later. One phosphorus environment indicates an axially symmetric chemical shift tensor, despite there being no symmetry reasons for attaining this axial symmetry. Methods for obtaining accurate principal components of the chemical shift tensor from spectra of MAS samples are known to have the greatest difficulty with axially or near axially symmetric species.<sup>116</sup>

Calculated phosphorus chemical shift tensors were obtained for both of the 50% occupancy structures,<sup>44</sup> labeled 'a' and 'b' in Appendix B. Both phosphorus chemical shift tensors computed for each of the two structures achieve reasonable agreement with the experimental values. The values of  $\delta_{ij}(\text{Calc})$  are very similar for structures 'a' and 'b', suggesting that the presence of disorder in the methyl group does not significantly affect the phosphorus shielding in  $\text{HN}({}^i\text{Pr}_2\text{PO})_2$ . This is consistent with the solid-state  ${}^{31}\text{P}$  NMR spectrum, Figure 5.2b, where no discernable difference in the line widths or line shapes of the two phosphorus environments was detected. In contrast to the calculated orientations of the phosphorus chemical shift tensors in  $\text{Ph}_2\text{P}(\text{OH})\text{NP}(\text{O})\text{Ph}_2$ , all four tensors for  $\text{HN}({}^i\text{Pr}_2\text{PO})_2$  are oriented similarly. The computations place  $\delta_{33}$  approximately along the O-P vector, and  $\delta_{22}$  perpendicular to the local O-P-N plane, with  $\delta_{11}$  perpendicular to O-P within the O-P-N plane.

#### 5.3.1.2 $\text{HN}(\text{R}_2\text{PS})_2$ ( $\text{R} = \text{Ph}, {}^i\text{Pr}$ )

The *anti* conformation of  $\text{HN}(\text{Ph}_2\text{PS})_2$ , with a S-P...P-S 'torsion' angle of  $156^\circ$  is similar to that of  $\text{Ph}_2\text{P}(\text{OH})\text{NP}(\text{O})\text{Ph}_2$ , while the nonlinear P-N-P angle  $133^\circ$  is consistent with a PNP backbone that possesses a protonated nitrogen.<sup>76-78</sup> The solid state structure consists of two  $\text{HN}(\text{Ph}_2\text{PS})_2$  molecules hydrogen bonded to form dimer pairs.<sup>76-78</sup> The  ${}^{31}\text{P}$  NMR parameters from the RACP MAS spectrum for  $\text{HN}(\text{Ph}_2\text{PS})_2$ , Figure 5.3a, are given in Table 5.1. The isotropic chemical shifts are in good agreement with the solution  ${}^{31}\text{P}$  NMR values of 55.1 ppm in THF,<sup>80</sup> and 58.2 ppm in  $\text{CDCl}_3$ .<sup>84</sup> The phosphorus chemical shift tensors for  $\text{HN}(\text{Ph}_2\text{PS})_2$  are more deshielded, possess larger spans and slightly more positive values of  $\kappa$  than those for  $\text{Ph}_2\text{P}(\text{OH})\text{NP}(\text{O})\text{Ph}_2$ .



**Figure 5.3** (a) RACP MAS  $^{31}\text{P}$  NMR spectrum (lower trace) for  $\text{HN}(\text{Ph}_2\text{PS})_2$  and its simulation (upper trace). Experimental conditions: 11.7 T, 64 scans, MAS at 3.0 kHz, 10 Hz of line broadening, a 3.0 ms contact time, and a 900 s recycle delay. (b) RACP MAS  $^{31}\text{P}$  NMR spectrum (lower trace) for  $\text{HN}(\text{iPr}_2\text{PS})_2$  and its simulation (upper trace). Experimental conditions: 11.7 T, 128 scans, MAS at 3.0 kHz, 5 Hz of line broadening, a 3.0 ms contact time, and a 9 s recycle delay. The isotropic peaks are marked with an asterisk (\*).

The DFT computations were performed on a dimer of  $\text{HN}(\text{Ph}_2\text{PS})_2$  units. The calculated principal components of the respective phosphorus chemical shift tensors slightly overestimate the corresponding experimental values. The orientations of the two calculated phosphorus chemical shift tensors are nearly identical and most closely resemble those calculated for  $\text{Ph}_2\text{P}(\text{OH})\text{NP}(\text{O})\text{Ph}_2$ , with  $\delta_{33}$  approximately parallel to the P-S vector,  $\delta_{11}$  perpendicular to the local S-P-N plane, and  $\delta_{22}$  nearly within the S-P-N plane perpendicular to P-S.

Similar to that of  $\text{HN}(\text{}^i\text{Pr}_2\text{PO})_2$ , the structure of  $\text{HN}(\text{}^i\text{Pr}_2\text{PS})_2$  contains a  $132^\circ$  P-N-P angle; however, the S-P $\cdots$ P-S ‘torsion’ angle is slightly larger at  $79^\circ$  and the X-ray structure reports no evidence of disorder.<sup>43</sup> The solid-state  $^{31}\text{P}$  NMR spectrum of  $\text{HN}(\text{}^i\text{Pr}_2\text{PS})_2$  is given Figure 5.3b. The isotropic chemical shifts for the two phosphorus environments are in good agreement with the value of 91.2 ppm reported for  $\text{HN}(\text{}^i\text{Pr}_2\text{PS})_2$  in  $\text{CDCl}_3$ .<sup>43</sup> Similar to the phosphorus chemical shift tensors of  $\text{HN}(\text{Ph}_2\text{PS})_2$  and  $\text{Ph}_2\text{P}(\text{OH})\text{NP}(\text{O})\text{Ph}_2$ , the two chemical shift tensors for  $\text{HN}(\text{}^i\text{Pr}_2\text{PS})_2$  are more deshielded and possess larger spans than those for  $\text{HN}(\text{}^i\text{Pr}_2\text{PO})_2$ . Solution  $^{31}\text{P}$  NMR for the mixed chalcogen system  $\text{}^i\text{Pr}_2\text{P}(\text{O})\text{NHP}(\text{S})\text{}^i\text{Pr}_2$  displays a comparable difference in the values of  $\delta_{\text{iso}}(^{31}\text{P})$ , 54.8 and 90.9 ppm.<sup>44</sup> Additionally, as with the E = O compounds, the phosphorus sites in  $\text{HN}(\text{}^i\text{Pr}_2\text{PS})_2$  are more deshielded and have larger positive skews than the phenyl derivative.

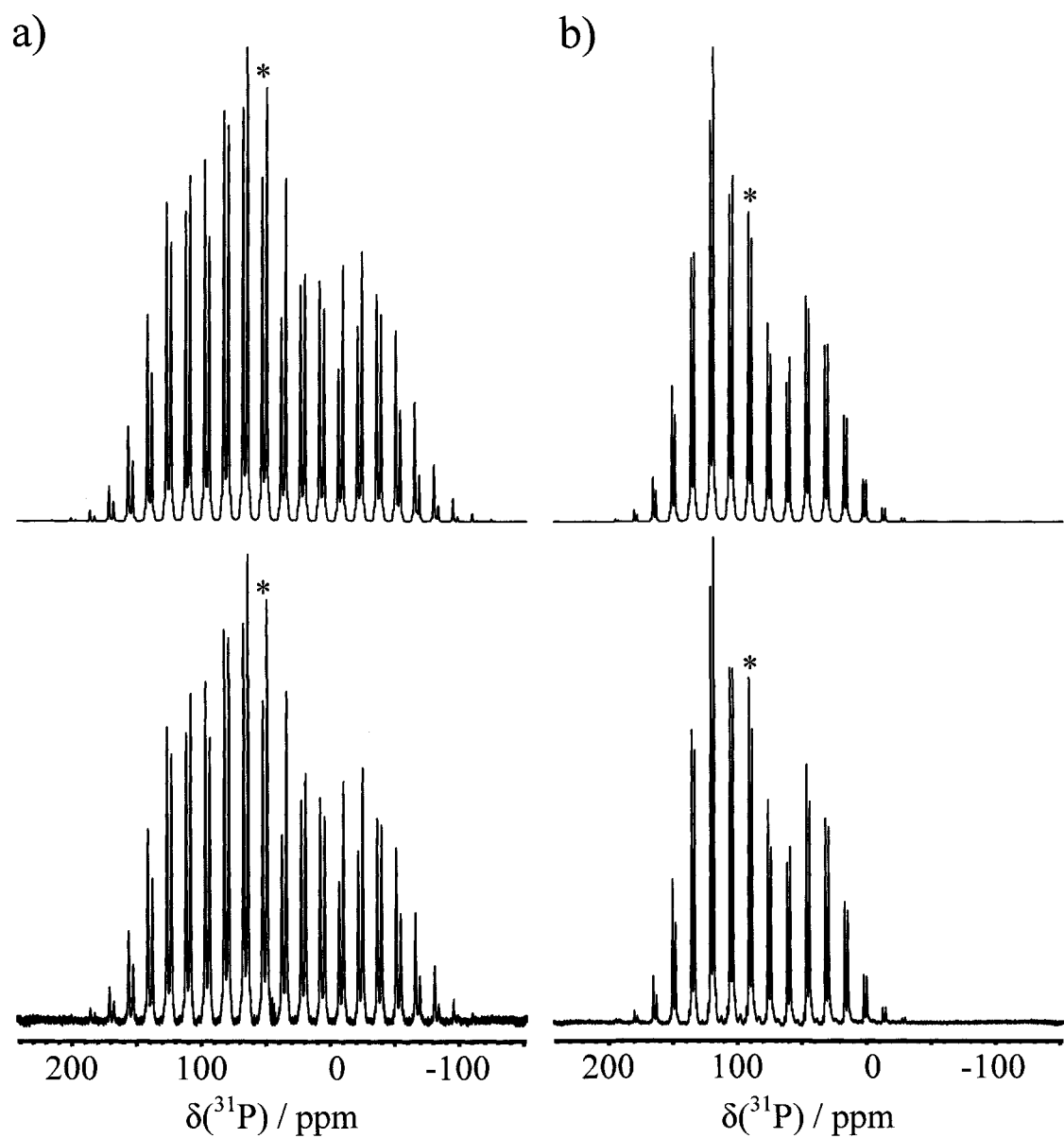
Calculated phosphorus chemical shift tensors for  $\text{HN}(\text{}^i\text{Pr}_2\text{PS})_2$  are given in Appendix B. The computed values of  $\delta_{\text{iso}}$ ,  $\delta_{\text{ii}}$ ,  $\Omega$ , and  $\kappa$  are in reasonable agreement with the experimentally obtained parameters. Similar to the calculated orientation of the tensors in  $\text{HN}(\text{}^i\text{Pr}_2\text{PO})_2$ , the two phosphorus chemical shift tensors for  $\text{HN}(\text{}^i\text{Pr}_2\text{PS})_2$  are

approximately identical and place  $\delta_{33}$  nearly parallel to the E-P vector; however, the directions of  $\delta_{11}$  and  $\delta_{22}$  are essentially reversed in  $\text{HN}(\text{}^i\text{Pr}_2\text{PS})_2$  with respect to  $\text{HN}(\text{}^i\text{Pr}_2\text{PO})_2$  with  $\delta_{11}$  perpendicular to the local S-P-N plane and  $\delta_{22}$  within the S-P-N plane perpendicular to S-P.

#### 5.3.1.3 $\text{HN}(\text{R}_2\text{PSe})_2$ ( $\text{R} = \text{Ph}, \text{}^i\text{Pr}$ )

Isomorphous with  $\text{HN}(\text{Ph}_2\text{PS})_2$ , the dimer structure of  $\text{HN}(\text{Ph}_2\text{PSe})_2$  possesses an *anti* conformation with a Se-P...P-Se ‘torsion’ angle of  $154^\circ$  and a P-N-P angle of  $132^\circ$ .<sup>10</sup> The phosphorus chemical shift parameters, along with an estimation of the one-bond selenium-phosphorus indirect spin-spin coupling constant,  $^1J(^{77}\text{Se}, ^{31}\text{P})_{\text{iso}}$ , from the MAS  $^{31}\text{P}$  NMR spectrum, Figure 5.4a, are reported in Table 5.1. The values of  $\delta_{\text{iso}}(^{31}\text{P})$  and  $^1J(^{77}\text{Se}, ^{31}\text{P})_{\text{iso}}$  are in good agreement with those from  $^{31}\text{P}$  NMR of methylene chloride and chloroform solutions of  $\text{HN}(\text{Ph}_2\text{PSe})_2$ , 53.0 ppm and  $(-)$ 793 Hz,<sup>10</sup> and 53.2 ppm,<sup>84</sup> respectively. The principal components of the phosphorus chemical shift tensors are very similar to those found for  $\text{HN}(\text{Ph}_2\text{PS})_2$ , see Table 5.1, suggesting that the impact of exchanging oxygen for sulfur in  $\text{HN}(\text{Ph}_2\text{PE})_2$  is larger than exchanging sulfur for selenium.

The phosphorus chemical shift tensors were calculated for a dimer of  $\text{HN}(\text{Ph}_2\text{PSe})_2$  molecules.<sup>10</sup> The calculations overestimate the values of  $\delta_{\text{iso}}$  and  $\Omega$  indicating that scalar relativistic effects may not be sufficient to accurately describe the shielding environment for  $\text{HN}(\text{Ph}_2\text{PSe})_2$  and that spin-orbit relativistic effects may be important. Similar to those of  $\text{HN}(\text{Ph}_2\text{PS})_2$ , the calculated orientations of the phosphorus chemical shift tensors in  $\text{HN}(\text{Ph}_2\text{PSe})_2$  place  $\delta_{11}$  perpendicular to the local Se-P-N plane,



**Figure 5.4** (a) RACP MAS  $^{31}\text{P}$  NMR spectrum (lower trace) for  $\text{HN}(\text{Ph}_2\text{PSe})_2$  and its simulation (upper trace). Experimental conditions: 11.7 T, 64 scans, MAS at 3.0 kHz, 10 Hz of line broadening, a 3.0 ms contact time, and a 900 s recycle delay. (b) RACP MAS  $^{31}\text{P}$  NMR spectrum (lower trace) for  $\text{HN}(\text{iPr}_2\text{PSe})_2$  and its simulation (upper trace). Experimental conditions: 11.7 T, 128 scans, MAS at 3.0 kHz, 10 Hz of line broadening, a 3.0 ms contact time, and a 18 s recycle delay. The isotropic peaks are marked with an asterisk (\*).

$\delta_{33}$  approximately along the P-Se vector, and  $\delta_{22}$  within the Se-P-N plane perpendicular to P-Se.

The structure of  $\text{HN}(\text{}^i\text{Pr}_2\text{PSe})_2$  more closely resembles that of  $\text{HN}(\text{}^i\text{Pr}_2\text{PS})_2$  with an  $80^\circ$  Se-P...P-Se ‘torsion’ angle, and a P-N-P angle of  $131^\circ$ .<sup>44</sup> However, similar with the structure of  $\text{HN}(\text{}^i\text{Pr}_2\text{PO})_2$ , the selenium analogue was refined where the location of one methyl carbon on one isopropyl group contained two 50% occupancy locations.<sup>44</sup> The isotropic chemical shifts and  ${}^1J({}^{77}\text{Se}, {}^{31}\text{P})_{\text{iso}}$  values extracted, Table 5.1, from the simulation of the solid-state  ${}^{31}\text{P}$  NMR spectrum of  $\text{HN}(\text{}^i\text{Pr}_2\text{PSe})_2$ , Figure 5.4b, are in good agreement with those from a chloroform solution  ${}^{31}\text{P}$  NMR study, 89.5 ppm and (-)757 Hz.<sup>44</sup> Similar to the solid-state  ${}^{31}\text{P}$  NMR spectrum of  $\text{HN}(\text{}^i\text{Pr}_2\text{PO})_2$ , Figure 5.2b, no evidence for the disorder in the methyl group was detected in the corresponding spectrum for iminobis(diisopropylphosphine selenide). As with the phosphorus chemical shift tensors of  $\text{HN}(\text{Ph}_2\text{PE})_2$  (E = S, Se), the two tensors for  $\text{HN}(\text{}^i\text{Pr}_2\text{PSe})_2$  are comparable to those found for  $\text{HN}(\text{}^i\text{Pr}_2\text{PS})_2$ , see Table 5.1. The isotropic phosphorus chemical shifts of the mixed chalcogen compound  ${}^i\text{Pr}_2\text{P}(\text{S})\text{NHP}(\text{Se}){}^i\text{Pr}_2$ , from a chloroform solution  ${}^{31}\text{P}$  NMR study, are also very similar at 89.2 and 92.1 ppm.<sup>44</sup>

Phosphorus chemical shift tensors were calculated for both of the 50% occupancy structures,<sup>44</sup> labeled ‘a’ and ‘b’ in Appendix B. The scalar relativistic calculated phosphorus chemical shift tensors for  $\text{HN}(\text{}^i\text{Pr}_2\text{PSe})_2$ , as with those for  $\text{HN}(\text{Ph}_2\text{PSe})_2$ , overestimate the experimental values. Analogous to those for  $\text{HN}(\text{}^i\text{Pr}_2\text{PO})_2$ , the calculated phosphorus chemical shift tensors for  $\text{HN}(\text{}^i\text{Pr}_2\text{PSe})_2$  structures ‘a’ and ‘b’ are nearly identical and suggest that evidence for the disorder is unlikely to come from the solid-state  ${}^{31}\text{P}$  NMR spectrum. As with the calculated orientations of the phosphorus

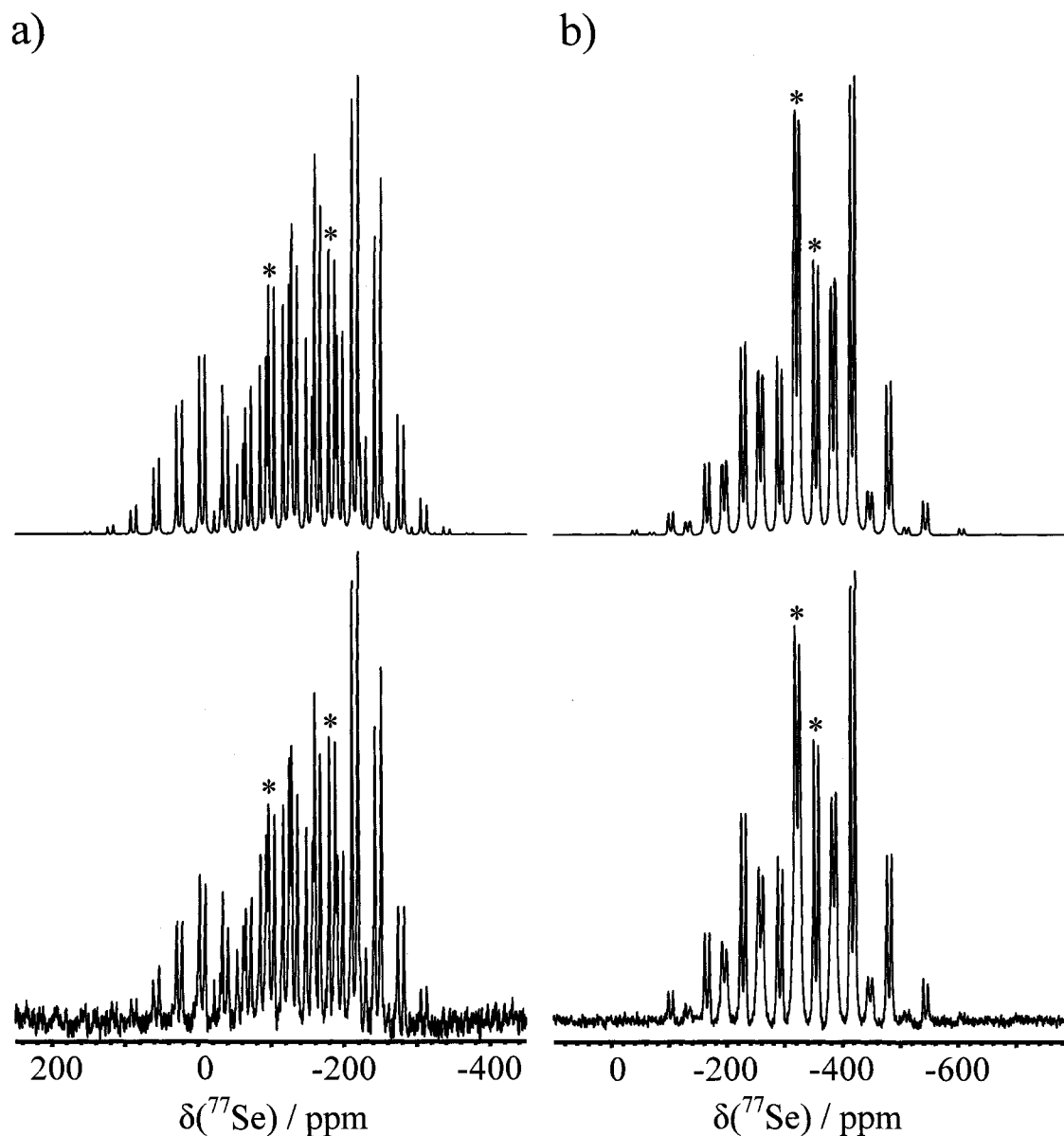
chemical shift tensors in  $\text{HN}(\text{iPr}_2\text{PO})_2$ , all four tensors for iminobis(diisopropylphosphine selenide) are identical; however, they are all oriented similarly to those of  $\text{HN}(\text{iPr}_2\text{PS})_2$ : Nearly along the P-Se vector is  $\delta_{33}$ , with  $\delta_{11}$  perpendicular to the local Se-P-N plane, and  $\delta_{22}$  within the Se-P-N plane perpendicular to P-Se.

### 5.3.2 Solid-State $^{77}\text{Se}$ NMR

The solid-state  $^{77}\text{Se}$  NMR spectrum for  $\text{HN}(\text{Ph}_2\text{PSe})_2$  is given in Figure 5.5a, and the  $^{77}\text{Se}$  NMR parameters extracted from its simulation are reported in Table 5.2. The values of  $^1J(^{77}\text{Se}, ^{31}\text{P})_{\text{iso}}$  are in agreement with those from solution  $^{31}\text{P}$  NMR<sup>10</sup> and with our solid-state  $^{31}\text{P}$  NMR values, Table 5.1 above. Similar to the large difference in isotropic phosphorus chemical shifts observed for  $\text{Ph}_2\text{P}(\text{OH})\text{NP}(\text{O})\text{Ph}_2$ , there is a significant difference between the two values of  $\delta_{\text{iso}}(\text{Se})$  in  $\text{HN}(\text{Ph}_2\text{PSe})_2$ . The spans of the selenium chemical shift tensors are both larger than any of the phosphorus chemical shift tensors obtained, which is consistent with the less symmetric environment of selenium in the iminobis(dialkylphosphine chalcogenide) systems and the larger chemical shift range of selenium with respect to that of phosphorus.<sup>117,118</sup>

The dimer structure of  $\text{HN}(\text{Ph}_2\text{PSe})_2$  was used to calculate the selenium chemical shift tensors. The computed principal components are in good agreement with the experimental values, particularly in the difference in shielding between the two chemical shift tensors. The calculations indicate that the selenium that participates in hydrogen bonding between the two  $\text{HN}(\text{Ph}_2\text{PSe})_2$  molecules is less shielded than the selenium that is not involved in hydrogen bonding. The calculated orientations of the two selenium chemical shift tensors are also different. For the selenium involved in hydrogen bonding





**Figure 5.5** (a) RACP MAS  ${}^{77}\text{Se}$  NMR spectrum (lower trace) for  $\text{HN}(\text{Ph}_2\text{PSe})_2$  and its simulation (upper trace). Experimental conditions: 11.7 T, 384 scans, MAS at 3.0 kHz, 50 Hz of line broadening, a 10.0 ms contact time, and a 840 s recycle delay. (b) RACP MAS  ${}^{77}\text{Se}$  NMR spectrum (lower trace) for  $\text{HN}({}^1\text{Pr}_2\text{PSe})_2$  and its simulation (upper trace). Experimental conditions: 11.7 T, 5288 scans, MAS at 6.0 kHz, 50 Hz of line broadening, a 6.5 ms contact time, and a 14 s recycle delay. The isotropic peaks are marked with an asterisk (\*).

**Table 5.2** Solid-state  $^{77}\text{Se}$  NMR parameters for  $\text{HN}(\text{R}_2\text{PSe})_2$  ( $\text{R} = \text{Ph}, \text{}^i\text{Pr}$ ).

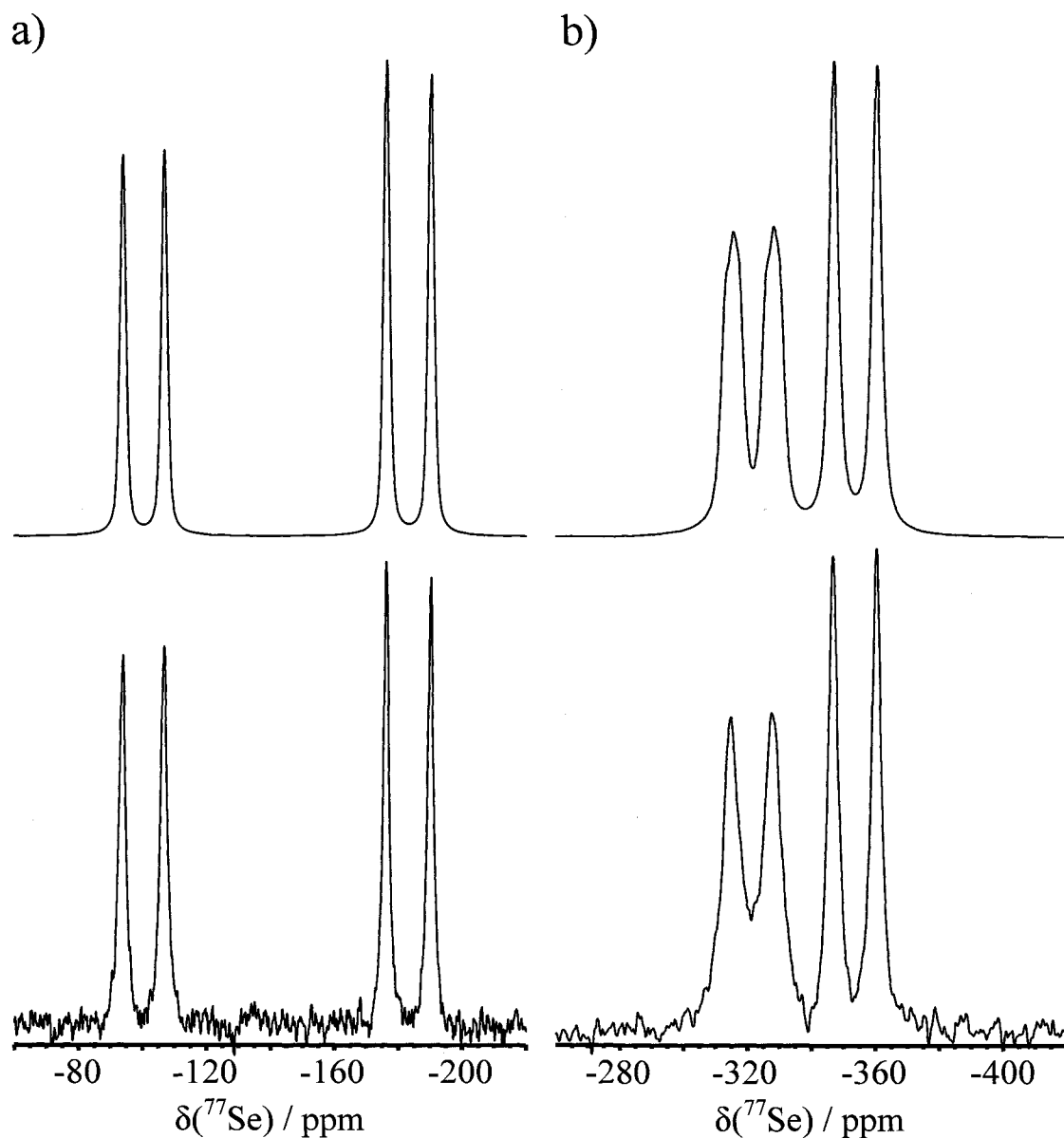
R	$\delta_{\text{iso}}$ ppm	$\delta_{11}$ ppm	$\delta_{22}$ ppm	$\delta_{33}$ ppm	$\Omega$ ppm	$\kappa$	$^1J(\text{Se,P})_{\text{iso}}^{\text{a}}$ Hz
Ph	-184	-41	-219	-291	250	-0.42	-800
	-101	79	-146	-236	317	-0.43	-740
$^i\text{Pr}$	-355	-135	-419	-511	376	-0.51	-760
	-322	-179	-352	-435	256	-0.36	-720

<sup>a</sup> For directly bonded selenium-77 and phosphorus-31 spin pairs, signs of  $^1J(^{77}\text{Se}, ^{31}\text{P})_{\text{iso}}$  are known to be negative for numerous analogous systems.<sup>113,114</sup>

between the dimers,  $\delta_{33}$  is nearly parallel to the Se-P vector,  $\delta_{11}$  perpendicular to the local Se-P-N plane, and  $\delta_{22}$  within the Se-P-N plane perpendicular to Se-P. The selenium that is not involved in hydrogen bonding possesses a chemical shift tensor that orients  $\delta_{22}$  approximately along Se-P, with  $\delta_{11}$  perpendicular to the local Se-P-N plane and  $\delta_{33}$  within the Se-P-N plane perpendicular to Se-P.

The  $^{77}\text{Se}$  NMR parameters from the solid-state  $^{77}\text{Se}$  NMR spectrum for  $\text{HN}(\text{}^i\text{Pr}_2\text{PSe})_2$ , Figure 5.5b, are given in Table 5.2. The two  $^1J(^{77}\text{Se}, ^{31}\text{P})_{\text{iso}}$  couplings are in good agreement with the reported values from solution<sup>44</sup> and solid-state (above)  $^{31}\text{P}$  NMR. Unlike those for  $\text{HN}(\text{Ph}_2\text{PSe})_2$ , the two isotropic selenium chemical shifts for iminobis(diisopropylphosphine selenide) are more shielded and significantly closer together. Additionally, in contrast to the solid-state  $^{31}\text{P}$  NMR spectra for  $\text{HN}(\text{}^i\text{Pr}_2\text{PE})_2$  ( $\text{E} = \text{O}, \text{Se}$ ), the solid-state  $^{77}\text{Se}$  NMR spectrum for  $\text{HN}(\text{}^i\text{Pr}_2\text{PSe})_2$  appears to be sensitive to the disorder of the methyl group in the structure.<sup>44</sup> Figure 5.6 displays the isotropic region of the solid-state  $^{77}\text{Se}$  NMR spectra for  $\text{HN}(\text{R}_2\text{PSe})_2$  ( $\text{R} = \text{Ph}, \text{}^i\text{Pr}$ ), where one of the two  $J$ -coupled isotropic peaks for  $\text{HN}(\text{}^i\text{Pr}_2\text{PSe})_2$  is visibly broader than the others.

The two calculated selenium chemical shift tensors for each of the two 50% occupancy structures also suggest that the impact of the disorder of the methyl group should be more pronounced in the solid-state  $^{77}\text{Se}$  NMR spectrum; however, the



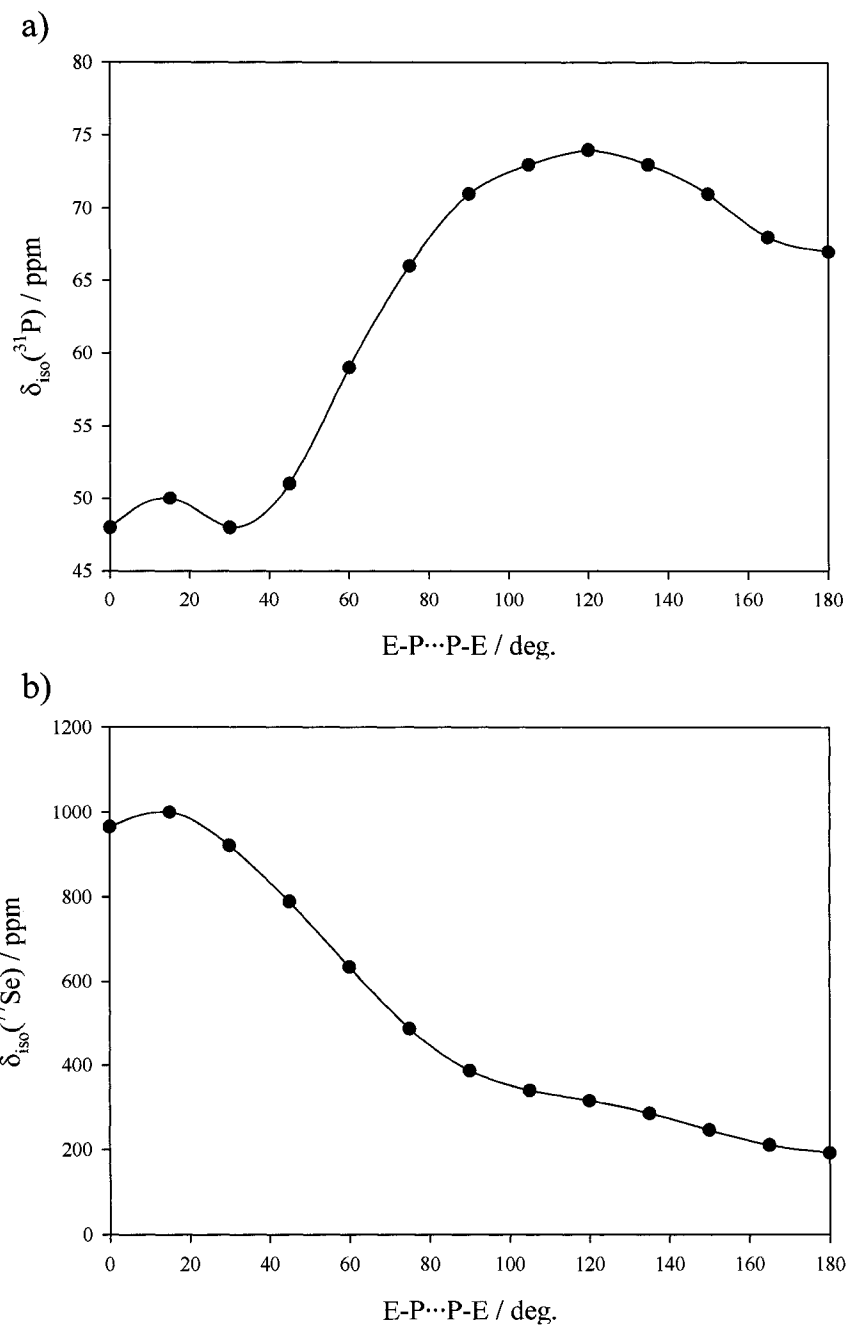
**Figure 5.6** Isotropic region of the  $^{77}\text{Se}$  NMR spectrum for (a)  $\text{HN}(\text{Ph}_2\text{PSe})_2$  and (b)  $\text{HN}(\text{}^i\text{Pr}_2\text{PSe})_2$  (lower traces) and their simulations (upper traces).

calculations indicate that both selenium environments should be influenced by the disorder. Additionally, the calculations predict that the selenium environment that is furthest from the methyl group should be affected more than the proximal selenium. The calculated orientations of the selenium chemical shift tensors are identical for structures

'a' and 'b', yet distinct. The chemical shift tensor for the selenium distal to the methyl disorder is oriented such that  $\delta_{33}$  is nearly along the Se-P vector,  $\delta_{11}$  is perpendicular to the local Se-P-N plane, while  $\delta_{22}$  lies within the Se-P-N plane perpendicular to Se-P. The selenium nearest the methyl disorder possesses a calculated chemical shift tensor that also places  $\delta_{11}$  approximately perpendicular to the local Se-P-N plane; however, the P-Se vector nearly bisects the  $\delta_{22}$ -Se- $\delta_{33}$  angle within the Se-P-N plane.

### 5.3.3 The Effect of the E-P...P-E 'Torsion' Angle

From Table 5.1 it is clear that the phosphorus environments in the  $\text{HN}(\text{Ph}_2\text{PE})_2$  (E = O, S, Se) systems, which all possess *anti* E-P...P-E 'torsion' angles, are all more shielded than their  $\text{HN}({}^i\text{Pr}_2\text{PE})_2$  counterparts that have *gauche* 'torsion' angles. Conversely, in Table 5.2, the selenium chemical shifts of  $\text{HN}(\text{Ph}_2\text{PSe})_2$  are both less shielded than those of  $\text{HN}({}^i\text{Pr}_2\text{PSe})_2$ . The consistent differences observed in the isotropic chemical shifts between the phenyl and isopropyl variants of  $\text{HN}(\text{R}_2\text{PE})_2$  (E = O, S, Se) are likely to arise from a combination of the electronic effects of the chosen alkyl group and the common steric differences between the structures. To probe the nature of these differences, nuclear magnetic shielding calculations were performed on a truncated system,  $\text{HN}(\text{Me}_2\text{PSe})_2$ . The  $\text{HN}(\text{Me}_2\text{PSe})_2$  structure was achieved by replacing the isopropyl groups of one of the two 50% occupancy structures of  $\text{HN}({}^i\text{Pr}_2\text{PSe})_2$  with methyl groups. Figure 5.7 displays the effect of rotation about the E-P...P-E 'torsion' angle from an eclipsed orientation,  $0^\circ$ , to a *trans* conformation,  $180^\circ$ , in  $15^\circ$  increments. For both the computed phosphorus and selenium chemical shifts, the calculations predict the opposite effect to what was observed experimentally; that is, the *anti* structures of



**Figure 5.7** Effect of rotation about the E-P...P-E 'torsion' angle for HN(Me<sub>2</sub>PSe)<sub>2</sub> on (a)  $\delta_{\text{iso}}(^{31}\text{P})$  and (b)  $\delta_{\text{iso}}(^{77}\text{Se})$ .

HN(Me<sub>2</sub>PSe)<sub>2</sub> possess less shielded phosphorus and more shielded selenium environments than any of the *gauche* structures. The outcome of these calculations

suggest that the electronic effect of the chosen alkyl group dominates the impact of the E-P...P-E 'torsion' angle, which is supported by the solution  $^{31}\text{P}$  NMR reported for the mixed alkyl system  $\text{Ph}_2\text{P}(\text{S})\text{NHP}(\text{S})^i\text{Pr}_2$ .<sup>119</sup> The isotropic phosphorus chemical shifts of  $\text{Ph}_2\text{P}(\text{S})\text{NHP}(\text{S})^i\text{Pr}_2$ , 100.0 and 51.5 ppm, display an even larger separation than those found between the phenyl and isopropyl compounds studied herein,  $\text{HN}(\text{R}_2\text{PE})_2$  (E = O, S, Se), Table 5.1. Rotation of the S-P...P-S angle in solution may effectively average the conformational impact on the phosphorus chemical shift present in the solid state. Thus, the electronic effect on the shielding of the alkyl group is not opposed to the same extent by the conformation of the EPNPE backbone and the isotropic phosphorus chemical shifts are found to be further apart.

#### 5.4 Summary

The iminobis(dialkylphosphine chalcogenide) systems,  $\text{HN}(\text{R}_2\text{PE})_2$  (E = O, S, Se; R = Ph,  $^i\text{Pr}$ ), have been investigated by solid-state  $^{31}\text{P}$  and  $^{77}\text{Se}$  NMR spectroscopy and DFT computational chemistry. The phosphorus chemical shift tensors of the  $\text{HN}(\text{Ph}_2\text{PE})_2$  (E = O, S, Se) systems all possessed more shielded environments, larger spans and smaller skews than the corresponding  $\text{HN}(^i\text{Pr}_2\text{PE})_2$  systems. Aside from  $\text{Ph}_2\text{P}(\text{OH})\text{NP}(\text{O})\text{Ph}_2$ , the calculated orientations of the two phosphorus chemical shift tensors in each  $\text{HN}(\text{R}_2\text{PE})_2$  system are essentially identical. The experimental and theoretical selenium chemical shift tensors in  $\text{HN}(\text{Ph}_2\text{PSe})_2$  were found to be sensitive to the presence of hydrogen bonding in its solid state dimer structure, while those of  $\text{HN}(^i\text{Pr}_2\text{PSe})_2$  were susceptible to the disorder found in its structure. The impact of the conformation of the EPNPE backbone via the E-P...P-E 'torsion' angle was studied by DFT nuclear magnetic

shielding calculations on a truncated system,  $\text{HN}(\text{Me}_2\text{PSe})_2$ . The steric impact of the Se-P...P-Se angle on the computed phosphorus and selenium isotropic chemical shifts was found to have the opposite effect to what was observed experimentally, indicating that the choice of phenyl or isopropyl group is more important than the conformational contributions to the phosphorus and selenium shielding in these systems.

## 5.5 References

- (1) Mehrotra, R. C.; Bohra, R.; Gaur, D. P. *Metal  $\beta$ -Diketonates and Allied Derivatives*; Academic Press: London, 1978.
- (2) Itoh, K.-I.; Matsumoto, O. *Thin Solid Films* **1999**, *345*, 29-33.
- (3) Toroyanov, S. I.; Kuzmina, N. P.; Soboleva, I. E.; Chugarov, N. V. *Electrochem. Soc. Proc.* **1997**, *97-25*, 886-892.
- (4) Gleizes, A. N. *Chem. Vap. Deposition* **2000**, *6*, 155-173.
- (5) Green, M.; O'Brien, P. *Chem. Commun.* **1999**, 2235-2241.
- (6) Pickett, N. L.; O'Brien, P. *Chem. Rec.* **2001**, *1*, 467-479.
- (7) Novosad, J.; Lindeman, S. V.; Marek, J.; Woollins, J. D.; Husebye, S. *Heteroat. Chem.* **1998**, *9*, 615-621.
- (8) Gilby, L. M.; Piggott, B. *Polyhedron* **1999**, *18*, 1077-1082.
- (9) Montiel-Palma, V.; Huitrón-Rattinger, E.; Cortés-Llamas, S.; Muñoz-Hernández, M.-Á.; García-Montalvo, V.; López-Honorato, E.; Silvestru, C. *Eur. J. Inorg. Chem.* **2004**, 3743-3750.
- (10) Bhattacharyya, P.; Novosad, J.; Phillips, J.; Slawin, A. M. Z.; Williams, D. J.; Woollins, J. D. *Dalton Trans.* **1995**, 1607-1613.
- (11) Knyazeva, A. N.; Shugam, E. A.; Shkol'nikova, L. M. *Zh. Strukt. Khim.* **1970**, *11*, 938-989.
- (12) Onuma, S.; Horioka, K.; Inoue, H.; Shibata, S. *Bull. Chem. Soc. Jpn.* **1980**, *53*, 2679-2680.
- (13) Woollins, J. D. *Dalton Trans.* **1996**, 2893-2901.
- (14) Valderrama, M.; Contreras, R.; Lamata, M. P.; Viguri, F.; Carmona, D.; Lahoz, F. J.; Elipe, S.; Oro, L. A. *J. Organomet. Chem.* **2000**, *607*, 3-11.
- (15) Bhattacharyya, P.; Woollins, J. D. *Polyhedron* **1995**, *14*, 3367-3388.
- (16) Bhattacharyya, P.; Slawin, A. M. Z.; Smith, M. B. *Dalton Trans.* **1998**, 2467-2475.
- (17) Pernin, C. G.; Ibers, J. A. *Inorg. Chem.* **1999**, *38*, 5478-5483.



- (18) Papadimitriou, C.; Veltsistas, P.; Novosad, J.; Cea-Olivares, R.; Toscano, A.; García y García, P.; Lopez-Cardosa, M.; Slawin, A. M. Z.; Woollins, J. D. *Polyhedron* **1997**, *16*, 2727-2729.
- (19) García-Montalvo, V.; Novosad, J.; Kilian, P.; Woollins, J. D.; Slawin, A. M. Z.; García y García, P.; López-Cardoso, M.; Espinosa-Pérez, G.; Cea-Olivares, R. *Dalton Trans.* **1997**, 1025-1029.
- (20) Cea-Olivares, R.; García-Montalvo, V.; Novosad, J.; Kilian, P.; Woollins, J. D.; Slawin, A. M. Z.; García y García, P.; López-Cardoso, M.; Espinosa-Pérez, G.; Toscano, R. A.; Hernández, S.; Canseco-Melchor, G.; Lima-Montaño, L.; Rodríguez-Narváez, C. *Phosphorus Sulfur Silicon Relat. Elem.* **1997**, *124*, 347-354.
- (21) Cea-Olivares, R.; Moya-Cabrera, M.; García-Montalvo, V.; Castro-Blanco, R.; Toscano, R. A.; Hernández-Ortega, S. *Dalton Trans.* **2005**, 1017-1018.
- (22) Novosad, J.; Necas, M.; Marek, J.; Veltsistas, P.; Papadimitriou, C.; Haiduc, I.; Watanabe, M.; Woollins, J. D. *Inorg. Chim. Acta* **1999**, *290*, 256-260.
- (23) Afzaal, M.; Crouch, D. J.; O'Brien, P.; Raftery, J.; Skabara, P. J.; White, A. J. P.; Williams, D. J. *J. Mater. Chem.* **2004**, *14*, 233-237.
- (24) Haiduc, I.; Silaghi-Dumitrescu, I. *Coord. Chem. Rev.* **1986**, *74*, 127-270.
- (25) Ly, T. Q.; Woollins, J. D. *Coord. Chem. Rev.* **1998**, *176*, 451-481.
- (26) Afzaal, M.; Crouch, D.; Malik, M. A.; Motevalli, M.; O'Brien, P.; Park, J.-H. *J. Mater. Chem.* **2003**, *13*, 639-640.
- (27) Crouch, D. J.; Helliwell, M.; O'Brien, P.; Park, J.-H.; Waters, J.; Williams, D. J. *Dalton Trans.* **2003**, 1500-1504.
- (28) Afzaal, M.; Aucott, S. M.; Crouch, D.; O'Brien, P.; Woollins, J. D.; Park, J.-H. *Chem. Vap. Deposition* **2002**, *8*, 187-189.
- (29) Afzaal, M.; Crouch, D.; Malik, M. A.; Motevalli, M.; O'Brien, P.; Park, J.-H.; Woollins, J. D. *Eur. J. Inorg. Chem.* **2004**, 171-177.
- (30) Malik, M. A.; Afzaal, M.; O'Brien, P.; Halliwell, M. *Polyhedron* **2006**, *25*, 864-868.
- (31) Afzaal, M.; Ellwood, K.; Pickett, N. L.; O'Brien, P.; Raftery, J.; Waters, J. *J. Mater. Chem.* **2004**, *14*, 1310-1315.

- (32) Park, J.-H.; Afzaal, M.; Helliwell, M.; Malik, M. A.; O'Brien, P.; Raftery, J. *Chem. Mat.* **2003**, *15*, 4205-4210.
- (33) Waters, J.; Crouch, D.; O'Brien, P.; Park, J.-H. *J. Mater. Sci.: Mater. Electron.* **2003**, *14*, 599-602.
- (34) Waters, J.; Crouch, D.; Raftery, J.; O'Brien, P. *Chem. Mat.* **2004**, *16*, 3289-3298.
- (35) Crouch, D. J.; O'Brien, P.; Malik, M. A.; Skabara, P. J.; Wright, S. P. *Chem. Commun.* **2003**, 1454-1455.
- (36) Singhal, A.; Dutta, D. P.; Kulshreshtha, S. K.; Mobin, S. M.; Mathur, P. J. *Organomet. Chem.* **2006**, *691*, 4320-4328.
- (37) Garje, S. S.; Copsey, M. C.; Afzaal, M.; O'Brien, P.; Chivers, T. *J. Mater. Chem.* **2006**, *16*, 4542-4547.
- (38) Garje, S. S.; Ritch, J. S.; Eisler, D. J.; Afzaal, M.; O'Brien, P.; Chivers, T. *J. Mater. Chem.* **2006**, *16*, 966-969.
- (39) Copsey, M. C.; Panneerselvam, A.; Afzaal, M.; Chivers, T.; O'Brien, P. *Dalton Trans.* **2007**, 1528-1538.
- (40) Ritch, J. S.; Chivers, T.; Afzaal, M.; O'Brien, P. *Chem. Soc. Rev.* **2007**, *36*, 1622-1631.
- (41) Rossi, R.; Marchi, A.; Marvelli, L.; Magon, L.; Peruzzini, M.; Casellato, U.; Graziani, R. *Dalton Trans.* **1993**, 723-729.
- (42) Silvestru, C.; Drake, J. E. *Coord. Chem. Rev.* **2001**, *223*, 117-216.
- (43) Cupertino, D.; Keyte, R.; Slawin, A. M. Z.; Williams, D. J.; Woollins, J. D. *Inorg. Chem.* **1996**, *35*, 2695-2697.
- (44) Cupertino, D.; Birdsall, D. J.; Slawin, A. M. Z.; Woollins, J. D. *Inorg. Chim. Acta* **1999**, *290*, 1-7.
- (45) Cea-Olivares, R.; Novosad, J.; Woollins, J. D.; Slawin, A. M. Z.; García-Montalvo, V.; Espinosa-Pérez, G.; García y García, P. *Chem. Commun.* **1996**, 519-520.
- (46) Williams, D. J.; Quicksall, C. O.; Barkigia, K. M. *Inorg. Chem.* **1982**, *21*, 2097-2100.
- (47) Cea-Olivares, R.; Toscano, R. A.; Carreón, G.; Valdés-Martínez, J. *Monatsh. Chem.* **1992**, *123*, 391-396.

- (48) García-Montalvo, V.; Zamora-Rosete, M. K.; Gorostieta, D.; Cea-Olivares, R.; Toscano, R. A.; Hernández-Ortega, S. *Eur. J. Inorg. Chem.* **2001**, 2279-2285.
- (49) Rodríguez, I.; Alvarez, C.; Gómez-Lara, J.; Cea-Olivares, R. *Lanthanide Actinide Res.* **1986**, *1*, 253-260.
- (50) Silvestru, C.; Haiduc, I.; Cea-Olivares, R.; Zimbron, A. *Polyhedron* **1994**, *13*, 3159-3165.
- (51) Cea-Olivares, R.; García-Montalvo, V.; Novosad, J.; Woollins, J. D.; Toscano, R. A.; Espinosa-Pérez, G. *Chem. Ber.* **1996**, *129*, 919-923.
- (52) García-Montalvo, V.; Cea-Olivares, R.; Williams, D. J.; Espinosa-Pérez, G. *Inorg. Chem.* **1996**, *35*, 3948-3953.
- (53) Rudler, H.; Denise, B.; Gregorio, J. R.; Vaissermann, J. *Chem. Commun.* **1997**, 2299-2300.
- (54) Goyal, M.; Novosad, J.; Necas, M.; Ishii, H.; Nagahata, R.; Sugiyama, J.-I.; Asai, M.; Ueda, M.; Takeuchi, K. *Appl. Organomet. Chem.* **2000**, *14*, 629-633.
- (55) Chatziapostolou, K. A.; Vallianatou, K. A.; Grigoropoulos, A.; Raptopoulou, C. P.; Terzis, A.; Kostas, I. D.; Kyritsis, P.; Pneumatikakis, G. *J. Organomet. Chem.* **2007**, *692*, 4129-4138.
- (56) du Preez, J. G. H.; Knabl, K. U.; Krüger, L.; van Brecht, B. J. A. M. *Solvent Extr. Ion Exch.* **1992**, *10*, 729-748.
- (57) Navrátil, O.; Herrmann, E.; Grossmann, G.; Teplý, J. *Collect. Czech. Chem. Commun.* **1990**, *55*, 364-371.
- (58) Herrmann, E.; Navrátil, O.; Nang, H. b.; Smola, J.; Friedrich, J.; Příhoda, J.; Dreyer, R.; Chalkin, V. A.; Kulpe, S. *Collect. Czech. Chem. Commun.* **1984**, *49*, 201-217.
- (59) Navrátil, O.; Cigánek, M.; Herrmann, E. *Collect. Czech. Chem. Commun.* **1983**, *48*, 2009-2014.
- (60) Navrátil, O.; Fofana, M.; Smola, J. *Z. Chem.* **1984**, *24*, 30.
- (61) Navrátil, O.; Herrmann, E.; Slezák, P. *Collect. Czech. Chem. Commun.* **1987**, *52*, 1708-1714.
- (62) Muñoz-Hernández, M.-Á.; Singer, A.; Atwood, D. A.; Cea-Olivares, R. *J. Organomet. Chem.* **1998**, *571*, 15-19.

- (63) Le, Q. T. H.; Umetani, S.; Matsui, M. *Dalton Trans.* **1997**, 3835-3840.
- (64) Platzer, N.; Rudler, H.; Alvarez, C.; Barkaoui, L.; Denise, B.; Goasdoué, N.; Rager, M.-N.; Vaissermann, J.; Daran, J.-C. *Bull. Soc. Chim. Fr.* **1995**, 132, 95-113.
- (65) Alvarez, C.; Barkaoui, L.; Goasdoué, N.; Daran, J.-C.; Platzer, N.; Rudler, H.; Vaissermann, J. *Chem. Commun.* **1989**, 1507-1509.
- (66) Alvarez, C.; Goasdoué, N.; Platzer, N.; Rodríguez, I.; Rudler, H. *Chem. Commun.* **1988**, 1002-1004.
- (67) Barkaoui, L.; Charrouf, M.; Rager, M.-N.; Denise, B.; Platzer, N.; Rudler, H. *Bull. Soc. Chim. Fr.* **1997**, 134, 167-175.
- (68) Rodríguez, I.; Alvarez, C.; Gómez-Lara, J.; Toscano, R. A.; Platzer, N.; Mulheim, C.; Rudler, H. *Chem. Commun.* **1987**, 1502-1503.
- (69) Magennis, S. W.; Parsons, S.; Corval, A.; Woollins, J. D.; Pikramenou, Z. *Chem. Commun.* **1999**, 61-62.
- (70) Bereman, R. D.; Wang, F. T.; Najdzionek, J.; Braitsch, D. M. *J. Am. Chem. Soc.* **1976**, 98, 7266-7268.
- (71) Sakaguchi, U.; Addison, A. W. *J. Am. Chem. Soc.* **1977**, 99, 5189-5190.
- (72) Siiman, O.; Vetuskey, J. *Inorg. Chem.* **1980**, 19, 1672-1680.
- (73) Hernández-Arganis, M.; Hernández-Ortega, S.; Toscano, R. A.; García-Montalvo, V.; Cea-Olivares, R. *Chem. Commun.* **2004**, 310-311.
- (74) Korshak, V. V.; Gribova, I. A.; Artamonova, T. V.; Bushmarina, A. N. *Vysokomol. Soedin.* **1960**, 2, 377-385.
- (75) Schmulbach, C. D. *Prog. Inorg. Chem.* **1962**, 4, 275-376.
- (76) Nöth, H. *Z. Naturforsch., B* **1982**, 37, 1491-1498.
- (77) Husebye, S.; Maartmann-Moe, K. *Acta Chem. Scand.* **1983**, A37, 439-441.
- (78) Hitchcock, P. B.; Nixon, J. F.; Silaghi-Dumitrescu, I.; Haiduc, I. *Inorg. Chim. Acta* **1985**, 96, 77-80.
- (79) Pernin, C. G.; Ibers, J. A. *Acta Crystallogr., Sect. C: Cryst. Struct. Commun.* **2000**, 56, 376-378.

- (80) Schmidpeter, A.; Groeger, H. *Z. Anorg. Allg. Chem.* **1966**, *345*, 106-118.
- (81) Wang, F. T.; Najdzionek, J.; Leneker, K. L.; Wasserman, H.; Braitsch, D. M. *Synth. React. Inorg. Met.-Org. Chem.* **1978**, *8*, 119-125.
- (82) McQuillan, G. P.; Oxtan, I. A. *Inorg. Chim. Acta* **1978**, *29*, 69-78.
- (83) Czernuszewicz, R.; Maslowsky, E.; Nakamoto, K. *Inorg. Chim. Acta* **1980**, *40*, 199-202.
- (84) Wrackmeyer, B.; Garcia-Baez, E.; Zuno-Cruz, F. J.; Sanchez-Cabrera, G.; Rosales, M. J. *Z. Naturforsch., B* **2000**, *55*, 185-188.
- (85) Haiduc, I. In *Inorganic Experiments*; Woollins, J. D., Ed.; VCH: New York; Basel; Cambridge; Tokyo, 1994, pp 145-149.
- (86) Williams, D. J. *Inorg. Nucl. Chem. Letters* **1980**, *16*, 189-193.
- (87) Metz, G.; Wu, X.; Smith, S. O. *J. Magn. Reson. Ser. A* **1994**, *110*, 219-227.
- (88) Bennett, A. E.; Rienstra, C. M.; Auger, M.; Lakshmi, K. V.; Griffin, R. G. *J. Chem. Phys.* **1995**, *103*, 6951-6958.
- (89) Bryce, D. L.; Bernard, G. M.; Gee, M.; Lumsden, M.; Eichele, K.; Wasylishen, R. E. *Can. J. Anal. Sci. Spectrosc.* **2001**, *46*, 46-82.
- (90) Collins, M. J.; Ratcliffe, C. I.; Ripmeester, J. A. *J. Magn. Reson.* **1986**, *68*, 172-179.
- (91) Maricq, M. M.; Waugh, J. S. *J. Chem. Phys.* **1979**, *70*, 3300-3316.
- (92) Herzfeld, J.; Berger, A. E. *J. Chem. Phys.* **1980**, *73*, 6021-6030.
- (93) Eichele, K.; Wasylishen, R. E.; 1.17.30 ed., 2001.
- (94) Mason, J. *Solid State Nucl. Magn. Reson.* **1993**, *2*, 285-288.
- (95) Schreckenbach, G.; Ziegler, T. *J. Phys. Chem.* **1995**, *99*, 606-616.
- (96) Schreckenbach, G.; Ziegler, T. *Int. J. Quantum Chem.* **1997**, *61*, 899-918.
- (97) Wolff, S. K.; Ziegler, T. *J. Chem. Phys.* **1998**, *109*, 895-905.
- (98) Baerends, E. J.; Ellis, D. E.; Ros, P. *Chem. Phys.* **1973**, *2*, 41-51.

- (99) Versluis, L.; Ziegler, T. *J. Chem. Phys.* **1988**, *88*, 322-328.
- (100) te Velde, G.; Baerends, E. J. *J. Comput. Phys.* **1992**, *99*, 84-98.
- (101) Fonseca Guerra, C.; Snijders, J. G.; te Velde, G.; Baerends, E. J. *Theor. Chem. Acc.* **1998**, *99*, 391-403.
- (102) Theoretical Chemistry, Vrije Universiteit, Amsterdam, <http://www.scm.com>.
- (103) Vosko, S. H.; Wilk, L.; Nusair, M. *Can. J. Phys.* **1980**, *58*, 1200-1211.
- (104) Becke, A. D. *Phys. Rev. A* **1988**, *38*, 3098-3100.
- (105) Perdew, J. P. *Phys. Rev. B* **1986**, *33*, 8822-8824.
- (106) Perdew, J. P. *Phys. Rev. B* **1986**, *34*, 7406.
- (107) Chang, C.; Pelissier, M.; Durand, P. *Phys. Scr.* **1986**, *34*, 394-404.
- (108) van Lenthe, E.; Baerends, E. J.; Snijders, J. G. *J. Chem. Phys.* **1993**, *99*, 4597-4610.
- (109) van Lenthe, E.; Baerends, E. J.; Snijders, J. G. *J. Chem. Phys.* **1994**, *101*, 9783-9792.
- (110) van Lenthe, E.; van Leeuwen, R.; Baerends, E. J.; Snijders, J. G. *Int. J. Quantum Chem.* **1996**, *57*, 281-293.
- (111) Jameson, C. J.; de Dios, A.; Jameson, A. K. *Chem. Phys. Lett.* **1990**, *167*, 575-582.
- (112) Demko, B. A.; Eichele, K.; Wasylishen, R. E. *J. Phys. Chem. A* **2006**, *110*, 13537-13550.
- (113) Jameson, C. J. In *Multinuclear NMR*; Mason, J., Ed.; Plenum Press: New York, 1987, pp 89-131.
- (114) Jameson, C. J. In *Phosphorus-31 NMR Spectroscopy in Stereochemical Analysis. Organic Compounds and Metal Complexes*; Verkade, J. G., Quin, L. D., Eds.; VCH Publishers, Inc.: Deerfield Beach, 1987; Vol. 8, pp 205-230.
- (115) Bryce, D. L.; Eichele, K.; Wasylishen, R. E. *Inorg. Chem.* **2003**, *42*, 5085-5096.
- (116) Clayden, N. J.; Dobson, C. M.; Lian, L.-Y.; Smith, D. J. *J. Magn. Reson.* **1986**, *69*, 476-487.

- (117) Duddeck, H. *Prog. Nucl. Magn. Reson. Spectrosc.* **1995**, *27*, 1-323.
- (118) Duddeck, H. *Annu. Rep. NMR Spectrosc.* **2004**, *52*, 105-166.
- (119) Birdsall, D. J.; Slawin, A. M. Z.; Woollins, J. D. *Polyhedron* **2001**, *20*, 125-134.

## Chapter 6

### A Solid-State NMR Investigation of Single-Source Precursors for Group 12 Metal Selenides; $M[N(^i\text{Pr}_2\text{PSe})_2]_2$ ( $M = \text{Zn, Cd, Hg}$ )<sup>†</sup>

#### 6.1 Introduction

Integrated applications of thin semiconducting films include light-emitting diodes,<sup>1</sup> and electrochromic display devices,<sup>2</sup> as well as use in infrared detectors.<sup>3,4</sup> Nanoparticles of semiconductor materials, or quantum dots, have applications ranging from single-electron transistors<sup>5</sup> to biomarkers,<sup>6</sup> due to a highly tuneable band gap. Crystals and thin films of metal chalcogenide materials have been utilized in variable energy radiation detectors, light emitting devices and optoelectronics,<sup>7</sup> as well as within solar selective coatings and photoelectrochemical devices.<sup>8-10</sup> The class of II-VI semiconductors is of current interest as one of the best known groups of semiconducting materials.

Conventional methods of preparing Group II metal chalcogenide materials involve hazardous organometallic compounds and highly toxic chalcogen sources reacting in the vapor phase or within a solution.<sup>11-16</sup> The nature of the reactants has led to considerable interest in identifying molecular single-source precursors for these solid-state materials.<sup>16-21</sup> Successful single-source precursors require a low degree of association and sufficient volatility for low-pressure deposition or solution thermolysis techniques, and depend in large part on the nature and purity of the precursors used.<sup>22</sup> Examples of such precursors for II-VI materials include metal(II) complexes of chalcogenolates  $[\text{EX}]^-$ , where  $E = \text{O, S, Se or Te}$  and  $X = \text{alkyl}^{14,23-29}$  or silyl,<sup>30,31</sup>

---

<sup>†</sup> A version of this chapter has been published: B.A. Demko and R.E. Wasylishen, *Dalton Transactions*, 2008, 481-490.



dichalcogenophosphinates  $[E_2PR_2]^-$ ,<sup>32,33</sup> and dichalcogenocarbamates  $[E_2CNR_2]^-$ .<sup>34-43</sup> Recently dichalcogenoimidodiphosphinato complexes,  $M^{n+}[N(R_2PE)_2]_n$ , have been utilized as single-source precursors for chemical vapor deposition<sup>16,19,20,22,44-51</sup> and quantum dot applications.<sup>45,49,52</sup> Dichalcogenoimidodiphosphinates overcome the often encountered involatility of metal organochalcogenolates,<sup>18</sup> are more thermally stable than the bulkier silylchalcogenolate ligands with cleaner thermolysis products and produce fewer degradation reactions of the ligand.<sup>23,27,52</sup> Additionally, diselenocarbamates are prepared using noxious carbon diselenide,<sup>20</sup> whereas diselenoimidodiphosphinates are obtained from facile oxidation of the corresponding bis(dialkylphosphine)amine with elemental selenium.

The chemistry involving dichalcogenoimidodiphosphinato complexes has been well reviewed.<sup>53-56</sup> In addition to applications as single-source precursors for solid-state materials, these bidentate ligands have found uses in the search for stereochemically active lone pairs,<sup>57-72</sup> in catalysis,<sup>73,74</sup> and in metal extraction processes,<sup>56,69,75-82</sup> as lanthanide shift reagents,<sup>69,83-87</sup> luminescent materials,<sup>88</sup> and as enzyme mimetics.<sup>89-91</sup> Often identified as main group inorganic analogues of acetylacetonate (*acac*), transition metal complexes of  $[N(R_2PE)_2]^-$  possess improved thermal and chemical stability over  $\beta$ -diketonates, which are susceptible to oxidation, polymerization and hydration, and generally makes *acac* complexes involatile.<sup>22,45,46,92-95</sup> The volatility of dichalcogenoimidodiphosphinato complexes can be manipulated by the functional choice of alkyl group.<sup>22</sup> Although considerably more attention has been given to the phenyl functionalized ligand in the literature, complexes of the isopropyl variant have shown an increase in volatility.<sup>22,54,62,96</sup> Careful tuning of the ligand in the choice of alkyl group

has afforded high quality CdSe quantum dots, prepared in a solvothermal reaction from the single-source precursor  $\text{Cd}[\text{N}(\text{}^i\text{Pr}_2\text{PSe})_2]_2$ .<sup>52</sup> The quantum dots obtained are highly monodispersed with diameters, and subsequently luminescent properties, that depend upon growth time.<sup>52</sup>

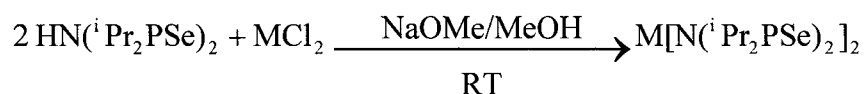
Characterization of dichalcogenoimidodiphosphinato complexes has to date been performed primarily by X-ray crystallography, as well as infrared and solution NMR spectroscopy.<sup>22,45,46,48,59,62-64,67,71,94,97-105</sup> Diselenoimidodiphosphate ligands possess numerous favorable NMR spin- $\frac{1}{2}$  nuclei, specifically  $^1\text{H}$  (99.99% N.A.,  $\Xi = 100$  MHz),  $^{13}\text{C}$  (1.07% N.A.,  $\Xi = 25.145$  MHz),  $^{31}\text{P}$  (100% N.A.,  $\Xi = 40.481$  MHz), and  $^{77}\text{Se}$  (7.63% N.A.,  $\Xi = 19.071$  MHz), however characterization has typically been limited to  $^1\text{H}$  and  $^{31}\text{P}$  solution NMR. Solid-state NMR, being potentially more informative than solution NMR spectroscopy, would appear to be an appropriate technique for characterizing the detailed molecular environment of dichalcogenoimidodiphosphate ligands and their complexes; however, there have been no reports of such investigations in the literature to our knowledge. The presented study of solid-state  $^{31}\text{P}$ ,  $^{77}\text{Se}$ ,  $^{113}\text{Cd}$ , and  $^{199}\text{Hg}$  NMR on the single-source precursors;  $\text{M}[\text{N}(\text{}^i\text{Pr}_2\text{PSe})_2]_2$  ( $\text{M} = \text{Zn}, \text{Cd}, \text{Hg}$ ), represents the first solid-state NMR investigation of dichalcogenoimidodiphosphinato complexes.

## 6.2 Experimental

### 6.2.1 Sample Preparation

Iminobis(diisopropylphosphine selenide),  $\text{HN}(\text{}^i\text{Pr}_2\text{PSe})_2$ , was prepared according to the two-step, condensation followed by oxidation, procedure outlined in Scheme 5.2.<sup>106</sup> The off-white powders of the zinc, cadmium and mercury complexes were

obtained by slow addition of the corresponding metal(II) chloride (Sigma-Aldrich) into a basic methanol solution of the tetraisopropyldiselenoimidodiphosphinate,  $[\text{N}(\text{}^i\text{Pr}_2\text{PSe})_2]^-$ , as shown in Scheme 6.1.<sup>48</sup> The single-source precursors were recrystallized by slow diffusion of methanol into chloroform solutions of the complexes. The crystal structures of the zinc,<sup>48</sup> cadmium,<sup>62</sup> and mercury<sup>22</sup> complexes have been previously determined by X-ray crystallography. All structures possess triclinic unit cells and indicate a single  $\text{M}[\text{N}(\text{}^i\text{Pr}_2\text{PSe})_2]_2$  molecule in the asymmetric unit.



**Scheme 6.1** Metal(II) tetraisopropyldiselenoimidodiphosphinate,  $\text{M}[\text{N}(\text{}^i\text{Pr}_2\text{PSe})_2]_2$  preparation.

### 6.2.2 NMR Experiments

Solid-state NMR investigations of powdered samples of  $\text{M}[\text{N}(\text{}^i\text{Pr}_2\text{PSe})_2]_2$  ( $\text{M} = \text{Zn, Cd, Hg}$ ) were obtained on 4.7 T, 7.0 T, and 11.7 T NMR spectrometers. The samples were packed in 4 mm (7.0 and 11.7 T) and 5 mm (4.7 T) o.d. zirconium oxide rotors and were placed within probes suitable for magic angle spinning, MAS, NMR experiments. A variable amplitude cross polarization, VACP, pulse sequence was used for all nuclei investigated on all spectrometers. Proton decoupling fields of approximately 60 kHz were achieved via two-pulse phase-modulation, TPPM.<sup>107</sup> All  $^{31}\text{P}$  NMR spectra were referenced with respect to 85%  $\text{H}_3\text{PO}_4$  (aq) by setting the  $^{31}\text{P}$  NMR peak of solid  $(\text{NH}_4)\text{H}_2\text{PO}_4$  to 0.81 ppm.<sup>108</sup> Similarly,  $^{77}\text{Se}$  NMR spectra were referenced to  $\text{Me}_2\text{Se}$  (*l*)

by setting the isotropic peak of solid ammonium selenate to 1040.2 ppm.<sup>108,109</sup>

Cadmium-113 NMR spectra were referenced with respect to a 0.1 M solution of Cd(ClO<sub>4</sub>)<sub>2</sub> in water by setting the solid-state <sup>113</sup>Cd NMR peak of Cd(NO<sub>3</sub>)<sub>2</sub>·4H<sub>2</sub>O to -100.0 ppm.<sup>108,110</sup> Solid-state <sup>199</sup>Hg NMR spectra were referenced to dimethyl mercury by setting the <sup>199</sup>Hg NMR peak of solid (NEt<sub>4</sub>)Na[Hg(CN)<sub>4</sub>] to -434 ppm.<sup>111</sup>

Solid-state <sup>31</sup>P NMR experiments were performed at frequencies of 81.0, 121.6 and 202.5 MHz at spinning frequencies ranging from 1.0 to 2.2 kHz. A total of between 64 and 512 scans were acquired per spectrum. Contact times between 2.0 and 4.5 ms, and pulse delays between 10 and 15 s were employed.

Solid-state <sup>77</sup>Se NMR measurements were performed at frequencies of 38.2, 57.3 and 95.4 MHz at spinning frequencies ranging from 2.4 to 15.0 kHz. A total of between 2952 and 23608 scans were acquired per spectrum. Contact times between 9.0 and 10.0 ms, and pulse delays between 10 and 15 s were employed.

Solid-state <sup>113</sup>Cd NMR experiments on Cd[N(<sup>1</sup>Pr<sub>2</sub>PSe)<sub>2</sub>]<sub>2</sub> were performed at frequencies of 44.4, 66.6 and 111.0 MHz at spinning frequencies ranging from 0.7 to 10.0 kHz. A total of between 128 and 6080 scans were acquired per spectrum. Contact times between 9.0 and 11.5 ms, and pulse delays between 7 and 12 s were employed.

Cadmium-113 NMR spectra were also acquired for stationary samples of Cd[N(<sup>1</sup>Pr<sub>2</sub>PSe)<sub>2</sub>]<sub>2</sub>, where a total of between 20000 and 23400 scans were acquired.

Solid-state <sup>199</sup>Hg NMR experiments on Hg[N(<sup>1</sup>Pr<sub>2</sub>PSe)<sub>2</sub>]<sub>2</sub> were performed at frequencies of 35.8, 53.8 and 89.5 MHz at spinning speeds ranging from 2.7 to 10.0 kHz. A total of between 8256 and 65808 scans were acquired per spectrum. Contact times between 10.0 and 11.5 ms, and pulse delays between 7 and 10 s were employed.

The principal components of the respective phosphorus, selenium, and mercury chemical shift tensors,  $\delta_{11} \geq \delta_{22} \geq \delta_{33}$ , were determined via the method of Herzfeld and Berger.<sup>112</sup> The cadmium chemical shift tensor principal components for  $\text{Cd}[\text{N}(\text{}^i\text{Pr}_2\text{PSe})_2]_2$  were identified directly from the discontinuities of the solid-state  $^{113}\text{Cd}$  NMR spectra of a stationary sample. All experimental (observed) solid-state NMR spectra were simulated using the determined values with the program WSOLIDS<sup>113</sup> to assess the quality of the obtained parameters. This procedure results in errors of  $\pm 0.2$  ppm in the isotropic chemical shift,  $\delta_{\text{iso}} = (1/3)(\delta_{11} + \delta_{22} + \delta_{33})$ , and errors in the principal components about 1-3% of the span,  $\Omega = \delta_{11} - \delta_{33}$ , of the respective chemical shift tensor.

### 6.2.3 DFT Computations

Theoretical calculation of NMR parameters, particularly for heavier nuclei where empirical interpretations are more difficult than those extracted from  $^1\text{H}$  or  $^{13}\text{C}$  NMR spectra, has become increasingly useful for spectroscopists.<sup>114</sup> Magnetic shielding tensors,  $\sigma$ , were calculated using the NMR module<sup>115-117</sup> of the Amsterdam Density Functional (ADF) program package.<sup>118-122</sup> The Vosko-Wilk-Nusair<sup>123</sup> local density approximation with the Becke88-Perdew86<sup>124-126</sup> generalized gradient approximation were used for the exchange-correlation functional. Scalar relativistic corrections were carried out based on the implementation of the zeroth order regular approximation, ZORA, formalism.<sup>127-130</sup> Triple- $\zeta$  doubly polarized, TZ2P, Slater-type ZORA basis sets were used for all atoms except for hydrogen, where double- $\zeta$  quality, DZ, basis functions were utilized. The calculations were performed on a Linux-based cluster with two AMD XP 1800+ Athlon processors operating in parallel. The corresponding phosphorus and

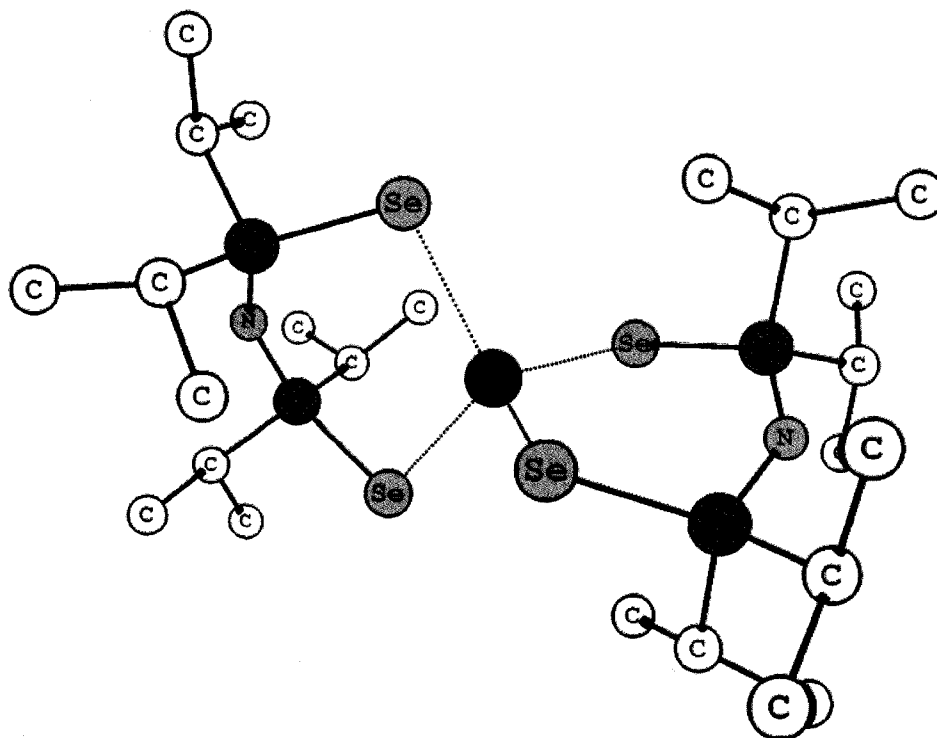
selenium chemical shift tensors were calculated from the magnetic shielding tensors using the relationship:

$$\delta_{ii}(sample) = \frac{\sigma_{iso}(ref) - \sigma_{ii}(sample)}{1 - \sigma_{iso}(ref)} \quad [6.1]$$

where  $\sigma_{iso}(ref)$  is the isotropic shielding of a standard reference. The absolute shielding scale for  $^{31}\text{P}$  has been determined, and the value of  $\sigma_{iso}(85\% \text{H}_3\text{PO}_4(aq))$  has been established to be 328.35 ppm.<sup>131</sup> We have previously investigated the selenium chemical shift tensors in a wide range of selenium containing compounds, and we have subsequently used the value of 1580 ppm determined therein for the reference shielding of a neat liquid of dimethyl selenide at 23 °C.<sup>132</sup> As a consistent standard for  $\sigma_{iso}(ref)$  has yet to be established for cadmium and mercury, the values have been reported as magnetic shielding where  $\sigma_{11} \leq \sigma_{22} \leq \sigma_{33}$ . Tables of traceless theoretical chemical shift tensors, along with the calculated phosphorus and selenium chemical shift and cadmium and mercury magnetic shielding tensors, are provided in Appendix C.

### 6.3 Results & Discussion

The single-source precursors investigated,  $\text{M}[\text{N}(\text{P}_2\text{PSe})_2]_2$  ( $\text{M} = \text{Zn}, \text{Cd}, \text{Hg}$ ), as determined by X-ray crystallography are isostructural, and a representation of the complexes is given in Figure 6.1. The structure at the metal center is best described as an approximate  $\text{MSe}_4$  tetrahedral core. The six-membered  $\text{MSe}_2\text{P}_2\text{N}$  heterocycle rings possess a pseudo-boat conformation. The single diselenoimidodiphosphinato complex in the asymmetric unit does not possess any symmetry elements that would provide

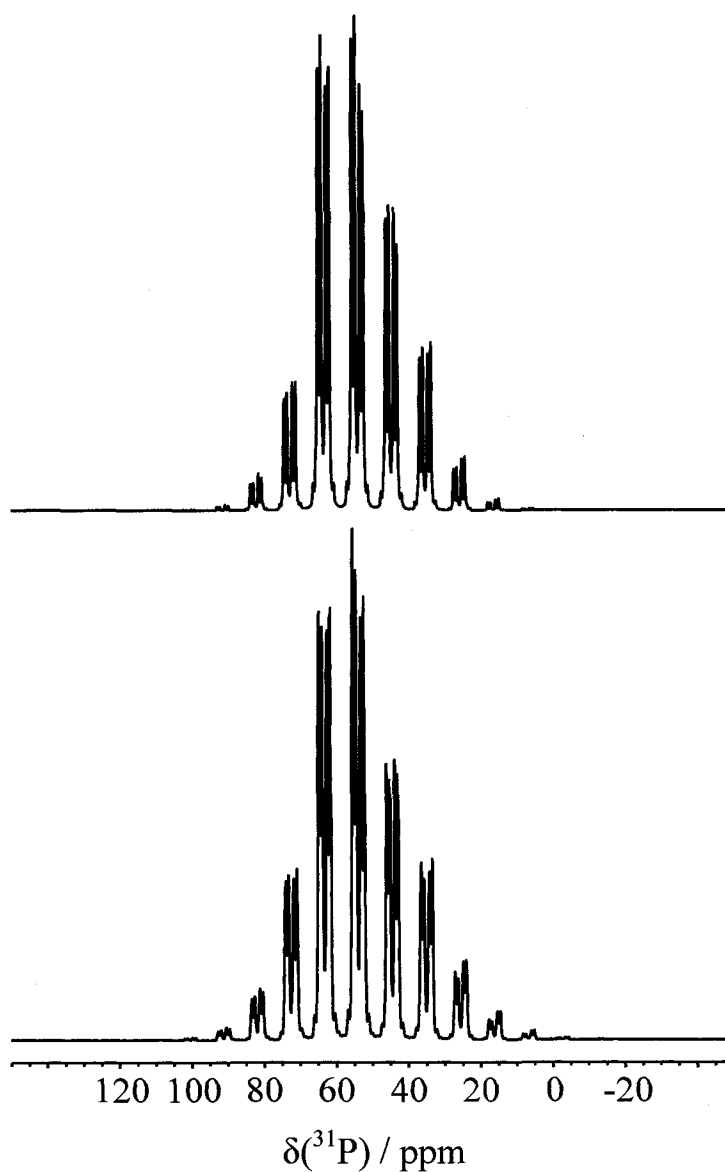


**Figure 6.1** Representation of the solid-state structure of  $M[N(^i\text{Pr}_2\text{PSe})_2]_2$  ( $M = \text{Zn}, ^{48}\text{Cd}, ^{62}\text{Hg}^{22}$ ). Hydrogen atoms have been removed for clarity.

chemical equivalence between any of the atoms within the molecule.<sup>22,48,62</sup> Thus, unique environments for each of the four phosphorus and four selenium atoms present in each complex are expected.

### 6.3.1 Solid-State $^{31}\text{P}$ NMR

Herzfeld-Berger analyses of each of the spinning sideband manifolds in the  $^{31}\text{P}$  spectra were performed for the zinc, cadmium and mercury diselenoimidodiphosphinato complexes, and a simulation of the entire  $^{31}\text{P}$  NMR spectrum of  $\text{Hg}[N(^i\text{Pr}_2\text{PSe})_2]_2$  at 11.7 T is given in Figure 6.2. This procedure yields the principal components of the phosphorus chemical shift tensors as well as an estimate of the indirect spin-spin coupling constant,  $^1J(^{77}\text{Se}, ^{31}\text{P})_{\text{iso}}$ , from the satellite peaks visible within the  $^{31}\text{P}$  NMR



**Figure 6.2** VACP MAS  $^{31}\text{P}$  NMR spectrum of  $\text{Hg}[\text{N}(\text{iPr}_2\text{PSe})_2]_2$  (lower trace) and its simulation (upper trace). Experimental conditions: 11.7 T, 512 scans, MAS at 1.9 kHz, 5 Hz of line broadening, a 2.0 ms contact time, and a 10 s recycle delay.

spectrum. The solid-state  $^{31}\text{P}$  NMR parameters for  $\text{M}[\text{N}(\text{iPr}_2\text{PSe})_2]_2$  ( $\text{M} = \text{Zn}, \text{Cd}, \text{Hg}$ ) are given in Table 6.1. The isotropic chemical shifts and  $^1J(^{77}\text{Se}, ^{31}\text{P})_{\text{iso}}$  agree well with chloroform solution  $^{31}\text{P}$  NMR values of 59.80 ppm and (-)539 Hz,<sup>62</sup> 56.60 ppm and (-)563 Hz,<sup>62</sup> and 56.80 ppm and (-)518 Hz<sup>22</sup> for the zinc, cadmium and mercury



**Table 6.1** Solid-state  $^{31}\text{P}$  NMR parameters for  $\text{M}[\text{N}(\text{iPr}_2\text{PSe})_2]_2$  ( $\text{M} = \text{Zn}, \text{Cd}, \text{Hg}$ ).

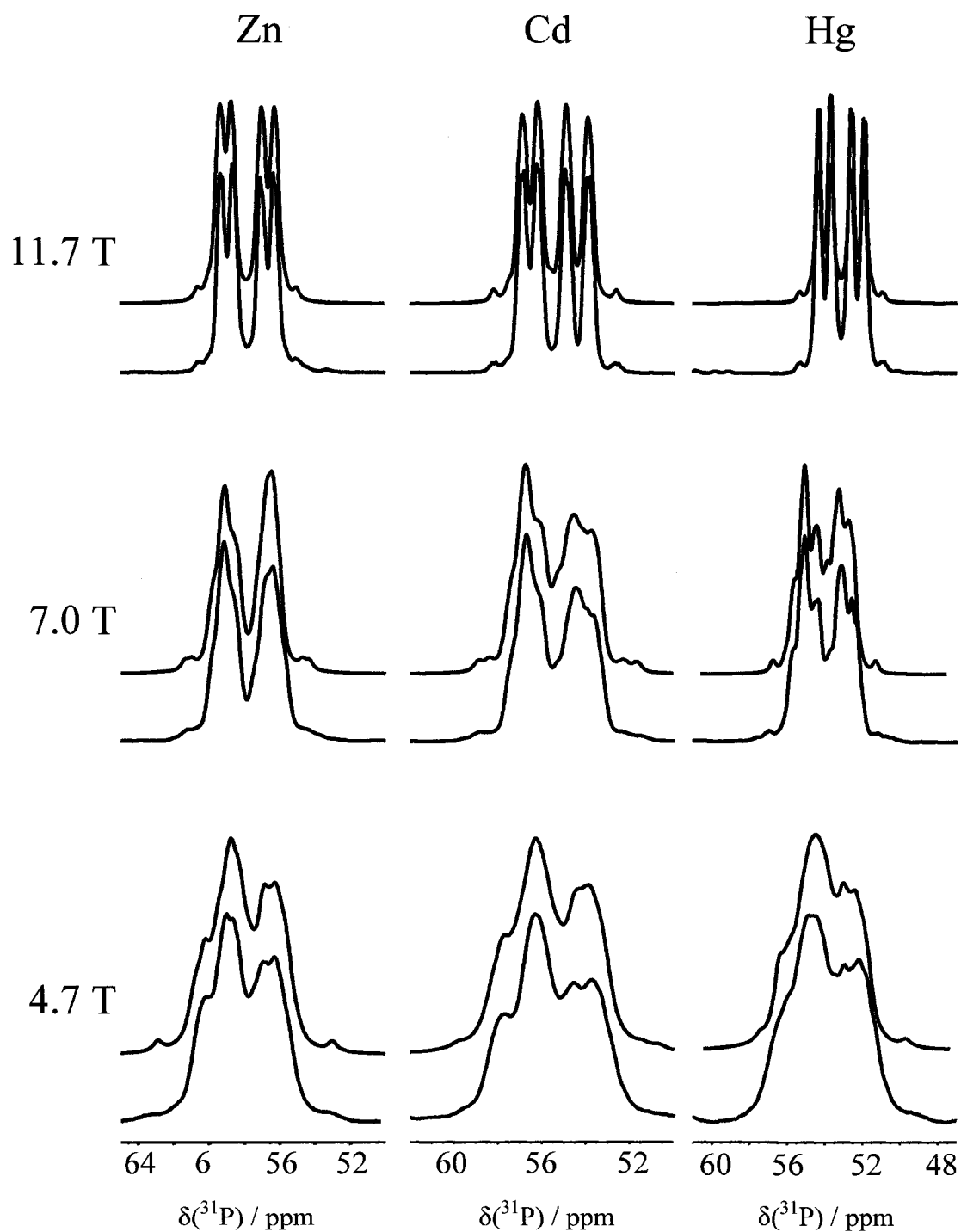
$\text{M}^{\text{II}}$	$\delta_{\text{iso}}$ ppm	$\delta_{11}$ ppm	$\delta_{22}$ ppm	$\delta_{33}$ ppm	$^1J(^{77}\text{Se}, ^{31}\text{P})_{\text{iso}}$ <sup>a</sup> Hz
Zn	59.3	79.6	65.0	33.4	-530
	58.8	79.2	65.4	31.8	-530
	57.0	81.0	62.7	27.3	-530
	56.3	78.4	62.2	28.4	-530
Cd	56.9	77.2	61.3	32.2	-520
	56.2	77.0	60.9	30.8	-520
	54.9	77.1	58.8	28.7	-520
	53.9	75.8	58.9	27.0	-520
Hg	55.4	76.6	59.5	30.2	-525
	54.6	75.8	58.7	29.3	-540
	53.2	76.7	56.5	26.3	-540
	52.4	75.0	57.3	24.8	-525

<sup>a</sup> For directly bonded selenium-77 and phosphorus-31 spin pairs, signs of  $^1J(^{77}\text{Se}, ^{31}\text{P})_{\text{iso}}$  are known to be negative for numerous analogous systems.<sup>133,134</sup>

complexes respectively. The average of the four experimental and calculated values of  $\delta_{\text{iso}}$  for the single-source precursors investigated shows a small yet consistent decrease as one progresses from the Zn to the Cd to the Hg complex. The decreasing trend is mimicked in each of the phosphorus chemical shift principal components,  $\delta_{ii}$ , indicating that the local environment of the phosphorus atoms becomes, on average, more shielded as one changes to a heavier Group 12 central metal. Increased phosphorus shielding by greater than 20 ppm has been linked to stronger metal-selenium bonding in Group 13 diselenoimidodiphosphinato complexes.<sup>81</sup> The average spans of the phosphorus chemical shift tensors,  $\Omega_{\text{avg}} = 48.3$  ppm, are considerably smaller, indicating a more symmetric shielding environment, than those found in tris-organophosphine selenides, whose  $\Omega_{\text{avg}} = 124$  ppm.<sup>135</sup> The magnetic shielding calculations provide the orientation of the phosphorus shielding tensors, which are unavailable from solid-state NMR investigations of powdered samples. Given the small spans, and similarity of the principal components of the  $^{31}\text{P}$  chemical shift tensors observed experimentally for the  $\text{M}[\text{N}(\text{iPr}_2\text{PSe})_2]_2$  ( $\text{M} =$

Zn, Cd, Hg) complexes, it is not surprising that the tensors have similar calculated orientations for all four phosphorus environments in each of the three complexes. The direction of least shielding,  $\sigma_{11}$ , is oriented perpendicular to the local Se-P-N plane, while the direction of greatest shielding,  $\sigma_{33}$ , lies approximately parallel to the phosphorus-nitrogen bond axis. The direction of intermediate shielding, orthogonal to the two other principal components, nearly bisects the Se-P-N angle.

The isotropic region of the solid-state  $^{31}\text{P}$  NMR spectra along with their simulations at 4.7 T, 7.0 T and 11.7 T is given in Figure 6.3. While the four unique phosphorus environments are readily discernable in the isotropic region of the spectra at 11.7 T, the spectra at the lower magnetic fields are considerably less well resolved. The lineshapes observed at 4.7 T and 7.0 T result from the adjacent  $^{14}\text{N}$  ( $I = 1$ , N.A. = 99.6%), which has previously been shown to influence solid-state  $^{31}\text{P}$  NMR spectra of mono- and cyclotri-phosphazenes.<sup>136-138</sup> As a quadrupolar nucleus, the energy levels of nitrogen-14 are quantized by both the applied magnetic field as well as the electric field gradient, EFG, at the  $^{14}\text{N}$  nucleus.<sup>139-141</sup> As a result, MAS cannot completely average the dipolar interaction between  $^{14}\text{N}$  and  $^{31}\text{P}$  and “residual dipolar coupling” effects between the two nuclei are manifested in the solid-state  $^{31}\text{P}$  NMR spectra. This broadening effect is inversely proportional to the Larmor frequency of the quadrupolar nucleus,  $\nu_{L, N} = \gamma_N B_0 / 2\pi$ ,<sup>139-141</sup> and thus produces a smaller effect at higher applied magnetic fields. Analyses of the  $^{31}\text{P}$  NMR spectra can yield values of the effective dipolar coupling constant,  $R_{eff}$ , and the isotropic one-bond indirect spin-spin coupling constant,  $^1J(^{31}\text{P}, ^{14}\text{N})_{iso}$ , as well as parameters describing the EFG at the nitrogen nucleus. The direct dipolar coupling constant,  $R_{DD}$ , is related to  $R_{eff}$  by



**Figure 6.3** Experimental (lower trace) isotropic  $^{31}\text{P}$  NMR regions, with spinning sidebands added to the isotropic region, and simulated (upper trace) for  $\text{M}[\text{N}(\text{}^1\text{Pr}_2\text{PSe})_2]_2$  ( $\text{M} = \text{Zn, Cd, Hg}$ ) at 4.7 T, 7.0 T, and 11.7 T. Experimental conditions: 64 – 512 scans, 5 Hz of line broadening, a 2.0 – 4.5 ms contact time, and a 10 – 15 s recycle delay.

$$R_{eff} = R_{DD} - \Delta J / 3 \quad [6.2]$$

where  $\Delta J = J_{33} - (J_{11} + J_{22})/2$  is the anisotropy of the phosphorus-nitrogen  $J$  tensor, and

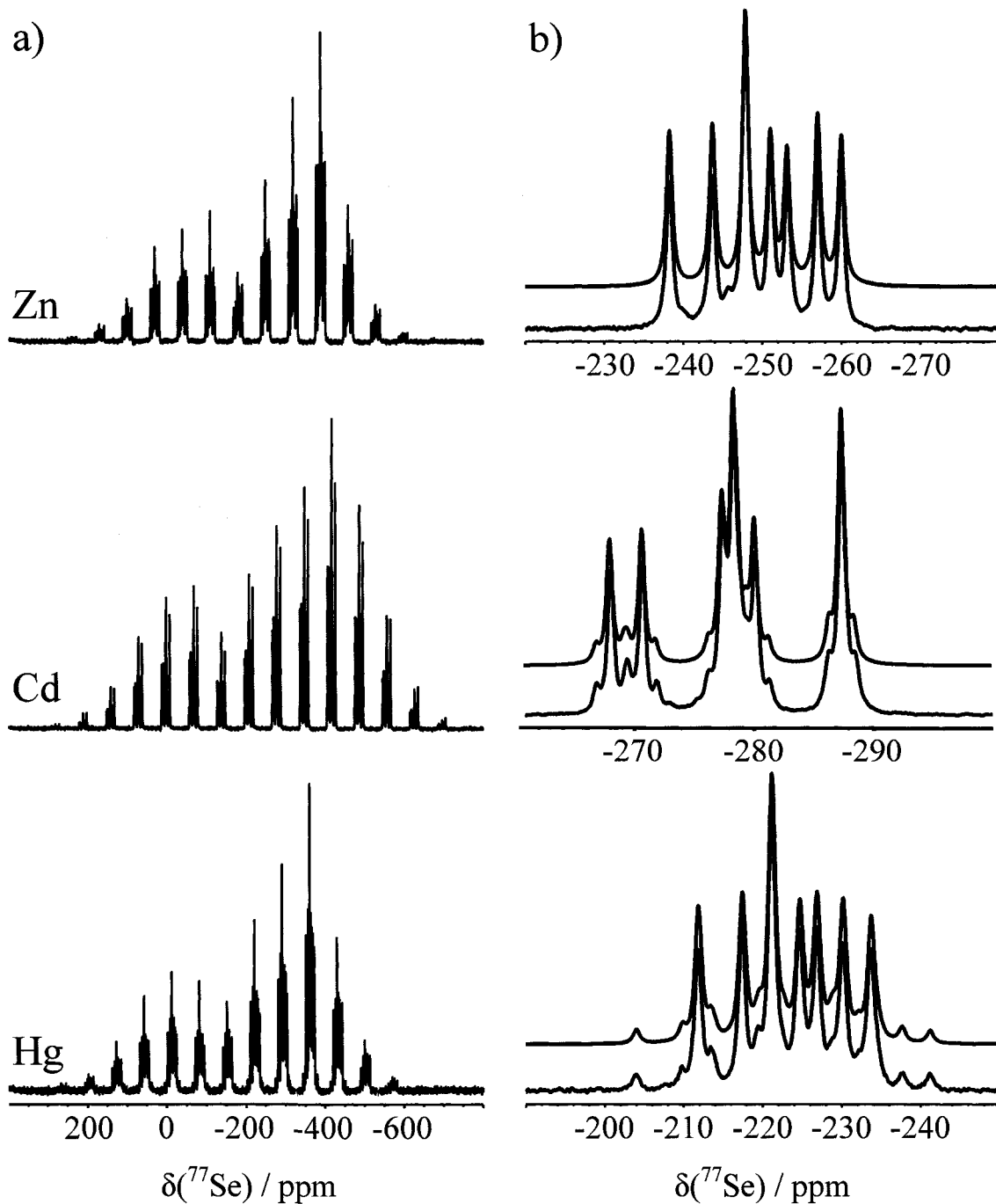
$$R_{DD} = \left( \frac{\mu_0}{4\pi} \right) \left( \frac{\hbar}{2\pi} \right) \left( \frac{\gamma_P \gamma_N}{\langle r_{PN}^3 \rangle} \right) \quad [6.3]$$

where  $\mu_0$  is the permeability of a vacuum,  $\gamma_P$  and  $\gamma_N$  are the magnetogyric ratios of  $^{31}\text{P}$  and  $^{14}\text{N}$ , and  $\langle r_{PN}^3 \rangle$  is the motionally-averaged cube of the distance between phosphorus and nitrogen. The contributions from  $\Delta J$  are expected to be negligible given the small magnitude for  $^1J(^{31}\text{P}, ^{15}\text{N})_{\text{iso}}$  determined for iminobis(diphenylphosphine selenide),  $\text{HN}(\text{Ph}_2\text{PSe})_2$ ,<sup>142</sup> and as a result  $R_{eff} = R_{DD}$  can be estimated directly from the phosphorus-nitrogen nuclear separation in the X-ray crystal structures. It is not feasible to assign a specific  $R_{DD}$ , i.e., a specific phosphorus-nitrogen distance, to a specific  $^{31}\text{P}$  NMR resonance, so an average  $r_{PN}$  was calculated from the four P-N distances within each complex. The resulting average  $R_{DD}$  was used in the simulations of all four sites in the  $^{31}\text{P}$  NMR spectra. The quadrupolar parameters required to describe the solid-state NMR spectrum of a spin- $1/2$  nucleus spin-spin coupled to a quadrupolar nucleus are the quadrupolar coupling constant,  $C_Q = eQV_{ZZ}/h$ , where  $e$  is the elementary charge,  $Q$  is the nuclear quadrupole moment, and  $V_{ZZ}$  is the largest component of the EFG tensor at the nucleus. Also required are the Euler angles,  $\alpha$  and  $\beta$ , which describe the orientation of the dipolar vector,  $r_{PN}$ , within the principal axis system of the EFG tensor at the quadrupolar nucleus. The values of the angles  $\alpha$  and  $\beta$  were initially obtained from DFT calculations of the nitrogen EFG tensors, and were subsequently optimized in the

simulations. For reasons analogous to those given above for  $R_{DD}$ , the simulations of all four phosphorus lineshapes were simulated using a single value of  ${}^1J({}^{31}\text{P}, {}^{14}\text{N})_{\text{iso}}$ ,  $C_Q$ ,  $\alpha$ , and  $\beta$ . The effect of using single average values of the residual dipolar coupling parameters does not appear to significantly influence the simulations for the  ${}^{31}\text{P}$  NMR spectra of the Zn, Cd, and Hg complexes given in Figure 6.3, where accurate lineshapes are achieved at all three applied magnetic fields employed. For  $\text{Zn}[\text{N}(\text{Pr}_2\text{PSe})_2]_2$ ,  $R_{DD} = 880(50)$  Hz from the average  $r_{\text{PN}}$  distance of  $1.588(30)$  Å,<sup>48</sup> and the azimuthal and polar angles were  $90(3)^\circ$  and  $27(3)^\circ$  respectively. The value of  $C_Q$  was  $3.05(20)$  MHz, and the indirect spin-spin coupling constant,  ${}^1J({}^{31}\text{P}, {}^{14}\text{N})_{\text{iso}}$ , was  $15(5)$  Hz. The parameters pertaining to residual dipolar coupling used in the simulations of the  ${}^{31}\text{P}$  NMR spectra of  $\text{Cd}[\text{N}(\text{Pr}_2\text{PSe})_2]_2$  were  $R_{DD} = 880(50)$  Hz,  $r_{\text{PN}} = 1.587(30)$  Å,<sup>62</sup>  $\alpha = 90(3)^\circ$ ,  $\beta = 26(4)^\circ$ ,  $C_Q = 3.00(20)$  MHz,  ${}^1J({}^{31}\text{P}, {}^{14}\text{N})_{\text{iso}} = 15(5)$  Hz. For  $\text{Hg}[\text{N}(\text{Pr}_2\text{PSe})_2]_2$ ,  $R_{DD} = 880(50)$  Hz,  $r_{\text{PN}} = 1.586(30)$  Å,<sup>22</sup>  $\alpha = 90(3)^\circ$ ,  $\beta = 26(4)^\circ$ ,  $C_Q = 3.00(20)$  MHz,  ${}^1J({}^{31}\text{P}, {}^{14}\text{N})_{\text{iso}} = 15(4)$  Hz were used. The EFG tensors at  ${}^{14}\text{N}$  in the three complexes are oriented similarly, such that the largest component lies within the P-N-P plane perpendicular to the P-N-P bisector, the intermediate component is parallel to the direction of the formal electron ‘lone pair’, and the smallest EFG component is perpendicular to the P-N-P plane. The magnitude of the quadrupolar coupling constants are all consistent with those found in other phosphorus-nitrogen systems where values of  $C_Q$  are not expected to exceed 4.0 MHz.<sup>136</sup> The values for  ${}^1J({}^{31}\text{P}, {}^{14}\text{N})_{\text{iso}}$  observed here are of similar magnitude, and in comparison with the corresponding  ${}^1J({}^{31}\text{P}, {}^{15}\text{N})_{\text{iso}}$  in  $\text{HN}(\text{Ph}_2\text{PSe})_2$ <sup>142</sup> confirm that the contributions of  $\Delta J$  are likely to be negligible in comparison to those of  $R_{DD}$ .

### 6.3.2 Solid-State $^{77}\text{Se}$ NMR

The entire spinning sideband manifolds for the solid-state  $^{77}\text{Se}$  NMR spectra for the single-source precursors investigated at 7.0 T are given in Figure 6.4a. The solid-state NMR parameters are detailed in Table 6.2. Solution-state  $^{77}\text{Se}$  NMR has not previously been reported for the  $\text{M}[\text{N}(\text{}^i\text{Pr}_2\text{PSe})_2]_2$  ( $\text{M} = \text{Zn, Cd, Hg}$ ) complexes. The values of  $\delta_{\text{iso}}(^{77}\text{Se})$  encountered vary by 66 ppm which are very similar given that the selenium chemical shift range exceeds 3000 ppm.<sup>143,144</sup> The apparent trend observed for the isotropic  $^{31}\text{P}$  chemical shifts and chemical shift principal components, where the shielding increases as the complexing metal went from zinc to cadmium to mercury, is not reproduced in the corresponding  $^{77}\text{Se}$  NMR values. The average of the isotropic  $^{77}\text{Se}$  chemical shifts decreases as one moves from the zinc to the cadmium complex; however,  $\text{Hg}[\text{N}(\text{}^i\text{Pr}_2\text{PSe})_2]_2$  possesses the least shielded selenium environments of the three complexes investigated. Theoretical calculations of the selenium chemical shift tensors reproduce the experimental values well, and agree with the experimentally observed order of average selenium magnetic shielding, i.e.,  $\sigma_{\text{iso,avg}}(^{77}\text{Se}; \text{M} = \text{Cd}) > \sigma_{\text{iso,avg}}(^{77}\text{Se}; \text{M} = \text{Zn}) > \sigma_{\text{iso,avg}}(^{77}\text{Se}; \text{M} = \text{Hg})$ , see Appendix C. The spans of the selenium chemical shift tensors investigated, unlike those for the  $^{31}\text{P}$  chemical shift tensors, are all larger than those found in tris-organophosphine selenides,<sup>132,145</sup> indicating that the presence of the metal is influencing the shielding environment of the selenium nuclei. Calculated orientations of selenium magnetic shielding tensors for tris-organophosphine selenide compounds,  $\text{R}_3\text{PSe}$ , were found to vary with the choice of R group.<sup>132</sup> The selenium magnetic shielding tensors for all four of the selenium environments for each of the zinc, cadmium and mercury complexes investigated as determined by DFT calculations,



**Figure 6.4** (a) VACP MAS  $^{77}\text{Se}$  NMR spectra for  $M[\text{N}(\text{iPr}_2\text{PSe})_2]_2$  ( $M = \text{Zn}, \text{Cd}, \text{Hg}$ ). (b) Expansion of the isotropic region of the  $^{77}\text{Se}$  NMR spectra (lower trace), with spinning sidebands added to the isotropic region, and the corresponding simulations (upper trace). Experimental conditions: 7.0 T, 6764 – 22064 scans, spinning at 4.0 kHz, 10 Hz of line broadening, a 9.0 – 10.0 ms contact time, and a 10 – 15 s recycle delay.

**Table 6.2** Solid-state  $^{77}\text{Se}$  NMR parameters for  $\text{M}[\text{N}(\text{}^1\text{Pr}_2\text{PSe})_2]_2$  ( $\text{M} = \text{Zn}, \text{Cd}, \text{Hg}$ ).

$\text{M}^{\text{II}}$	$\delta_{\text{iso}}$ ppm	$\delta_{11}$ ppm	$\delta_{22}$ ppm	$\delta_{33}$ ppm	$^1J(^{77}\text{Se}, ^{31}\text{P})_{\text{iso}}$ <sup>a</sup> Hz	$^1J(\text{M}, ^{77}\text{Se})_{\text{iso}}$ <sup>b,c</sup> Hz
Zn	-242	178	-416	-489	-544	
	-248	172	-399	-516	-540	
	-252	151	-407	-499	-516	
	-255	184	-414	-534	-521	
Cd	-272	166	-386	-596	-522	$\pm 135$
	-275	161	-373	-613	-537	$\pm 135$
	-282	162	-383	-626	-518	$\pm 120$
	-282	162	-383	-626	-518	$\pm 120$
Hg	-216	189	-338	-499	-550	-900
	-221	186	-339	-511	-550	-880
	-224	180	-345	-508	-512	-860
	-229	197	-359	-524	-526	-850

<sup>a</sup> For directly bonded selenium-77 and phosphorus-31 spin pairs, signs of  $^1J(^{77}\text{Se}, ^{31}\text{P})_{\text{iso}}$  are known to be negative for numerous analogous systems.<sup>133,134</sup>

<sup>b</sup> Signs of  $^1J(^{199}\text{Hg}, ^{77}\text{Se})_{\text{iso}}$  are reported as negative based on double resonance experiments performed on  $\text{Hg}(\text{SePBu}_3)_2$  ( $\text{X} = \text{Cl}, \text{Br}, \text{I}, \text{SCN}$ ) complexes.<sup>146</sup>

<sup>c</sup> Couplings to  $^{111}\text{Cd}$  and  $^{113}\text{Cd}$  could not be resolved from each other.

possess similar orientations, suggesting that the variation of the central metal does not significantly impact the orientation of the selenium magnetic shielding tensor. The directions of least and greatest shielding,  $\sigma_{11}$  and  $\sigma_{33}$ , were found to orient nearly parallel with the metal-selenium and selenium-phosphorus bond axes, respectively. Orthogonal to the other principal components, the direction of intermediate shielding,  $\sigma_{22}$ , was oriented perpendicular to the local M-Se-P plane.

Experimental spectra of the isotropic region at 7.0 T, with spinning sideband addition, from the corresponding  $^{77}\text{Se}$  NMR spectra are given in Figure 6.4b, along with their simulations. The isotropic region for  $\text{Zn}[\text{N}(\text{}^1\text{Pr}_2\text{PSe})_2]_2$  exhibits seven peaks in an approximate 1:1:2:1:1:1:1 fashion. This intensity profile is consistent with the expected four selenium environments from the crystal structure, each of which experiences indirect spin-spin coupling from the adjacent  $^{31}\text{P}$  (N.A. 100%). Zinc-67 is the only NMR-active nuclide of zinc, and because of its quadrupolar nature,  $I = 5/2$ , low 4.10% natural



abundance, and small frequency ratio,  $\Xi = 6.257$  MHz, it is expected that the influence of  $^{67}\text{Zn}$  on the selenium-77 NMR spectra would be negligible. Exploiting the magnetic field dependence of the chemical shift and the field independence of the indirect spin-spin coupling interactions permits the simulation of the  $^{77}\text{Se}$  NMR spectrum in Figure 6.4b, along with the simulations of the  $^{77}\text{Se}$  NMR spectra at 4.7 T and 11.7 T (not shown), to extract the values of  $\delta_{\text{iso}}$ ,  $\delta_{\text{ii}}$ , and  $^1J(^{77}\text{Se}, ^{31}\text{P})_{\text{iso}}$  given in Table 6.2. The values of  $^1J(^{77}\text{Se}, ^{31}\text{P})_{\text{iso}}$  are in good agreement with the magnitude of (-)539 Hz from the  $^{31}\text{P}$  NMR spectrum of a chloroform solution of  $\text{Zn}[\text{N}(\text{}^i\text{Pr}_2\text{PSe})_2]_2$ ,<sup>62</sup> and those from the above solid-state  $^{31}\text{P}$  NMR investigation, Table 6.1.

The isotropic region for  $\text{Cd}[\text{N}(\text{}^i\text{Pr}_2\text{PSe})_2]_2$  shows considerably more fine structure at the base of the more intense peaks whose intensity profile at 7.0 T displays a 1:1:1:2:1:2 pattern, Figure 6.4b. The  $^{77}\text{Se}$  NMR spectra for  $\text{Cd}[\text{N}(\text{}^i\text{Pr}_2\text{PSe})_2]_2$  were simulated at all three magnetic fields employed with only three unique selenium environments, in a 1:1:2 intensity ratio, despite the absence of any symmetry elements relating any two selenium atoms in the crystal structure.<sup>62</sup> While the four calculated selenium chemical shift tensors for  $\text{Cd}[\text{N}(\text{}^i\text{Pr}_2\text{PSe})_2]_2$  are very similar, no two are identical, as expected. The fine structure in the spectrum is a result of indirect spin-spin coupling from  $^{111}\text{Cd}$  ( $I = 1/2$ , 12.80 % N.A.,  $\Xi = 21.215$  MHz) and  $^{113}\text{Cd}$  ( $I = 1/2$ , 12.22 % N.A.,  $\Xi = 21.193$  MHz). The values of  $^1J(^{111/113}\text{Cd}, ^{77}\text{Se})_{\text{iso}}$  are of a similar order of magnitude to those found in  $(\text{NMe}_4)_2[\text{Cd}(\text{Se}_4)_2]$  by solid-state  $^{77}\text{Se}$  NMR,<sup>147</sup> and to those in cadmium(II) phenylselenolate complexes by solution  $^{77}\text{Se}$  and  $^{113}\text{Cd}$  NMR.<sup>148</sup> The  $^1J(^{77}\text{Se}, ^{31}\text{P})_{\text{iso}}$  values agree well with those from the satellites in the solution,  $^1J(^{77}\text{Se}, ^{31}\text{P})_{\text{iso}} = (-)563$  Hz,<sup>62</sup> and solid-state  $^{31}\text{P}$  NMR data given in Table 6.1.

The isotropic region in the  $^{77}\text{Se}$  NMR spectrum for  $\text{Hg}[\text{N}(\text{}^i\text{Pr}_2\text{PSe})_2]_2$  appears similar to the isotropic region in the corresponding zinc complex with the addition of satellite peaks resulting from  $^1J(^{199}\text{Hg}, ^{77}\text{Se})_{\text{iso}}$  due to the presence of  $^{199}\text{Hg}$  ( $I = 1/2$ , 16.87 % N.A.,  $\Xi = 17.911$  MHz), Figure 6.4b. Mercury possesses a second NMR-active isotope  $^{201}\text{Hg}$  ( $I = 3/2$ , 13.18 % N.A.,  $\Xi = 6.612$  MHz); however, similar to  $^{67}\text{Zn}$ , its quadrupolar nature, natural abundance and frequency ratio produce a negligible detectable impact on the  $^{77}\text{Se}$  NMR spectra. The values of  $^1J(^{77}\text{Se}, ^{31}\text{P})_{\text{iso}}$  given in Table 6.2 are in good agreement with the magnitude of (-)518 Hz from the solution  $^{31}\text{P}$  NMR spectrum,<sup>22</sup> and the solid-state values, Table 6.1. The large values of  $^1J(^{199}\text{Hg}, ^{77}\text{Se})_{\text{iso}}$  agree well with the  $^{199}\text{Hg}$  NMR value of (-)855 Hz from a chloroform solution of  $\text{Hg}[\text{N}(\text{}^i\text{Pr}_2\text{PSe})_2]_2$ ,<sup>22</sup> and are of a similar order of magnitude to those found in  $\text{HgX}_2(\text{Bu}_3\text{PSe})_2$  ( $X = \text{Cl, Br, I, SCN}$ ) by solution  $^{77}\text{Se}$  and  $^{199}\text{Hg}$  NMR,<sup>146</sup> and in  $(\text{NMe}_4)_2[\text{Hg}(\text{Se}_4)_2]$  by solid-state  $^{77}\text{Se}$  NMR.<sup>147</sup>

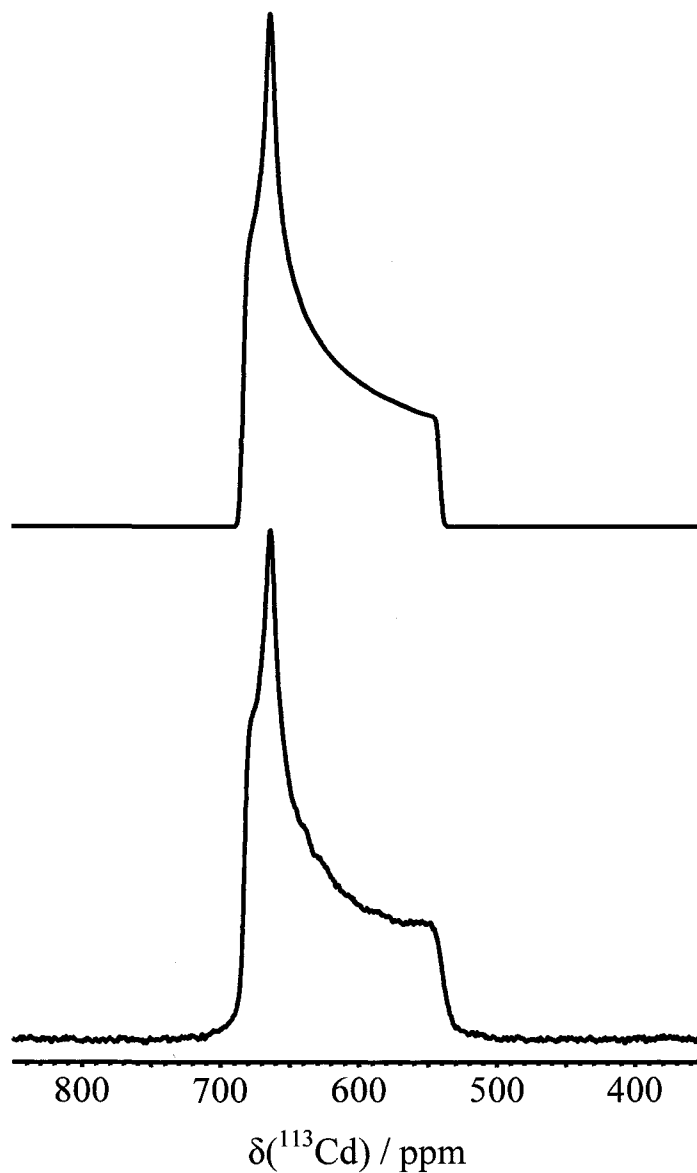
The internuclear phosphorus-selenium distances for the zinc, cadmium and mercury complexes range from 2.177-2.183 Å,<sup>48</sup> 2.168-2.188 Å,<sup>62</sup> and 2.180-2.191 Å<sup>22</sup> respectively. Not surprisingly, all of the  $\text{M}[\text{N}(\text{}^i\text{Pr}_2\text{PSe})_2]_2$  ( $\text{M} = \text{Zn, Cd, Hg}$ ) complexes have similar values of  $^1J(^{77}\text{Se}, ^{31}\text{P})_{\text{iso}}$  from solid-state  $^{31}\text{P}$  and  $^{77}\text{Se}$  NMR spectroscopy, see Tables 6.1 and 6.2. These  $^1J(^{77}\text{Se}, ^{31}\text{P})_{\text{iso}}$  values are all considerably smaller in magnitude than the corresponding solution value of (-)757 Hz in the ‘free’  $\text{HN}(\text{}^i\text{Pr}_2\text{PSe})_2$  ligand.<sup>62</sup> The decrease in the magnitude of  $^1J(^{77}\text{Se}, ^{31}\text{P})_{\text{iso}}$  values upon complexation has been observed upon coordination of  $\text{R}_3\text{PSe}$  with  $\text{Cd}(\text{II})$ ,<sup>149</sup> or  $\text{HgX}_2$  ( $X = \text{Cl, Br, I}$ ),<sup>150</sup> and it has been suggested to result from a lowering of the P-Se bond order upon complexation as the P-Se distance increases from 2.092 and 2.103 Å found for the solid-state structure

of  $\text{HN}(\text{}^1\text{Pr}_2\text{PSe})_2$ .<sup>62</sup> The complexing strength of  $[\text{N}(\text{}^1\text{Pr}_2\text{PSe})_2]^-$  has been shown in its ability to displace coordinated triphenylphosphine,<sup>151</sup> and a reduction in the magnitude of the phosphorus-selenium coupling constant from the ‘free’ ligand indicates metal-selenium bonding.<sup>81</sup>

The ranges of internuclear metal-selenium distances for the cadmium and mercury complexes are very similar, 2.622-2.636 Å and 2.625-2.636 Å respectively. Scaling of  ${}^1J(\text{}^{113}\text{Cd}, \text{}^{77}\text{Se})_{\text{iso}} = 120\text{-}135$  Hz and  ${}^1J(\text{}^{199}\text{Hg}, \text{}^{77}\text{Se})_{\text{iso}} = 850\text{-}900$  Hz by  $4\pi^2/\text{hr}\gamma_{\text{Cd/Hg}}\gamma_{\text{Se}}$  yields the respective reduced coupling constants  ${}^1K(\text{Cd}, \text{Se})_{\text{iso}} = 234\text{-}263 \times 10^{19} \text{ T}^2 \text{ J}^{-1}$  and  ${}^1K(\text{Hg}, \text{Se})_{\text{iso}} = 2038\text{-}2158 \times 10^{19} \text{ T}^2 \text{ J}^{-1}$  allowing for direct comparison. The approximate order of magnitude difference between cadmium and mercury in the values of  ${}^1J(\text{M}, \text{Se})_{\text{iso}}$  is upheld when considering the corresponding  ${}^1K(\text{M}, \text{Se})_{\text{iso}}$ . An increase in the magnitude of the reduced coupling constant as one moves down a group in the periodic table is a well known trend for various Group 14 couplings,<sup>152-158</sup> and appears to hold for the Group 12 metal coupling with selenium in the complexes investigated.

### 6.3.3 Solid-State ${}^{113}\text{Cd}$ NMR

The solid-state  ${}^{113}\text{Cd}$  NMR spectrum of a stationary sample of  $\text{Cd}[\text{N}(\text{}^1\text{Pr}_2\text{PSe})_2]_2$  at 11.7 T is given in Figure 6.5 along with its simulation. The low natural abundance of selenium-77 (7.63 %) prevents any significant impact of  ${}^1J(\text{}^{113}\text{Cd}, \text{}^{77}\text{Se})_{\text{iso}}$  on the simulation of the acquired spectrum, and the value of  ${}^2J(\text{}^{113}\text{Cd}, \text{}^{31}\text{P})_{\text{iso}} = 30.8$  Hz<sup>62</sup> from a solution  ${}^{31}\text{P}$  NMR spectrum is too small to observe in any of the solid-state  ${}^{113}\text{Cd}$  measurements at the applied magnetic fields used. The principal components of the single cadmium chemical shift tensor are given in Table 6.3. The nearly axial symmetric



**Figure 6.5** VACP  $^{113}\text{Cd}$  NMR spectrum of stationary  $\text{Cd}[\text{N}(\text{iPr}_2\text{PSe})_2]_2$  (lower trace) and its simulation (upper trace). Experimental conditions: 11.7 T, 20000 scans, 100 Hz of line broadening, an 11.5 ms contact time, and a 12 s recycle delay.

$^{113}\text{Cd}$  chemical shift tensor, Figure 6.5, arises due to the approximate  $S_4$  symmetry axis present at the metal center. The presence of an improper 4-fold rotation axis about the metal center was initially found in the X-ray crystal structure determination of  $\text{Zn}[\text{N}(\text{iPr}_2\text{PS})_2]_2$ ,<sup>61</sup> which was ultimately revisited<sup>48</sup> and refined to be isostructural with

**Table 6.3** Solid-state  $^{113}\text{Cd}$  and  $^{199}\text{Hg}$  NMR parameters for  $\text{M}[\text{N}(\text{}^i\text{Pr}_2\text{PSe})_2]_2$  ( $\text{M} = \text{Cd}, \text{Hg}$ ).

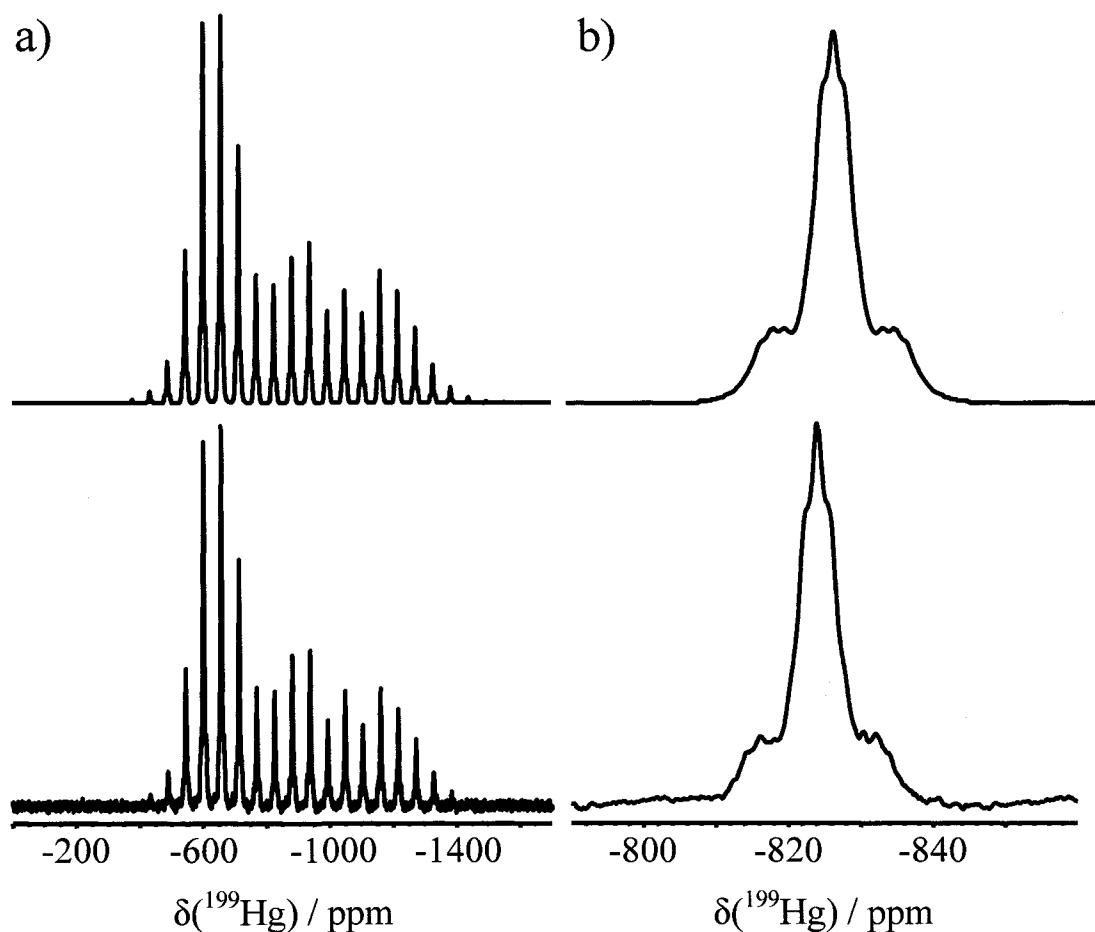
$\text{M}^{\text{II}}$	$\delta_{\text{iso}}$ ppm	$\delta_{11}$ ppm	$\delta_{22}$ ppm	$\delta_{33}$ ppm	${}^2J(\text{M}, {}^{31}\text{P})_{\text{iso}}^{\text{a}}$ Hz	${}^1J(\text{M}, {}^{77}\text{Se})_{\text{iso}}^{\text{a}}$ Hz
Cd	629	683	663	540		
Hg	-826	-530	-600	-1348	-80	-870

<sup>a</sup> Signs of  ${}^1J({}^{199}\text{Hg}, {}^{77}\text{Se})_{\text{iso}}$  and  ${}^2J({}^{199}\text{Hg}, {}^{31}\text{P})_{\text{iso}}$  are reported as negative based on double resonance resonance experiments performed on  $\text{Hg}(\text{SePBu}_3)\text{X}_2$  ( $\text{X} = \text{Cl}, \text{Br}, \text{I}, \text{SCN}$ ) complexes.<sup>146</sup>

the  $\text{M}[\text{N}(\text{}^i\text{Pr}_2\text{PSe})_2]_2$  ( $\text{M} = \text{Zn}, \text{Cd}, \text{Hg}$ ) complexes. Near axial symmetry was also found in the calculated magnetic shielding tensor for the cadmium complex. While there are no solution-state  $^{113}\text{Cd}$  NMR values for  $\text{Cd}[\text{N}(\text{}^i\text{Pr}_2\text{PSe})_2]_2$  for comparison, the isotropic  $^{113}\text{Cd}$  chemical shift is reasonable given those found for cadmium(II) phenylselenolate complexes from a solution  $^{113}\text{Cd}$  NMR study.<sup>148</sup>

#### 6.3.4 Solid-State $^{199}\text{Hg}$ NMR

The solid-state  $^{199}\text{Hg}$  NMR spectrum of  $\text{Hg}[\text{N}(\text{}^i\text{Pr}_2\text{PSe})_2]_2$  at 7.0 T is given in Figure 6.6a, and the isotropic region with spinning sideband addition is shown in Figure 6.6b. The solid-state parameters extracted from this as well as the spectra at 4.7 T and 11.7 T (not shown) are given in Table 6.3. Similar to the solid-state  $^{113}\text{Cd}$  NMR spectrum of  $\text{Cd}[\text{N}(\text{}^i\text{Pr}_2\text{PSe})_2]_2$  in Figure 6.5, the solid-state  $^{199}\text{Hg}$  NMR spectrum of the mercury analogue in Figure 6.6a displays a nearly axially symmetric chemical shift tensor arising from an approximate  $S_4$  axis about the mercury center. Near axial symmetry has been observed for  $^{199}\text{Hg}$  chemical shift tensors in mercury(II) complexes with monoanionic bidentate carboxylate ligands,<sup>159,160</sup> and in the calculated magnetic shielding tensor for  $\text{Hg}[\text{N}(\text{}^i\text{Pr}_2\text{PSe})_2]_2$  given in Appendix C. The isotropic  $^{199}\text{Hg}$  chemical



**Figure 6.6** (a) VACP MAS  $^{199}\text{Hg}$  NMR spectrum of  $\text{Hg}[\text{N}(\text{}^i\text{Pr}_2\text{PSe})_2]_2$  (lower trace) and its simulation (upper trace). (b) Expansion of the isotropic region of the  $^{199}\text{Hg}$  NMR spectrum (lower trace), with spinning sideband addition, and the simulation (upper trace). Experimental conditions: 7.0 T, 22896 scans, spinning at 3.0 kHz, 20 Hz of line broadening, a 11.5 ms contact time, and a 10 s recycle delay.

shift, -826 ppm, agrees well with the solution  $^{199}\text{Hg}$  NMR value of -859 ppm.<sup>22</sup> The simulation of the isotropic peak, Figure 6.6b, requires the presence of four  ${}^2J(^{199}\text{Hg}, {}^{31}\text{P})_{\text{iso}}$  to properly describe the observed lineshape. The average value of  ${}^2J(^{199}\text{Hg}, {}^{31}\text{P})_{\text{iso}}$ , -80 Hz, correctly produces the approximate 1:4:6:4:1 splitting pattern, and agrees with the value of (-)127 Hz as determined by solution  $^{199}\text{Hg}$  NMR,<sup>22</sup> and is of a similar magnitude to two-bond mercury-phosphorus coupling constants found in  $\text{HgX}_2(\text{Bu}_3\text{PSe})_2$  ( $\text{X} = \text{Cl}$ ,

Br, I, SCN).<sup>146,161</sup> The single  $^1J(^{199}\text{Hg}, ^{77}\text{Se})_{\text{iso}}$  value used to simulate the  $^{199}\text{Hg}$  NMR spectrum at all applied magnetic fields employed agrees well with the value from the  $^{199}\text{Hg}$  NMR value reported for a chloroform solution of  $\text{Hg}[\text{N}(\text{iPr}_2\text{PSe})_2]_2$ ,  $^1J(^{199}\text{Hg}, ^{77}\text{Se})_{\text{iso}} = (-)855 \text{ Hz}$ ,<sup>22</sup> as well as with the values determined from the solid-state  $^{77}\text{Se}$  NMR investigation given from this study in Table 6.2. The one-bond indirect mercury-selenium isotropic coupling constant, Table 6.3, is also consistent with those found in mercury(II) halide complexes of tributylphosphine selenide from solution  $^{77}\text{Se}$  and  $^{199}\text{Hg}$  NMR,<sup>146</sup> and in  $(\text{NMe}_4)_2[\text{Hg}(\text{Se}_4)_2]$  by solid-state  $^{77}\text{Se}$  NMR.<sup>147</sup>

#### 6.4 Summary

The single-source precursors,  $\text{M}[\text{N}(\text{iPr}_2\text{PSe})_2]_2$  ( $\text{M} = \text{Zn}, \text{Cd}, \text{Hg}$ ), for solid-state metal selenide materials were investigated by solid-state  $^{31}\text{P}$ ,  $^{77}\text{Se}$ ,  $^{113}\text{Cd}$ , and  $^{199}\text{Hg}$  NMR. Magnetic shielding calculations support many of the experimentally observed trends and values, specifically in the calculated orientations of the  $^{14}\text{N}$  EFG tensors, and magnetic shielding tensors. The slight increase in shielding for the phosphorus nuclei observed as one moves down the Group 12 period, is not nearly as significant as was observed in dialkyl Group 13 complexes,  $\text{R}'_2\text{M}[\text{N}(\text{R}_2\text{PSe})_2]$  ( $\text{M} = \text{Al}, \text{Ga}$ ).<sup>81</sup> The approximately equal values for  $^1J(^{77}\text{Se}, ^{31}\text{P})_{\text{iso}}$  in all three complexes investigated suggest that the metal-selenium bond order is similar in all  $\text{M}[\text{N}(\text{iPr}_2\text{PSe})_2]_2$  ( $\text{M} = \text{Zn}, \text{Cd}, \text{Hg}$ ) complexes. Residual dipolar coupling between  $^{31}\text{P}$  and  $^{14}\text{N}$  was found to significantly influence the solid-state  $^{31}\text{P}$  NMR spectra at 4.7 T and 7.0 T. Analysis of the phosphorus-31 NMR spectra at all three applied magnetic fields yielded additional information about the local environments of the phosphorus and nitrogen nuclei within the single-source precursors.

Aside from the principal components of the respective chemical shift tensors, nearly identical parameters were used to simulate the solid-state  $^{31}\text{P}$  NMR spectra at 4.7 T, 7.0 T and 11.7 T for all three complexes investigated, indicating that the local environments for phosphorus and nitrogen are very similar regardless of whether  $[\text{N}(\text{}^i\text{Pr}_2\text{PSe})_2]^-$  is coordinated to zinc, cadmium or mercury. While four distinct  $^{31}\text{P}$  environments are observed for  $\text{Cd}[\text{N}(\text{}^i\text{Pr}_2\text{PSe})_2]_2$  as expected, only three selenium environments were found in the solid-state  $^{77}\text{Se}$  NMR spectra. The occurrence of two selenium environments possessing identical isotropic  $^{77}\text{Se}$  chemical shifts within the cadmium complex is fortuitous. Solid-state  $^{77}\text{Se}$  NMR, in general, provides more accurate values of indirect spin-spin coupling constants, primarily due to the larger natural abundances of  $^{31}\text{P}$ ,  $^{111/113}\text{Cd}$ , and  $^{199}\text{Hg}$  with respect to  $^{77}\text{Se}$ . The solid-state  $^{113}\text{Cd}$  and  $^{199}\text{Hg}$  NMR spectra yield information on the type of environment provided by two diselenoimido-diphosphinato ligands oriented in a spirobicyclic fashion around the central metal. The solid-state  $^{113}\text{Cd}$  NMR spectra give a chemical shift tensor spanning less than 150 ppm, with little detectable evidence for cadmium-selenium one-bond or cadmium-phosphorus two-bond indirect spin-spin coupling; whereas, the  $^{199}\text{Hg}$  chemical shift tensor spans over 800 ppm, and displays evidence of both  $^1J(^{199}\text{Hg}, ^{77}\text{Se})_{\text{iso}}$  and  $^2J(^{199}\text{Hg}, ^{31}\text{P})_{\text{iso}}$ . The asymmetric nature of the  $^{113}\text{Cd}$  and  $^{199}\text{Hg}$  chemical shift tensors clearly show sensitivity to the distortions from tetrahedral symmetry about the  $\text{MSe}_4$  core.



## 6.5 References

- (1) Gustafsson, G.; Cao, Y.; Treacy, G. M.; Klavetter, F.; Colaneri, N.; Heeger, A. J. *Nature* **1992**, *357*, 477-479.
- (2) Dhawan, S. K.; Trivedi, D. C. *J. Appl. Electrochem.* **1992**, *22*, 563-570.
- (3) Balcerak, R.; Gibson, J. F.; Gutierrez, W. A.; Pollard, J. H. *Opt. Eng.* **1987**, *26*, 191-200.
- (4) Rogalski, A. *Opt. Eng.* **1994**, *33*, 1395-1412.
- (5) Sato, T.; Ahmed, H.; Brown, D.; Johnson, B. F. G. *J. Appl. Phys.* **1997**, *82*, 696-701.
- (6) Slot, J. W.; Geuze, H. J. *J. Cell Biol.* **1981**, *90*, 533-536.
- (7) Mycielski, A.; Szadkowski, A.; Kaliszek, W.; Witkowska, B. *Proc. SPIE-Int. Soc. Opt. Eng.* **2001**, *4412*, 38-45.
- (8) Yesugade, N. S.; Lokhande, C. D.; Bhosale, C. H. *Thin Solid Films* **1995**, *263*, 145-149.
- (9) Bhattacharya, R. N.; Pramanik, P. *J. Electrochem. Soc.* **1982**, *129*, 332-335.
- (10) Sankapal, B. R.; Lokhande, C. D. *Mater. Chem. Phys.* **2002**, *73*, 151-155.
- (11) Manasevit, H. M.; Simpson, W. I. *J. Electrochem. Soc.* **1971**, *118*, 644-647.
- (12) Murray, C. B.; Norris, D. J.; Bawendi, M. G. *J. Am. Chem. Soc.* **1993**, *115*, 8706-8715.
- (13) Pickett, N. L.; Riddell, F. G.; Foster, D. F.; Cole-Hamilton, D. J.; Fryer, J. R. *J. Mater. Chem.* **1997**, *7*, 1855-1865.
- (14) Pickett, N. L.; Lawson, S.; Thomas, W. G.; Riddell, F. G.; Foster, D. F.; Cole-Hamilton, D. J.; Fryer, J. R. *J. Mater. Chem.* **1998**, *8*, 2769-2776.
- (15) Peng, Z. A.; Peng, X. *J. Am. Chem. Soc.* **2001**, *123*, 183-184.
- (16) Green, M.; O'Brien, P. *Chem. Commun.* **1999**, 2235-2241.
- (17) Arnold, J. *Prog. Inorg. Chem.* **1995**, *43*, 353-417.
- (18) O'Brien, P.; Nomura, R. *J. Mater. Chem.* **1995**, *5*, 1761-1773.

- (19) Gleizes, A. N. *Chem. Vap. Deposition* **2000**, *6*, 155-173.
- (20) Pickett, N. L.; O'Brien, P. *Chem. Rec.* **2001**, *1*, 467-479.
- (21) Bochmann, M. *Chem. Vap. Deposition* **1996**, *2*, 85-96.
- (22) Crouch, D. J.; Hatton, P. M.; Helliwell, M.; O'Brien, P.; Raftery, J. *Dalton Trans.* **2003**, 2761-2766.
- (23) Osakada, K.; Yamamoto, T. *Chem. Commun.* **1987**, 1117-1118.
- (24) Steigerwald, M. L.; Sprinkle, C. R. *J. Am. Chem. Soc.* **1987**, *109*, 7200-7201.
- (25) Brennan, J. G.; Siegrist, T.; Carroll, P. J.; Stuczynski, S. M.; Brus, L. E.; Steigerwald, M. L. *J. Am. Chem. Soc.* **1989**, *111*, 4141-4143.
- (26) Bochmann, M.; Webb, K.; Harman, M.; Hursthouse, M. B. *Angew. Chem., Int. Ed. Engl.* **1990**, *29*, 638-639.
- (27) Brennan, J. G.; Siegrist, T.; Carroll, P. J.; Stuczynski, S. M.; Reynders, P.; Brus, L. E.; Steigerwald, M. L. *Chem. Mat.* **1990**, *2*, 403-409.
- (28) Bochmann, M.; Webb, K. J.; Hails, J. E.; Wolverson, D. *Eur. J. Solid State Inorg. Chem.* **1992**, *29*, 155-166.
- (29) Park, H. S.; Mokhtari, M.; Roesky, H. W. *Chem. Vap. Deposition* **1996**, *2*, 135-139.
- (30) Arnold, J.; Walker, J. M.; Yu, K. M.; Bonasia, P. J.; Seligson, A. L.; Bourret, E. *D. J. Cryst. Growth* **1992**, *124*, 647-653.
- (31) Seligson, A. L.; Bonasia, P. J.; Arnold, J.; Yu, K. M.; Walker, J. M.; Bourret, E. *D. Mater. Res. Soc. Symp. Proc.* **1993**, *282*, 665-670.
- (32) Takahashi, Y.; Yuki, R.; Sugiura, M.; Motojima, S.; Sugiyama, K. *J. Cryst. Growth* **1980**, *50*, 491-497.
- (33) Evans, M. A. H.; Williams, J. O. *Thin Solid Films* **1982**, *87*, L1-L2.
- (34) Frigo, D. M.; Khan, O. F. Z.; O'Brien, P. *J. Cryst. Growth* **1989**, *96*, 989-992.
- (35) Hursthouse, M. B.; Malik, M. A.; Motevalli, M.; O'Brien, P. *Polyhedron* **1992**, *11*, 45-48.

- (36) Pike, R. D.; Cui, H.; Kershaw, R.; Dwight, K.; Wold, A.; Blanton, T. N.; Wernberg, A. A.; Gysling, H. J. *Thin Solid Films* **1993**, *224*, 221-226.
- (37) Nomura, R.; Murai, T.; Toyosaki, T.; Matsuda, H. *Thin Solid Films* **1995**, *271*, 4-7.
- (38) Trindade, T.; O'Brien, P. *Adv. Mater.* **1996**, *8*, 161-163.
- (39) O'Brien, P.; Walsh, J. R.; Watson, I. M.; Motevalli, M.; Henriksen, L. *Dalton Trans.* **1996**, 2491-2496.
- (40) Trindade, T.; O'Brien, P.; Zhang, X.-M. *Chem. Mat.* **1997**, *9*, 523-530.
- (41) Ludolph, B.; Malik, M. A.; O'Brien, P.; Revaprasadu, N. *Chem. Commun.* **1998**, 1849-1850.
- (42) Revaprasadu, N.; Malik, M. A.; O'Brien, P.; Zulu, M. M.; Wakefield, G. *J. Mater. Chem.* **1998**, *8*, 1885-1888.
- (43) Revaprasadu, N.; Malik, M. A.; O'Brien, P.; Wakefield, G. *Chem. Commun.* **1999**, 1573-1574.
- (44) Afzaal, M.; Crouch, D.; Malik, M. A.; Motevalli, M.; O'Brien, P.; Park, J.-H. *J. Mater. Chem.* **2003**, *13*, 639-640.
- (45) Afzaal, M.; Crouch, D. J.; O'Brien, P.; Raftery, J.; Skabara, P. J.; White, A. J. P.; Williams, D. J. *J. Mater. Chem.* **2004**, *14*, 233-237.
- (46) Crouch, D. J.; Helliwell, M.; O'Brien, P.; Park, J.-H.; Waters, J.; Williams, D. J. *Dalton Trans.* **2003**, 1500-1504.
- (47) Afzaal, M.; Aucott, S. M.; Crouch, D.; O'Brien, P.; Woollins, J. D.; Park, J.-H. *Chem. Vap. Deposition* **2002**, *8*, 187-189.
- (48) Afzaal, M.; Crouch, D.; Malik, M. A.; Motevalli, M.; O'Brien, P.; Park, J.-H.; Woollins, J. D. *Eur. J. Inorg. Chem.* **2004**, 171-177.
- (49) Malik, M. A.; Afzaal, M.; O'Brien, P.; Halliwell, M. *Polyhedron* **2006**, *25*, 864-868.
- (50) Garje, S. S.; Ritch, J. S.; Eisler, D. J.; Afzaal, M.; O'Brien, P.; Chivers, T. *J. Mater. Chem.* **2006**, *16*, 966-969.
- (51) Afzaal, M.; Ellwood, K.; Pickett, N. L.; O'Brien, P.; Raftery, J.; Waters, J. *J. Mater. Chem.* **2004**, *14*, 1310-1315.

- (52) Crouch, D. J.; O'Brien, P.; Malik, M. A.; Skabara, P. J.; Wright, S. P. *Chem. Commun.* **2003**, 1454-1455.
- (53) Haiduc, I.; Silaghi-Dumitrescu, I. *Coord. Chem. Rev.* **1986**, *74*, 127-270.
- (54) Woollins, J. D. *Dalton Trans.* **1996**, 2893-2901.
- (55) Ly, T. Q.; Woollins, J. D. *Coord. Chem. Rev.* **1998**, *176*, 451-481.
- (56) Bhattacharyya, P.; Woollins, J. D. *Polyhedron* **1995**, *14*, 3367-3388.
- (57) Rossi, R.; Marchi, A.; Marvelli, L.; Magon, L.; Peruzzini, M.; Casellato, U.; Graziani, R. *Dalton Trans.* **1993**, 723-729.
- (58) Cea-Olivares, R.; García-Montalvo, V.; Novosad, J.; Kilian, P.; Woollins, J. D.; Slawin, A. M. Z.; García y García, P.; López-Cardoso, M.; Espinosa-Pérez, G.; Toscano, R. A.; Hernández, S.; Canseco-Melchor, G.; Lima-Montaño, L.; Rodríguez-Narváez, C. *Phosphorus Sulfur Silicon Relat. Elem.* **1997**, *124*, 347-354.
- (59) Cea-Olivares, R.; Moya-Cabrera, M.; García-Montalvo, V.; Castro-Blanco, R.; Toscano, R. A.; Hernández-Ortega, S. *Dalton Trans.* **2005**, 1017-1018.
- (60) Silvestru, C.; Drake, J. E. *Coord. Chem. Rev.* **2001**, *223*, 117-216.
- (61) Cupertino, D.; Keyte, R.; Slawin, A. M. Z.; Williams, D. J.; Woollins, J. D. *Inorg. Chem.* **1996**, *35*, 2695-2697.
- (62) Cupertino, D.; Birdsall, D. J.; Slawin, A. M. Z.; Woollins, J. D. *Inorg. Chim. Acta* **1999**, *290*, 1-7.
- (63) Bhattacharyya, P.; Novosad, J.; Phillips, J.; Slawin, A. M. Z.; Williams, D. J.; Woollins, J. D. *Dalton Trans.* **1995**, 1607-1613.
- (64) Cea-Olivares, R.; Novosad, J.; Woollins, J. D.; Slawin, A. M. Z.; García-Montalvo, V.; Espinosa-Pérez, G.; García y García, P. *Chem. Commun.* **1996**, 519-520.
- (65) Williams, D. J.; Quicksall, C. O.; Barkigia, K. M. *Inorg. Chem.* **1982**, *21*, 2097-2100.
- (66) Cea-Olivares, R.; Toscano, R. A.; Carreón, G.; Valdés-Martínez, J. *Monatsh. Chem.* **1992**, *123*, 391-396.
- (67) García-Montalvo, V.; Novosad, J.; Kilian, P.; Woollins, J. D.; Slawin, A. M. Z.; García y García, P.; López-Cardoso, M.; Espinosa-Pérez, G.; Cea-Olivares, R. *Dalton Trans.* **1997**, 1025-1029.

- (68) García-Montalvo, V.; Zamora-Rosete, M. K.; Gorostieta, D.; Cea-Olivares, R.; Toscano, R. A.; Hernández-Ortega, S. *Eur. J. Inorg. Chem.* **2001**, 2279-2285.
- (69) Rodríguez, I.; Alvarez, C.; Gómez-Lara, J.; Cea-Olivares, R. *Lanthanide Actinide Res.* **1986**, *1*, 253-260.
- (70) Silvestru, C.; Haiduc, I.; Cea-Olivares, R.; Zimbron, A. *Polyhedron* **1994**, *13*, 3159-3165.
- (71) Cea-Olivares, R.; García-Montalvo, V.; Novosad, J.; Woollins, J. D.; Toscano, R. A.; Espinosa-Pérez, G. *Chem. Ber.* **1996**, *129*, 919-923.
- (72) García-Montalvo, V.; Cea-Olivares, R.; Williams, D. J.; Espinosa-Pérez, G. *Inorg. Chem.* **1996**, *35*, 3948-3953.
- (73) Rudler, H.; Denise, B.; Gregorio, J. R.; Vaissermann, J. *Chem. Commun.* **1997**, 2299-2300.
- (74) Goyal, M.; Novosad, J.; Necas, M.; Ishii, H.; Nagahata, R.; Sugiyama, J.-I.; Asai, M.; Ueda, M.; Takeuchi, K. *Appl. Organomet. Chem.* **2000**, *14*, 629-633.
- (75) du Preez, J. G. H.; Knabl, K. U.; Krüger, L.; van Brecht, B. J. A. M. *Solvent Extr. Ion Exch.* **1992**, *10*, 729-748.
- (76) Navrátil, O.; Herrmann, E.; Grossmann, G.; Teplý, J. *Collect. Czech. Chem. Commun.* **1990**, *55*, 364-371.
- (77) Herrmann, E.; Navrátil, O.; Nang, H. b.; Smola, J.; Friedrich, J.; Příhoda, J.; Dreyer, R.; Chalkin, V. A.; Kulpe, S. *Collect. Czech. Chem. Commun.* **1984**, *49*, 201-217.
- (78) Navrátil, O.; Cigánek, M.; Herrmann, E. *Collect. Czech. Chem. Commun.* **1983**, *48*, 2009-2014.
- (79) Navrátil, O.; Fofana, M.; Smola, J. *Z. Chem.* **1984**, *24*, 30.
- (80) Navrátil, O.; Herrmann, E.; Slezák, P. *Collect. Czech. Chem. Commun.* **1987**, *52*, 1708-1714.
- (81) Muñoz-Hernández, M.-Á.; Singer, A.; Atwood, D. A.; Cea-Olivares, R. *J. Organomet. Chem.* **1998**, *571*, 15-19.
- (82) Le, Q. T. H.; Umetani, S.; Matsui, M. *Dalton Trans.* **1997**, 3835-3840.
- (83) Platzer, N.; Rudler, H.; Alvarez, C.; Barkaoui, L.; Denise, B.; Goasdoué, N.; Rager, M.-N.; Vaissermann, J.; Daran, J.-C. *Bull. Soc. Chim. Fr.* **1995**, *132*, 95-113.

- (84) Alvarez, C.; Barkaoui, L.; Goasdoué, N.; Daran, J.-C.; Platzer, N.; Rudler, H.; Vaissermann, J. *Chem. Commun.* **1989**, 1507-1509.
- (85) Alvarez, C.; Goasdoué, N.; Platzer, N.; Rodríguez, I.; Rudler, H. *Chem. Commun.* **1988**, 1002-1004.
- (86) Barkaoui, L.; Charrouf, M.; Rager, M.-N.; Denise, B.; Platzer, N.; Rudler, H. *Bull. Soc. Chim. Fr.* **1997**, *134*, 167-175.
- (87) Rodríguez, I.; Alvarez, C.; Gómez-Lara, J.; Toscano, R. A.; Platzer, N.; Mulheim, C.; Rudler, H. *Chem. Commun.* **1987**, 1502-1503.
- (88) Magennis, S. W.; Parsons, S.; Corval, A.; Woollins, J. D.; Pikramenou, Z. *Chem. Commun.* **1999**, 61-62.
- (89) Bereman, R. D.; Wang, F. T.; Najdzionek, J.; Braitsch, D. M. *J. Am. Chem. Soc.* **1976**, *98*, 7266-7268.
- (90) Sakaguchi, U.; Addison, A. W. *J. Am. Chem. Soc.* **1977**, *99*, 5189-5190.
- (91) Siiman, O.; Vetuskey, J. *Inorg. Chem.* **1980**, *19*, 1672-1680.
- (92) Mehrotra, R. C.; Bohra, R.; Gaur, D. P. *Metal  $\beta$ -Diketonates and Allied Derivatives*; Academic Press: London, 1978.
- (93) Berg, E. W.; Truemper, J. T. *Anal. Chim. Acta* **1965**, *32*, 245-252.
- (94) Gilby, L. M.; Piggott, B. *Polyhedron* **1999**, *18*, 1077-1082.
- (95) Graddon, D. P. *Coord. Chem. Rev.* **1969**, *4*, 1-28.
- (96) Bhattacharyya, P.; Slawin, A. M. Z.; Smith, M. B. *Dalton Trans.* **1998**, 2467-2475.
- (97) Birdsall, D. J.; Novosad, J.; Slawin, A. M. Z.; Woollins, J. D. *Dalton Trans.* **2000**, 435-439.
- (98) Béreau, V.; Sekar, P.; McLauchlan, C. C.; Ibers, J. A. *Inorg. Chim. Acta* **2000**, *308*, 91-96.
- (99) Cea-Olivares, R.; Canseco-Melchor, G.; García-Montalvo, V.; Hernández-Ortega, S.; Novosad, J. *Eur. J. Inorg. Chem.* **1998**, 1573-1576.
- (100) Gaunt, A. J.; Scott, B. L.; Neu, M. P. *Chem. Commun.* **2005**, 3215-3217.

- (101) Papadimitriou, C.; Veltsistas, P.; Novosad, J.; Cea-Olivares, R.; Toscano, A.; García y García, P.; Lopez-Cardosa, M.; Slawin, A. M. Z.; Woollins, J. D. *Polyhedron* **1997**, *16*, 2727-2729.
- (102) Pernin, C. G.; Ibers, J. A. *Inorg. Chem.* **2000**, *39*, 1222-1226.
- (103) Wilton-Ely, J. D. E. T.; Schier, A.; Schmidbaur, H. *Dalton Trans.* **2001**, 3647-3651.
- (104) Gaunt, A. J.; Scott, B. L.; Neu, M. P. *Angew. Chem., Int. Ed. Engl.* **2006**, *45*, 1638-1641.
- (105) Chivers, T.; Eisler, D. J.; Ritch, J. S. *Dalton Trans.* **2005**, 2675-2677.
- (106) Haiduc, I. In *Inorganic Experiments*; Woollins, J. D., Ed.; VCH: New York; Basel; Cambridge; Tokyo, 1994, pp 145-149.
- (107) Bennett, A. E.; Rienstra, C. M.; Auger, M.; Lakshmi, K. V.; Griffin, R. G. *J. Chem. Phys.* **1995**, *103*, 6951-6958.
- (108) Bryce, D. L.; Bernard, G. M.; Gee, M.; Lumsden, M.; Eichele, K.; Wasylshen, R. E. *Can. J. Anal. Sci. Spectrosc.* **2001**, *46*, 46-82.
- (109) Collins, M. J.; Ratcliffe, C. I.; Ripmeester, J. A. *J. Magn. Reson.* **1986**, *68*, 172-179.
- (110) Mennitt, P. G.; Shatlock, M. P.; Bartuska, V. J.; Maciel, G. E. *J. Phys. Chem.* **1981**, *85*, 2087-2091.
- (111) Eichele, K.; Kroeker, S.; Wu, G.; Wasylshen, R. E. *Solid State Nucl. Magn. Reson.* **1995**, *4*, 295-300.
- (112) Herzfeld, J.; Berger, A. E. *J. Chem. Phys.* **1980**, *73*, 6021-6030.
- (113) Eichele, K.; Wasylshen, R. E.; 1.17.30 ed., 2001.
- (114) Pulay, P. In *Calculation of NMR and EPR Parameters*; Kaupp, M., Bühl, M., Malkin, V. G., Eds.; Wiley-VCH Verlag GmbH & Co. KGaA: Weinheim, 2004, p XIII.
- (115) Schreckenbach, G.; Ziegler, T. *J. Phys. Chem.* **1995**, *99*, 606-616.
- (116) Schreckenbach, G.; Ziegler, T. *Int. J. Quantum Chem.* **1997**, *61*, 899-918.
- (117) Wolff, S. K.; Ziegler, T. *J. Chem. Phys.* **1998**, *109*, 895-905.

- (118) Baerends, E. J.; Ellis, D. E.; Ros, P. *Chem. Phys.* **1973**, *2*, 41-51.
- (119) Versluis, L.; Ziegler, T. *J. Chem. Phys.* **1988**, *88*, 322-328.
- (120) te Velde, G.; Baerends, E. J. *J. Comput. Phys.* **1992**, *99*, 84-98.
- (121) Fonseca Guerra, C.; Snijders, J. G.; te Velde, G.; Baerends, E. J. *Theor. Chem. Acc.* **1998**, *99*, 391-403.
- (122) Theoretical Chemistry, Vrije Universiteit, Amsterdam, <http://www.scm.com>.
- (123) Vosko, S. H.; Wilk, L.; Nusair, M. *Can. J. Phys.* **1980**, *58*, 1200-1211.
- (124) Becke, A. D. *Phys. Rev. A* **1988**, *38*, 3098-3100.
- (125) Perdew, J. P. *Phys. Rev. B* **1986**, *33*, 8822-8824.
- (126) Perdew, J. P. *Phys. Rev. B* **1986**, *34*, 7406.
- (127) Chang, C.; Pelissier, M.; Durand, P. *Phys. Scr.* **1986**, *34*, 394-404.
- (128) van Lenthe, E.; Baerends, E. J.; Snijders, J. G. *J. Chem. Phys.* **1993**, *99*, 4597-4610.
- (129) van Lenthe, E.; Baerends, E. J.; Snijders, J. G. *J. Chem. Phys.* **1994**, *101*, 9783-9792.
- (130) van Lenthe, E.; van Leeuwen, R.; Baerends, E. J.; Snijders, J. G. *Int. J. Quantum Chem.* **1996**, *57*, 281-293.
- (131) Jameson, C. J.; de Dios, A.; Jameson, A. K. *Chem. Phys. Lett.* **1990**, *167*, 575-582.
- (132) Demko, B. A.; Eichele, K.; Wasylishen, R. E. *J. Phys. Chem. A* **2006**, *110*, 13537-13550.
- (133) Jameson, C. J. In *Multinuclear NMR*; Mason, J., Ed.; Plenum Press: New York, 1987, pp 89-131.
- (134) Jameson, C. J. In *Phosphorus-31 NMR Spectroscopy in Stereochemical Analysis. Organic Compounds and Metal Complexes*; Verkade, J. G., Quin, L. D., Eds.; VCH Publishers, Inc.: Deerfield Beach, 1987; Vol. 8, pp 205-230.
- (135) Robert, J. B.; Wiesenfeld, L. *Mol. Phys.* **1981**, *44*, 319-327.



- (136) Power, W. P.; Wasylshen, R. E.; Curtis, R. D. *Can. J. Chem.* **1989**, *67*, 454-459.
- (137) Comotti, A.; Gallazzi, M. C.; Simonutti, R.; Sozzani, P. *Chem. Mat.* **1998**, *10*, 3589-3596.
- (138) Comotti, A.; Simonutti, R.; Stramare, S.; Sozzani, P. *Nanotechnology* **1999**, *10*, 70-76.
- (139) Olivieri, A. C. *J. Magn. Reson.* **1989**, *81*, 201-205.
- (140) Zumbulyadis, N.; Henrichs, P. M.; Young, R. H. *J. Chem. Phys.* **1981**, *75*, 1603-1611.
- (141) Hexem, J. G.; Frey, M. H.; Opella, S. J. *J. Chem. Phys.* **1982**, *77*, 3847-3856.
- (142) Wrackmeyer, B.; Garcia-Baez, E.; Zuno-Cruz, F. J.; Sanchez-Cabrera, G.; Rosales, M. J. *Z. Naturforsch., B* **2000**, *55*, 185-188.
- (143) Duddeck, H. *Prog. Nucl. Magn. Reson. Spectrosc.* **1995**, *27*, 1-323.
- (144) Duddeck, H. *Annu. Rep. NMR Spectrosc.* **2004**, *52*, 105-166.
- (145) Grossmann, G.; Potrzebowski, M. J.; Fleischer, U.; Krüger, K.; Malkina, O. L.; Ciesielski, W. *Solid State Nucl. Magn. Reson.* **1998**, *13*, 71-85.
- (146) Colquhoun, I. J.; McFarlane, W. *Dalton Trans.* **1981**, 658-660.
- (147) Barrie, P. J.; Clark, R. J. H.; Withnall, R.; Chung, D.-Y.; Kim, K.-W.; Kanatzidis, M. G. *Inorg. Chem.* **1994**, *33*, 1212-1216.
- (148) Carson, G. K.; Dean, P. A. W. *Inorg. Chim. Acta* **1982**, *66*, 37-39.
- (149) Dean, P. A. W.; Hughes, M. K. *Can. J. Chem.* **1980**, *58*, 180-190.
- (150) Grim, S. O.; Walton, E. D.; Satek, L. C. *Inorg. Chim. Acta* **1978**, *27*, L115-L116.
- (151) Novosad, J.; Necas, M.; Marek, J.; Veltsistas, P.; Papadimitriou, C.; Haiduc, I.; Watanabe, M.; Woollins, J. D. *Inorg. Chim. Acta* **1999**, *290*, 256-260.
- (152) Dreeskamp, H.; Stegmeier, G. *Z. Naturforsch., A* **1967**, *22*, 1458-1464.
- (153) Kennedy, J. D.; McFarlane, W.; Pyne, G. S.; Wrackmeyer, B. *Dalton Trans.* **1975**, 386-390.

- (154) Kennedy, J. D.; McFarlane, W.; Wrackmeyer, B. *Inorg. Chem.* **1976**, *16*, 1299-1302.
- (155) Wrackmeyer, B.; Horchler, K. *Magn. Reson. Chem.* **1990**, *28*, 56-61.
- (156) Wrackmeyer, B.; Zhou, H. *Magn. Reson. Chem.* **1990**, *28*, 1066-1069.
- (157) Christendat, D.; Butler, I. S.; Gilson, D. F. R.; Morin, F. G. *Can. J. Chem.* **1999**, *77*, 1892-1898.
- (158) Willans, M. J.; Demko, B. A.; Wasylshen, R. E. *Phys. Chem. Chem. Phys.* **2006**, *8*, 2733-2743.
- (159) Groombridge, C. J. *Magn. Reson. Chem.* **1993**, *31*, 380-387.
- (160) Natan, M. J.; Millikan, C. F.; Wright, J. G.; O'Halloran, T. V. *J. Am. Chem. Soc.* **1990**, *112*, 3255-3257.
- (161) Grim, S. O.; Walton, E. D.; Satek, L. C. *Can. J. Chem.* **1980**, *58*, 1476-1479.

## Chapter 7

### Comparing Main Group and Transition Metal Square-Planar

### Complexes of the Diselenoimidodiphosphinate Anion: A Solid-State

### NMR Investigation of $M[N(\text{}^i\text{Pr}_2\text{PSe})_2]_2$ ( $M = \text{Se, Te; Pd, Pt}$ )<sup>†</sup>

#### 7.1 Introduction

The diselenoimidodiphosphinate anion,  $[N(\text{R}_2\text{PSe})_2]^-$  ( $\text{R} = \text{alkyl}$ ), a bidentate ligand often referred to as the inorganic analogue of acetylacetonate, has been utilized in the preparation of homoleptic square-planar complexes of both main-group<sup>1-5</sup> and transition metal<sup>6-8</sup> centers. Dichalcogenoimidodiphosphinato complexes,  $M^{n+}[N(\text{R}_2\text{PE})_2]_n$  ( $\text{E} = \text{O, S, Se, Te}$ ), are known to exhibit various binding geometries about the metal center that depend on the choice of chalcogen, organic group, and complexing metal.<sup>9-13</sup> The flexibility of the dichalcogenoimidodiphosphinate system has been called one of its greatest advantages, permitting the EPNPE skeleton to adjust to various coordination geometries desired by the central metal,<sup>11,14</sup> along with the large chalcogen-chalcogen ‘bite’, which aids in forming regular coordination spheres with large central atoms.<sup>15</sup> These bidentate ligands have found applications as single-source precursors for solid-state metal chalcogenide materials,<sup>16-34</sup> in the search for stereochemically active lone pairs,<sup>2,3,6,8,11,35-46</sup> in catalysis,<sup>47-49</sup> and in metal extraction processes,<sup>13,43,50-57</sup> as lanthanide shift reagents,<sup>43,58-62</sup> luminescent materials,<sup>63</sup> and as enzyme mimetics.<sup>64-66</sup>

---

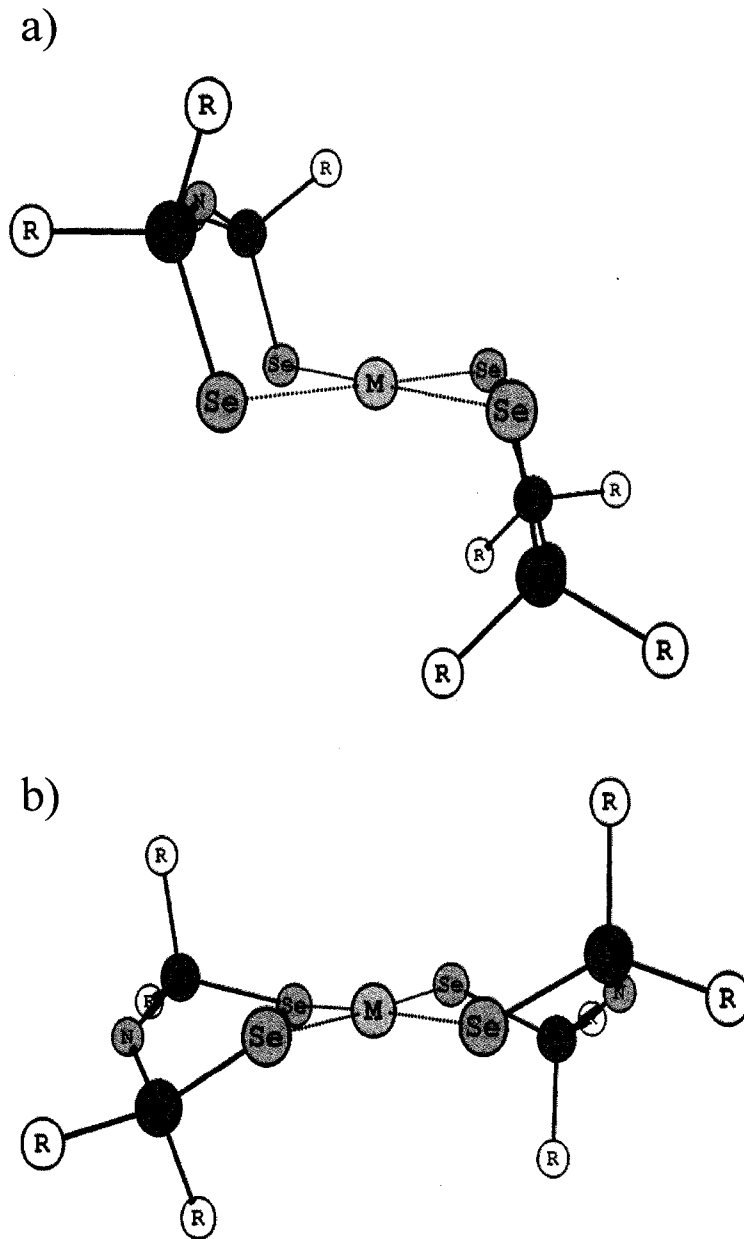
<sup>†</sup> A version of this chapter has been accepted for publication: B.A. Demko and R.E. Wasylishen, *Inorganic Chemistry*, **2008**, *47*, 2786-2797.

Considerable interest persists for square-planar complexes, yet appropriate comparisons between main-group and transition metal centers are difficult as few analogous systems exist. The homoleptic Group 10 and 16 tetraisopropyldiselenoimido-diphosphinato complexes,  $M[N(^iPr_2PSe)_2]_2$  ( $M = Pd, Pt$  and  $Se, Te$ , respectively), offer a rare opportunity to probe the differences between main-group and traditional transition metal square-planar systems. Solid-state NMR is aptly suited for investigating the detailed molecular environments of the diselenoimidodiphosphinato complexes. In the present study, a combined density functional theory, DFT, and experimental solid-state  $^{31}P$ ,  $^{77}Se$ ,  $^{125}Te$ , and  $^{195}Pt$  NMR investigation of the square-planar  $M[N(^iPr_2PSe)_2]_2$  ( $M = Pd, Pt; Se, Te$ ) complexes is reported.

## 7.2 Experimental

### 7.2.1 Sample Preparation

Iminobis(diisopropylphosphine selenide),  $HN(^iPr_2PSe)_2$ , was prepared according to the two-step, condensation followed by oxidation, procedure outlined in Scheme 5.2.<sup>67</sup> The transition metal complexes were obtained by slow addition of the corresponding dichloro(1,5-cyclooctadiene)metal(II) (Aldrich) into a basic methanol solution of tetraisopropyldiselenoimidodiphosphinate,  $[N(^iPr_2PSe)_2]^-$ , as described by Scheme 6.1.<sup>8</sup> The main-group complexes were prepared in a similar fashion from  $[N(^iPr_2PSe)_2]^-$  with  $Se[S_2P(O^iPr)_2]_2$  and  $Te(thiourea)_4Cl_2 \cdot 2H_2O$ , respectively according to literature procedures.<sup>3,4</sup> Crystal structures have previously been determined for the square-planar complexes,  $M[N(^iPr_2PSe)_2]_2$  ( $M = Pt$ ,<sup>8</sup>  $Se$ ,<sup>3</sup>  $Te$ <sup>4</sup>), and a representation of their structures is given in Figure 7.1. All structures indicate a single  $M[N(^iPr_2PSe)_2]_2$  molecule in the



**Figure 7.1** Representation of the solid-state structures of  $M[N(R_2PSe)_2]_2$  ( $R = {}^i\text{Pr}, \text{Ph}$ ) (a)  $M = \text{Se}, \text{Te}$ ; (b)  $M = \text{Pd}, \text{Pt}$ .

asymmetric unit; however, the main-group centered structures (Figure 7.1a) crystallize within the  $P2_1/c$  space group while the transition metal structure (Figure 7.1b) crystallizes in the  $C2/c$  space group.

## 7.2.2 NMR Experiments

Solution  $^{77}\text{Se}$  and  $^{195}\text{Pt}$  NMR spectra for a  $\text{CDCl}_3$  solution of  $\text{Pt}[\text{N}(\text{}^i\text{Pr}_2\text{PSe})_2]_2$  were acquired, at 76.3 MHz and 85.6 MHz respectively, on a 9.4 T spectrometer in order to deduce the magnitudes of the platinum-selenium and platinum-phosphorus indirect spin-spin coupling constants.

Solid-state NMR investigations of powdered samples of  $\text{M}[\text{N}(\text{}^i\text{Pr}_2\text{PSe})_2]_2$  ( $\text{M} = \text{Pd, Pt; Se, Te}$ ) were obtained on 4.7 T, 7.0 T and 11.7 T NMR spectrometers. The samples were packed in 4 mm (7.0 T and 11.7 T) and 7.5 mm (4.7 T) o.d. zirconium oxide rotors and were placed within probes suitable for magic angle spinning, MAS, NMR experiments. A variable amplitude cross polarization, VACP, pulse sequence was used to acquire all spectra.<sup>68</sup> Proton decoupling fields of approximately 60 kHz were achieved via two-pulse phase-modulation, TPPM.<sup>69</sup> The  $^{31}\text{P}$  NMR spectra were referenced with respect to 85%  $\text{H}_3\text{PO}_4$  (*aq*) by setting the isotropic  $^{31}\text{P}$  NMR peak of solid  $(\text{NH}_4)\text{H}_2\text{PO}_4$  to 0.81 ppm.<sup>70</sup> Similarly,  $^{77}\text{Se}$  NMR spectra were referenced to  $\text{Me}_2\text{Se}$  (*l*) by setting the isotropic peak of solid ammonium selenate to 1040.2 ppm.<sup>70,71</sup> Tellurium-125 NMR spectra were referenced with respect to a dimethyl telluride by setting the high frequency solid-state  $^{125}\text{Te}$  NMR peak of telluric acid to 692.2 ppm.<sup>70,72</sup> Solid-state  $^{195}\text{Pt}$  NMR spectra were referenced to potassium hexachloroplatinate by setting the  $^{195}\text{Pt}$  NMR peak of solid  $\text{K}_2\text{Pt}(\text{OH})_6$  to 3476 ppm.<sup>70,73</sup>

Solid-state  $^{31}\text{P}$  NMR experiments were performed at Larmor frequencies of 81.0, 121.6 and 202.5 MHz, and at spinning frequencies ranging from 1.50 to 5.00 kHz. A total of between 32 and 512 scans were acquired per spectrum. Contact times between 1.5 and 6.5 ms, and pulse delays between 5 and 20 s were employed.

Solid-state  $^{77}\text{Se}$  NMR measurements were performed at Larmor frequencies of 38.2, 57.3 and 95.4 MHz, and at spinning frequencies ranging from 2.35 to 12.00 kHz. A total of between 880 and 31808 scans were acquired per spectrum. Contact times between 7.0 and 10.0 ms, and pulse delays between 5 and 11 s were employed.

Solid-state  $^{125}\text{Te}$  NMR experiments on  $\text{Te}[\text{N}(\text{}^i\text{Pr}_2\text{PSe})_2]_2$  were performed at Larmor frequencies of 63.2 and 94.8 MHz, and at spinning frequencies ranging from 5.00 to 12.00 kHz. A total of between 25616 and 41520 scans were acquired per spectrum. Contact times between 8.0 and 11.0 ms, and pulse delays between 8 and 20 s were employed.

Solid-state  $^{195}\text{Pt}$  NMR experiments on  $\text{Pt}[\text{N}(\text{}^i\text{Pr}_2\text{PSe})_2]_2$  were performed at 42.8 MHz at spinning speeds ranging from 6.00 to 6.75 kHz. A total of between 19904 and 84656 scans were acquired per spectrum. Contact times and pulse delays of 11.0 ms and 9 s were employed, respectively.

The principal components of the respective phosphorus, selenium, tellurium and platinum chemical shift tensors,  $\delta_{11} \geq \delta_{22} \geq \delta_{33}$ , were determined from the experimental spectra via the procedure of Herzfeld and Berger.<sup>74,75</sup> All experimental solid-state NMR spectra were simulated using the determined values with the program WSOLIDS<sup>76</sup> to assess the quality of the obtained parameters. This procedure results in errors of  $\pm 0.2$  ppm in the isotropic chemical shift,  $\delta_{\text{iso}} = (1/3)(\delta_{11} + \delta_{22} + \delta_{33})$ , and errors in the principal components about 1-3% of the span,  $\Omega = \delta_{11} - \delta_{33}$ , of the respective chemical shift tensor. Another useful quantity for describing the appearance of chemical shift tensors is the skew,  $\kappa = 3(\delta_{22} - \delta_{\text{iso}})/\Omega$ .<sup>77</sup>

### 7.2.3 DFT Computations

Theoretical calculation of NMR parameters, particularly for heavier nuclei where interpretations are more difficult than those extracted from  $^{13}\text{C}$  NMR spectra, has become increasingly useful for spectroscopists.<sup>78</sup> Magnetic shielding tensors,  $\sigma$ , were calculated using the EPR<sup>79</sup> and NMR<sup>80-82</sup> modules of the Amsterdam Density Functional (ADF) program package,<sup>83-87</sup> and are tabulated in Appendix D. The Vosko-Wilk-Nusair<sup>88</sup> local density approximation with the Becke88-Perdew86<sup>89-91</sup> generalized gradient approximation were used for the exchange-correlation functional. ADF numerical integration parameters were increased from the default, 4.0, setting *accint* = 5.0 and *accsph* = 6.0 to better describe the core regions of the molecular orbitals. Scalar as well as scalar with spin-orbit relativistic corrections were carried out based on the implementation of the zeroth order regular approximation, ZORA, formalism.<sup>92-95</sup> Triple- $\zeta$  doubly polarized, TZ2P, Slater-type ZORA basis sets were used for all atoms except for hydrogen, where double- $\zeta$  quality, DZ, basis functions were utilized. While the X-ray structures of the  $\text{M}[\text{N}(\text{}^i\text{Pr}_2\text{PSe})_2]_2$  ( $\text{M} = \text{Se}, \text{Te}, \text{Pt}$ ) complexes were used directly, optimized structures of  $\text{Pd}[\text{N}(\text{}^i\text{Pr}_2\text{PSe})_2]_2$  as well as the chemical shift reference compounds were obtained using non-relativistic ADF basis sets of comparable quality to those used in the magnetic shielding tensor calculations. Relativistic geometry optimizations were not performed due to a noted energy-potential mismatch in the ZORA approach.<sup>87</sup> The optimized structure of  $\text{Pd}[\text{N}(\text{}^i\text{Pr}_2\text{PSe})_2]_2$  converged at a complex very similar to the platinum analogue (Figure 7.1b), an expected result given that the palladium and platinum complexes of the phenyl-derivatized ligand,  $\text{M}[\text{N}(\text{Ph}_2\text{PSe})_2]_2$  ( $\text{M}$



= Pd, Pt), are known to be isostructural.<sup>6,7</sup> The corresponding calculated chemical shift tensors were calculated from the magnetic shielding tensors using the relationship:

$$\delta_{ii}(sample) = \frac{\sigma_{iso}(ref) - \sigma_{ii}(sample)}{1 - \sigma_{iso}(ref)} \quad [7.1]$$

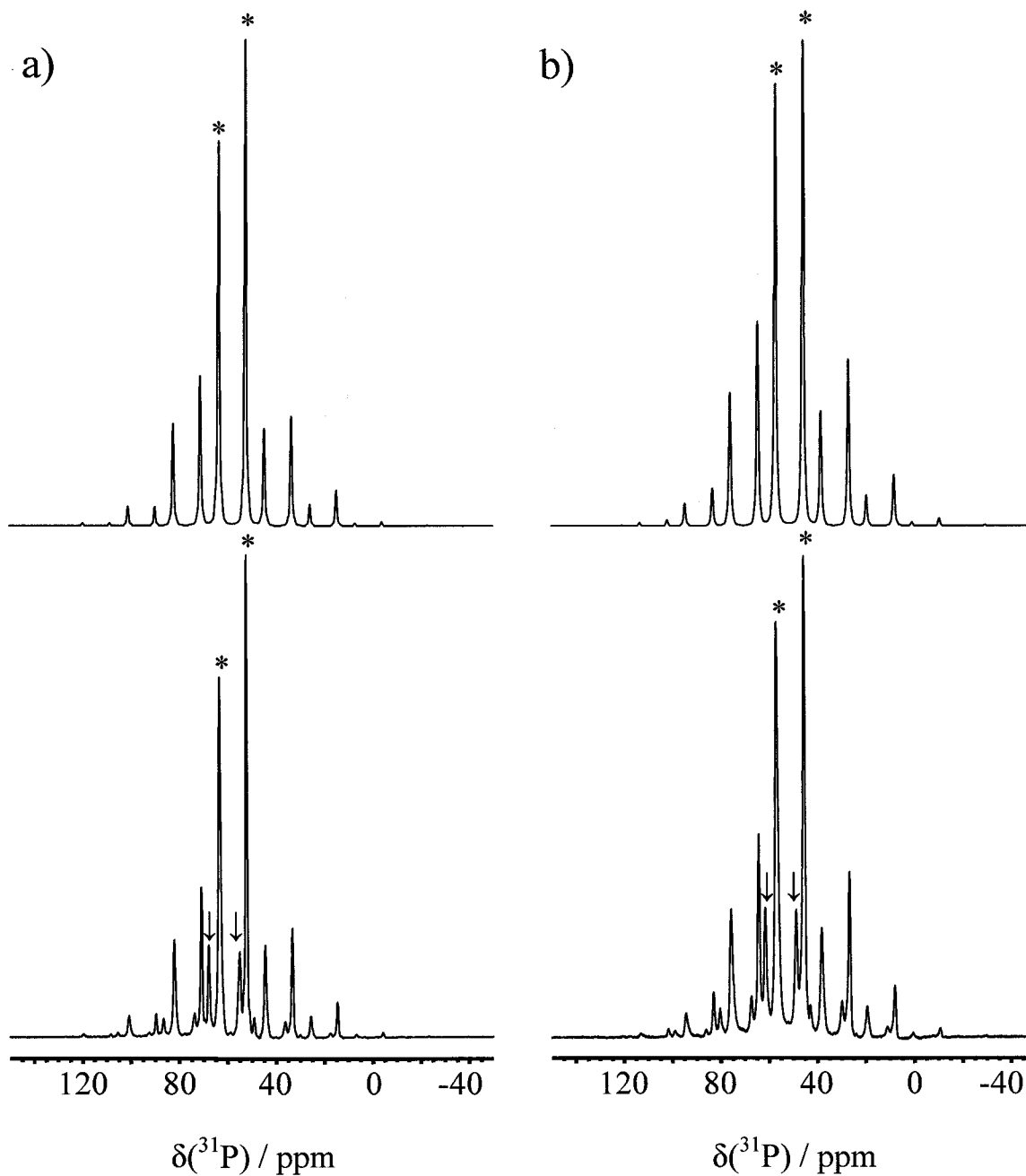
where  $\sigma_{iso}(ref)$  is the isotropic shielding of a standard reference. The absolute shielding scale for  $^{31}\text{P}$  has been determined, and the value of  $\sigma_{iso}(85\% \text{H}_3\text{PO}_{4(aq)})$  is 328.35 ppm.<sup>96</sup> Magnetic shielding calculations on optimized structures of the selenium, tellurium, and platinum reference compounds, dimethyl selenide, dimethyl telluride, and the hexachloroplatinate anion, respectively, have been performed; however, as solvent and vibrational effects have been omitted the calculations serve only as a qualitative understanding of the chemical shift tensors obtained. We have previously investigated the selenium chemical shift tensors in a wide range of compounds, and found the absolute isotropic magnetic shielding constant for a neat liquid of dimethyl selenide at 23 °C to be 1580 ppm for calculations with scalar relativistic corrections (hereafter denoted SR) included, and 1745 ppm for calculations including scalar with spin-orbit relativistic corrections (hereafter SO).<sup>97</sup> Using a similar method  $\sigma_{iso}(ref) = 2352$  ppm (SR) and 3060 ppm (SO) were calculated for the absolute Te shielding from a non-relativistically optimized structure of  $\text{Me}_2\text{Te}$ , in good agreement with an earlier study of calculated  $^{125}\text{Te}$  chemical shifts.<sup>98</sup> The absolute Pt shieldings,  $\sigma_{iso}(ref)$ , were calculated on an optimized structure of  $[\text{PtCl}_6]^{2-}$ , yielding values of -3471 ppm (SR) and -338 ppm (SO).

### 7.3 Results & Discussion

The square-planar complexes investigated,  $M[N(^1Pr_2PSe)_2]_2$  ( $M = Pd, Pt; Se, Te$ ) as determined by computational chemistry or X-ray crystallography, display distinct structures depending on the central atom. The selenium and tellurium square-planar complexes are isostructural possessing a step-like structure with approximate  $90^\circ$  angles between the SePNPSe planes and the  $MSe_4$  plane; whereas in the palladium and platinum complexes, the SePNPSe planes are considerably closer to coplanar with the  $MSe_4$  plane (Figure 7.1). The  $MSe_2P_2N$  heterocycles for the Pd(II) and Pt(II) complexes possess a pseudo-boat conformation; however, the six-membered rings of the Se(II) and Te(II) complexes have a distorted-chair conformation. Symmetry elements within each presented square-planar complex impose magnetic equivalence on two pairs of phosphorus and selenium environments, and as a result only two unique phosphorus and selenium sites are expected in the corresponding solid-state NMR spectra. The results of the solid-state  $^{31}P$  NMR investigation of the  $M[N(^1Pr_2PSe)_2]_2$  ( $M = Pd, Pt; Se, Te$ ) complexes will be presented first, followed by the results of the solid-state  $^{77}Se$  NMR spectra from the diselenoimidodiphosphinato selenium environments of the square-planar complexes. Finally the parameters from the solid-state  $^{77}Se$ ,  $^{125}Te$ , and  $^{195}Pt$  NMR investigation for the central atom will be discussed. In each case, the results for the traditional transition metal square-planar complexes will be presented first, followed by those for the main-group square-planar complexes highlighting any observed differences.

### 7.3.1 Solid-State $^{31}\text{P}$ NMR

The solid-state  $^{31}\text{P}$  NMR spectra for  $\text{M}[\text{N}(\text{iPr}_2\text{PSe})_2]_2$  ( $\text{M} = \text{Pd}, \text{Pt}$ ) are given in Figure 7.2 along with their simulations. In each of these samples there exists a small impurity evident in the solid-state  $^{31}\text{P}$  NMR spectra. The presence of these impurities did not hamper the spectral analysis, and no impurities were detected in the subsequent  $^{77}\text{Se}$  and  $^{195}\text{Pt}$  NMR investigations (vide infra), and thus no effort was made to remove the impurity within the sample. The phosphorus chemical shift tensor parameters are summarized in Table 7.1, along with estimations for the one-bond indirect selenium-phosphorus coupling constant,  $^1J(^{77}\text{Se}, ^{31}\text{P})_{\text{iso}}$ , from the observed satellite peaks in the  $^{31}\text{P}$  NMR spectrum. The isotropic chemical shifts and  $^1J(^{77}\text{Se}, ^{31}\text{P})_{\text{iso}}$  values agree well with those measured for chloroform solutions; 55.9 ppm and (-)590 Hz for the palladium complex, and 50.1 ppm and (-)536 Hz for the platinum complex.<sup>8</sup> Increasingly shielded phosphorus environments as the complexing metal becomes heavier has previously been reported for the tetraisopropyldiselenoimidodiphosphinato Group 12 complexes,  $\text{M}[\text{N}(\text{iPr}_2\text{PSe})_2]_2$  ( $\text{M} = \text{Zn}, \text{Cd}, \text{Hg}$ ).<sup>99</sup> The spans of the phosphorus chemical shift tensors ( $\leq 70$  ppm) are small, indicating a more symmetric electronic environment than those found in tris-organophosphine selenides, whose average  $\Omega$  is 124 ppm.<sup>100</sup> The DFT calculations are insufficiently accurate for definitive assignments of  $^{31}\text{P}$  resonances to specific phosphorus sites within the respective crystal structures. The SR DFT calculations overestimate the isotropic  $^{31}\text{P}$  chemical shifts as well as the principal components,  $\delta_{ii}$ ; however, calculated phosphorus chemical shift tensors that include the SO term achieve much better agreement with the experimental values, Table 7.1. Given the similarity of the principal components of the  $^{31}\text{P}$  chemical shift tensors observed



**Figure 7.2** (a) VACP MAS  $^{31}\text{P}$  NMR spectrum (lower trace) for  $\text{Pd}[\text{N}(\text{}^1\text{Pr}_2\text{PSe})_2]_2$  and its simulation (upper trace). (b) VACP MAS  $^{31}\text{P}$  NMR spectrum (lower trace) for  $\text{Pt}[\text{N}(\text{}^1\text{Pr}_2\text{PSe})_2]_2$  and its simulation (upper trace). Experimental conditions: 11.7 T, 128 scans, MAS at 3.8 kHz, 5 Hz of line broadening, a 3.0 ms contact time, and a 9 s recycle delay. The isotropic peaks are marked with an asterisk (\*), while those of impurities are marked with arrows ( $\downarrow$ ).

**Table 7.1** Experimental and theoretical solid-state  $^{31}\text{P}$  NMR parameters for  $\text{M}[\text{N}(\text{}^i\text{Pr}_2\text{PSe})_2]_2$  (M = Pd, Pt; Se, Te).

$\text{M}^{\text{II}}$		$\delta_{\text{iso}}$ ppm	$\delta_{11}$ ppm	$\delta_{22}$ ppm	$\delta_{33}$ ppm	$\Omega$ ppm	$^1J(^{77}\text{Se}, ^{31}\text{P})_{\text{iso}}$ <sup>a</sup> Hz
Pd	Expt <sup>b</sup>	52.1	78.4	58.8	19.3	59.1	-520
		63.3	92.5	64.3	33.0	59.5	-520
	SR	107.2	150.6	111.2	59.7	90.9	
		119.2	185.7	101.2	70.8	114.9	
	SO	67.4	90.0	82.5	29.8	60.2	
		84.3	125.9	76.8	50.1	75.8	
Pt	Expt <sup>b</sup>	45.6	78.4	49.5	8.9	69.5	-480
		57.0	86.0	60.2	24.6	61.4	-480
	SR	95.3	140.1	94.8	51.0	89.1	
		112.1	178.1	82.0	76.1	102.0	
	SO	51.1	80.6	59.4	13.2	67.4	
		73.4	109.0	73.9	37.3	71.7	
Se	Expt <sup>c</sup>	52.8	82.3	63.7	12.3	70.0	-520
		55.7	84.1	59.2	23.6	60.5	-540
	SR	115.0	162.1	111.7	71.2	90.8	
		118.6	159.1	120.1	76.6	82.4	
	SO	56.0	89.2	63.3	15.6	73.6	
		58.4	88.3	62.9	23.8	64.4	
Te	Expt <sup>c</sup>	50.1	77.7	61.0	11.5	66.2	-500
		52.0	80.2	57.0	18.9	61.3	-530
	SR	89.8	127.0	89.1	56.4	70.6	
		91.3	134.4	89.4	50.2	84.2	
	SO	53.8	79.4	60.5	21.4	58.0	
		55.2	85.9	64.5	15.0	70.9	

<sup>a</sup> For directly bonded selenium-77 and phosphorus-31 spin pairs, signs of  $^1J(^{77}\text{Se}, ^{31}\text{P})_{\text{iso}}$  are known to be negative for numerous analogous systems.<sup>101,102</sup> Estimated errors of  $^1J(^{77}\text{Se}, ^{31}\text{P})_{\text{iso}}$  are  $\pm 10$ -20 Hz.

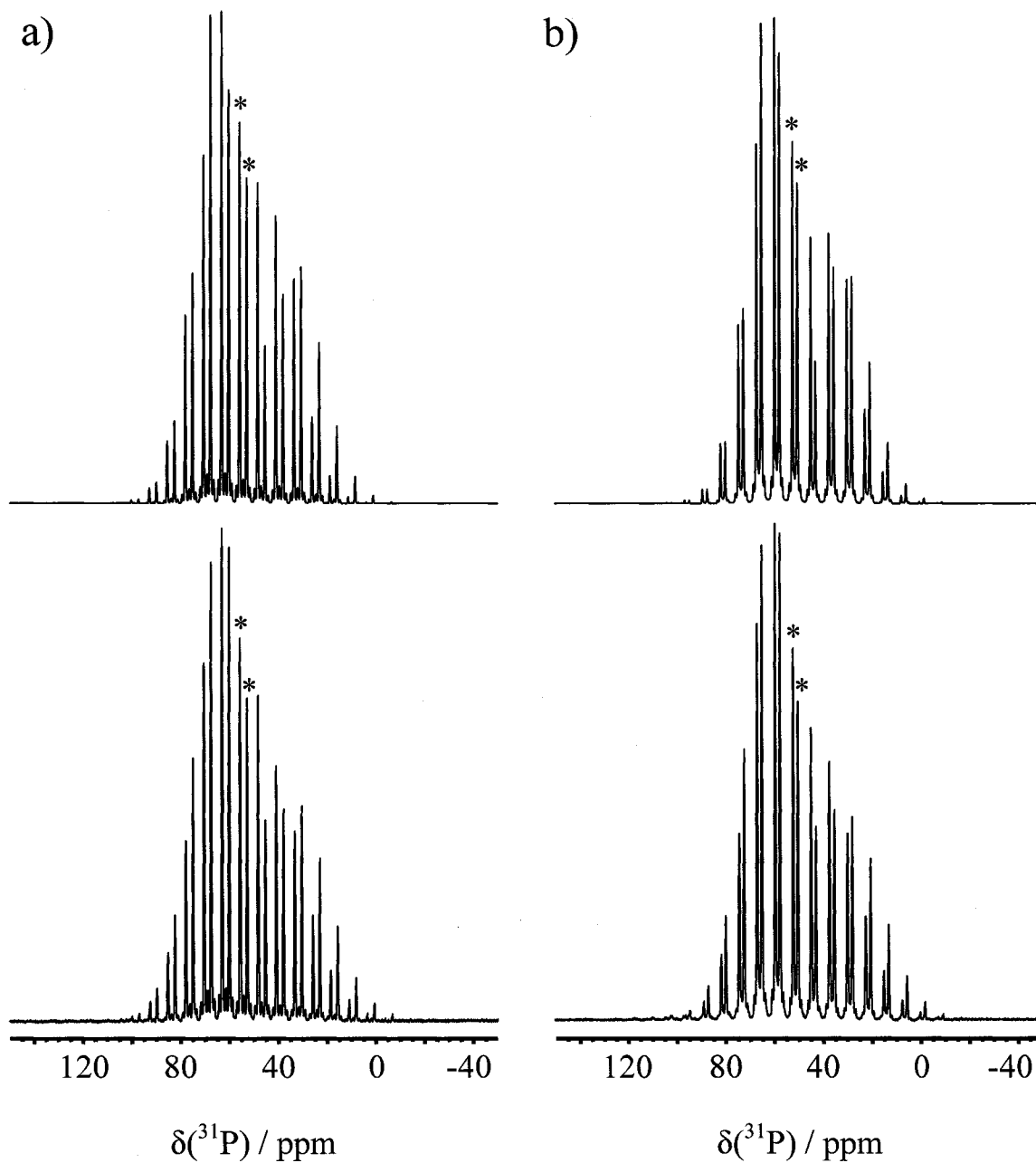
<sup>b</sup> Estimated errors in  $\delta_{ii}$  are  $\pm 1.2$  ppm.

<sup>c</sup> Estimated errors in  $\delta_{ii}$  are  $\pm 0.8$  ppm.

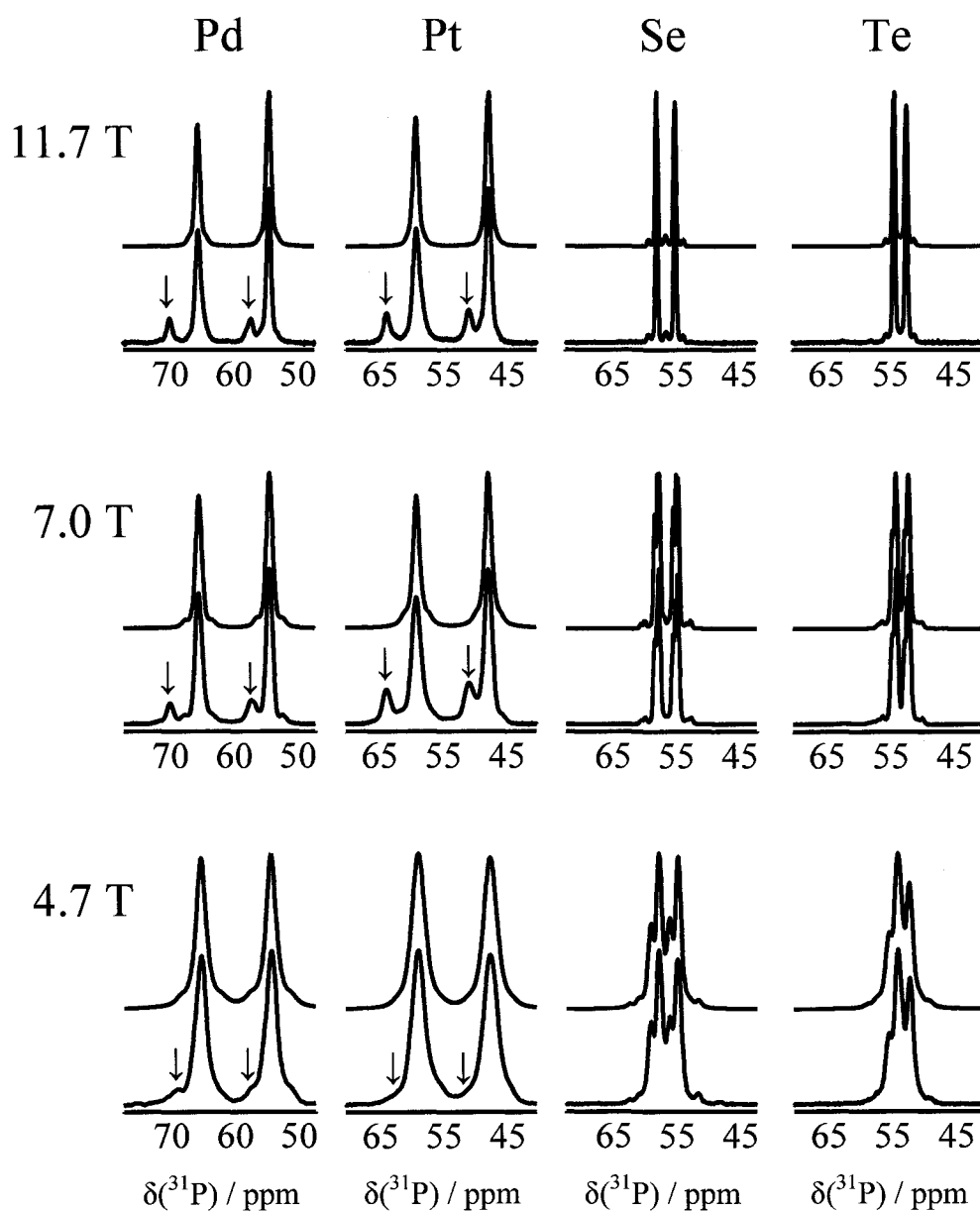
experimentally for the palladium and platinum complexes, it is not surprising that the tensors have similar calculated orientations for all of the phosphorus environments. The direction of  $\delta_{11}$  is oriented perpendicular to the local Se-P-N plane, while  $\delta_{33}$  lies approximately parallel to the phosphorus-nitrogen bond axis. The intermediate principal component,  $\delta_{22}$ , nearly bisects the Se-P-N angle. Similar orientations have been calculated for the phosphorus chemical shift tensors in  $\text{M}[\text{N}(\text{}^i\text{Pr}_2\text{PSe})_2]_2$  (M = Zn, Cd, Hg) complexes.<sup>99</sup>

The corresponding  $^{31}\text{P}$  VACP MAS spectra for the  $\text{M}[\text{N}(\text{}^i\text{Pr}_2\text{PSe})_2]_2$  ( $\text{M} = \text{Se}, \text{Te}$ ) complexes are given in Figure 7.3. The isotropic chemical shifts and  $^1J(^{77}\text{Se}, ^{31}\text{P})_{\text{iso}}$  values are in agreement with the chloroform solution  $^{31}\text{P}$  NMR values of 69.9 ppm and (-)526 Hz,<sup>3</sup> and 58.7 ppm and (-)528 Hz<sup>4</sup> for the selenium and tellurium complexes, respectively. Similar values of  $\delta_{\text{iso}}(^{31}\text{P})$  and  $\Omega(^{31}\text{P})$  to those found in the Pd(II) and Pt(II) complexes are obtained, as well as a slight increase in phosphorus shieldings in the tellurium relative to the selenium complex. The SR calculated phosphorus chemical shift tensors are also overestimated for the Se(II) and Te(II) complexes; whereas, the SO calculations again achieve improved agreement with experimental values. The orientations found at both the SR and SO levels are nearly identical to those described for the Pd(II) and Pt(II) complexes.

The principal difference observed between the transition metal and main-group square-planar complexes is apparent in the  $^{31}\text{P}$  NMR spectra at lower applied magnetic fields. Figure 7.4 displays the isotropic  $^{31}\text{P}$  regions for the four complexes at 4.7 T, 7.0 T and 11.7 T. While the two unique phosphorus environments are readily discernable for all four complexes in the isotropic region of the spectra at 11.7 T, the spectra for the selenium and tellurium complexes at the lower magnetic fields show significant fine structure as well as line broadening. The lineshapes observed at 4.7 T and 7.0 T result from the adjacent  $^{14}\text{N}$  ( $I = 1$ , N.A. = 99.6%), which has previously been shown to influence solid-state  $^{31}\text{P}$  NMR spectra of  $\text{M}[\text{N}(\text{}^i\text{Pr}_2\text{PSe})_2]_2$  ( $\text{M} = \text{Zn}, \text{Cd}, \text{Hg}$ ) complexes.<sup>99</sup> The energy levels of nitrogen-14 are quantized by both the applied magnetic field as well as the electric field gradient, EFG, at the  $^{14}\text{N}$  nucleus.<sup>103-105</sup> As a result, MAS can not completely average the dipolar interaction between  $^{14}\text{N}$  and  $^{31}\text{P}$  and



**Figure 7.3** (a) VACP MAS  $^{31}\text{P}$  NMR spectrum (lower trace) for  $\text{Se}[\text{N}(\text{}^1\text{Pr}_2\text{PSe})_2]_2$  and its simulation (upper trace). (b) VACP MAS  $^{31}\text{P}$  NMR spectrum (lower trace) for  $\text{Te}[\text{N}(\text{}^1\text{Pr}_2\text{PSe})_2]_2$  and its simulation (upper trace). Experimental conditions: 11.7 T, 128 scans, MAS at 1.5 kHz, 5 Hz of line broadening, a 3.0 ms contact time, and a 9 s recycle delay. The isotropic peaks are marked with an asterisk (\*).



**Figure 7.4** Experimental (lower trace) isotropic  $^{31}\text{P}$  NMR regions, with spinning sidebands added to the isotropic region, and simulated (upper trace) for  $\text{M}[\text{N}(\text{Pr}_2\text{PSe})_2]_2$  ( $\text{M} = \text{Pd}, \text{Pt}; \text{Se}, \text{Te}$ ) at 4.7 T, 7.0 T, and 11.7 T. The isotropic peaks of the impurities are marked with arrows ( $\downarrow$ ).

“residual dipolar coupling” effects between the two nuclei are manifested in solid-state  $^{31}\text{P}$  NMR spectra. This broadening effect is inversely proportional to the Larmor



frequency of the quadrupolar nucleus,  $\nu_{L, N} = \gamma_N B_0 / 2\pi$ ,<sup>103-105</sup> and thus produces a smaller effect at higher applied magnetic fields.

Analyses of these <sup>31</sup>P NMR spectra can yield values of the effective dipolar coupling constant,  $R_{eff}$ , and the isotropic indirect spin-spin coupling constant,  ${}^1J(^{31}\text{P}, {}^{14}\text{N})_{iso}$ , as well as parameters describing the EFG at the nitrogen nucleus. The direct dipolar coupling constant,  $R_{DD}$ , is related to  $R_{eff}$  by

$$R_{eff} = R_{DD} - \Delta J / 3 \quad [7.2]$$

where  $\Delta J = J_{33} - (J_{11} + J_{22})/2$  is the anisotropy of the phosphorus-nitrogen  $J$  tensor, and

$$R_{DD} = \left( \frac{\mu_0}{4\pi} \right) \left( \frac{\hbar}{2\pi} \right) \left( \frac{\gamma_P \gamma_N}{\langle r_{PN}^3 \rangle} \right) \quad [7.3]$$

where  $\mu_0$  is the permeability of a vacuum,  $\gamma_P$  and  $\gamma_N$  are the magnetogyric ratios of <sup>31</sup>P and <sup>14</sup>N, and  $\langle r_{PN}^3 \rangle$  is the motionally-averaged cube of the distance between phosphorus and nitrogen.<sup>106,107</sup> The contributions from  $\Delta J$  are expected to be negligible given the small magnitude for  ${}^1J(^{31}\text{P}, {}^{15}\text{N})_{iso}$  determined for iminobis(diphenylphosphine selenide),  $\text{HN}(\text{Ph}_2\text{PSe})_2$ ,<sup>108</sup> and similarly small values of  ${}^1J(^{31}\text{P}, {}^{14}\text{N})_{iso}$  found previously for the Group 12 complexes of  $[\text{N}(\text{Pr}_2\text{PSe})_2]$ .<sup>99</sup> As a result  $R_{eff}$  can be estimated directly from the phosphorus-nitrogen nuclear separation determined by X-ray diffraction. It is not possible to assign a specific  $R_{DD}$ , i.e., a specific phosphorus-nitrogen distance, to a specific <sup>31</sup>P NMR resonance, so an average  $r_{PN}$  was calculated from the two P-N distances within each complex. The resulting average  $R_{DD}$  was used in the simulations

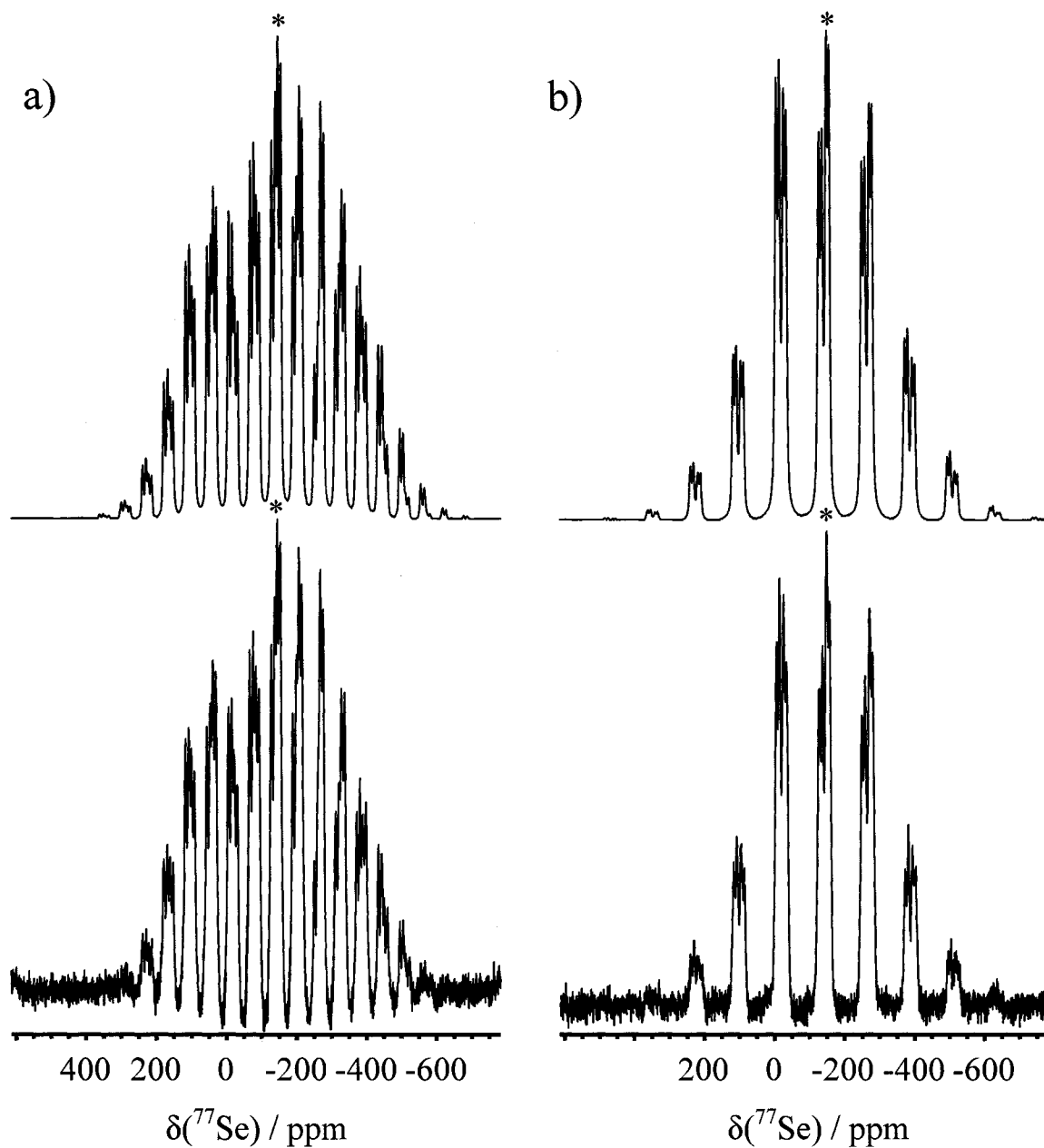
for both sites in the  $^{31}\text{P}$  NMR spectra. The quadrupolar parameters required to describe the solid-state NMR spectrum of a spin- $1/2$  nucleus spin-spin coupled to a quadrupolar nucleus include the quadrupolar coupling constant,  $C_Q = eQV_{ZZ}/h$ , where  $e$  is the elementary charge,  $Q$  is the nuclear quadrupole moment, and  $V_{ZZ}$  is the largest component of the EFG tensor at the nucleus. Also required are the Euler angles,  $\alpha$  and  $\beta$ , which describe the orientation of the dipolar vector,  $r_{\text{PN}}$ , within the principal axis system of the EFG tensor at the quadrupolar nucleus. Preliminary values of  $C_Q$ , as well as the angles  $\alpha$  and  $\beta$  used herein were obtained from DFT calculations of the nitrogen EFG tensors. For reasons analogous to those given above for  $R_{\text{DD}}$ , the simulations of both phosphorus lineshapes in each spectrum were obtained using a single value of  $^1J(^{31}\text{P}, ^{14}\text{N})_{\text{iso}}$ ,  $C_Q$ ,  $\alpha$ , and  $\beta$ . The effect of using single average values of the residual dipolar coupling parameters does not appear to significantly impair the quality of the simulations for the  $^{31}\text{P}$  NMR spectra of the Se(II) and Te(II) complexes given in Figure 7.4, where accurate lineshapes are achieved at all three applied magnetic fields employed.

For  $\text{Se}[\text{N}(\text{Pr}_2\text{PSe})_2]_2$ ,  $R_{\text{DD}} = 890(50)$  Hz from the average  $r_{\text{PN}}$  distance of  $1.583(30)$  Å,<sup>3</sup> and the azimuthal and polar angles were  $90(3)^\circ$  and  $18(5)^\circ$  respectively. The value of  $C_Q$  was  $2.50(20)$  MHz, and the indirect spin-spin coupling constant,  $^1J(^{31}\text{P}, ^{14}\text{N})_{\text{iso}}$ , was  $15(4)$  Hz. The parameters pertaining to residual dipolar coupling used in the simulations of the  $^{31}\text{P}$  NMR spectra of  $\text{Te}[\text{N}(\text{Pr}_2\text{PSe})_2]_2$  were  $R_{\text{DD}} = 890(50)$  Hz,  $r_{\text{PN}} = 1.583(30)$  Å,<sup>4</sup>  $\alpha = 90(3)^\circ$ ,  $\beta = 16(5)^\circ$ ,  $C_Q = 2.55(20)$  MHz,  $^1J(^{31}\text{P}, ^{14}\text{N})_{\text{iso}} = 16(5)$  Hz. These residual dipolar coupling parameters are consistent with those found in other diselenoimidodiphosphinato complexes,<sup>99</sup> and the magnitude of the quadrupolar coupling constants are reasonable in comparison with other phosphorus-nitrogen systems where

values of  $C_Q$  are not expected to exceed 4.0 MHz.<sup>109</sup> The EFG tensors at  $^{14}\text{N}$  in the selenium and tellurium complexes are oriented similarly, such that the largest component,  $V_{ZZ}$ , lies within the P-N-P plane perpendicular to the P-N-P bisector, the intermediate component is parallel to the direction of the formal electron ‘lone pair’ on the nitrogen, and the smallest EFG component is perpendicular to the P-N-P plane. In contrast the calculated  $^{14}\text{N}$  EFG tensors for the palladium and platinum complexes, despite possessing similar calculated quadrupolar coupling constants to those in the Se(II) and Te(II) complexes, are oriented such that it is the largest component that is perpendicular to the P-N-P plane, and the smallest EFG component within the P-N-P plane perpendicular to the P-N-P bisector. Such a tensor results in values of  $25^\circ$  for  $\alpha$ , and  $90^\circ$  for  $\beta$ , which would not produce discernable fine structure in the  $^{31}\text{P}$  MAS lineshapes due to residual dipolar coupling from nitrogen even at low magnetic field strengths.

### 7.3.2 Solid-State $^{77}\text{Se}$ NMR Results of the Diselenoimidodiphosphinato Selenium Environments

The entire spinning-sideband manifolds for the solid-state  $^{77}\text{Se}$  NMR spectra for the transition metal square-planar complexes investigated at 7.0 T are given in Figure 7.5. The solid-state NMR parameters from simulations of the spectra for the diselenoimidodiphosphinato selenium environments are detailed in Table 7.2. Differences in the relative intensities of the respective  $J$ -coupled spectra were insufficient for the extraction of meaningful values of the selenium-phosphorus coupling parameters,  $R_{eff}$  and  $\Delta J$ . The  $^{77}\text{Se}$  NMR parameters for the palladium and platinum complexes are very similar with isotropic chemical shifts that are all within 20 ppm, indicating very



**Figure 7.5** (a) VACP MAS  $^{77}\text{Se}$  NMR spectra for  $\text{Pd}[\text{N}(\text{}^1\text{Pr}_2\text{PSe})_2]_2$ . Experimental conditions: 7.0 T, 30128 scans, spinning at 3.5 kHz, 20 Hz of line broadening, a 9.0 ms contact time, and an 8 s recycle delay. (b) VACP MAS  $^{77}\text{Se}$  NMR spectra for  $\text{Pt}[\text{N}(\text{}^1\text{Pr}_2\text{PSe})_2]_2$ . Experimental conditions: 7.0 T, 15560 scans, spinning at 7.0 kHz, 20 Hz of line broadening, a 10.0 ms contact time, and a 5 s recycle delay. Simulated spectra are shown in the upper traces. The isotropic peaks are marked with an asterisk (\*).

**Table 7.2** Experimental and theoretical solid-state  $^{77}\text{Se}$  NMR parameters for the anion of  $\text{M}[\text{N}(\text{Pr}_2\text{PSe})_2]_2$  (M = Pd, Pt; Se, Te).

$\text{M}^{\text{II}}$	$\delta_{\text{iso}}$ ppm	$\delta_{11}$ ppm	$\delta_{22}$ ppm	$\delta_{33}$ ppm	$\Omega$ ppm	$^1J(^{77}\text{Se}, ^{31}\text{P})_{\text{iso}}^{\text{a}}$ Hz	$^1J(\text{M}, ^{77}\text{Se})_{\text{iso}}$ Hz
Pd	Expt <sup>b</sup>	-133	228	-92	-536	764	-560
		-150	195	-194	-450	645	-485
	SR	55	447	113	-395	842	
		47	399	-22	-236	635	
	SO	48	422	142	-421	843	
		30	356	-23	-244	600	
Pt	Expt <sup>b</sup>	-132	209	-102	-502	711	-510
		-152	170	-152	-475	645	-450
	SR	-28	335	41	-459	794	
		-24	320	-52	-342	662	
	SO	-42	283	28	-436	719	
		-49	263	-72	-337	600	
Se	Expt <sup>c</sup>	120	383	108	-131	514	$\pm 405$
		32	333	14	-250	583	$\pm 435$
	SR	178	558	188	-211	769	
		111	563	132	-363	926	
	SO	120	500	82	-223	723	
		58	488	34	-347	835	
Te	Expt <sup>c</sup>	-11	162	24	-219	381	$\pm 1120$
		-105	163	-152	-327	490	$\pm 1270$
	SR	-17	174	23	-248	422	
		-78	232	-97	-368	600	
	SO	-18	207	-5	-255	461	
		-81	232	-123	-353	586	

<sup>a</sup> For directly bonded selenium-77 and phosphorus-31 spin pairs, signs of  $^1J(^{77}\text{Se}, ^{31}\text{P})_{\text{iso}}$  are known to be negative for numerous analogous systems.<sup>101,102</sup> Estimated errors of  $^1J(^{77}\text{Se}, ^{31}\text{P})_{\text{iso}}$  are  $\pm 5$ -10 Hz.

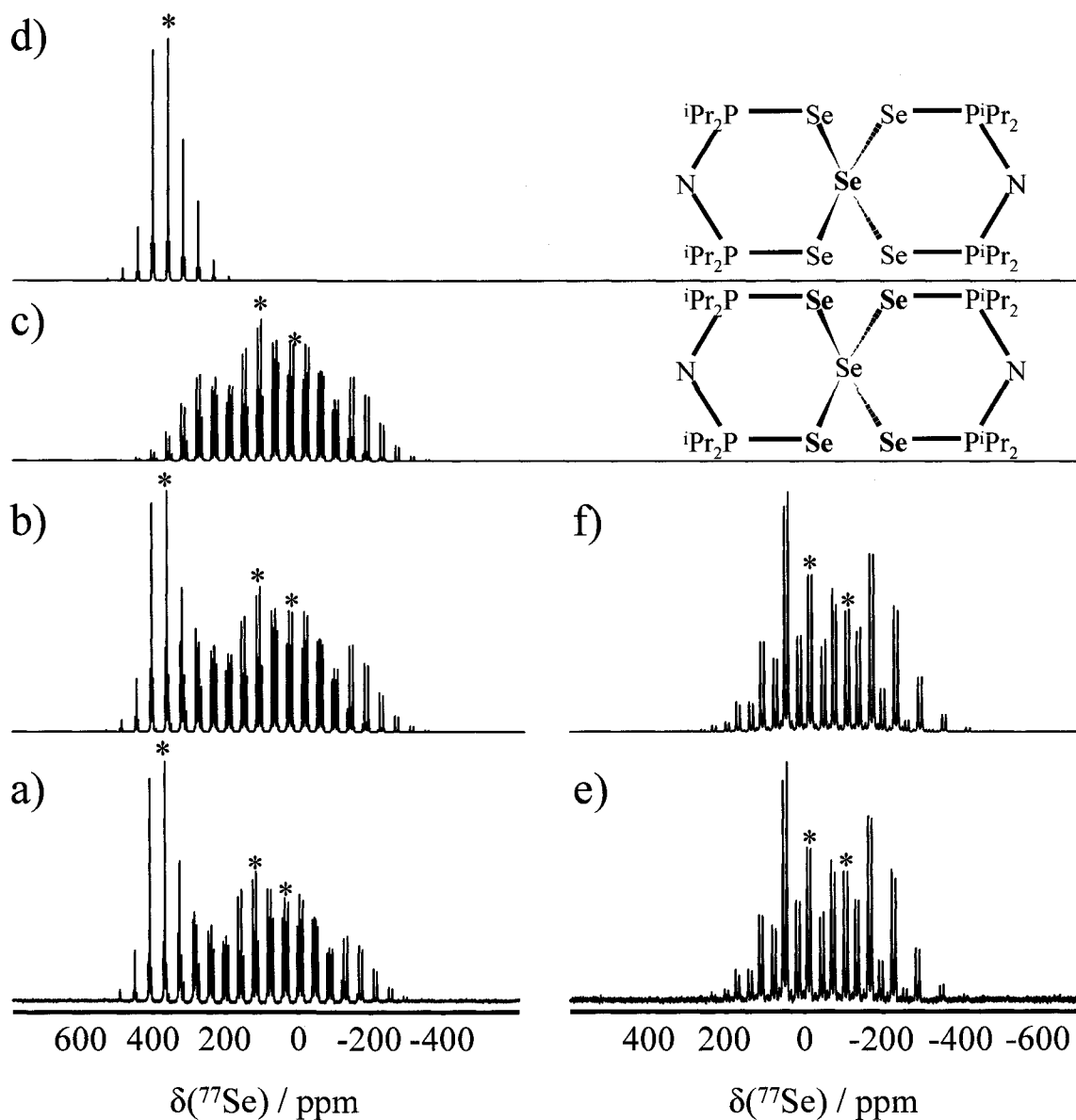
<sup>b</sup> Estimated errors in  $\delta_{ii}$  are  $\pm 14$  ppm.

<sup>c</sup> Estimated errors in  $\delta_{ii}$  are  $\pm 8$  ppm.

comparable selenium environments considering that the selenium chemical shift range exceeds 3000 ppm.<sup>110,111</sup> The solid-state  $^{77}\text{Se}$  NMR spectra of the Group 12 complexes,  $\text{M}[\text{N}(\text{Pr}_2\text{PSe})_2]$  (M = Zn, Cd, Hg), also shows little variation in the selenium chemical shift parameters between the selenium sites present in those complexes.<sup>99</sup> Theoretical calculations of the selenium chemical shift tensors reproduce the experimental values well (Table 7.2). The indirect selenium-phosphorus coupling,  $^1J(^{77}\text{Se}, ^{31}\text{P})_{\text{iso}}$ , values of -485 and -560 Hz for  $\text{Pd}[\text{N}(\text{Pr}_2\text{PSe})_2]_2$  agree well with the single value from solution  $^{31}\text{P}$

NMR, (-)590 Hz,<sup>8</sup> and the values determined from the <sup>31</sup>P solid-state NMR spectra (Table 7.1). Similarly for the Pt(II) complex, the <sup>1</sup>J(<sup>77</sup>Se, <sup>31</sup>P)<sub>iso</sub> values of -450 and -510 Hz are in agreement with the solid-state <sup>31</sup>P NMR value above, and the magnitude from a chloroform solution <sup>31</sup>P NMR spectrum of Pt[N(<sup>i</sup>Pr<sub>2</sub>PSe)<sub>2</sub>]<sub>2</sub>, (-)536 Hz.<sup>8</sup> There was no evidence of <sup>1</sup>J(<sup>195</sup>Pt, <sup>77</sup>Se)<sub>iso</sub> in the solid-state <sup>77</sup>Se NMR spectrum of Pt[N(<sup>i</sup>Pr<sub>2</sub>PSe)<sub>2</sub>]<sub>2</sub>. This prompted us to investigate the complex via solution <sup>77</sup>Se NMR yielding an isotropic chemical shift of -137 ppm consistent with the solid-state values in Table 7.2, and a <sup>1</sup>J(<sup>195</sup>Pt, <sup>77</sup>Se)<sub>iso</sub> value of 90 Hz, which is well within the linewidths in the corresponding solid-state <sup>77</sup>Se NMR spectrum. Calculated orientations of selenium magnetic shielding tensors for tris-organophosphine selenide compounds, R<sub>3</sub>PSe, were found to be sensitive to the nature of the R group.<sup>97</sup> However, the selenium magnetic shielding tensors for the transition metal complexes, as determined by the DFT calculations, possess similar orientations with the directions of δ<sub>11</sub> and δ<sub>33</sub>, oriented nearly parallel with the metal-selenium and selenium-phosphorus bond axes, respectively. The intermediate component, δ<sub>22</sub>, is oriented perpendicular to the local M-Se-P plane.

The solid-state <sup>77</sup>Se NMR spectrum for the ligands of the Se[N(<sup>i</sup>Pr<sub>2</sub>PSe)<sub>2</sub>]<sub>2</sub> complex overlaps with the spectrum for the central selenium atom, see Figure 7.6. The experimentally observed solid-state <sup>77</sup>Se NMR spectrum (Figure 7.6a) agrees well with the simulation of all selenium environments (Figure 7.6b), which is comprised of the simulations for the ligand (Figure 7.6c) and that of the central selenium atom (Figure 7.6d). The solid-state <sup>77</sup>Se NMR spectrum for Te[N(<sup>i</sup>Pr<sub>2</sub>PSe)<sub>2</sub>]<sub>2</sub> at 7.0 T along with its simulation is given in Figures 7.6e and 7.6f, respectively. The experimental solid-state <sup>77</sup>Se NMR parameters for the ligand for both of the main-group square-planar complexes



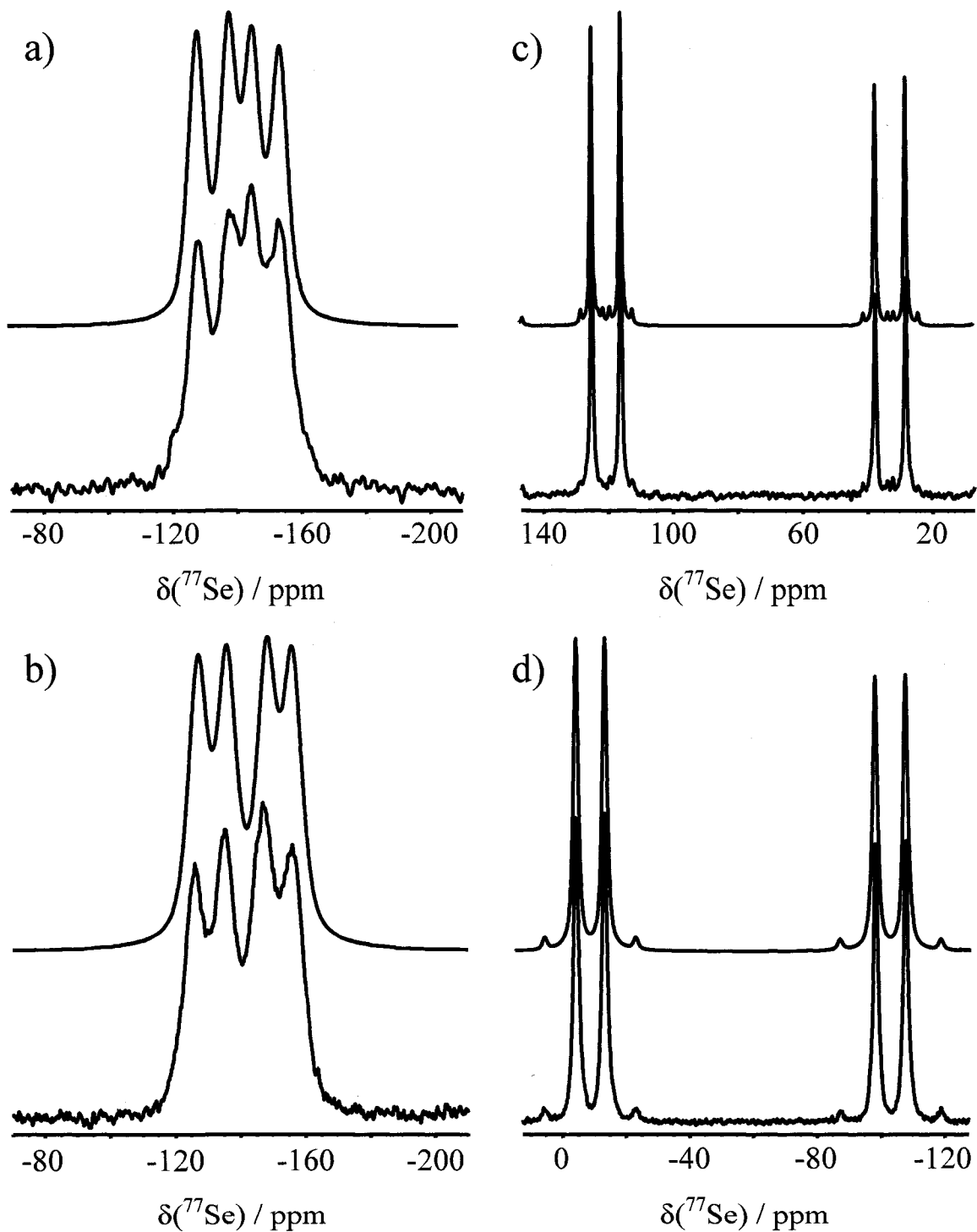
**Figure 7.6** (a) Experimental VACP MAS  $^{77}\text{Se}$  NMR spectrum for  $\text{Se}[\text{N}(\text{iPr}_2\text{PSe})_2]_2$ . Experimental conditions: 7.0 T, 31808 scans, 5 Hz of line broadening, a 9.0 ms contact time, and a 5 s recycle delay. (b) Total simulation of all selenium environments for  $\text{Se}[\text{N}(\text{iPr}_2\text{PSe})_2]_2$ . (c) Simulation of the  $^{77}\text{Se}$  MAS spectrum for the anion of  $\text{Se}[\text{N}(\text{iPr}_2\text{PSe})_2]_2$ . (d) Simulation of the  $^{77}\text{Se}$  MAS spectrum for the central selenium in  $\text{Se}[\text{N}(\text{iPr}_2\text{PSe})_2]_2$ . (e) VACP MAS  $^{77}\text{Se}$  NMR spectrum for  $\text{Te}[\text{N}(\text{iPr}_2\text{PSe})_2]_2$ . Experimental conditions: 7.0 T, 10896 scans, 10 Hz of line broadening, an 11.0 ms contact time, and an 8 s recycle delay. (f) Simulation of the  $^{77}\text{Se}$  MAS spectrum for  $\text{Te}[\text{N}(\text{iPr}_2\text{PSe})_2]_2$ . The isotropic peaks are marked with an asterisk (\*).

are well reproduced by the DFT calculations, Table 7.2. The significant difference between the values of  $\delta_{\text{iso}}(\text{Se})$  for the two selenium sites within the Se(II) and Te(II) complexes, along with the consistent reproduction of this difference by the DFT computations, permits the assignment of these resonances to specific selenium environments within the  $\text{M}[\text{N}(\text{Pr}_2\text{PSe})_2]_2$  structures. For both main-group complexes, the site with the larger isotropic chemical shift corresponds to the selenium site within the crystal structure with smaller M-Se and Se-P distances, as well as smaller M-Se-P angle; whereas, the site with the smaller value of  $\delta_{\text{iso}}(\text{Se})$  corresponded to the selenium site with larger M-Se and Se-P distances, and larger M-Se-P angle. The  $^1J(^{77}\text{Se}, ^{31}\text{P})_{\text{iso}}$  values of -520 and -535 Hz for  $\text{Se}[\text{N}(\text{Pr}_2\text{PSe})_2]_2$  agree well with the solution  $^{31}\text{P}$  NMR magnitude of (-)526 Hz,<sup>3</sup> and the solid-state  $^{31}\text{P}$  NMR value given in Table 7.1. Additionally, the indirect spin-spin couplings between the central selenium and the selenium nuclei from the ligands,  $^1J(^{77}\text{Se}, ^{77}\text{Se})_{\text{iso}} = \pm 405$  and  $\pm 435$  Hz, from the ~7.63% relative intensity satellite peaks, are in good agreement with the magnitude of 391 Hz for selenium-selenium one-bond coupling in  $\text{Se}[\text{Se}_2\text{CN}(\text{tBu})_2]_2$ ,<sup>112</sup> which was previously recognized as the largest known value of  $^1J(^{77}\text{Se}, ^{77}\text{Se})_{\text{iso}}$ .<sup>110</sup> The  $^1J(^{77}\text{Se}, ^{31}\text{P})_{\text{iso}}$  values for the tellurium complex, -520 and -540 Hz, are in agreement with our solid-state  $^{31}\text{P}$  NMR value above and the coupling observed from a chloroform solution, (-)528 Hz.<sup>4</sup> The magnitudes of  $^1J(^{125}\text{Te}, ^{77}\text{Se})_{\text{iso}}$ , 1120 and 1270 Hz, appear to be the largest tellurium-selenium couplings reported, over 500 Hz larger than those found in polychalcogenides.<sup>113-115</sup> Scaling of these  $^1J(^{125}\text{Te}, ^{77}\text{Se})_{\text{iso}}$  and the values of  $^1J(^{77}\text{Se}, ^{77}\text{Se})_{\text{iso}}$  for the Se(II) complex by  $4\pi^2/h\gamma_{\text{M}}\gamma_{\text{Se}}$  yields the reduced coupling constants  $^1K(\text{M}, \text{Se})_{\text{iso}}$ , which allows for direct comparison. The values of  $^1K(\text{Se}, \text{Se})_{\text{iso}}$ ,  $918 \times 10^{19} \text{ T}^2 \text{ J}^{-1}$  and  $986 \times 10^{19} \text{ T}^2 \text{ J}^{-1}$ , are of a



similar order of magnitude yet smaller than the corresponding  ${}^1K(\text{Te,Se})_{\text{iso}}$ ,  $1529 \times 10^{19} \text{ T}^2 \text{ J}^{-1}$  and  $1734 \times 10^{19} \text{ T}^2 \text{ J}^{-1}$ , found for  $\text{Te}[\text{N}(\text{}^1\text{Pr}_2\text{PSe})_2]_2$ . Increasing magnitudes of  ${}^1K_{\text{iso}}$  as one moves down a group in the periodic table is a well known trend for various Group 14 couplings,<sup>116-122</sup> and has also been observed in the coupling of the Group 12 metal centers, cadmium and mercury, with selenium in diselenoimidodiphosphinato complexes.<sup>99</sup>

There are a number of notable differences between the solid-state  ${}^{77}\text{Se}$  NMR parameters for the diselenoimidodiphosphinato selenium environments in the transition metal square-planar complexes and those for the main-group complexes. The first observed difference involves the isotropic region of the  ${}^{77}\text{Se}$  NMR spectra. It is readily apparent from Figure 7.7 that the isotropic shifts within the  ${}^{77}\text{Se}$  NMR spectra of the Pd(II) (Figure 7.7a) and Pt(II) (Figure 7.7b) complexes are considerably closer together than those for the Se(II) (Figure 7.7c) and Te(II) (Figure 7.7d) complexes. While the selenium isotropic shifts of the transition metal complexes are approximately 20 ppm apart, the  ${}^{77}\text{Se}$  resonances for the main group square-planar complexes are nearly 90 ppm separated from each other. Additionally, the selenium chemical shifts for the transition metal complexes do not vary much when the complexing metal is changed from palladium to platinum,  $\Delta\delta_{\text{iso}} \leq 2 \text{ ppm}$ ; however, the isotropic  ${}^{77}\text{Se}$  NMR peaks for the  $[\text{N}(\text{}^1\text{Pr}_2\text{PSe})_2]^-$  selenium environments are separated by more than 130 ppm, depending on whether the central atom is selenium or tellurium (Table 7.2). Secondly, the spans of the selenium chemical shift tensors of the diselenoimidodiphosphinato selenium environments in the selenium and tellurium complexes are on the order of 200 ppm smaller than those for the transition metal complexes; however, all spans of the selenium



**Figure 7.7** Expansion of the isotropic regions of the  $^{77}\text{Se}$  NMR spectra at 7.0 T (lower trace) and the corresponding simulations (upper traces) for the diselenoimidodiphosphate anion of the square-planar complexes  $\text{M}[\text{N}(\text{Pr}_2\text{PSe})_2]_2$ ,  $\text{M} =$  (a) Pd, (b) Pt, (c) Se, (d) Te.

chemical shift tensors investigated are still larger than those typically found in tris-organophosphine selenides.<sup>97,123</sup> Finally, the calculated orientation of the  $[\text{N}(\text{}^1\text{Pr}_2\text{PSe})]^-$  selenium chemical shift tensors depend on whether the complexing center is palladium and platinum or selenium and tellurium. For the main-group square planar complexes,  $\delta_{33}$  is oriented nearly parallel to the metal-selenium bond axis,  $\delta_{11}$  is approximately aligned with the selenium-phosphorus bond axis, with  $\delta_{22}$  perpendicular to the local M-Se-P plane. These are distinctly different from the orientation of the selenium chemical shift tensors in the palladium and platinum complexes where  $\delta_{11}$  was calculated parallel to the metal-selenium axis and  $\delta_{33}$  parallel to the selenium-phosphorus axis. The difference in the magnitude of the spans and orientations of the selenium chemical shift tensors may be a result of the difference between the selenium environment being within a  $\text{MSe}_2\text{P}_2\text{N}$  heterocyclic ring with a distorted-chair conformation,  $\text{M} = \text{Se}$  or  $\text{Te}$ , rather than a pseudo-boat conformation as seen above with the palladium and platinum complexes as well as previously observed for the tetraisopropyldiselenoimido-diphosphinato Group 12 complexes,  $\text{M}[\text{N}(\text{}^1\text{Pr}_2\text{PSe})_2]_2$  ( $\text{M} = \text{Zn}, \text{Cd}, \text{Hg}$ ), which also possess similarly oriented selenium chemical shift tensors and spans greater than 650 ppm within their pseudo-boat heterocyclic ring structures.<sup>99</sup>

### 7.3.3 Solid-State NMR of the Central Atom of $\text{M}[\text{N}(\text{}^1\text{Pr}_2\text{PSe})_2]_2$ ( $\text{M} = \text{}^{195}\text{Pt}, \text{}^{77}\text{Se}, \text{}^{125}\text{Te}$ )

The results of the solid-state  $^{77}\text{Se}$ ,  $^{125}\text{Te}$ , and  $^{195}\text{Pt}$  NMR investigation on the spin- $1/2$  nuclei of the central atoms in the  $\text{M}[\text{N}(\text{}^1\text{Pr}_2\text{PSe})_2]_2$  ( $\text{M} = \text{Pt}, \text{Se}, \text{Te}$ ) complexes are given in Table 7.3. Palladium-105 is a low- $\gamma$  quadrupolar nucleus,  $S = 5/2$ , with a large quadrupolar moment,  $Q = 66.0 \text{ fm}^2$ ,<sup>124</sup> making it impractical to study at the moderate

**Table 7.3** Experimental and theoretical solid-state NMR parameters for  $M[N(\text{}^i\text{Pr}_2\text{PSe})_2]_2$  ( $M = {}^{105}\text{Pd}, {}^{195}\text{Pt}, {}^{77}\text{Se}, {}^{125}\text{Te}$ ).

$M^{\text{II}}$	$\delta_{\text{iso}}$ ppm	$\delta_{11}$ ppm	$\delta_{22}$ ppm	$\delta_{33}$ ppm	$\Omega$ ppm	$\kappa$	${}^1J(M, {}^{77}\text{Se})_{\text{iso}}$ Hz	
Pd <sup>a</sup>	SR	0	1801	-796	-1005	2806	-0.87	
	SO	0	1866	-818	-1049	2915	-0.86	
Pt	Expt <sup>b</sup>	-4580	-2412	-5623	-5706	3294	-0.95	
	SR	-6017	-4651	-6611	-6790	2146	-0.83	
	SO	-6347	-4648	-7076	-7319	2671	-0.82	
Se	Expt <sup>c</sup>	367	457	389	255	202	0.32	$\pm 424$
	SR	296	523	245	119	404	-0.37	
	SO	373	446	399	275	171	0.45	
Te	Expt <sup>d</sup>	645	1330	1073	-468	1798	0.71	$\pm 1200$
	SR	295	817	99	-30	848	-0.68	
	SO	508	963	741	-179	1142	0.59	

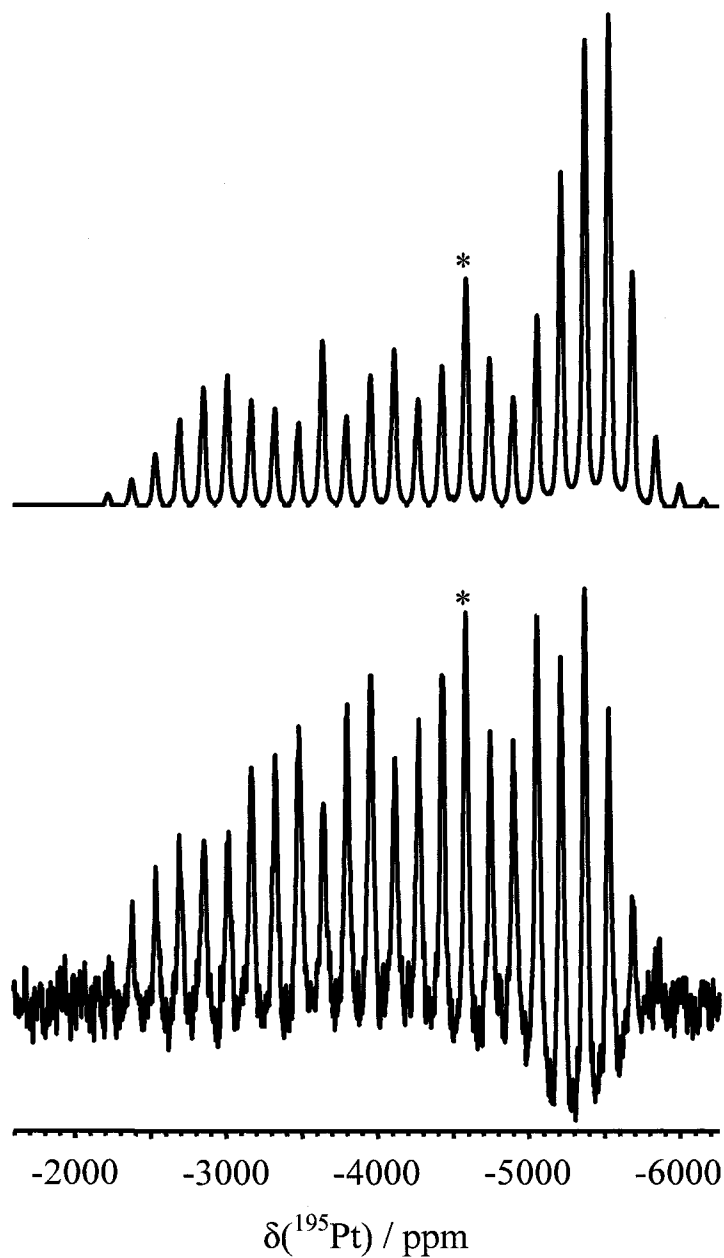
<sup>a</sup> Pd-105 chemical shift tensors are given as a traceless representation.

<sup>b</sup> Estimated errors in  $\delta_{ii}$  are  $\pm 80$  ppm.

<sup>c</sup> Estimated errors in  $\delta_{ii}$  are  $\pm 5$  ppm.

<sup>d</sup> Estimated errors in  $\delta_{ii}$  are  $\pm 40$  ppm.

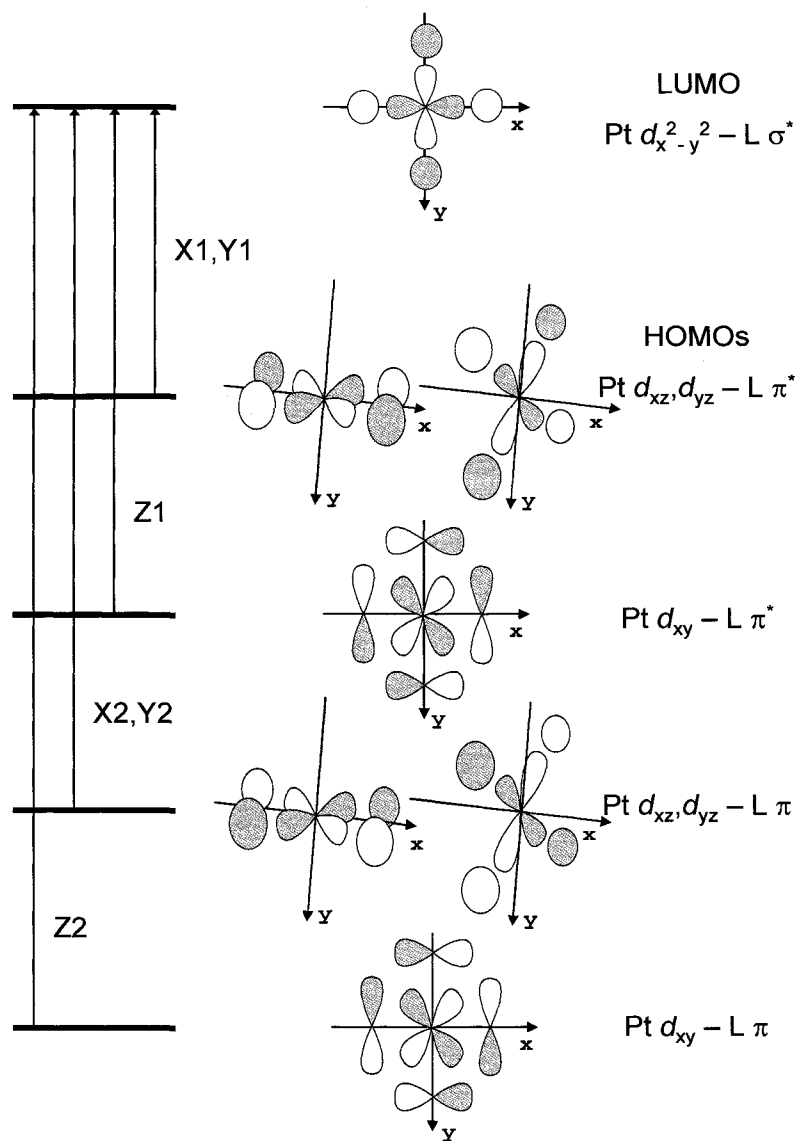
magnetic fields employed; however, DFT computations of the  ${}^{105}\text{Pd}$  chemical shift tensor were performed and are included in Table 7.3. The solid-state  ${}^{195}\text{Pt}$  NMR spectrum of  $\text{Pt}[N(\text{}^i\text{Pr}_2\text{PSe})_2]_2$  at 4.7 T is given in Figure 7.8 along with its simulation. The isotropic  ${}^{195}\text{Pt}$  chemical shift, -4580 ppm, agrees well with the solution  ${}^{195}\text{Pt}$  NMR value, -4308 ppm, as well as that for the phenyl-derivated complex,  $\text{Pt}[N(\text{Ph}_2\text{PSe})_2]_2$ , -4240 ppm.<sup>6,7</sup> The broad spectrum spanning over 3000 ppm affords rather low resolution, and provides no evidence for splittings due to platinum-selenium coupling; however, the solution-state  ${}^{195}\text{Pt}$  NMR spectrum displays a  ${}^1J({}^{195}\text{Pt}, {}^{77}\text{Se})_{\text{iso}}$  of 92 Hz consistent with the solution-state  ${}^{77}\text{Se}$  NMR value, as well as a  ${}^2J({}^{195}\text{Pt}, {}^{31}\text{P})_{\text{iso}}$  value of 94 Hz. Despite being of a similar order of magnitude with other platinum-selenium couplings,<sup>110</sup> the small value of  ${}^1J({}^{195}\text{Pt}, {}^{77}\text{Se})_{\text{iso}}$  was unexpected given the large  ${}^1J({}^{125}\text{Te}, {}^{77}\text{Se})_{\text{iso}}$  couplings observed herein



**Figure 7.8** VACP MAS  $^{195}\text{Pt}$  NMR spectrum of  $\text{Pt}[\text{N}(\text{iPr}_2\text{PSe})_2]_2$  (lower trace) and its simulation (upper trace). Experimental conditions: 4.7 T, 84656 scans, spinning at 6.75 kHz, 200 Hz of line broadening, a 10.0 ms contact time, and a 9 s recycle delay. The isotropic peak is marked with an asterisk (\*).

for  $\text{Te}[\text{N}(\text{}^i\text{Pr}_2\text{PSe})_2]_2$ ,  $\pm 1120$  and  $\pm 1270$  Hz, as well as the  ${}^1J({}^{199}\text{Hg}, {}^{77}\text{Se})_{\text{iso}}$  values found for  $\text{Hg}[\text{N}(\text{}^i\text{Pr}_2\text{PSe})_2]_2$  ranging from  $-850$  to  $-900$  Hz.<sup>99</sup>

The principal components of the palladium and platinum chemical shift tensors indicate nearly axially symmetric environments about the central transition metal centers in  $\text{M}[\text{N}(\text{}^i\text{Pr}_2\text{PSe})_2]_2$ ,  $\text{M} = \text{Pd}, \text{Pt}$ , consistent with experimental  ${}^{195}\text{Pt}$  chemical shift tensors determined for other square-planar platinum complexes.<sup>125-128</sup> Orbital interpretations of paramagnetic shielding contributions have been successful in understanding the physical origin of the observed chemical shift tensors for numerous molecular systems.<sup>129,130</sup> Gilbert and Ziegler have utilized qualitative molecular orbital theory along with ZORA DFT calculations to describe the  ${}^{195}\text{Pt}$  shielding environments for several square-planar platinum complexes.<sup>131</sup> Their results show that platinum chemical shift tensors with negative skews (i.e.,  $\delta_{22} \sim \delta_{33}$ ) arise from large deshielding paramagnetic contributions perpendicular to the square plane resulting from the magnetic-dipole allowed mixing of  $d_{xy} \rightarrow d_{x^2-y^2}$ ; occupied  $\rightarrow$  virtual orbital mixing, Z1 and Z2 in Figure 7.9.<sup>131</sup> The SR and SO calculated platinum chemical shift tensors for  $\text{Pt}[\text{N}(\text{}^i\text{Pr}_2\text{PSe})_2]_2$  are in fair agreement with experiment given that the  ${}^{195}\text{Pt}$  chemical shift range covers 13000 ppm.<sup>132</sup> The discrepancy between the calculations suggests that scalar ZORA relativistic corrections are not completely able to detail the local platinum environment. The inclusion of spin-orbit relativistic corrections yield better agreement, indicating that these effects are important for describing the local environment of this heavy transition metal. The calculations do however perform well in describing the shape and size of the platinum chemical shift tensor, as shown in the comparable values of the skew and magnitudes of the span, see Table 7.3. The calculated orientation of the platinum chemical shift tensor

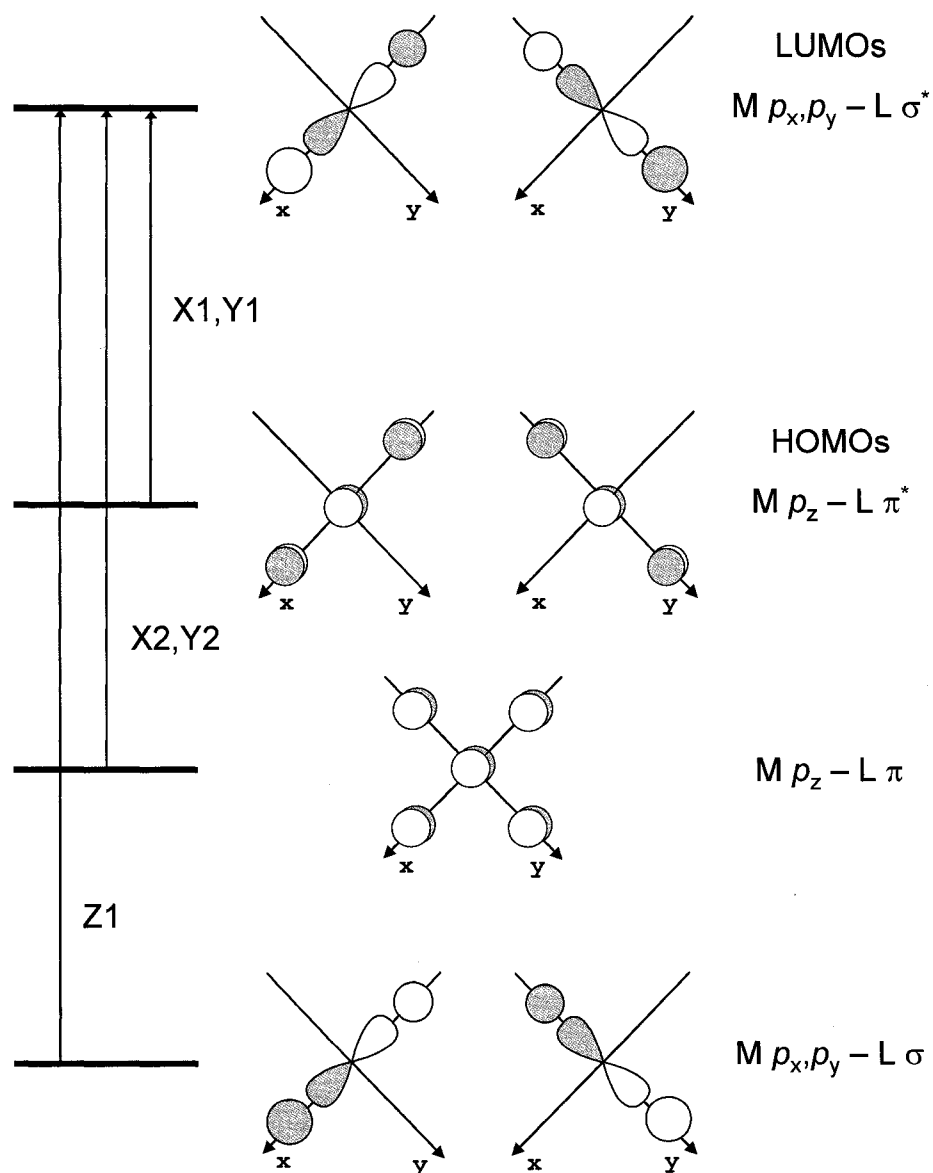


**Figure 7.9** Molecular orbital diagram for an idealized Pt<sup>II</sup>L<sub>4</sub> anion adapted from ref [131]. X and Y magnetic-dipole allowed mixing lead to paramagnetic contributions within the square plane; whereas, Z mixing lead to deshielding contributions perpendicular to the molecular plane.

also correctly predicts a nearly axially symmetric tensor, suggesting that directions of  $\delta_{33}$  and  $\delta_{22}$  are coincident within the PtSe<sub>4</sub> plane, and that  $\delta_{11}$  is oriented perpendicular to the square plane.

The solid-state  $^{77}\text{Se}$  NMR spectrum for  $\text{Se}[\text{N}(\text{}^i\text{Pr}_2\text{PSe})_2]_2$  at 7.0 T is shown in Figure 7.6. The simulation of the central selenium site (Figure 7.6d) shows a selenium chemical shift tensor that possesses a considerably smaller span than the ligand selenium environments, Figure 7.6c and Tables 7.2 and 7.3. The isotropic  $^{77}\text{Se}$  chemical shift, 367 ppm, is consistent with those found in other selenium(II) centers,<sup>112,133</sup> and the observed  $^1J(^{77}\text{Se}, ^{77}\text{Se})_{\text{iso}}$ ,  $\pm 424$  Hz, from the  $4 \times 7.63\% = 30.52\%$  relative intensity satellite peaks, is in good agreement with the indirect one-bond selenium-selenium coupling constants found from the diselenoimidodiphosphinato selenium environments within the same spectrum given in Table 7.2. The small span, positive skew, and non axially symmetric  $^{77}\text{Se}$  chemical shift tensor are in stark contrast to the corresponding platinum chemical shift tensor for  $\text{Pt}[\text{N}(\text{}^i\text{Pr}_2\text{PSe})_2]_2$ , with its large span, near axial symmetry and negative  $\kappa$ . The difference between the skews of the respective central selenium and platinum chemical shift tensors can also be understood via qualitative molecular orbital theory. Figure 7.10 displays the dominant magnetic-dipole allowed mixing of orbitals, obtained using the EPR module from the DFT computations, for describing the shielding for the central atom within the main-group square-planar complexes investigated. Deshielding paramagnetic contributions arise within the molecular square plane due to  $p_z \rightarrow p_{x,y}$  mixing (X1,Y1 and X2,Y2 in Figure 7.10); whereas, the majority of the deshielding perpendicular to the plane results from the  $p_{x,y}(\text{occupied}) \rightarrow p_{y,x}(\text{virtual})$  mixing (Z1 in Figure 7.10). Since the paramagnetic contributions from the X1,Y1 and X2,Y2 mixing are larger than those from Z1, the principal components approximately within the  $\text{SeSe}_4$  plane are more deshielded than the component perpendicular to the plane and a chemical shift tensor with a positive skew is found. The scalar relativistic calculated selenium



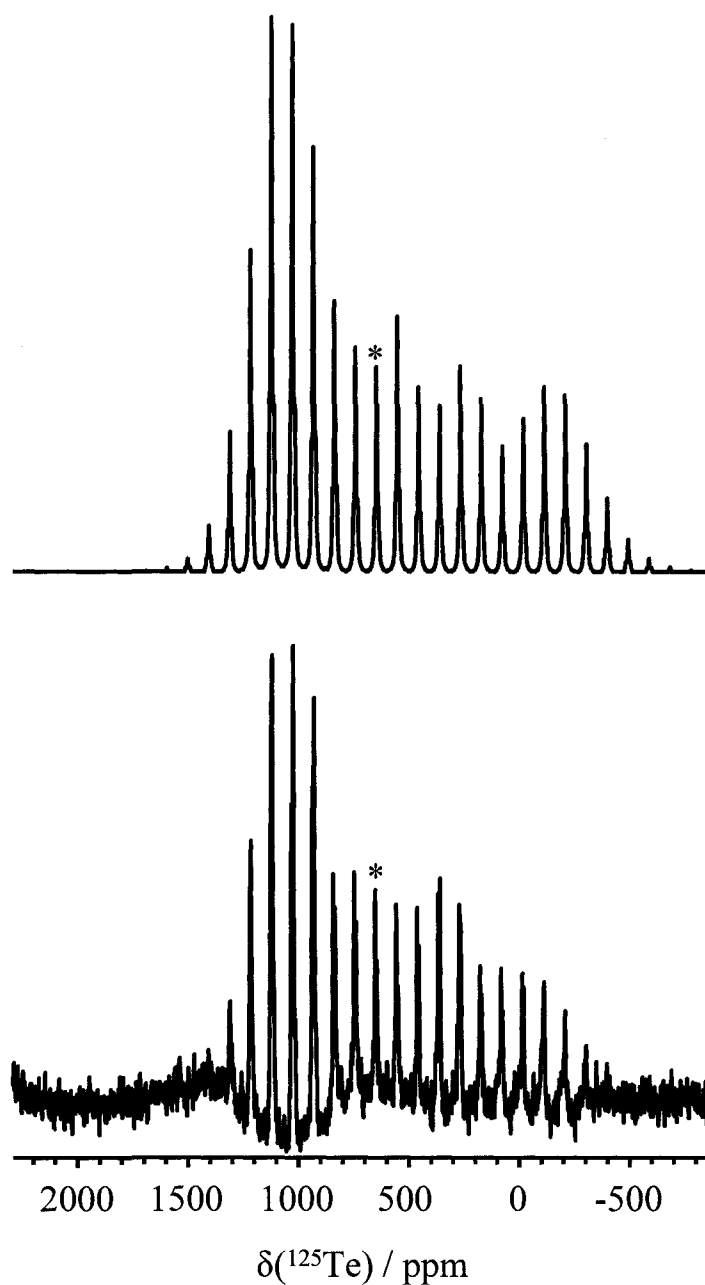


**Figure 7.10** Molecular orbital diagram for an idealized  $M^{II}L_4$  ( $M = Se, Te$ ) anion. X and Y magnetic-dipole allowed mixing lead to paramagnetic contributions within the square plane; whereas, Z mixing lead to deshielding contributions perpendicular to the molecular plane.

chemical shift tensor has difficulty reproducing all of the experimental values, predicting a  $^{77}Se$  chemical shift tensor with a skew of the opposite sign; however, the SO calculation achieves improved agreement in  $\delta_{iso}$ ,  $\delta_{ii}$ ,  $\Omega$  and arrives at a positive  $\kappa$  indicating that spin-orbit relativistic corrections are necessary in providing an accurate description of the

shielding environment for the central selenium in  $\text{Se}[\text{N}(\text{}^i\text{Pr}_2\text{PSe})_2]_2$  (Table 7.3). The orientation of the selenium chemical shift tensor calculated at the SR level is clearly incorrect given that the calculated skew is of opposite sign to that determined experimentally. The SO DFT calculation orients the  $^{77}\text{Se}$  chemical shift tensor with the intermediate component almost in the  $\text{SeSe}_4$  plane, while the square plane nearly bisects the  $\delta_{11}\text{-Se-}\delta_{33}$  angle. The origin of the change in  $\kappa$  arises primarily from a large spin-orbit shielding perpendicular to the  $\text{SeSe}_4$  plane that results in the principal component perpendicular to this plane changing from the least shielded component,  $\delta_{11}$  in the scalar calculation, to a more shielded  $\delta_{33}$  component in the SO calculation.

The solid-state  $^{125}\text{Te}$  NMR spectrum of  $\text{Te}[\text{N}(\text{}^i\text{Pr}_2\text{PSe})_2]_2$  at 4.7 T is given in Figure 7.11 along with its simulation. Similar to the  $^{77}\text{Se}$  chemical shift tensor of the selenium(II) complex, the tellurium chemical shift tensor has a positive skew; however, it possesses a considerably larger span and is closer to being axially symmetric than was found for the Se(II) center. The isotropic  $^{125}\text{Te}$  chemical shift, 645 ppm, is similar to the value of 797 ppm found from a solution  $^{125}\text{Te}$  NMR study of  $\text{C}_4\text{H}_8\text{TeI}[\text{N}(\text{Ph}_2\text{PSe})_2]$ ,<sup>42</sup> considering the tellurium chemical shift range exceeds 7000 ppm.<sup>134</sup> The value of  $^1J(^{125}\text{Te}, ^{77}\text{Se})_{\text{iso}}, \pm 1200$  Hz, agrees well with the indirect one-bond tellurium-selenium coupling constants from the solid-state  $^{77}\text{Se}$  NMR results above, Table 7.2. Analogous to the molecular orbital theory description of the shielding explaining the positive skew for the selenium chemical shift tensor in  $\text{Se}[\text{N}(\text{}^i\text{Pr}_2\text{PSe})_2]_2$ , Figure 7.10 illustrates the dominant magnetic-dipole allowed mixing of orbitals involved in determining the tellurium chemical shift tensor. Similar to the calculations for the Se(II) complex, the calculated tellurium chemical shift tensor at the SR level of theory achieves poor



**Figure 7.11** VACP MAS  $^{125}\text{Te}$  NMR spectrum of  $\text{Te}[\text{N}(\text{}^i\text{Pr}_2\text{PSe})_2]_2$  (lower trace) and its simulation (upper trace). Experimental conditions: 4.7 T, 25616 scans, spinning at 6.0 kHz, 100 Hz of line broadening, a 8.0 ms contact time, and a 20 s recycle delay. The isotropic peak is marked with an asterisk (\*).

agreement with the values of  $\delta_{ii}$ , and a negative skew, while the SO calculation provides closer agreement to the experimental  $^{125}\text{Te}$  chemical shift tensor and a positive skew.

The SO calculation orients the  $^{125}\text{Te}$  chemical shift tensor such that  $\delta_{33}$  lies nearly perpendicular to the  $\text{TeSe}_4$  plane, with  $\delta_{22}$  within and  $\delta_{11}$  slightly out of the square plane itself. The change in  $\kappa$  is, again, due primarily to a large spin-orbit shielding perpendicular to the  $\text{TeSe}_4$  plane that essentially makes  $\delta_{11}(\text{SR})$ ,  $\delta_{33}$  in the SO calculation. This shielding is, not surprisingly, larger than that found for the central selenium in the  $\text{Se}[\text{N}(\text{Pr}_2\text{PSe})_2]_2$ , which results in a tellurium chemical shift tensor with a larger positive skew, see Table 7.3.

#### 7.4 Summary

Solid-state  $^{31}\text{P}$ ,  $^{77}\text{Se}$ ,  $^{125}\text{Te}$ , and  $^{195}\text{Pt}$  NMR spectroscopy was found to be a powerful comparative technique for the investigation of square-planar complexes of Group 10 ( $\text{Pd}^{\text{II}}$ ,  $\text{Pt}^{\text{II}}$ ) and 16 ( $\text{Se}^{\text{II}}$ ,  $\text{Te}^{\text{II}}$ ) centers coordinated with the tetraisopropyldiselenoimido-diphosphate anion,  $[\text{N}(\text{Pr}_2\text{PSe})_2]^-$ . Density functional theory calculations support many of the experimentally observed trends and values in the chemical shift tensors, as well as provide orientations for the  $^{14}\text{N}$  EFG tensors. Residual dipolar coupling effects between phosphorus and nitrogen were manifested in the  $^{31}\text{P}$  MAS spectra for the selenium and tellurium complexes, but not for the palladium and platinum complexes. Very different orientations for the  $^{14}\text{N}$  EFG tensors between the transition metal and main-group square-planar complexes account for the differences observed in solid-state  $^{31}\text{P}$  NMR spectra at 4.7 T and 7.0 T. Differences between the Group 10 and 16 complexes were also found in the  $^{77}\text{Se}$  MAS spectra of the diselenoimidodiphosphinato selenium environments, where considerably more variation is observed in the isotropic selenium chemical shifts of the  $\text{Se}(\text{II})$  and  $\text{Te}(\text{II})$  complexes than is found for those of  $\text{Pd}(\text{II})$  and  $\text{Pt}(\text{II})$ . Additionally,

characteristic spans and orientations for the selenium chemical shift tensors were found to differentiate diselenoimidodiphosphinato selenium environments within pseudo-boat versus distorted-chair  $MSe_2P_2N$  heterocycles. The solid-state  $^{77}Se$ ,  $^{125}Te$ , and  $^{195}Pt$  NMR spectra for the central atom of the square-planar complexes investigated were found to have chemical shift tensors with positive skew values for the main-group square-planar complexes, and a negative  $\kappa$  in the platinum complex. The different skews of the chemical shift tensors for the central atoms were rationalized with qualitative molecular orbital theory.

## 7.5 References

- (1) Cea-Olivares, R.; Canseco-Melchor, G.; García-Montalvo, V.; Hernández-Ortega, S.; Novosad, J. *Eur. J. Inorg. Chem.* **1998**, 1573-1576.
- (2) Cea-Olivares, R.; Novosad, J.; Woollins, J. D.; Slawin, A. M. Z.; García-Montalvo, V.; Espinosa-Pérez, G.; García y García, P. *Chem. Commun.* **1996**, 519-520.
- (3) Cea-Olivares, R.; Moya-Cabrera, M.; García-Montalvo, V.; Castro-Blanco, R.; Toscano, R. A.; Hernández-Ortega, S. *Dalton Trans.* **2005**, 1017-1018.
- (4) Birdsall, D. J.; Novosad, J.; Slawin, A. M. Z.; Woollins, J. D. *Dalton Trans.* **2000**, 435-439.
- (5) Novosad, J.; Lindeman, S. V.; Marek, J.; Woollins, J. D.; Husebye, S. *Heteroat. Chem.* **1998**, *9*, 615-621.
- (6) Bhattacharyya, P.; Novosad, J.; Phillips, J.; Slawin, A. M. Z.; Williams, D. J.; Woollins, J. D. *Dalton Trans.* **1995**, 1607-1613.
- (7) Papadimitriou, C.; Veltsistas, P.; Novosad, J.; Cea-Olivares, R.; Toscano, A.; García y García, P.; Lopez-Cardosa, M.; Slawin, A. M. Z.; Woollins, J. D. *Polyhedron* **1997**, *16*, 2727-2729.
- (8) Cupertino, D.; Birdsall, D. J.; Slawin, A. M. Z.; Woollins, J. D. *Inorg. Chim. Acta* **1999**, *290*, 1-7.
- (9) Haiduc, I.; Silaghi-Dumitrescu, I. *Coord. Chem. Rev.* **1986**, *74*, 127-270.
- (10) Woollins, J. D. *Dalton Trans.* **1996**, 2893-2901.
- (11) Silvestru, C.; Drake, J. E. *Coord. Chem. Rev.* **2001**, *223*, 117-216.
- (12) Ly, T. Q.; Woollins, J. D. *Coord. Chem. Rev.* **1998**, *176*, 451-481.
- (13) Bhattacharyya, P.; Woollins, J. D. *Polyhedron* **1995**, *14*, 3367-3388.
- (14) Balazs, L.; Stanga, O.; Breunig, H. J.; Silvestru, C. *Dalton Trans.* **2003**, 2237-2242.
- (15) Darwin, K.; Gilby, L. M.; Hodge, P. R.; Piggott, B. *Polyhedron* **1999**, *18*, 3729-3733.
- (16) Afzaal, M.; Crouch, D.; Malik, M. A.; Motevalli, M.; O'Brien, P.; Park, J.-H. *J. Mater. Chem.* **2003**, *13*, 639-640.

- (17) Afzaal, M.; Crouch, D. J.; O'Brien, P.; Raftery, J.; Skabara, P. J.; White, A. J. P.; Williams, D. J. *J. Mater. Chem.* **2004**, *14*, 233-237.
- (18) Crouch, D. J.; Helliwell, M.; O'Brien, P.; Park, J.-H.; Waters, J.; Williams, D. J. *Dalton Trans.* **2003**, 1500-1504.
- (19) Pickett, N. L.; O'Brien, P. *Chem. Rec.* **2001**, *1*, 467-479.
- (20) Green, M.; O'Brien, P. *Chem. Commun.* **1999**, 2235-2241.
- (21) Gleizes, A. N. *Chem. Vap. Deposition* **2000**, *6*, 155-173.
- (22) Afzaal, M.; Aucott, S. M.; Crouch, D.; O'Brien, P.; Woollins, J. D.; Park, J.-H. *Chem. Vap. Deposition* **2002**, *8*, 187-189.
- (23) Afzaal, M.; Crouch, D.; Malik, M. A.; Motevalli, M.; O'Brien, P.; Park, J.-H.; Woollins, J. D. *Eur. J. Inorg. Chem.* **2004**, 171-177.
- (24) Malik, M. A.; Afzaal, M.; O'Brien, P.; Halliwell, M. *Polyhedron* **2006**, *25*, 864-868.
- (25) Afzaal, M.; Ellwood, K.; Pickett, N. L.; O'Brien, P.; Raftery, J.; Waters, J. *J. Mater. Chem.* **2004**, *14*, 1310-1315.
- (26) Park, J.-H.; Afzaal, M.; Helliwell, M.; Malik, M. A.; O'Brien, P.; Raftery, J. *Chem. Mat.* **2003**, *15*, 4205-4210.
- (27) Waters, J.; Crouch, D.; O'Brien, P.; Park, J.-H. *J. Mater. Sci.: Mater. Electron.* **2003**, *14*, 599-602.
- (28) Waters, J.; Crouch, D.; Raftery, J.; O'Brien, P. *Chem. Mat.* **2004**, *16*, 3289-3298.
- (29) Crouch, D. J.; O'Brien, P.; Malik, M. A.; Skabara, P. J.; Wright, S. P. *Chem. Commun.* **2003**, 1454-1455.
- (30) Singhal, A.; Dutta, D. P.; Kulshreshtha, S. K.; Mobin, S. M.; Mathur, P. J. *Organomet. Chem.* **2006**, *691*, 4320-4328.
- (31) Garje, S. S.; Copey, M. C.; Afzaal, M.; O'Brien, P.; Chivers, T. *J. Mater. Chem.* **2006**, *16*, 4542-4547.
- (32) Garje, S. S.; Ritch, J. S.; Eisler, D. J.; Afzaal, M.; O'Brien, P.; Chivers, T. *J. Mater. Chem.* **2006**, *16*, 966-969.

- (33) Copsey, M. C.; Panneerselvam, A.; Afzaal, M.; Chivers, T.; O'Brien, P. *Dalton Trans.* **2007**, 1528-1538.
- (34) Ritch, J. S.; Chivers, T.; Afzaal, M.; O'Brien, P. *Chem. Soc. Rev.* **2007**, *36*, 1622-1631.
- (35) Rossi, R.; Marchi, A.; Marvelli, L.; Magon, L.; Peruzzini, M.; Casellato, U.; Graziani, R. *Dalton Trans.* **1993**, 723-729.
- (36) Cea-Olivares, R.; García-Montalvo, V.; Novosad, J.; Kilian, P.; Woollins, J. D.; Slawin, A. M. Z.; García y García, P.; López-Cardoso, M.; Espinosa-Pérez, G.; Toscano, R. A.; Hernández, S.; Canseco-Melchor, G.; Lima-Montaño, L.; Rodríguez-Narváez, C. *Phosphorus Sulfur Silicon Relat. Elem.* **1997**, *124*, 347-354.
- (37) Chivers, T.; Konu, J.; Ritch, J. S.; Copsey, M. C.; Eisler, D. J.; Tuononen, H. M. *J. Organomet. Chem.* **2007**, *692*, 2658-2668.
- (38) Cupertino, D.; Keyte, R.; Slawin, A. M. Z.; Williams, D. J.; Woollins, J. D. *Inorg. Chem.* **1996**, *35*, 2695-2697.
- (39) Williams, D. J.; Quicksall, C. O.; Barkigia, K. M. *Inorg. Chem.* **1982**, *21*, 2097-2100.
- (40) Cea-Olivares, R.; Toscano, R. A.; Carreón, G.; Valdés-Martínez, J. *Monatsh. Chem.* **1992**, *123*, 391-396.
- (41) García-Montalvo, V.; Novosad, J.; Kilian, P.; Woollins, J. D.; Slawin, A. M. Z.; García y García, P.; López-Cardoso, M.; Espinosa-Pérez, G.; Cea-Olivares, R. *Dalton Trans.* **1997**, 1025-1029.
- (42) García-Montalvo, V.; Zamora-Rosete, M. K.; Gorostieta, D.; Cea-Olivares, R.; Toscano, R. A.; Hernández-Ortega, S. *Eur. J. Inorg. Chem.* **2001**, 2279-2285.
- (43) Rodríguez, I.; Alvarez, C.; Gómez-Lara, J.; Cea-Olivares, R. *Lanthanide Actinide Res.* **1986**, *1*, 253-260.
- (44) Silvestru, C.; Haiduc, I.; Cea-Olivares, R.; Zimbron, A. *Polyhedron* **1994**, *13*, 3159-3165.
- (45) Cea-Olivares, R.; García-Montalvo, V.; Novosad, J.; Woollins, J. D.; Toscano, R. A.; Espinosa-Pérez, G. *Chem. Ber.* **1996**, *129*, 919-923.
- (46) García-Montalvo, V.; Cea-Olivares, R.; Williams, D. J.; Espinosa-Pérez, G. *Inorg. Chem.* **1996**, *35*, 3948-3953.



- (47) Rudler, H.; Denise, B.; Gregorio, J. R.; Vaissermann, J. *Chem. Commun.* **1997**, 2299-2300.
- (48) Goyal, M.; Novosad, J.; Necas, M.; Ishii, H.; Nagahata, R.; Sugiyama, J.-I.; Asai, M.; Ueda, M.; Takeuchi, K. *Appl. Organomet. Chem.* **2000**, *14*, 629-633.
- (49) Chatziapostolou, K. A.; Vallianatou, K. A.; Grigoropoulos, A.; Raptopoulou, C. P.; Terzis, A.; Kostas, I. D.; Kyritsis, P.; Pneumatikakis, G. *J. Organomet. Chem.* **2007**, *692*, 4129-4138.
- (50) du Preez, J. G. H.; Knabl, K. U.; Krüger, L.; van Brecht, B. J. A. M. *Solvent Extr. Ion Exch.* **1992**, *10*, 729-748.
- (51) Navrátil, O.; Herrmann, E.; Grossmann, G.; Teplý, J. *Collect. Czech. Chem. Commun.* **1990**, *55*, 364-371.
- (52) Herrmann, E.; Navrátil, O.; Nang, H. b.; Smola, J.; Friedrich, J.; Příhoda, J.; Dreyer, R.; Chalkin, V. A.; Kulpe, S. *Collect. Czech. Chem. Commun.* **1984**, *49*, 201-217.
- (53) Navrátil, O.; Cigánek, M.; Herrmann, E. *Collect. Czech. Chem. Commun.* **1983**, *48*, 2009-2014.
- (54) Navrátil, O.; Fofana, M.; Smola, J. *Z. Chem.* **1984**, *24*, 30.
- (55) Navrátil, O.; Herrmann, E.; Slezák, P. *Collect. Czech. Chem. Commun.* **1987**, *52*, 1708-1714.
- (56) Muñoz-Hernández, M.-Á.; Singer, A.; Atwood, D. A.; Cea-Olivares, R. *J. Organomet. Chem.* **1998**, *571*, 15-19.
- (57) Le, Q. T. H.; Umetani, S.; Matsui, M. *Dalton Trans.* **1997**, 3835-3840.
- (58) Platzer, N.; Rudler, H.; Alvarez, C.; Barkaoui, L.; Denise, B.; Goasdoué, N.; Rager, M.-N.; Vaissermann, J.; Daran, J.-C. *Bull. Soc. Chim. Fr.* **1995**, *132*, 95-113.
- (59) Alvarez, C.; Barkaoui, L.; Goasdoué, N.; Daran, J.-C.; Platzer, N.; Rudler, H.; Vaissermann, J. *Chem. Commun.* **1989**, 1507-1509.
- (60) Alvarez, C.; Goasdoué, N.; Platzer, N.; Rodríguez, I.; Rudler, H. *Chem. Commun.* **1988**, 1002-1004.
- (61) Barkaoui, L.; Charrouf, M.; Rager, M.-N.; Denise, B.; Platzer, N.; Rudler, H. *Bull. Soc. Chim. Fr.* **1997**, *134*, 167-175.

- (62) Rodríguez, I.; Alvarez, C.; Gómez-Lara, J.; Toscano, R. A.; Platzner, N.; Mulheim, C.; Rudler, H. *Chem. Commun.* **1987**, 1502-1503.
- (63) Magennis, S. W.; Parsons, S.; Corval, A.; Woollins, J. D.; Pikramenou, Z. *Chem. Commun.* **1999**, 61-62.
- (64) Bereman, R. D.; Wang, F. T.; Najdzionek, J.; Braitsch, D. M. *J. Am. Chem. Soc.* **1976**, *98*, 7266-7268.
- (65) Sakaguchi, U.; Addison, A. W. *J. Am. Chem. Soc.* **1977**, *99*, 5189-5190.
- (66) Siiman, O.; Vetuskey, J. *Inorg. Chem.* **1980**, *19*, 1672-1680.
- (67) Haiduc, I. In *Inorganic Experiments*; Woollins, J. D., Ed.; VCH: New York; Basel; Cambridge; Tokyo, 1994, pp 145-149.
- (68) Metz, G.; Wu, X.; Smith, S. O. *J. Magn. Reson. Ser. A* **1994**, *110*, 219-227.
- (69) Bennett, A. E.; Rienstra, C. M.; Auger, M.; Lakshmi, K. V.; Griffin, R. G. *J. Chem. Phys.* **1995**, *103*, 6951-6958.
- (70) Bryce, D. L.; Bernard, G. M.; Gee, M.; Lumsden, M.; Eichele, K.; Wasylshen, R. E. *Can. J. Anal. Sci. Spectrosc.* **2001**, *46*, 46-82.
- (71) Collins, M. J.; Ratcliffe, C. I.; Ripmeester, J. A. *J. Magn. Reson.* **1986**, *68*, 172-179.
- (72) Collins, M. J.; Ripmeester, J. A. *J. Am. Chem. Soc.* **1987**, *109*, 4113-4115.
- (73) Harris, R. K.; Sebald, A. *Magn. Reson. Chem.* **1987**, *25*, 1058-1062.
- (74) Maricq, M. M.; Waugh, J. S. *J. Chem. Phys.* **1979**, *70*, 3300-3316.
- (75) Herzfeld, J.; Berger, A. E. *J. Chem. Phys.* **1980**, *73*, 6021-6030.
- (76) Eichele, K.; Wasylshen, R. E.; 1.17.30 ed., 2001.
- (77) Mason, J. *Solid State Nucl. Magn. Reson.* **1993**, *2*, 285-288.
- (78) Pulay, P. In *Calculation of NMR and EPR Parameters*; Kaupp, M., Bühl, M., Malkin, V. G., Eds.; Wiley-VCH Verlag GmbH & Co. KGaA: Weinheim, 2004, p XIII.
- (79) Schreckenbach, G.; Ziegler, T. *J. Phys. Chem. A* **1997**, *101*, 3388-3399.
- (80) Schreckenbach, G.; Ziegler, T. *J. Phys. Chem.* **1995**, *99*, 606-616.

- (81) Schreckenbach, G.; Ziegler, T. *Int. J. Quantum Chem.* **1997**, *61*, 899-918.
- (82) Wolff, S. K.; Ziegler, T. *J. Chem. Phys.* **1998**, *109*, 895-905.
- (83) Baerends, E. J.; Ellis, D. E.; Ros, P. *Chem. Phys.* **1973**, *2*, 41-51.
- (84) Versluis, L.; Ziegler, T. *J. Chem. Phys.* **1988**, *88*, 322-328.
- (85) te Velde, G.; Baerends, E. J. *J. Comput. Phys.* **1992**, *99*, 84-98.
- (86) Fonseca Guerra, C.; Snijders, J. G.; te Velde, G.; Baerends, E. J. *Theor. Chem. Acc.* **1998**, *99*, 391-403.
- (87) Theoretical Chemistry, Vrije Universiteit, Amsterdam, <http://www.scm.com>.
- (88) Vosko, S. H.; Wilk, L.; Nusair, M. *Can. J. Phys.* **1980**, *58*, 1200-1211.
- (89) Becke, A. D. *Phys. Rev. A* **1988**, *38*, 3098-3100.
- (90) Perdew, J. P. *Phys. Rev. B* **1986**, *33*, 8822-8824.
- (91) Perdew, J. P. *Phys. Rev. B* **1986**, *34*, 7406.
- (92) Chang, C.; Pelissier, M.; Durand, P. *Phys. Scr.* **1986**, *34*, 394-404.
- (93) van Lenthe, E.; Baerends, E. J.; Snijders, J. G. *J. Chem. Phys.* **1993**, *99*, 4597-4610.
- (94) van Lenthe, E.; Baerends, E. J.; Snijders, J. G. *J. Chem. Phys.* **1994**, *101*, 9783-9792.
- (95) van Lenthe, E.; van Leeuwen, R.; Baerends, E. J.; Snijders, J. G. *Int. J. Quantum Chem.* **1996**, *57*, 281-293.
- (96) Jameson, C. J.; de Dios, A.; Jameson, A. K. *Chem. Phys. Lett.* **1990**, *167*, 575-582.
- (97) Demko, B. A.; Eichele, K.; Wasylishen, R. E. *J. Phys. Chem. A* **2006**, *110*, 13537-13550.
- (98) Ruiz-Morales, Y.; Schreckenbach, G.; Ziegler, T. *J. Phys. Chem. A* **1997**, *101*, 4121-4127.
- (99) Demko, B. A.; Wasylishen, R. E. *Dalton Trans.* **2008**, 481-490.

- (100) Robert, J. B.; Wiesenfeld, L. *Mol. Phys.* **1981**, *44*, 319-327.
- (101) Jameson, C. J. In *Multinuclear NMR*; Mason, J., Ed.; Plenum Press: New York, 1987, pp 89-131.
- (102) Jameson, C. J. In *Phosphorus-31 NMR Spectroscopy in Stereochemical Analysis. Organic Compounds and Metal Complexes*; Verkade, J. G., Quin, L. D., Eds.; VCH Publishers, Inc.: Deerfield Beach, 1987; Vol. 8, pp 205-230.
- (103) Olivieri, A. C. *J. Magn. Reson.* **1989**, *81*, 201-205.
- (104) Zumbulyadis, N.; Henrichs, P. M.; Young, R. H. *J. Chem. Phys.* **1981**, *75*, 1603-1611.
- (105) Hexem, J. G.; Frey, M. H.; Opella, S. J. *J. Chem. Phys.* **1982**, *77*, 3847-3856.
- (106) Wasylishen, R. E. In *Encyclopedia of Nuclear Magnetic Resonance*; Grant, D. M., Harris, R. K., Eds.; John Wiley and Sons, Ltd.: Chichester, 1996, pp 1685-1695.
- (107) Wasylishen, R. E. In *Encyclopedia of Nuclear Magnetic Resonance*; Grant, D. M., Harris, R. K., Eds.; John Wiley and Sons, Ltd.: Chichester, 2002; Vol. 9, pp 274-282.
- (108) Wrackmeyer, B.; Garcia-Baez, E.; Zuno-Cruz, F. J.; Sanchez-Cabrera, G.; Rosales, M. J. *Z. Naturforsch., B* **2000**, *55*, 185-188.
- (109) Power, W. P.; Wasylishen, R. E.; Curtis, R. D. *Can. J. Chem.* **1989**, *67*, 454-459.
- (110) Duddeck, H. *Prog. Nucl. Magn. Reson. Spectrosc.* **1995**, *27*, 1-323.
- (111) Duddeck, H. *Annu. Rep. NMR Spectrosc.* **2004**, *52*, 105-166.
- (112) Mazaki, Y.; Kobayashi, K. *Tetrahedron Lett.* **1989**, *30*, 2813-2816.
- (113) Schrobilgen, G. J.; Burns, R. C.; Granger, P. *J. Chem. Soc.-Chem. Commun.* **1978**, 957-960.
- (114) Björgvinsson, M.; Schrobilgen, G. J. *Inorg. Chem.* **1991**, *30*, 2540-2547.
- (115) Björgvinsson, M.; Sawyer, J. F.; Schrobilgen, G. J. *Inorg. Chem.* **1991**, *30*, 4238-4245.
- (116) Dreeskamp, H.; Stegmeier, G. *Z. Naturforsch., A* **1967**, *22*, 1458-1464.
- (117) Kennedy, J. D.; McFarlane, W.; Pyne, G. S.; Wrackmeyer, B. *Dalton Trans.* **1975**, 386-390.

- (118) Kennedy, J. D.; McFarlane, W.; Wrackmeyer, B. *Inorg. Chem.* **1976**, *16*, 1299-1302.
- (119) Wrackmeyer, B.; Horchler, K. *Magn. Reson. Chem.* **1990**, *28*, 56-61.
- (120) Wrackmeyer, B.; Zhou, H. *Magn. Reson. Chem.* **1990**, *28*, 1066-1069.
- (121) Christendat, D.; Butler, I. S.; Gilson, D. F. R.; Morin, F. G. *Can. J. Chem.* **1999**, *77*, 1892-1898.
- (122) Willans, M. J.; Demko, B. A.; Wasylishen, R. E. *Phys. Chem. Chem. Phys.* **2006**, *8*, 2733-2743.
- (123) Grossmann, G.; Potrzebowski, M. J.; Fleischer, U.; Krüger, K.; Malkina, O. L.; Ciesielski, W. *Solid State Nucl. Magn. Reson.* **1998**, *13*, 71-85.
- (124) Harris, R. K.; Becker, E. D.; Crabral de Menezes, S. M.; Goodfellow, R.; Granger, P. *Pure Appl. Chem.* **2001**, *73*, 1795-1818.
- (125) Harris, R. K.; McNaught, I. J.; Reams, P.; Packer, K. J. *Magn. Reson. Chem.* **1991**, *29*, S60-S72.
- (126) Harris, R. K.; Reams, P.; Packer, K. J. *Dalton Trans.* **1986**, 1015-1020.
- (127) Austin, E. J.; Barrie, P. J.; Clark, R. J. H. *Chem. Commun.* **1993**, 1404-1405.
- (128) Duer, M. J.; Khan, M. S.; Kakkar, A. K. *Solid State Nucl. Magn. Reson.* **1992**, *1*, 13-16.
- (129) Jameson, C. J.; Gutowsky, H. S. *J. Chem. Phys.* **1964**, *40*, 1714-1724.
- (130) Grutzner, J. B. In *Recent Advances in Organic NMR Spectroscopy*; Lambert, J. B., Rittner, R., Eds.; Norell Press: Landsville, NJ, 1987, pp 17-42.
- (131) Gilbert, T. M.; Ziegler, T. *J. Phys. Chem. A* **1999**, *103*, 7535-7543.
- (132) Still, B. M.; Kumar, P. G. A.; Aldrich-Wright, J. R.; Prize, W. S. *Chem. Soc. Rev.* **2007**, *36*, 665-686.
- (133) Dietzsch, W.; Olk, R.-M.; Hoyer, E.; Meiler, W.; Robien, W. *Magn. Reson. Chem.* **1988**, *26*, 653-657.
- (134) Luthra, N. P.; Odom, J. D. In *The Chemistry of Organic Selenium and Tellurium Compounds*; Patai, S., Rappoport, Z., Eds.; John Wiley & Sons: New York, 1986; Vol. 1, pp 189-241.

## Chapter 8

### Conclusions and Outlook

#### 8.1 Conclusions

The research presented within this thesis was undertaken in order to improve the knowledge and understanding of  $^{77}\text{Se}$  NMR parameters, predominantly the nuclear magnetic shielding and indirect spin-spin coupling interactions. The significant results and advances put forth in the preceding chapters are summarized below, highlighting three fundamental areas of impact. First, the additions to the known experimental solid-state  $^{77}\text{Se}$  NMR parameters obtained within Chapters 4 through 7 are discussed in terms of their contribution to the reported literature (Chapter 2). Second, insights into the theoretical calculation of NMR parameters involving selenium, particularly nuclear magnetic shielding, are reviewed from all of the experimental chapters. Finally, revisited is the chemical information extracted from the molecular systems focused upon; imino-bis(dialkylphosphine selenide),  $\text{HN}(\text{R}_2\text{PSe})_2$ , in Chapter 5, and the tetraalkyldiselenoimidodiphosphinato complexes,  $\text{M}[\text{N}(\text{Pr}_2\text{PSe})_2]_2$ , from Chapters 6 and 7.

While the body of this thesis details the most significant research performed, particularly in regards to  $^{77}\text{Se}$  NMR interaction tensors, there are a number of additional areas where contributions were made and research experience was gained during the course of my graduate program. The specific projects undertaken include additional ab initio computations of selenium chemical shift tensors, synthetic pursuits of substituted diphenyl diselenides, a solid-state NMR study of triphenyl-Group 14 chlorides,  $\text{Ph}_3\text{XCl}$  ( $\text{X} = \text{C}, \text{Si}, \text{Sn}, \text{Pb}$ ), and hyperpolarized  $^{129}\text{Xe}$  NMR of xenon within the porous

framework of AlPO<sub>4</sub>-18. The role of the research I performed and the results yielded from the investigations are summarized in Appendix E.

### 8.1.1 Experimental Solid-State <sup>77</sup>Se NMR Parameters

The solid-state <sup>77</sup>Se NMR investigations described in Chapter 4 covered a vast variety of selenium chemical environments. While some of the selenium-containing species had previously been investigated by solid-state NMR, the majority of the <sup>77</sup>Se NMR parameters for the compounds studied were characterized for the first time. Two new organoselenium compounds were reported; *N*-methylbenzothiazole-2-selone and diphenylselenium dichloride. The X-ray crystal structure investigation of *N*-methylbenzothiazole-2-selone was only able to characterize one of two crystalline forms,<sup>1</sup> indicating two molecular species in the asymmetric unit; whereas, the solid-state <sup>77</sup>Se NMR investigation was capable of characterizing four selenium chemical shift tensors from a bulk sample of *N*-methylbenzothiazole-2-selone. The selenium chemical shift tensors were more deshielded than other seleno-carbonyl systems that have been investigated by solid-state <sup>77</sup>Se NMR (Chapter 2), yet possess isotropic selenium chemical shifts that are consistent with similar C=Se environments where the carbon is bonded to one or more nitrogen atoms.<sup>2,3</sup> That all four selenium chemical shift tensors are similar indicates comparable chemical environments and that the observed differences are likely a result of minor conformational differences and crystal packing forces. Diphenylselenium dichloride was investigated as a four coordinate organoselenium compound. The axially symmetric selenium chemical shift tensor may be evidence for significant motion of the phenyl ligands about the Cl-Se-Cl axis, as there are no

symmetry reasons from the crystal structure of  $\text{Ph}_2\text{SeCl}_2$  for the attained axial symmetry.<sup>4</sup> Motion could also be contributing to the relatively small span for the selenium chemical shift tensor, 160 ppm. Residual dipolar coupling from the quadrupolar  $^{35/37}\text{Cl}$  nuclei permitted the extraction of the coupling parameters,  $R_{\text{eff}}$  and  $^1J(^{77}\text{Se}, ^{35}\text{Cl})_{\text{iso}}$  from the simulation of the solid-state  $^{77}\text{Se}$  NMR spectrum, Figure 4.7. The magnitude of  $^1J(^{77}\text{Se}, ^{35}\text{Cl})_{\text{iso}}$ , 110 Hz, was the first reported coupling constant between selenium and chlorine in either solution<sup>2,3</sup> or solid-state  $^{77}\text{Se}$  NMR, see Table 2.5.

The organophosphine selenides studied in Chapter 4 add significantly to the known solid-state  $^{77}\text{Se}$  NMR literature of phosphine selenone systems in general. Five novel organophosphine selenides were investigated along with two that had previously been studied using 70% enriched selenium-77. The selenium chemical shift tensors and indirect one-bond selenium-phosphorus coupling constants,  $^1J(^{77}\text{Se}, ^{31}\text{P})_{\text{iso}}$ , for tris-(*tert*-butyl)phosphine selenide, tri-cyclohexylphosphine selenide, 5-phenyldibenzophosphine selenide, tri-*para*-tolylphosphine selenide, and tris-2,4,6-trimethoxyphenylphosphine selenide expanded the range of isotropic selenium chemical shifts from solid-state NMR for all phosphine selenones to -437 ppm from  $(\text{C}_6\text{H}_{11})_3\text{PSe}$  at the most shielded extreme, and to -30 ppm from  $[\text{C}_6\text{H}_2(\text{OMe})_3]_3\text{PSe}$  as the most deshielded organophosphine selenide selenium environment. Similarly, the value of -768 Hz for one of the two  $^1J(^{77}\text{Se}, ^{31}\text{P})_{\text{iso}}$  for 5-phenyldibenzophosphine selenide is the largest coupling in magnitude observed for organophosphine selenides from solid-state  $^{77}\text{Se}$  NMR.

The solid-state  $^{77}\text{Se}$  NMR investigation of ammonium selenotungstate yielded three inorganic selenium chemical shift tensors. The isotropic selenium chemical shifts were all relatively deshielded selenium environments, and the nearly axially symmetric



selenium chemical shift tensors were consistent with the terminal selenium moieties in  $(\text{NH}_4)_2\text{WSe}_4$ . In addition, the largest spans of any experimental selenium chemical shift tensor determined in this thesis were found for the three ammonium selenotungstate selenium sites.

The iminobis(dialkylphosphine selenide) systems,  $\text{HN}(\text{R}_2\text{PSe})_2$  ( $\text{R} = \text{Ph}, ^i\text{Pr}$ ), studied by solid-state  $^{77}\text{Se}$  NMR in Chapter 5 display similar selenium chemical shift tensors and indirect one-bond selenium-phosphorus coupling constants,  $^1J(^{77}\text{Se}, ^{31}\text{P})_{\text{iso}}$ , to those of the phosphine selenes reported in Chapters 2 and 4. Despite comparable values of  $^1J(^{77}\text{Se}, ^{31}\text{P})_{\text{iso}}$ , the selenium chemical shift tensors of  $\text{HN}(^i\text{Pr}_2\text{PSe})_2$  were found to be more shielded and possess larger spans than the corresponding iminobis(diphenylphosphine selenide).

The tetraisopropyldiselenoimidodiphosphinato complexes,  $\text{M}[\text{N}(^i\text{Pr}_2\text{PSe})_2]_2$  ( $\text{M} = \text{Zn}, \text{Se}, \text{Pd}, \text{Cd}, \text{Te}, \text{Pt}, \text{Hg}$ ) contain a novel environment for selenium that had not previously been investigated by solid-state  $^{77}\text{Se}$  NMR spectroscopy. All of the complexes studied in Chapters 6 and 7 contain M-Se-P moieties and, aside from  $\text{Se}[\text{N}(^i\text{Pr}_2\text{PSe})_2]_2$ , possess non-symmetric inorganic X-Se-Y linkages where neither X nor Y are another selenium atom. Previously, the only non-symmetric inorganic X-Se-Y systems that had been investigated by solid-state  $^{77}\text{Se}$  NMR were phosphorus diselenides, P-Se-Se, and metal polyselenides, M-Se-Se. The selenium chemical shift tensor for the central selenium in  $\text{Se}[\text{N}(^i\text{Pr}_2\text{PSe})_2]_2$ , despite possessing a square-planar  $\text{SeSe}_4$  environment, has a smaller span than the bridging Se-Se-P sites. All of the indirect one-bond selenium-phosphorus coupling constants,  $^1J(^{77}\text{Se}, ^{31}\text{P})_{\text{iso}}$ , for the tetraisopropyldiselenoimidodiphosphinato complexes are smaller in magnitude than those for

$\text{HN}(\text{}^i\text{Pr}_2\text{PSe})_2$ , but consistent with numerous other  $[\text{N}(\text{R}_2\text{PSe})_2]^-$  systems. The magnitudes of  ${}^1J({}^{111/113}\text{Cd}, {}^{77}\text{Se})_{\text{iso}}$  and  ${}^1J({}^{199}\text{Hg}, {}^{77}\text{Se})_{\text{iso}}$  from  $\text{Cd}[\text{N}(\text{}^i\text{Pr}_2\text{PSe})_2]_2$  and  $\text{Hg}[\text{N}(\text{}^i\text{Pr}_2\text{PSe})_2]_2$ , respectively, are within the known ranges of one-bond cadmium- and mercury-selenium couplings; however, the indirect one-bond selenium-selenium and tellurium-selenium coupling constants,  ${}^1J({}^{77}\text{Se}, {}^{77}\text{Se})_{\text{iso}}$  and  ${}^1J({}^{125}\text{Te}, {}^{77}\text{Se})_{\text{iso}}$ , for  $\text{Se}[\text{N}(\text{}^i\text{Pr}_2\text{PSe})_2]_2$  and  $\text{Te}[\text{N}(\text{}^i\text{Pr}_2\text{PSe})_2]_2$ , respectively, were found to have the largest magnitudes of any such couplings from solution or solid-state NMR.

### 8.1.2 Theoretical Insight into ${}^{77}\text{Se}$ Nuclear Magnetic Shielding

The calculations of nuclear magnetic shielding tensors in the experimental chapters of this thesis have sought to provide one or more of three potential contributions. All computations yield the orientation of the nuclear magnetic shielding tensor with respect to the molecular frame, while some calculations are able to discern the difference between the nuclear magnetic shielding of one selenium site with respect to another within the solid state structure used for the computation. Still some other calculated nuclear magnetic shielding tensors, when converted to chemical shift tensors and compared to experimentally determined values, are able to highlight the importance of relativistic effects in the accurate reproduction of the corresponding experimental selenium chemical shift tensors.

The calculated selenium chemical shift tensors for the organoselenium compounds studied in Chapter 4 highlighted that different orientations are possible for seleno-carbonyls as demonstrated with *N,N*-dimethylselenourea and *N*-methylbenzothiazole-2-selone. The chemical shift tensor orientations of the bridging selenium

environments in seleno-DL-methionine and tetramethyltetraselenafulvalene showed similarities in that  $\delta_{22}$  was always predicted to be perpendicular to the C-Se-C plane. The calculated orientations of the selenium chemical shift tensors for the organophosphine selenides investigated showed that nearly any orientation with respect to the P=Se vector is possible for these terminal selenium moieties. Additionally, the small deshieldings noted along the direction of the P-Se bond suggest that the bonding environment most closely resembles a polarized,  $R_3P^+-Se^-$ , form. The selenium chemical shift tensors for the selenate and selenotungstate anions were similarly oriented in that  $\delta_{33}$  was calculated to be parallel with the O-Se vector of  $(NH_4)_2SeO_4$ , and with the Se-W vector of  $(NH_4)_2WSe_4$ . The calculated orientations of the selenium chemical shift tensors of the iminobis(dialkylphosphine selenide) systems and tetraisopropylidiselenoimido-diphosphinato complexes studied in Chapters 5 through 7 were useful in comparing and contrasting the computed orientations with the known structures of the chemical systems investigated. These observations will be discussed in more detail in the following section.

Differentiation between selenium environments in a solid-state  $^{77}Se$  NMR spectrum based upon the calculation of the corresponding selenium chemical shift tensors is typically only reliable if the isotropic selenium chemical shifts of the sites being distinguished differ by more than 50 ppm for both the experimental and theoretical selenium chemical shift tensors. For the two selenium chemical shift tensors of iminobis(diphenylphosphine selenide), the calculations were able to discern that the selenium involved in hydrogen bonding between the dimer pair of  $HN(Ph_2PSe)_2$  molecules is more deshielded than the selenium environment that is oriented *anti* with respect to the

hydrogen bonding selenium. Similarly, the diselenoimidodiphosphate selenium environments of  $M[N(^1\text{Pr}_2\text{PSe})_2]_2$  ( $M = \text{Se}, \text{Te}$ ) were differentiated based upon their experimental and computed chemical shift tensors. In both complexes, the more deshielded selenium environment corresponded to the selenium with the smaller M-Se and Se-P distances as well as smaller M-Se-P angle, while the more shielded selenium site belonged to the selenium with larger M-Se and Se-P distances and larger M-Se-P angle.

The inclusion of relativistic effects in the calculation of selenium nuclear magnetic shieldings was investigated primarily in Chapter 4. The general conclusions found therein suggested that isotropic selenium chemical shifts as well as the orientations of the selenium chemical shift tensors were calculated generally equally well with and without applied relativistic corrections. When the selenium site being computed was located near a heavy atom, such as tungsten in  $(\text{NH}_4)_2\text{WSe}_4$ , the use of relativistic calculations was found to be necessary for the reproduction of the experimental selenium chemical shift tensor(s). Evaluation of the computed principal components of the respective chemical shift tensors indicated that, in comparison with experimentally determined values, scalar with spin-orbit relativistic calculations generally achieved the best results. Spin-orbit relativistic corrections were found to be very important in the accurate calculated selenium chemical shift tensor for the central selenium in  $\text{Se}[N(^1\text{Pr}_2\text{PSe})_2]_2$  (Chapter 7), where non-relativistic and scalar relativistic computations arrive at tensors with the wrong skew.

### 8.1.3 Specific Chemical Information

Relationships between solid-state NMR parameters and the local chemical structure of the nucleus under investigation are widely sought. In the process of investigating the iminobis(dialkylphosphine selenide) systems,  $\text{HN}(\text{R}_2\text{PSe})_2$  ( $\text{R} = \text{Ph}, ^i\text{Pr}$ ), and numerous metal(II) complexes of the tetrakispropyldiselenoimidodiphosphate anion,  $\text{M}[\text{N}(^i\text{Pr}_2\text{PSe})_2]_2$ , certain insights into the dependence of the solid-state  $^{77}\text{Se}$  NMR parameters and the chemical environment of the selenium nucleus have been obtained.

Unlike the corresponding phosphorus chemical shift tensors, the selenium chemical shift tensors of the  $\text{HN}(\text{R}_2\text{PSe})_2$  molecules were found to be sensitive to subtle differences in their local structures. This is likely due to a combination of the larger selenium chemical shift range and the fact that the selenium atoms lie on the periphery of the molecule while the phosphorus does not. The experimental and theoretical selenium chemical shift tensors, along with their calculated orientations, of iminobis(diphenylphosphine selenide) were found to be diagnostic with respect to whether or not the selenium atom was a participant in the hydrogen bonding between the dimer pairs of  $\text{HN}(\text{Ph}_2\text{PSe})_2$  units. Similarly, the selenium chemical shift tensors, and their orientations, for  $\text{HN}(^i\text{Pr}_2\text{PSe})_2$  were susceptible to the presence of methyl disorder in one of the isopropyl groups noting a significant difference in  $^{77}\text{Se}$  NMR line widths of the two selenium environments.

The indirect one-bond selenium-phosphorus coupling constants,  $^1J(^{77}\text{Se}, ^{31}\text{P})_{\text{iso}}$ , for the  $\text{HN}(\text{R}_2\text{PSe})_2$  ( $\text{R} = \text{Ph}, ^i\text{Pr}$ ) and  $\text{M}[\text{N}(^i\text{Pr}_2\text{PSe})_2]_2$  systems were found to be sensitive to the presence of the acidic N-H proton. The values of  $^1J(^{77}\text{Se}, ^{31}\text{P})_{\text{iso}}$  for  $\text{HN}(\text{R}_2\text{PSe})_2$  ( $\text{R} =$

Ph, <sup>i</sup>Pr) are all less than -700 Hz, while those for the M[N(<sup>i</sup>Pr<sub>2</sub>PSe)<sub>2</sub>]<sub>2</sub> complexes are all greater than -600 Hz.

The local structures of the selenium environments in the tetraisopropylidisenoidimidodiphosphinato complexes were able to be differentiated by their solid-state <sup>77</sup>Se NMR parameters. Due to the flexibility of the SePNPSe backbone the six-membered MSe<sub>2</sub>P<sub>2</sub>N rings generally attain one of two conformations, pseudo-boat or distorted chair. The spans of the selenium chemical shift tensors for M[N(<sup>i</sup>Pr<sub>2</sub>PSe)<sub>2</sub>]<sub>2</sub> (M = Zn, Pd, Cd, Pt, Hg), which possess pseudo-boat heterocyclic rings are on the order of 100-200 ppm larger than complexes with distorted chair MSe<sub>2</sub>P<sub>2</sub>N rings, such as for Se[N(<sup>i</sup>Pr<sub>2</sub>PSe)<sub>2</sub>]<sub>2</sub> and Te[N(<sup>i</sup>Pr<sub>2</sub>PSe)<sub>2</sub>]<sub>2</sub>. The calculated orientations for the selenium chemical shift tensors also depend on whether pseudo-boat or distorted chair six-membered rings are found in the structures of the metal(II) tetraisopropylimidodiphosphate complexes. The pseudo-boat heterocyclic rings found in M[N(<sup>i</sup>Pr<sub>2</sub>PSe)<sub>2</sub>]<sub>2</sub> (M = Zn, Pd, Cd, Pt, Hg) all possess calculated selenium chemical shift tensors where δ<sub>11</sub> is oriented nearly parallel to the M-Se vector, and δ<sub>33</sub> approximately aligned with Se-P, with δ<sub>22</sub> perpendicular to the local M-Se-P plane. The orientations of the distorted chair selenium chemical shift tensors of the diselenoidimidodiphosphate sites within M[N(<sup>i</sup>Pr<sub>2</sub>PSe)<sub>2</sub>]<sub>2</sub> (M = Se, Te), in contrast, place δ<sub>33</sub> near parallel to M-Se and δ<sub>11</sub> approximately along Se-P.

## 8.2 Outlook

Besides other interesting M<sup>n+</sup>[N(R<sub>2</sub>PSe)<sub>2</sub>]<sub>n</sub> complexes, such as those involving lanthanide or actinide centers,<sup>5-8</sup> there are a number of straightforward extensions of the work

presented in this thesis available for research pursuits. Summarized below are the aims, concerns and interests of three such projects.

### 8.2.1 Lone Electron Pair Stereochemical Activity

The stereochemistry observed in  $AL_6X$  systems when L is a hard donor such as fluorine or oxygen produce complexes where the lone electron pair, X, appears stereoactive; however, when L is a soft donor such as sulfur or selenium the stereochemical activity of the lone pair is not expressed.<sup>9,10</sup> The  $Bi[N(R_2PE)_2]_3$  (E = O, S, Se) complexes have shown to be a good system to study the stereochemical impact of the lone electron pair on the bismuth as a function of the binding chalcogen atom.<sup>11-17</sup> As demonstrated in Chapters 5 through 7, the solid-state  $^{31}P$  and  $^{77}Se$  NMR parameters for these complexes should be sensitive to the local phosphorus and selenium environments, respectively. The phosphorus and selenium chemical shift tensors, as well as their calculated orientations, are likely to be susceptible to the distortions of the six-membered  $BiE_2P_2N$  rings caused by stereochemistry imposed by the activity of the lone electron pair on the  $BiE_6$  pseudo-octahedron.

### 8.2.2 Paramagnetic Systems

Another extension to the work presented in this thesis would be to add an additional interaction to the  $^{77}Se$  NMR Hamiltonian. One such interaction would involve the influence of unpaired electrons on the NMR spectra. Paramagnetic compounds have the benefit of rapid nuclear relaxation such that the delay between FID transient acquisition is significantly reduced; however, there are also a number of disadvantages.<sup>18</sup>

One such challenge in acquiring NMR spectra of paramagnetic systems involves considerable line broadening of the NMR signals in the vicinity of the paramagnetic center, while another impact of the presence of an unpaired electron involves the hyperfine shift to the nuclear magnetic shielding.<sup>18</sup> The contribution of the hyperfine shift towards the chemical shift of heavier nuclear, such as selenium, can be on the order of thousands of parts per million.<sup>19</sup> The influence of an unpaired electron on similar systems to those investigated in Chapters 6 and 7 may be sought from the diselenoimidodiphosphinato complexes of nickel(II), Ni[N(R<sub>2</sub>PSe)<sub>2</sub>]<sub>2</sub>.<sup>20</sup> The square-planar nickel(II) complexes, like those of the Pd(II) and Pt(II) studied in Chapter 7, are diamagnetic; however, there exists a tetrahedral form of Ni[N(R<sub>2</sub>PSe)<sub>2</sub>]<sub>2</sub> that is paramagnetic. The comparison of the <sup>31</sup>P and <sup>77</sup>Se solid-state NMR parameters, particularly the NMR line widths and chemical shift tensors, between the diamagnetic and paramagnetic forms of Ni[N(R<sub>2</sub>PSe)<sub>2</sub>]<sub>2</sub> would provide insight into the impact of unpaired electrons on the NMR spectra of nuclei that are one and two bonds away from a paramagnetic center.

### 8.2.3 Tellurium Analogues

Due to the presence of <sup>123</sup>Te (*I* = ½, 0.89% N.A.) and <sup>125</sup>Te (*I* = ½, 7.07% N.A.), tellurium analogues of the dichalcogenoimidodiphosphinate anions are of interest for solid-state NMR investigations as, similar to the [N(R<sub>2</sub>PSe)<sub>2</sub>]<sup>-</sup> systems, spectra for the chalcogen are readily obtained. However, [N(R<sub>2</sub>PTe)<sub>2</sub>]<sup>-</sup> systems have only recently been prepared as their synthesis is not as straightforward as the corresponding oxygen, sulfur and selenium derivatives. While HN(R<sub>2</sub>PE)<sub>2</sub> (E = O, S, Se) may be obtained by facile



oxidation of  $\text{HN}(\text{R}_2\text{P})_2$  with hydrogen peroxide, elemental sulfur or elemental selenium, respectively, reaction of elemental tellurium with  $\text{HN}(\text{R}_2\text{P})_2$  produces only the monotelluride,  $\text{R}_2\text{P}(\text{Te})\text{NHPR}_2$ , in low yields.<sup>21</sup> Recently, the ditelluride has been prepared by the reaction of Te with  $\text{Na}[\text{N}(\text{R}_2\text{P})_2]$  in the presence of tetramethylethylenediamine.<sup>22</sup> As a result, metal complexes of the ditelluroimidodiphosphate anion,  $[\text{N}(\text{R}_2\text{P}\text{Te})_2]^-$ , have appeared in the literature. Solid-state  $^{31}\text{P}$  and  $^{125}\text{Te}$  NMR investigations of analogous complexes to those studied in Chapter 6,  $\text{M}[\text{N}(\text{R}_2\text{P}\text{Te})_2]_2$  ( $\text{M} = \text{Zn}, \text{Cd}, \text{Hg}$ ),<sup>23</sup> which have been utilized as single source precursors for metal telluride materials,<sup>24,25</sup> are now possible. Additionally, the investigation of lanthanide- and actinide-tellurium bonding by solid-state  $^{125}\text{Te}$  NMR is also available for a number of reported structures.<sup>8,26</sup>

### 8.3 References

- (1) Husebye, S.; Lindeman, S. V.; Rudd, M. D. *Acta Crystallogr. Sect. C-Cryst. Struct. Commun.* **1997**, *53*, 809-811.
- (2) Duddeck, H. *Prog. Nucl. Magn. Reson. Spectrosc.* **1995**, *27*, 1-323.
- (3) Duddeck, H. *Annu. Rep. NMR Spectrosc.* **2004**, *52*, 105-166.
- (4) McCullough, J. D.; Hamburger, G. *J. Am. Chem. Soc.* **1942**, *64*, 508-513.
- (5) Pernin, C. G.; Ibers, J. A. *Inorg. Chem.* **2000**, *39*, 1216-1221.
- (6) Gaunt, A. J.; Scott, B. L.; Neu, M. P. *Chem. Commun.* **2005**, 3215-3217.
- (7) Sekar, P.; Ibers, J. A. *Inorg. Chim. Acta* **2006**, *359*, 2751-2755.
- (8) Gaunt, A. J.; Reilly, S. D.; Enriquez, A. E.; Scott, B. L.; Ibers, J. A.; Sekar, P.; Ingram, K. I. M.; Kaltsoyannis, N.; Neu, M. P. *Inorg. Chem.* **2008**, *47*, 29-41.
- (9) Wynne, K. J. *J. Chem. Educ.* **1973**, *50*, 328-330.
- (10) Williams, D. J. *Inorg. Nucl. Chem. Letters* **1980**, *16*, 189-193.
- (11) Williams, D. J.; Quicksall, C. O.; Barkigia, K. M. *Inorg. Chem.* **1982**, *21*, 2097-2100.
- (12) Cea-Olivares, R.; Toscano, R. A.; Carreón, G.; Valdés-Martínez, J. *Monatsh. Chem.* **1992**, *123*, 391-396.
- (13) Cea-Olivares, R.; Novosad, J.; Woollins, J. D.; Slawin, A. M. Z.; García-Montalvo, V.; Espinosa-Pérez, G.; García y García, P. *Chem. Commun.* **1996**, 519-520.
- (14) Cea-Olivares, R.; García-Montalvo, V.; Novosad, J.; Woollins, J. D.; Toscano, R. A.; Espinosa-Pérez, G. *Chem. Ber.* **1996**, *129*, 919-923.
- (15) Cea-Olivares, R.; García-Montalvo, V.; Novosad, J.; Kilian, P.; Woollins, J. D.; Slawin, A. M. Z.; García y García, P.; López-Cardoso, M.; Espinosa-Pérez, G.; Toscano, R. A.; Hernández, S.; Canseco-Melchor, G.; Lima-Montaño, L.; Rodríguez-Narváez, C. *Phosphorus Sulfur Silicon Relat. Elem.* **1997**, *124*, 347-354.
- (16) García-Montalvo, V.; Cea-Olivares, R.; Williams, D. J.; Espinosa-Pérez, G. *Inorg. Chem.* **1996**, *35*, 3948-3953.
- (17) García-Montalvo, V.; Novosad, J.; Kilian, P.; Woollins, J. D.; Slawin, A. M. Z.;

- García y García, P.; López-Cardoso, M.; Espinosa-Pérez, G.; Cea-Olivares, R. *Dalton Trans.* **1997**, 1025-1029.
- (18) Bertini, I.; Turano, P.; Vila, A. J. *Chem. Rev.* **1993**, *93*, 2833-2932.
- (19) Mao, J.; Zhang, Y.; Oldfield, E. *J. Am. Chem. Soc.* **2002**, *124*, 13911-13920.
- (20) Papadimitriou, C.; Veltsistas, P.; Novosad, J.; Cea-Olivares, R.; Toscano, A.; García y García, P.; Lopez-Cardosa, M.; Slawin, A. M. Z.; Woollins, J. D. *Polyhedron* **1997**, *16*, 2727-2729.
- (21) Chivers, T.; Konu, J.; Ritch, J. S.; Copsey, M. C.; Eisler, D. J.; Tuononen, H. M. *J. Organomet. Chem.* **2007**, *692*, 2658-2668.
- (22) Briand, G. G.; Chivers, T.; Parvez, M. *Angew. Chem., Int. Ed. Engl.* **2002**, *41*, 3468-3470.
- (23) Chivers, T.; Eisler, D. J.; Ritch, J. S. *Dalton Trans.* **2005**, 2675-2677.
- (24) Garje, S. S.; Ritch, J. S.; Eisler, D. J.; Afzaal, M.; O'Brien, P.; Chivers, T. *J. Mater. Chem.* **2006**, *16*, 966-969.
- (25) Ritch, J. S.; Chivers, T.; Afzaal, M.; O'Brien, P. *Chem. Soc. Rev.* **2007**, *36*, 1622-1631.
- (26) Gaunt, A. J.; Scott, B. L.; Neu, M. P. *Angew. Chem., Int. Ed. Engl.* **2006**, *45*, 1638-1641.

## Appendix A

**Table A1** Linear Fit Parameters for Experimental vs. Calculated Selenium Chemical Shift Tensors.

	NR	SR	SO	
$\delta_{180}$	slope	1.12	1.08	1.07
	intercept	-20	-7	-15
	mean absolute deviation <sup>a)</sup>	91	71	66
$\delta_{11}$	slope	1.15	1.07	1.07
	intercept	52	98	50
	mean absolute deviation <sup>a)</sup>	171	164	120
$\delta_{22}$	slope	0.96	0.92	0.93
	intercept	-4	14	2
	mean absolute deviation <sup>a)</sup>	126	133	132
$\delta_{33}$	slope	1.37	1.18	1.13
	intercept	-15	-85	-67
	mean absolute deviation <sup>a)</sup>	247	165	124
$\Omega$	slope	0.69	0.91	0.99
	intercept	350	283	164
	mean absolute deviation <sup>a)</sup>	276	240	164

a) mean absolute deviation via  $\sum_i^n \frac{|(x_i^{Expt.} - x_i^{Calc.})|}{n}$

## Appendix B

**Table B1** Theoretical phosphorus chemical shift tensors for  $\text{HN}(\text{R}_2\text{PE})_2$  ( $\text{E} = \text{O}, \text{S}, \text{Se}$ ;  $\text{R} = \text{Ph}, {}^i\text{Pr}$ ).

E	R	$\delta_{\text{iso}}$ ppm	$\delta_{11}$ ppm	$\delta_{22}$ ppm	$\delta_{33}$ ppm	$\Omega$ ppm	$\kappa$
O	Ph	19.0	85.7	35.8	-64.6	150.3	0.34
		24.4	127.4	51.6	-105.9	233.3	0.35
	<sup>i</sup> Pr a	62.2	137.9	124.0	-75.2	213.1	0.87
		68.9	144.3	123.9	-61.4	205.7	0.80
	<sup>i</sup> Pr b	59.1	131.1	122.3	-76.2	207.3	0.92
		69.1	144.7	124.0	-61.4	206.1	0.80
S	Ph	75.4	203.9	129.2	-106.9	310.8	0.52
		76.5	195.3	118.0	-83.8	279.1	0.45
	<sup>i</sup> Pr	102.2	206.1	142.6	-41.9	248.0	0.49
		108.2	190.3	164.3	-29.9	220.2	0.76
Se	Ph	98.6	235.0	139.3	-78.6	313.6	0.39
		101.8	249.3	153.9	-97.8	347.1	0.45
	<sup>i</sup> Pr a	129.8	245.8	170.2	-26.5	272.3	0.44
		130.3	215.2	192.8	-17.1	232.3	0.81
	<sup>i</sup> Pr b	129.9	243.4	170.9	-24.6	268.0	0.46
		130.5	225.2	184.4	-18.3	243.5	0.66

**Table B2** Theoretical selenium chemical shift tensors for  $\text{HN}(\text{R}_2\text{PSe})_2$  ( $\text{R} = \text{Ph}, \text{}^i\text{Pr}$ ).

R	$\delta_{\text{iso}}$ ppm	$\delta_{11}$ ppm	$\delta_{22}$ ppm	$\delta_{33}$ ppm	$\Omega$ ppm	$\kappa$
Ph	-201	-30	-248	-325	295	-0.48
	-115	97	-133	-331	408	-0.13
<sup>i</sup> Pr a	-495	-140	-609	-735	595	-0.58
	-436	-222	-512	-575	353	-0.64
<sup>i</sup> Pr b	-518	-307	-608	-638	331	-0.82
	-465	-265	-528	-603	337	-0.55

## Appendix C

**Table C1** Theoretical phosphorus chemical shift tensors for  $M[N(^i\text{Pr}_2\text{PSe})_2]_2$  ( $M = \text{Zn}, \text{Cd}, \text{Hg}$ ).

$M^{\text{II}}$	$\delta_{\text{iso}}$ ppm	$\delta_{11}$ ppm	$\delta_{22}$ ppm	$\delta_{33}$ ppm
Zn	98.7	137.8	103.1	55.3
	97.3	136.3	99.2	56.3
	95.3	132.6	97.3	56.0
	95.2	131.5	98.1	55.9
Cd	100.5	140.2	100.1	61.4
	96.8	137.7	94.3	58.6
	93.2	135.4	86.0	58.2
	88.6	128.3	89.0	48.4
Hg	96.5	138.3	90.9	60.2
	93.0	132.2	94.2	52.4
	92.4	131.0	91.0	55.1
	91.8	131.1	88.6	55.7

**Table C2** Theoretical selenium chemical shift tensors for  $M[N(^i\text{Pr}_2\text{PSe})_2]_2$  ( $M = \text{Zn}, \text{Cd}, \text{Hg}$ ).

$M^{\text{II}}$	$\delta_{\text{iso}}$ ppm	$\delta_{11}$ ppm	$\delta_{22}$ ppm	$\delta_{33}$ ppm
Zn	-291	138	-444	-566
	-292	136	-434	-578
	-292	153	-445	-584
	-293	135	-443	-572
Cd	-320	161	-424	-696
	-337	153	-452	-712
	-341	133	-455	-702
	-348	117	-460	-703
Hg	-235	183	-375	-515
	-243	183	-372	-540
	-246	188	-393	-535
	-249	175	-393	-530



**Table C3** Theoretical cadmium and mercury magnetic shielding tensors for  $M[N(^1\text{Pr}_2\text{PSe})_2]_2$  ( $M = \text{Cd}, \text{Hg}$ ).

$M^{II}$	$\sigma_{\text{iso}}$ ppm	$\sigma_{11}$ ppm	$\sigma_{22}$ ppm	$\sigma_{33}$ ppm
Cd	2809	2798	2801	2828
Hg	5463	5417	5438	5534

**Table C4** Traceless phosphorus chemical shift tensors for  $M[N(^i\text{Pr}_2\text{PSe})_2]_2$  ( $M = \text{Zn, Cd, Hg}$ ).

$M^{II}$		$\delta_{\text{iso}}$ ppm	$\delta_{11}$ ppm	$\delta_{22}$ ppm	$\delta_{33}$ ppm		
Zn	Expt	0	20.3	5.7	-25.9		
		0	20.4	6.6	-27.0		
		0	24.0	5.7	-29.7		
		0	22.1	5.9	-27.9		
	Calc	0	39.1	4.4	-43.4		
		0	39.0	1.9	-41.0		
		0	37.3	2.0	-39.3		
		0	36.3	2.9	-39.3		
		Cd	Expt	0	20.3	4.4	24.7
				0	20.8	4.7	-25.4
0	22.2			3.9	-26.2		
0	21.9			5.0	-26.9		
Calc	0		39.7	-0.4	-39.1		
	0		40.9	-2.5	-38.2		
	0		42.2	-7.2	-35.0		
	0		39.7	0.4	-40.2		
	Hg		Expt	0	21.2	4.1	-25.2
				0	21.2	4.1	-25.3
0		23.5		3.3	-26.9		
0		22.6		4.9	-27.6		
Calc		0	41.8	-5.6	-36.3		
		0	39.2	1.2	-40.6		
		0	38.6	-1.4	-37.3		
		0	39.3	-3.2	-36.1		

**Table C5** Traceless selenium chemical shift tensors for  $M[N(^i\text{Pr}_2\text{PSe})_2]_2$  ( $M = \text{Zn, Cd, Hg}$ ).

$M^{\text{II}}$		$\delta_{\text{iso}}$ ppm	$\delta_{11}$ ppm	$\delta_{22}$ ppm	$\delta_{33}$ ppm	
Zn	Expt	0	420	-174	-247	
		0	420	-151	-269	
		0	403	-155	-247	
		0	439	-159	-279	
	Calc	0	429	-153	-275	
		0	428	-142	-286	
		0	445	-153	-292	
		0	428	-150	-279	
	Cd	Expt	0	438	-114	-324
			0	436	-98	-338
0			444	-101	-344	
0			444	-101	-344	
Calc		0	481	-104	-376	
		0	490	-115	-375	
		0	474	-114	-361	
		0	465	-112	-355	
Hg		Expt	0	405	-122	-283
			0	407	-118	-290
	0		404	-121	-284	
	0		426	-130	-295	
	Calc	0	418	-140	-280	
		0	426	-129	-297	
		0	434	-147	-289	
		0	424	-144	-281	

**Table C6** Traceless cadmium and mercury chemical shift tensors for  $M[N(\text{Pr}_2\text{PSe})_2]_2$  ( $M = \text{Cd, Hg}$ ).

$M^{II}$		$\delta_{iso}$ ppm	$\delta_{11}$ ppm	$\delta_{22}$ ppm	$\delta_{33}$ ppm
Cd	Expt	0	54	34	-89
	Calc	0	11	8	-19
Hg	Expt	0	296	226	-522
	Calc	0	46	25	-71

## Appendix D

**Table D1** Theoretical phosphorus shielding tensors for  $M[N(^i\text{Pr}_2\text{PSe})_2]_2$  ( $M = \text{Pd, Pt; Se, Te}$ ).

$M^{II}$		$\sigma_{\text{iso}}$ ppm	$\sigma_{11}$ ppm	$\sigma_{22}$ ppm	$\sigma_{33}$ ppm	$\Omega$ ppm
Pd	SR	222	178	218	269	91
		210	143	228	258	115
	SO	261	239	246	299	60
		244	203	252	278	75
Pt	SR	233	189	234	278	89
		217	151	247	253	102
	SO	277	248	269	315	67
		255	220	255	291	71
Se	SR	214	167	217	257	90
		210	170	209	252	82
	SO	273	239	265	313	74
		270	240	266	305	65
Te	SR	239	202	240	275	73
		237	194	239	278	84
	SO	275	249	268	307	58
		273	243	264	313	70

**Table D2** Theoretical selenium shielding tensors for the anion of  $M[N(^i\text{Pr}_2\text{PSe})_2]_2$  ( $M = \text{Pd, Pt; Se, Te}$ ).

$M^{II}$		$\sigma_{\text{iso}}$ ppm	$\sigma_{11}$ ppm	$\sigma_{22}$ ppm	$\sigma_{33}$ ppm	$\Omega$ ppm
Pd	SR	1526	1140	1468	1968	828
		1534	1187	1602	1812	625
	SO	1698	1331	1606	2159	828
		1716	1395	1767	1985	590
Pt	SR	1607	1250	1540	2032	782
		1604	1265	1631	1916	651
	SO	1986	1467	1717	2174	707
		1793	1487	1815	2077	590
Se	SR	1404	1031	1395	1788	757
		1471	1026	1450	1937	911
	SO	1628	1254	1665	1965	711
		1688	1265	1712	2086	821
Te	SR	1597	1409	1557	1824	415
		1657	1352	1676	1942	590
	SO	1763	1542	1751	1996	454
		1825	1517	1866	2092	575

**Table D3** Theoretical shielding tensors for nucleus M of  $M[N(iPr_2PSe)_2]_2$  ( $M = {}^{105}Pd, {}^{195}Pt, {}^{77}Se, {}^{125}Te$ ).

$M^{II}$		$\sigma_{iso}$ ppm	$\sigma_{11}$ ppm	$\sigma_{22}$ ppm	$\sigma_{33}$ ppm	$\Omega$ ppm	$\kappa$
Pd	SR	498	-1336	1309	1521	2837	-0.86
	SO	1004	-909	1842	2079	2988	-0.84
Pt	SR	3097	1726	3692	3872	2146	-0.83
	SO	5700	3941	6453	6705	2764	-0.82
Se	SR	1289	1065	1338	1463	398	-0.37
	SO	1378	1307	1353	1475	168	0.45
Te	SR	2063	1554	2255	2382	828	-0.69
	SO	2567	2127	2342	3234	1107	0.61

## Appendix E

Prior to the use of ADF for the computation of the selenium chemical shift tensors investigated in this thesis, Gaussian98 was employed in calculating the corresponding nuclear magnetic shielding tensors for many of the compounds studied in Chapter 4. Restricted Hartree-Fock, hybrid DFT utilizing the B3LYP exchange-correlation functional, and Møller-Plesset second order perturbation theory calculations were performed in order to assess the importance of electron correlation to the computations. Basis sets ranging from 6-31G to 6-311++G(3df, 2pd) were employed to provide an estimate on the minimum number of basis functions required to eliminate the effects of an incomplete basis set. The results of the above calculations were consistent with previous studies in their ability to reproduce isotropic selenium chemical shifts,<sup>1-13</sup> and led to the pursuit of accurate reproduction of the principal components,  $\delta_{ii}$ , of the selenium chemical shift tensors in general, and the importance of relativistic effects on the computations carried out using ZORA DFT in Chapter 4.

While the theoretical basis for many of the calculations subsequently performed was being identified, synthetic approaches to the production of substituted diphenyl diselenides,  $\text{Ar}_2\text{Se}_2$ , were being pursued. Initial attempts proceeded through an aryl selenocyanate,  $\text{ArSeCN}$ , intermediate that was subsequently oxidized to the  $\text{Ar}_2\text{Se}_2$ . The  $\text{ArSeCN}$  species were arrived at via the diazotization reaction between  $\text{KSeCN}$  and the substituted aniline,  $\text{ArNH}_2$ ,<sup>14</sup> and subsequent oxidation was achieved via literature procedures.<sup>15</sup> However, efforts at obtaining pure *ortho*-, *meta*-, and *para*-substituted  $\text{XPh}_2\text{Se}_2$  ( $\text{X} = \text{F}, \text{Cl}, \text{Br}, \text{NO}_2$ ) were unsuccessful. An alternate approach to  $\text{Ar}_2\text{Se}_2$



species via the aryl selenol, ArSeH, was then attempted. The aryl selenols were synthesized via a modified Grignard reaction involving aryl bromides, magnesium turnings, and elemental selenium. While some halo-substituted diphenyl diselenides were prepared in this manner, the vast majority remained as liquids or oils thwarting the goal of characterizing the orientation dependent NMR interaction tensors via solid-state  $^{77}\text{Se}$  NMR.

The pursuit of the NMR interaction tensors involving selenium was the focus of my graduate research; however, there were a couple of additional projects that I was involved with that did not involve selenium. Mathew Willans and I collaborated on an introductory project involving the study of triphenyl-Group 14 chlorides,  $\text{Ph}_3\text{XCl}$  ( $\text{X} = \text{C}, \text{Si}, \text{Sn}, \text{Pb}$ ), via solid-state  $^{13}\text{C}$ ,  $^{29}\text{Si}$ ,  $^{117/119}\text{Sn}$ , and  $^{207}\text{Pb}$  NMR spectroscopy and ZORA DFT computations. This project introduced me to the concept of residual dipolar coupling between quadrupolar and spin- $\frac{1}{2}$  nuclei. A manuscript on this research entitled *An NMR and Relativistic DFT Study of Spin-Spin Coupling in Solid Triphenyl Group-14 Chlorides* was published in *Physical Chemistry Chemical Physics*.<sup>16</sup> The role I provided in this project involved performing some of the solid-state  $^{13}\text{C}$ ,  $^{29}\text{Si}$ ,  $^{117/119}\text{Sn}$ , and  $^{207}\text{Pb}$  NMR spectroscopy, simulation of a number of the experimental spectra, calculation of the corresponding nuclear magnetic shielding and indirect spin-spin coupling tensors, and assistance with the preparation of the manuscript.

When I came to the University of Alberta, I brought samples of the intermediate formation of the molecular sieve  $\text{AlPO}_4\text{-18}$  from my honours research project with me from Dr. Huang's lab at the University of Western Ontario. The purpose was to calcine the samples I had prepared, and flow hyperpolarized xenon through the microporous

material from which their porous nature could be investigated by  $^{129}\text{Xe}$  NMR. The project gave me experience in the operation of a hyperpolarizer and the manipulation of gases in the preparation of sealed samples. The article, *Formation of Porous Aluminophosphate Frameworks Monitored by Hyperpolarized  $^{129}\text{Xe}$  NMR Spectroscopy* was published in Chemistry of Materials.<sup>17</sup> The research role I provided in this project involved preparation and calcination of the samples, preparation of sealed xenon samples, acquisition of hyperpolarized and thermally polarized  $^{129}\text{Xe}$  NMR spectra, and assistance with the preparation of the published article.

## References

- (1) Sefzik, T. H.; Turco, D.; Iuliucci, R. J.; Facelli, J. C. *J. Phys. Chem. A* **2005**, *109*, 1180-1187.
- (2) Yates, J. R.; Pickard, C. J.; Payne, M. C.; Mauri, F. *J. Chem. Phys.* **2003**, *118*, 5746-5753.
- (3) Bayse, C. A. *J. Chem. Theory Comput.* **2005**, *1*, 1119-1127.
- (4) Magyarfalvi, G.; Pulay, P. *Chem. Phys. Lett.* **1994**, *225*, 280-284.
- (5) Bühl, M.; Gauss, J.; Stanton, J. F. *Chem. Phys. Lett.* **1995**, *241*, 248-252.
- (6) Bühl, M.; Thiel, W.; Fleischer, U.; Kutzelnigg, W. *J. Phys. Chem.* **1995**, *99*, 4000-4007.
- (7) Schreckenbach, G.; Ruiz-Morales, Y.; Ziegler, T. *J. Chem. Phys.* **1996**, *104*, 8605-8612.
- (8) Nakanishi, W.; Hayashi, S. *Chem. Lett.* **1998**, 523-524.
- (9) Bayse, C. A. *Inorg. Chem.* **2004**, *43*, 1208-1210.
- (10) Bernard, G. M.; Eichele, K.; Wu, G.; Kirby, C. W.; Wasylshen, R. E. *Can. J. Chem.* **2000**, *78*, 614-625.
- (11) Chesnut, D. B. *Chem. Phys.* **2004**, *305*, 237-241.
- (12) Tattershall, B. W.; Sandham, E. L. *J. Chem. Soc.-Dalton Trans.* **2001**, 1834-1840.
- (13) Wilson, P. J. *Mol. Phys.* **2001**, *99*, 363-367.
- (14) Schmid, G. H.; Garratt, D. G. *J. Org. Chem.* **1983**, *48*, 4169-4172.
- (15) Krief, A.; Dumont, W.; Delmotte, C. *Angew. Chem., Int. Ed. Engl.* **2000**, *39*, 1669-1672.
- (16) Willans, M. J.; Demko, B. A.; Wasylshen, R. E. *Phys. Chem. Chem. Phys.* **2006**, *8*, 2733-2743.
- (17) Sears, D. N.; Demko, B. A.; Ooms, K. J.; Wasylshen, R. E.; Huang, Y. *Chem. Mat.* **2005**, *17*, 5481-5488.